Graded organisation of fibronectin to tune cell behaviour

Eleni Grigoriou

(BSc, MRes)

Submitted in fulfilment of the requirements for the Degree of Doctor of Philosophy (PhD)

College of Science and Engineering

School of Engineering

University of Glasgow

Glasgow, G12 8LT

July 2017

Thesis abstract

Cells are in constant and dynamic interactions with the extracellular environment. They receive several inputs involved in the regulation of cell behaviour. Fibronectin, an abundant protein of the ECM, contains multiple binding domains and binds to cell receptors, growth factors and other ECM proteins. FN undergoes conformational changes through cell-generated contractile forces which consequently affects cell response. Tissue engineering aims at engineering biomaterials that recreate the *in vivo* ECM. In addition to biomaterials, stem cells have emerged as a promising source due to their inherent differentiation potential.

In this work, the role of poly acrylates in controlling human mesenchymal stem cell behaviour (hMSCs) was explored. Particularly, a series of copolymers with specific ratio of ethyl(acrylate), EA, and methyl(acrylate), MA, were used. It is known that poly(ethyl)acrylate, PEA, triggers a network-like conformation of FN upon adsorption, whereas poly(methyl)acrylate, PMA, elicits a globular conformation. It was found that a different degree of FN organisation can be obtained dependent on the EA/MA ratio, with the network being more connected with increased EA ratio. This differential conformation was shown to affect the availability of critical binding sites. This system was further used to study hMSCs response in terms of adhesion and osteogenic differentiation. All surfaces support cell growth and focal adhesion formation. However, increased cell size and spreading was promoted on surfaces with higher EA concentration. Next, the potential of the surfaces after sequential adsorption of FN and the growth factor BMP-2 to drive osteogenic commitment was explored. Enhanced expression of the osteogenic markers RUNX2 and OCN was found with higher concentration of EA whereas the opposite was observed with ALP expression. Another part of this work involved investigating cell migration on PEA and PMA. Higher cell speed was found on PEA where FN adopts a more extended conformation. Moreover, the protein composition of focal adhesions was evaluated by proteomic analysis.

The findings of this work give further insights into how the surface with well-defined chemical properties can modulate FN conformation and how these changes affect cellular processes.

Table of Contents

List of Tables

Chapter 1

Chapter 2

Chapter 4

List of figures

Chapter 1

Chapter 2

Chapter 3

Chapter 4

Chapter 5

Presentations

(2016) Oral presentation at the Glasgow Orthopaedic Research Initiative (GLORI), Glasgow, UK: E Grigoriou, M Cantini, MJ Dalby, M Salmeron-Sanchez. Graded organisation of fibronectin on polymer surfaces to tune cell response

(2016) Poster presentation at the British Orthopaedic Research Society (BORS), Glasgow, UK: E Grigoriou, M Cantini, MJ Dalby, M Salmeron-Sanchez. Graded Organisation of Fibronectin on Polymer Surfaces to Tune Mesenchymal Stem Cell Response

(2016) Poster presentation at the Biointerfaces International Conference, Zurich, Switzerland: E Grigoriou, M Cantini, MJ Dalby, M Salmeron-Sanchez. Graded organisation of fibronectin on polymer surfaces to control growth factor presentation and cell response

(2015) Poster presentation at the Tissue and Cell Engineering Society (TCES), Southampton, UK: E Grigoriou, M Cantini, MJ Dalby, M Salmeron-Sanchez. Graded organisation of fibronectin on polymer surfaces to tune cell response.

Publications

Grigoriou, E. Cantini, M. Dalby, M. J. Petersen, A. Salmeron-Sanchez, M., Cell migration on material-driven fibronectin microenvironments. Biomaterials Science 2017, 5 (7), 1326-1333.

Mnatsakanyan, H. Rico, P. Grigoriou, E. Candelas, A. M. Rodrigo-Navarro, A. Salmeron-Sanchez, M. Sabater i Serra, R., Controlled Assembly of Fibronectin Nanofibrils Triggered by Random Copolymer Chemistry. ACS Applied Materials & Interfaces 2015, 7 (32), 18125-18135.

Awards

Best poster communication at Tissue and Cell Engineering Society conference in Southampton, 2015

Acknowledgements

Firstly, I would like to thank Manuel Salmeron Sanchez for giving me the opportunity to be part of his group. He always offered his guidance and his support through these years.

I would also like to thank my second supervisors Matthew Dalby for giving me advice when needed and Marco Cantini for helping me any time I needed. Of course I would like to thank all the people I have met in MiMe group for their support and advice in the lab as well as all for providing a friendly and supportive working environment. Many thanks also to Virgina Llopis Hernandez for being so awesome! It was a pleasure working with you. Also, I would like to thank my friends Andria and Ross for always being there for me in the moments of crisis.

Finally, I would like to say a massive thank you to my parents for supporting me practically and emotionally all these years. It would not have been possible without them.

Author’s Declaration

I hereby declare that the research presented within this thesis is my own work unless otherwise stated, and has not been submitted elsewhere for any other academic degree.

List of abbreviations

µl……..……..……microletre

µm ……micrometre

ACA……..Advancing contact angle

AFM……..Atomic force microscopy

ALP……Alkaline phosphate activity

AMIDAS……..Adjacent site to MIDAS

ANOVA…….Analysis of variance

Arg, R……Arginine

ASC……..Adult stem cells

Asn……...Asparagine

Asp, D……Aspartic acid

BMPs……..……Bone morphogenetic proteins

BSA……...Bovine serum albumin

BSA……Micro-bicinchoninic acid

BTE…….……..Bone TE

Ca^{2}+……...Calcium

DAPI ……4’6-diamidino-2-phenylindole

DAVID ……Database for Annotation, Visualization and Integrated Discovery

DBSCs……...Dental bud stem cells

DPBS……..…Dulbecco’s phosphate buffered saline

EA……...Ethyacrylate

ECM……Extracellular matrix

EDTA ……..…Ethylenediaminetetraacetic acid

EGF……Epidermal growth factor

ELISA……Enzyme-linked immunosorbent assay

emPAI…….……Exponentially modified protein abundance index

ERK1/2……..……Extracellular-regulated kinases 1/2

ESC……..….Embryonic stem cells

ESI……Electrospray ionization

FAK……...Focal adhesion kinase

FAs……..Focal adhesions

FASP……Filtered-aided sample preparation

FBS……..Foetal bovine serum

FD……..……..Fractal dimension

FGF……..…Fibroblast growth factor

FITC……Fluorescein

FN……Fibronectin

FRET……Förster resonance energy transfer

GAGs…….……..Glycosaminoglycans

GDP……...…Guanosine diphosphate

GFOGER ……..……...Gly-Phe-Hyp-Gly-Glu-Arg

GFs……Growth factors

Glu……Glutamic acid

Gly……...Glycine

GO……Gene Ontology

Grbp2……..Growth factor receptor-bound protein 2

GTP……Guonosine triphosphate

GTPase……Guanosine triphosphatase

HA……..Hydroxyapatite

HGF……..…Hepatocyte growth factor

His……Histidine

hMSCs……hMSCs

HRP……Horseradish peroxidase

HSCs……Hematopoietic stem cell precursors

Hyp……...Hydroxyprline

ICW……...In-Cell Western

iPSCs……..Induced pluripotent stem cells

ISCT…… International Society for Cellular Therapy

KEGG……Kyoto Encyclopedia of Genes and Genomes

m/z……...Mass-to-charge ratio

MA……..Methylacrylate

MALDI……Matrix assisted laser desorption/ionization

MAPK……Mitogen-activated protein kinase

Mg^{2}+……Magnesium

MH…….……Mad-homology

MIDAS……..Metal ion-dependent adhesion sites

MS…….....……..……...Mass spectrometry

MSCs……Mesenchymal stem cells

NaH_2PO_4……Sodium phosphate monobasic

Nas……Nascent adhesions
NGF……..……Nerve growth factor
NLK……Nemo-like kinase
Nm……Nanometre
OCN……Osteocalcin
OPN……Osteopontin
PANTHER …..……Protein Analysis THrough Evolutionary Relationships
PCA……..Principal component analysis
PCL……Poly(caprolactone)
PDGF……...Platelet-derived growth factor
PEA……..…….Poly(ethyl acrylate)
PEG……Polyethylene glycol
PGA……..Poly(glycolic acid)
Phe……..Phenylalanine
PHSRN……Pro-His-Ser-Arg-Asn
PLLA……Poly(L-lactic acid)
PMA ……..……Poly(methyl acrylate)
Pro……Proline
RCA……Receding contact angle
RGD……..Rrginine-glycine-aspartate
RTK……..Tyrosine kinase
RUNX2……Runt-related transcription factor 2
SAMs……..Self-assembled monolayers
SCA……...Static contact angle
SD……Standard deviation
SDS……Sodium dodecyl sulfate
Ser……Serine
SH2……...Src homology 2
siRNAs……Small interfering RNAs
Smad……Mothers against decapentaplegic homolog
SOS……Son of sevenless
TCP……Tissue culture plastic
TE……Tissue engineering
TEA……..Triethanolamine
TGF……Transforming growth factor beta

UV……..Ultraviolet

VEGF……..……Vascular endothelial growth factor

VN…….Vitronectin

WCA…….Water contact angle

1. Introduction

1.1 Introduction

Regenerative medicine is a multidisciplinary field that aims to replace, restore and improve the function of injured and diseased tissues. Tissue engineering (TE) is an important component of regenerative medicine and its goal is to develop biological substitutes of tissues[1]. Current approaches of TE require a suitable cell source, engineered biomaterials and the delivery of biomolecules. This field has contributed to understanding the mechanisms that regulate major cell functions as well as cell-biomaterials interactions[2]. Essentially, the objective of TE is to deconstruct the complexity of the in *vivo* environment and to recapitulate the cell physiological environment.

1.2 Extracellular matrix

The extracellular matrix (ECM) is the cell native environment and it is a three-dimensional non-cellular heterogeneous network composed of a meshwork of proteoglycans, glycoproteins and soluble growth factors[3, 4]. The ECM serves multiple and fundamental functions. It provides structural support to the cells and thus it defines the shape of organs and tissues. Deregulation of ECM components and biophysical properties are associated with the development of pathologies, such as skin diseases, fibrosis and cancer[5]. ECM is a rather dynamic entity that undergoes constant remodelling and its composition and topology is tissue-specific. It is also a source of signals and growth factors that allow cells to carry out important processes for their proliferation and survival[6]. All cell types synthesize and secrete matrix proteins, a process which is highly regulated.

1.3 Cell adhesion

Cells sense the biochemical and physical cues coming from the ECM and they are then converted to biochemical signals which regulate cell processes such as differentiation and survival. Signal transduction is mediated *via* cell adhesion receptors known as integrins formed at the sites of cell-ECM interactions. These complexes are physically bound to specific amino acid sequences of ECM proteins, such as fibronectin (FN), vitronectin (VN), collagen and laminin and mechanically link the actin cytoskeleton to the ECM[7]. Transduction of

external signals *via* integrins results in changes in ECM architecture and instigate signalling pathways important for cell response[8].

1.3.1 Integrins

Integrins are bidirectional cell surfaces receptors and mediate divalent cation-dependent interactions with components of the ECM. They are heterodimeric type I transmembrane receptors and are composed of non-covalently bound α and β glycoprotein subunits. Each receptor recognises specific ECM ligands with different affinities[7]. Integrin structure and function have been extensively studied since their discovery and classification in the 1980s[9]. In mammals, there are 18 α subunits and 8 β subunits which are composed of several domains and are assembled into 24 different receptors. Each subunit consists of a large extracellular domain, a spanning transmembrane helix and a short cytoplasmic domain. The solved crystal structure of the extracellular domain of $\alpha_v\beta_3$ integrin has given important insights into the structural conformations integrins obtain upon ligand binding[10]. Half of the α subunits contain an extra domain known as inserted αI domain and is the major ligand binding site. For the integrins that lack the αI domain, such as $\alpha_v\beta_3$, $\alpha_{IIb}\beta_3$ and $\alpha_5\beta_1$, ligand binding occurs at the largest interface between the two subunits and the βI domain which is homologous to αI[11, 12].

Most integrins are not constitutively active. Their regulation is achieved through tight temporal and spatial control of their affinity for ECM ligands. Three distinct integrin structures associated with ligand affinity have been described; bent with a closed headpiece, extended with a closed headpiece, and extended with an open headpiece. Conversion from low-affinity to high-affinity state is induced by both extracellular and intracellular signals[13]. Low-affinity integrins, represented by a bend and inverted V-like conformation[10, 14], indicate the inactive state of integrins which does not favour the recognition and binding of ligands. Activation of integrins is triggered by the binding of small ligand molecules (Mg^{2+}, Mn^{2+} and Ca^{2+}). This leads to rapid conformation changes characterised by a more open and extended configuration[14]. These changes have been shown to alter the structure of metal ion-dependent adhesion sites (MIDAS) in αI and βI domains and the adjacent site to MIDAS (AMIDAS)[12].

Conformational changes and integrin clustering are required for the transmission of outside-in signalling. However, it is still not clear how signals are transmitted across the plasma membrane through the transmembrane domain. Recent studies showed that association of the α and β subunit transmembrane domains results in the stabilisation of the inactive integrin state. The separation of the transmembrane domain, induced by binding of the β subunit cytoplasmic domain to intracellular molecules, contribute to the high-affinity conformation and integrin activation[15-17] (Figure 1.1).

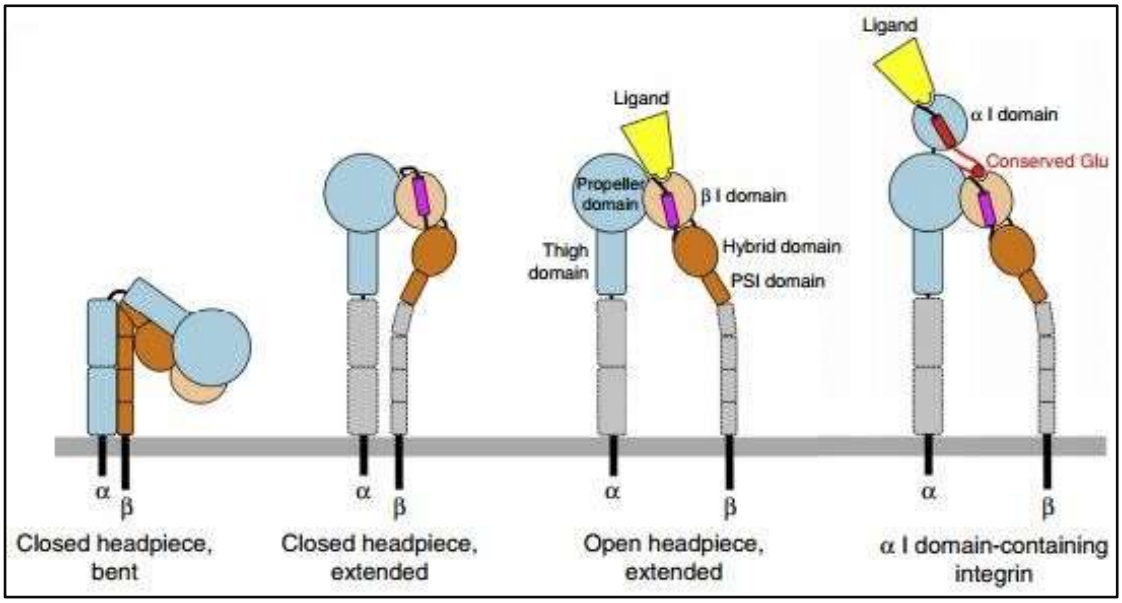

Figure 1.1 Schematic representation of integrin activation. Integrin structure, activation and interactions[18].

1.3.2 Focal adhesions

Conformational changes induced by ligand binding result in the assembly of an intracellular multiprotein structure. The activating step is followed by binding of the anchoring protein talin which interacts with the intracellular β subunit of integrins *via* the N-terminal while the C-terminal binds to actin[19]. Talin also contributes to the upright conformation of integrins. Expression of talin in talin knockout cells rescued integrin activation and cell spreading[20]. In addition, disruption of talin in endothelial cells impaired organization into vessels, leading to embryonic death at gastrulation[21]. Kindlin, another anchoring protein, co-operates with talin and is essential for integrin activation[4]. Lack of either talin or kindlin failed to activate β1 integrins[22].

Binding of talin to kindlin elicits the recruitment of various proteins in the cytoplasmic tail resulting in the assembly of focal adhesions (FAs). One of the best characterised protein is vinculin which is considered a mechanosensitive protein. Constitutively active forms of vinculin were shown to induce an increase in the size of FAs as well a reduced rate of turnover[23]. In contrast, loss of intracellular tension caused by blebbistatin promoted rapid dissociation of vinculin from FAs[24]. Vinculin binds to talin *via* its N-terminal and triggers the clustering of activated integrins and actin complexes. By binding to actin *via* its C-terminal, vinculin act as a molecular clutch and is essential in development of stable focal adhesion complexes[25]. Talin-vinculin interactions are regulated by conformational changes. Vinculin also reinforces the link between talin and actin. Suppression of vinculin binding to talin results in the inactivation of the actin-binding domain of talin and in the formation of unstable short-lived focal complexes[20].

The first adhesion structure is formed away from the leading edge between lamellipodia (membrane extensions formed at the cell front[26]) and the lamella (structures found behind the lamellipodia[26]) and are short-lived nascent adhesions (NAs) (> 1 μm length)[27]. These focal points transmit traction forces and they undergo rapid disassembly. Some of them grow in size and develop into longer mature FAs in the lamellum (1.0–10 μm^2). These structures contain multiple proteins such as vinculin, talin and paxillin. FAs are tightly attached to the ECM and to the cytoskeleton *via* F-actin. They thus contribute to cell response to chemical and physical features coming from the ECM and to signal transmission. For example, fibroblasts seeded on rigid surfaces displayed large and uniformly oriented FAs[28, 29].

Mechanotransduction *via* FAs is transimitted by a non-receptor tyrosine kinase known as focal adhesion kinase (FAK). Upon integrin clustering, FAK is activated by autophosphorylation on the Y397. This triggers the binding of Src to the autophosphorylated sites leading to an increase in Src–FAK activation[30]. Src is another non-receptor tyrosine kinase and phosphorylates other sites of FAK[31] and other FA proteins such as paxillin[30]. Previous studies suggest that the FAK-Src are involved in the control of FA dynamics which subsequently has an impact on downstream signalling pathways[32].

1.4 Fibronectin

FN is one of the most abundant components of the ECM and is widely involved in physiological events such as development and tissue regeneration. FN knockout mice fail to develop beyond embryonic day 10 or 11[33]. It can also influence pathological conditions such as tumour metastasis[34]. Within the ECM, FN is organised into a network of elongated fibrils which can be stretched in a cell-mediated process[35]. FN is encoded by a single gene, however various isoforms are generated by alternative splicing[3]. FN is synthesised by a variety of cells and two main forms have been described; plasma FN, predominantly secreted by hepatocytes, and cellular FN[36].

FN is a dimeric protein and consists of two subunits of ~250 kDa covalently linked by disulphide bonds at their C-terminus[37]. Each dimer contains multiple recognition domains that mediate interactions with other ECM proteins, such as collagen, heparin and fibrin, FN molecules, glycosaminoglycans (GAGs) and cell surface receptors[38] . There are three types of FN repeating units; type I, type II and type III [39]. Each module consists of 12 type I repeats, 2 type II repeats and 15-17 type III repeats (Figure 1.2). The structure of type I and type II repeats is stabilised by pairs of intramolecular disulphide bridges, whereas type III repeats are 7-stranded β-barrel structures which are stabilised by hydrogen bonds and Van der Waals forces[40]. Due to the lack of disulphate bonds, type III repeats are flexible and can undergo conformation changes under mechanical or chemical stimuli[41].

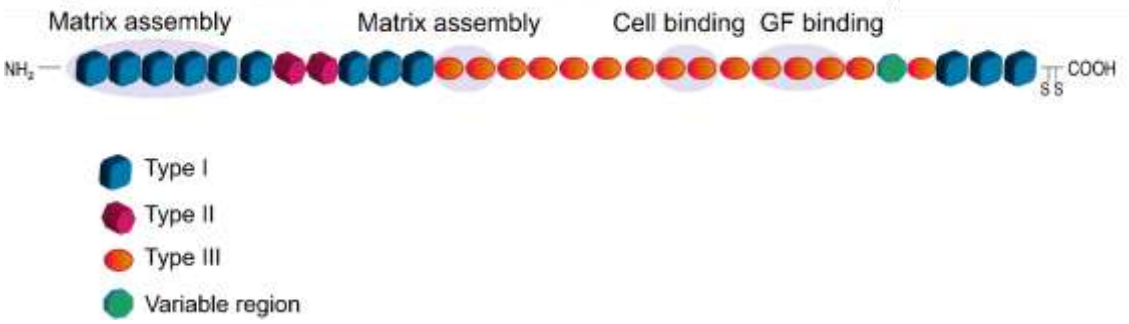

Figure 1.2. FN subunit and its molecular recognition sites. Each dimer consists of three types of domains; type I, type II and type III.

FN has been associated with a wide range of cellular processes. It contributes to the homeostasis of the ECM as well as to the stability and assembly of other ECM components. In addition, it is required for the deposition of other ECM proteins such as collagen. In a study where FN null cells were used, FN polymerisation was found to be a prerequisite for the deposition of collagen I and thrombosponin-1[42]. Furthermore, using Förster resonance energy transfer (FRET) labelled FN, it was found that collagen I fibres interact preferentially with more relaxed FN. Once collagen I is assembled, it restrict the ability of fibroblasts to further stretch and mechanically unfold FN fibres[43].

1.4.1 Fibronectin matrix assembly

FN can be categorised into soluble plasma and insoluble cellular molecules. FN can be found in different conformations which in turn affect the protein biological function. Consequently, a critical event in FN biological activity is the assembly of FN molecules into interconnected fibres which ultimately result in a fibrillar network. This is a cell-dependent process and occurs in an elaborate step-wise way which is not yet fully understood. The dimeric protein is secreted in a soluble and compact form. In this form, FN is inactive and its activation is required for matrix assembly. The initial step involves binding to cell surface receptors such as syndecans and integrins. Cell attachment is mediated primarily through binding of $\alpha_5\beta_1$ integrin to the RGD (arginine-glycine-aspartate) sequence located in the $FNIII_{10}$ repeat and to the adjacent PHSRN (Pro-His-Ser-Arg-Asn) synergy domain located in a loop in $FNIII_9$ repeat[39, 44-46]. An RGD-independent assembly of FN has been also reported to occur through binding of $\alpha_4\beta_1$ integrin to the alternatively spliced V region near the C terminus of FN[47].

Cell attachment to FN supports actin stress fibre formation and enhances cell contractility *via* the activation of small guanosine triphosphatase (GTPase) Rho[48]. This event leads to an increase in the concentration of integrin-bound FN which is organised into short fibrils. In addition, actin-myosin interactions generate forces sufficient to extent FN molecules. Such conformational changes lead to protein unravelling and the exposure of cryptic binding sites which allowing FN molecule to interact laterally and promote the formation of thicker fibrils. It has been suggested that unfolding of the $FNIII_{10}$ repeat

contributes to FN fibrillogenesis[49]. The compact form of FN is maintained by intramolecular association of several binding sites such as binding of $FNIII_{2-3}$ and $FNIII_{12-14}$ repeats[50]. Disruption of these interactions promote fibrillogenesis and allow intermolecular interactions. Further unfolding of type III repeats have been proposed to contribute to fibril extensibility[51]. Other binding domains contribute to this process too. The $FNIII_{1-2}$ repeat has been shown to regulate fibrillogenesis *via* binding to FN. Blocking of $FNIII_1$[52] or deletion of the $FNIII_{1-2\ site}$ significantly reduced matrix assembly[53]. For example, the FNIII1-5 site at N-terminal binds directly to other binding regions across FN. Additionally, covalent interactions of the subunits are also required involving a pair of the C-terminal bonds [39, 54].

1.4.2 Fibronectin activity

Cells interact with FN *via* integrins which recognise and bind to its multiple domains. Integrin binding is a highly regulated process and a specific pattern of binding can direct cell behaviour. The major cell binding site recognised by numerous integrins is the RGD sequence which is incorporated into many adhesive ECM proteins[55]. The RGD sequence is recognised by the five α_V integrins, two β1 integrins (α_5, α_8) and $\alpha_{IIb}\beta_3$[56] and it has described as the minimal adhesive motif. Adjacent to RGD site, FN harbours the synergy domain PHRSN which binds $\alpha_5\beta_1$ and $\alpha_{IIb}\beta3$ integrins but not α_v-class integrins[57]. In vitro studies have demonstrated that the PHSRN domain contributes to the binding affinity of the α5β1 to FN[58] and to the overall increase in cell adhesion[59]. These two sequences can mimic the adhesive properties of native FN[60].

A large body of evidence suggests that FN conformational state affects integrin binding. Both the RGD and PHRSN are required for the binding of the $\alpha_5\beta_1$ integrin which assumes an open conformation upon binding[61]. Other integrins engage FN through RGD including $\alpha IIb\beta_3$, $\alpha_V\beta_3$, $\alpha_V\beta_6$, $\alpha_V\beta_1$ and $\alpha_8\beta_1$[62]. The spatial organisation of the RGD and PHSRN sites have critical implication in the affinity of integrin binding. They are separated by about 32 Å when FN is relaxed. Under tension, the $FNIII_{10}$ repeat unfolds resulting essentially in translocation of the RGD from the PHSRN site from 32 Å to approximately 55 Å[63]. It has been shown that when they are in closer proximity, the binding of

$\alpha_5\beta_1$ integrin is enhanced. In contrast, a stretched state of FN results in a decrease in the binding affinity. Further evidence to support the effect of RGD-PHSRN distance in integrin binding is shown when the $FNIII_9$ repeat was stabilised by a Leu-Pro mutation resulting in an increased affinity of $\alpha_5\beta_1$[64]. Another study reported decreased binding of the integrin subunits α_3 and α_5 on $FNIII_{10}$ compared to increased binding found on the $FNIII_{9\text{-}10}$ repeat. In contrast, binding of the a_v integrins was not affected by the lack of synergy domain[65]. Altering the binding of integrins to FN has been shown to affect cell phenotype. Garcia *et al*. demonstrated that the levels of bound $\alpha_5\beta_1$ could regulate the switch between the proliferation and differentiation of murine myoblasts[66]. In another study, cells bound to substrates through $\alpha_5\beta_1$ exert higher forces than if they were bound through $\alpha_v\beta_3$[67]. In another study, blocking of $\alpha_5\beta_1$ had an effect only on highly affine substrates where FN fragments presented both the RGD and PHSRN domain. In contrast, full-length FN and fragments containing only the RGD site sustained cell growth[64].

Aside from FN-integrin interactions, FN binds various growth factors including transforming growth factor beta (TGF)-β1[68] and hepatocyte growth factor (HGF)[69] *via* growth factor binding domains. More specifically, the $FNIII_{12\text{-}14}$ is known as a binding site for several GFs. Martino *et al*. reported high affinity of platelet-derived growth factor (PDGF), fibroblast growth factor (FGF), TGF-β, and neurotrophin families to engineered $FNIII_{12\text{-}14}$ fragments[70]. Furthermore, VEGF has been shown to bind to this site. When the lysine and arginine of repeats 13 and 14 were mutated to serine, the binding of vascular endothelial growth factor (VEGF) was abolished. Interestingly, in the same study it was also demonstrated that the VEGF biological activity required the synergy of both cell-binding and VEGF-binding domains to promote the VEGF activity[71].

1.5 Stem cells

Stem cells are characterised by prolonged self-renewal capacity and the ability to differentiate and commit to one or more cell lineages. Due to their inherent differentiation potential, they have long been recognised as an ideal cell source in developing cell-based therapies for the regeneration of injured or diseased tissues. Strategies combing the use of appropriate materials and stem cells are promising in treating several conditions[72].

Stem cells reside in a specialised microenvironment, the niche, in which cells remain in a quiescent state or are activated in response to specific stimuli and differentiate[73]. Stem cells are broadly divided into embryonic stem cells (ESC), adult stem cells (ASC) and induced pluripotent stem cells (iPSCs). ESCs were first isolated from mice [74, 75] and are derived from the inner cell mass of the blastocyst. They are pluripotent cells since they can differentiate into all somatic germ layers (mesoderm, endoderm and ectoderm) [76, 77]. ASCs are isolated from various tissues like bone marrow, adipose tissue, dental pulp and brain tissue. Their self-renewal capacity is similar to ESCs. However, their differentiation potential is more restricted and they give rise to a tissue-specific cell type[78]. More recently, the development of a new class of stem cells, iPSCs has been reported. iPSCs were first established by Takahashi and Yamada and they were obtained from genetically reprogramming adult cells into a de-differentiated state. They are characterised by over expression of four key transcription factors; Oct3/4, Sox2, c-Myc, and Klf4 which were inserted into the nuclei of mouse fibroblasts by using a retroviral vector[79]. iPSCs exhibit similar characteristics to ESCs and have attracted much interest recently as a cell source because they do not have the limitations ESCs present. They also represent a promising source of autologous pluripotent stem cells obtained from adult tissues.

1.5.1 Mesenchymal stem cells

Mesenchymal stem cells (MSCs) are a population of ASCs. They were first isolated by Friedenstein from bone marrow, but since then they have been identified in several tissues of the body such as adipose and dermis tissue, umbilical cord, pancreas and muscles. Their regenerative potential was first indicated by Cohnheim who hypothesised that MSCs can contribute to wound healing by migrating through the blood stream to sites of injuries and differentiate into functional cells[80]. MSCs are fibroblastic multipotent stromal stem cells characterised by the ability to differentiate into cells of the mesodermal lineage (Figure 1.3)[81]. According to the International Society for Cellular Therapy (ISCT), MSCs meet the following criteria: they adhere to plastic, they express the markers CD105, CD73, CD90 and they lack the expression of CD45, CD34, CD14or CD11b, CD79a or CD19, HLA-DR, and

they can differentiate into osteoblasts, adipocytes, and chondrocytes[82]. It should be noted that MSC characterisation has been updated in 2016[83]. MSCs are a potential cell source in stem cell-bases therapies due to their potent immunomodulatory properties[84] and their intrinsic ability to differentiate into multiple cell linages.

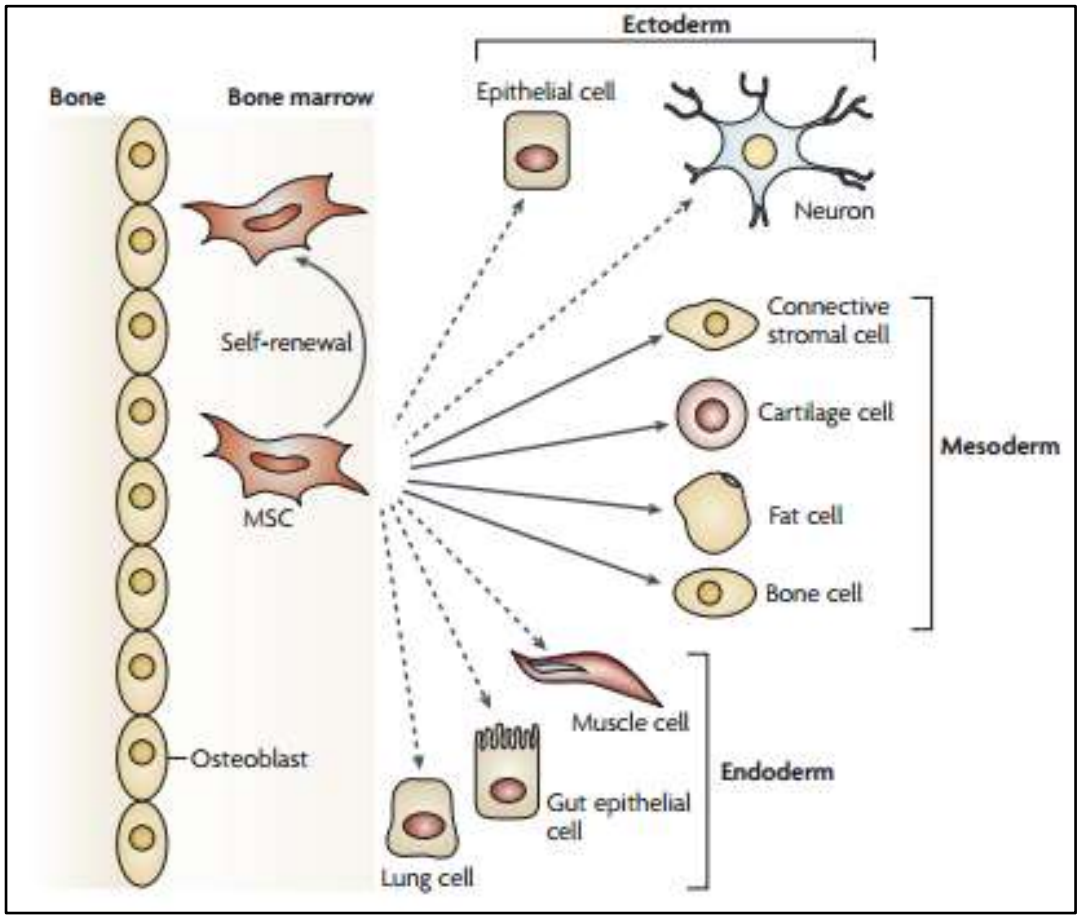

Figure 1.3. MSCs differentiation. The differentiation potential of MSCs into osteoblastic, chondrogenic, myogenic, smooth muscle, and neurogenic differentiation[85].

1.6 Stem cell differentiation

Stem cells are found in numerous mammalian tissues and throughout life they produce a variety of functionally specialized mature cells while they maintain their renewal capacity. MSC differentiation is a two-step process; however, the exact mechanism is not fully understood[86]. It requires the switch of MSCs to lineage-specific progenitors and the subsequent maturation which indicates the progression from progenitor cells to specific cell types. This switch from renewal to committed state requires the cross-talk of a complex network of

signalling pathways. It is well known that the mitogen-activated protein kinases (MAPKs) play a fundamental role in converting diverse extracellular signals into cellular responses including cell proliferation, differentiation and apoptosis. For example, MAPK-mediated integrin signalling is required for maintaining the stemness of epidermal SCs[87].

MAPKs are protein Ser/Thr kinases and typical MAPKs include at least four distinctly regulated groups: the extracellular-regulated kinases 1/2 (ERK1/2), c-Jun N-terminal kinases 1-3 (JNK1-3), p38 proteins (p38α/β/γ/δ) and ERK5 and are activated by specific MAPKs. There are additional MAPKs such as ERK3/4, ERK7/8, and nemo-like kinase (NLK); however, their enzymatic activity is incompletely understood[88]. The most studied are the ERK1/2, JNKs, and p38 isoforms MAPKs. Essentially they consist of a linear array of three kinases (Figure 1.4).

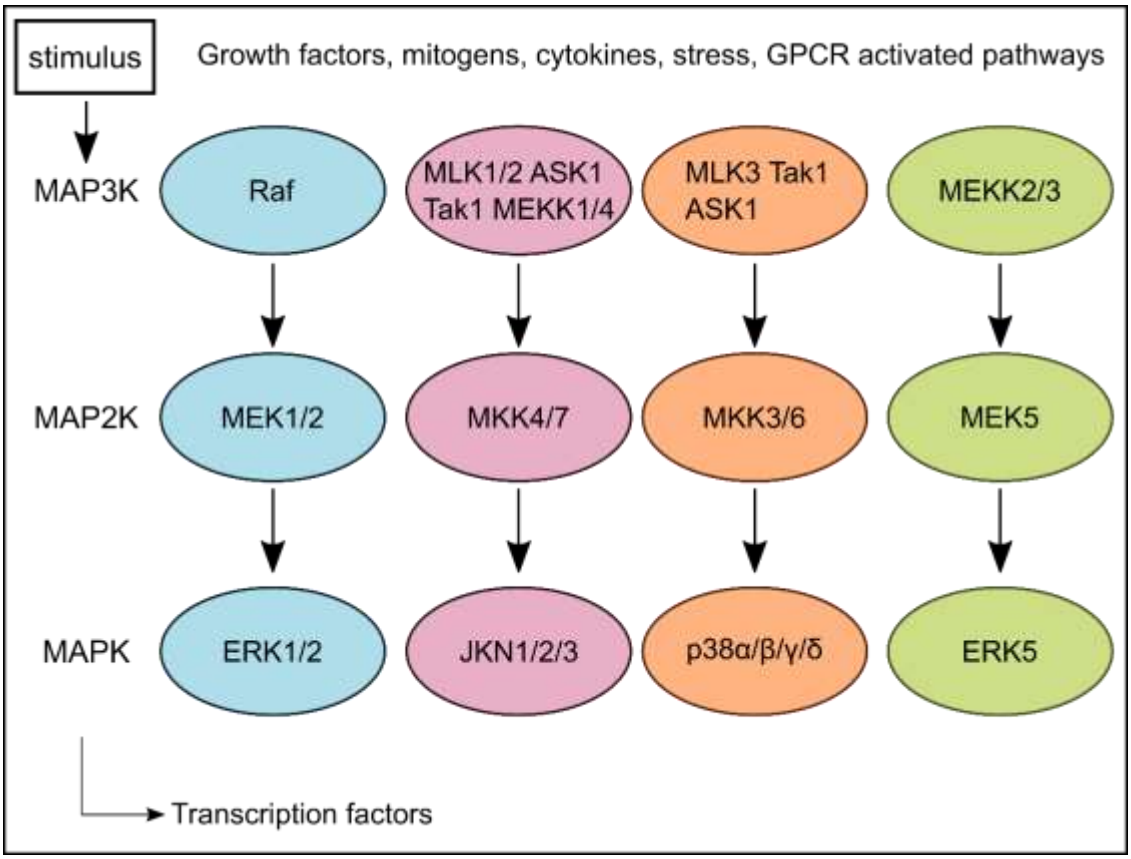

Figure 1.4. The MAPK signalling pathway. Redrawn and adapted[89].

They are activated by a wide variety of extracellular stimuli such as GFs, cytokines, mitogens, and stress. MAP3Ks are often phosphorylated as a result

of their interaction with a small (guanosine triphosphate) GTP-binding protein. This is followed by the phosphorylation of Ser/Thr residues on MAP2Ks which in turn activate MAPKs through phosphorylation on Thr and Tyr residues. MAPKs translocate directly into the nucleus or activate additional kinases in the cytoplasm[90-92].

1.6.1 ERK pathway

The ERK cascade, comprising of Raf, MEK and ERK, is the most extensively investigated. Signal transduction is initiated when an extracellular signal binds to a cell specific receptor tyrosine kinase (RTK). Upon binding, the inactive monomers dimerise promoting autophosphorylation of Tyr residues in the intracellular domain and activation[93]. The phosphorylated residues act as binding sites for proteins containing Src homology 2 (SH2) or phosphotyrosine binding (PTB) domains, including the adaptor proteins Shc and the growth factor receptor-bound protein 2 (Grbp2). Grbp2 or Shc interact with the son of sevenless (SOS) which is recruited from the cytosol to the plasma membrane. SOS contributes to the exchange of guanosine diphosphate (GDP) bound to Ras by (GTP) [94, 95]. This event positively regulates Ras which in turn activates Raf. All Raf members can activate MEK1/2 which subsequently activates ERK1/2 through phosphorylation on the threonine/tyrosine residues[96]. This event results in the phosphorylation of a wide range of targets, such as nuclear transcription factors. Cell response is determined by the activation of a specific set of factors[97].

The control of ERK pathway is subjected to both positive and negative regulatory events which ultimately affect its biological activity. For example, stimulation of PC-12 cells with nerve growth factor (NGF) or epidermal growth factor (EGF) resulted in neuronal differentiation or proliferation respectively. These results were associated with the transient MAP2K activation by EGF as opposed to the sustained activation by NGF[98]. ERK is subjected to spatial regulation as well which enhances the complexity of this pathway. The subcellular localisation of activated ERK can affect its signalling activity[99].

ERK signalling is involved in cell cycle progression[100, 101] and proliferation[102]. It has been also suggested that FAK-mediated activation of ERK promotes cell survival[103]. Another work has shown that FN stimulated ERK pathway *via* FAK/Src activation[104]. Integrin-ECM interactions have been shown to regulate the phosphorylation and activation of the ERK pathway. For example, diminished ERK activation was shown when endothelial cells were treated with integrin $\alpha_v\beta_3$ antagonists[105]. ERK signaling is also involved in the pluripotency maintenance and in regulation of stem cell differentiation. It has been reported that inhibition of ERK activity obstructed the differentiation of ESCs[106]. However, other studies showed that ERK activation may be dispensable for propagation of undifferentiated mouse ESCs[107].

1.7 Osteogenic differentiation of MSCs

MSCs are a promising cell source for cell-based TE strategies. In particular, the osteogenic capacity of MSCs *in vitro* has been the focus of a large body of research. Bone formation by osteoblasts and resorption by osteoclasts is a dynamic and highly regulated process which ultimately leads to the formation of bone tissue. Osteoclasts are derived from hematopoietic stem cell precursors (HSCs) along the myeloid differentiation lineage. Osteoblasts originate from bone marrow MSCs[108].

The progression of MSCs towards osteogenic differentiation is divided *in vitro* into three stages. The initial stage which lasts from 1 to 4 days is characterised by cell proliferation and expression of osteoblast markers. This is followed by loss of cell expansion from days 5 to 14 and the synthesis of ECM, mainly collagen type I[109]. ECM maturation follows, marked by an increase in alkaline phosphate activity (ALP). ALP is a metalloenzyme expressed in many tissues such as kidney, bone and liver and is considered an early osteoblast marker. By using antisense RNA approaches, knockout mice and small interfering RNAs (siRNAs), absence of osteoblasts was indicated as well as defects and inhibition of matrix mineralisation[110-112]. In the third stage from days 14 to 28, the level of ALP decreases and an upregulation in osteocalcin (OCN) and osteopontin (OPN) expression follows. This event leads to the deposition of calcium and phosphate. OCN is the most abundant noncollagenous bone matrix-bound protein and is produced by osteoblasts. It has been suggested

that OCN binds to the hydroxyapatite (HA) mineral component of bone [113]. However, its precise function in bone formation is not fully understood. OPN is a soluble protein and can function extracellularly through interactions with various integrins. Its increased expression in MSCs has been implicated in numerous processes including osteogenic differentiation[114]

Recently the role of integrins in osteogenic differentiation has been demonstrated in several studies. Martino *et al*. showed that the binding affinity of $\alpha_5\beta_1$ to FN fragments containing both the RGD and PHSRN sequence influenced the osteogenic differentiation of human MSCs (hMSCs)[64]. Other studies have shown that this cell receptor upregulated the expression of osteogenic markers. Increased expression of the α_5 subunit has been found in undifferentiated dental bud stem cells (DBSCs) and formed a complex with β_1 when cells differentiated[115].

1.7.1 RUNX2

RUNX2, also known as Cbfa1, is a major regulator of osteoblast differentiation. RUNX2 is a Runt-related transcription factor and contains the DNA binding domain runt. Its critical role in osteoblast differentiation and mineralisation during bone formation has been demonstrated in several studies. RUNX2 deficient mice were characterised by absence of ossification [116, 117]. Moreover, accelerated bone repair in a critical-sized defects was demonstrated when Runx2-modified MSCs were used[118], while enhanced bone accumulation was found in developing mice upon ERK-MAPK activation through changes in the RUNX2 posphorylation[119]. In addition, upregulation of RUNX2 induced MSC differentiation into immature osteoblasts while it inhibits adipogenic differentiation[120].

During osteoblast differentiation, most signalling pathways already discussed are targeted at RUNX2. Activation of MAPK resulted in increased RUNX2 phosphorylation[121], while introduction of specific mutations at RUNX2 phosphorylation sites led to inhibited MAPK activation and to reduced osteoblast-specific gene expression[122]. Similarly, ERK1/2 activation was shown to control RUNX2 activation which resulted in osteoblast differentiation[123]. FAK-mediated activation of ERK1/2 and p38 phosphorylated RUNX2 inducing

increased osteogenic differentiation of immature osteoblast-like cells[124]. RUNX2 has been also shown to upregulate the expression of osteogenic marker genes such as ALP, OCN and OPN[125]. However, downregulation of RUNX2 expression is required for differentiation into mature osteoblasts underlying its role in directing pluripotent mesenchymal cells to the osteoblast lineage[126].

1.7.2 Osteogenesis and integrins

The role of cell adhesion in guiding stem cell fate has gained significant interest. FAK has been shown to phosphorylate and activate ERK1/2 contributing to bone formation[127] or expression of RUNX2 in hMSCs[128]. Inhibition of FAK disrupted the activation of MAPK pathway causing decreased expression of osteogenic differentiation markers[129]. The integrins $\alpha_v\beta_3$ and $\alpha_5\beta_1$ have been implicated in stem cell osteogenic differentiation too; however, their role is not fully understood. *In vivo* and *in vitro* expression of β_1 and β_5 subunits in osteoblasts from human bone has been reported[130, 131]. In addition, interaction with increased specificity of $\alpha_5\beta_1$ integrin with FN fragments resulted in upregulated ALP activity and osteogenic gene expression in MSCs[64]. In line with these results, upregulated osteoblast gene expression and osteogenic differentiation of MSC was observed *in vitro* and *in vivo* with induced expression of $\alpha_5\beta_1$ integrin[132]. Improved osseointegration was also reported when titanium implants specific to $\alpha_5\beta_1$ integrin were implanted in rats[133]. Similarly, decreased levels of $\alpha_5\beta_1$ were associated with bone loss[134].

The role of $\alpha_v\beta_3$ in osteogenesis remains controversial. Blocking antibodies against $\alpha_v\beta_3$ and RGD-containing peptides had a negative impact on bone resorption[135, 136]. In addition, osteogenic differentiation of hMSCs was promoted on monolayers functionalized with an RGD peptide with high affinity with the $\alpha_v\beta_3$ integrin[137]. In contrast, decreased osteoblastic differentiation has been reported in a murine osteoblastic cell line overexpressing $\alpha_v\beta_3$[138]. Blocking $\alpha_v\beta_3$ binding also increased the ratio of ALP positive MSCs[139]. Other integrins have been implicated in bone formation as well. Administration of a peptidomimetic ligand of activated $\alpha_4\beta_1$ conjugated with a bone seeking component and ectopic expression of $\alpha_4\beta_1$ on MSCs increased MSC bone homing[140, 141]. In addition,

knocking down the α_2 and α_{11} subunits in hMSCs cultured on collagen I inhibited the deposition of mineralized matrix[142].

1.8 Bone morphogenetic proteins

Growth factors (GFs) are proteins which regulate fundamental cell functions such cell proliferation and embryonic development. GFs are secreted by cells into the ECM and bind to specific receptors on the cell surface in order to exert their biological functions in an autocrine, paracrine or endocrine way. Bone morphogenetic proteins (BMPs) belong to the TGF-β superfamily and around 20 BMP ligands have been identified. At the cellular level, BMPs regulate many processes like apoptosis, differentiation and migration[143, 144]. They are dimeric molecules and are synthesised as inactive peptide precursors. They consist of an N-terminal signal peptide, a non-conserved prodomain for folding and secretion, and a mature peptide located at the C-terminal[145]. They can be divided into four categories according to their structural homology and function: 1) BMPs -2 and -4 2) BMP -5, -6, -7, -8a, and -8b; 3) BMP -9, -10, and 4) BMP -12, -13 and -14[146]. Different members affect MSCs differentiation in a dose-dependent way. For instance, low doses of BMP-2 induced adipogenic differentiation of embryonic stem cells whereas chondrogenic and osteogenic differentiation was triggered at higher doses[147].

Name	Main function
BMP1	Induces cartilage formation.
BMP2	Plays a role in bone and cartilage formation. Also involved in osteoblast differentiation.
BMP4	Induces bone and cartilage formation. Also involved in tooth development, limp formation and fracture repair.
BMP5	Induces cartilage formation.
BMP6	Involved in the regulation of bone and cartilage formation. Also involved in the regulation of the number of HSCs.
BMP7	Induces bone and cartilage formation. Plays a role in renal and kidney development.
BMP8a	Play a role in the development of the reproductive system.
BMP8b	Involved in thermogenesis in brown adipose tissue.
BMP9	Involved in angiogenesis.
BMP10	Plays a role in maintaining cardiac growth.
BMP11	Involved in skeletal patterning during development.
BMP12	Involved in the joint and ligament formation.
BMP13	Inhibits bone formation.
BMP14	Involved bone and joint formation.

Table 1.1. Biological role of BMP members.

The osteoinductive activity of bone morphogenetic proteins 2 (BMP-2) was first characterised in 1960s[148] and since then several growth factors have been used to induce bone formation. Even though BMPs were initially identified as components which induce ectopic bone formation, some BMPs act as inhibitors of bone formation or they contribute to the maintenance of several tissues. For example, BMP-3 is a negative regulator of bone density, and BMP-13 is a strong inhibitor of bone formation[149]. BMP-4 and BMP-7 have been reported to stimulate adipogenesis[150, 151].BMP-2, BMP-4, BMP-7 and BMP-9 are the most well-known osteoinductive BMPs [152, 153]. BMP-2 and its involvement in osteogenic differentiation is the focus of a large body of research. Katagiri *et al*. demonstrated that BMP-2 inhibited myotube formation of C2C12 cells and initiated the production of osteogenic markers[154]. Another study showed that transduction of MSCs with BMP-2 enhanced osteogenesis[155]. Currently, BMP-2 has become the most powerful osteoinductive growth factor. Recombinant BMP-2 in combination with a collagen sponge is used for the treatment of open long cone fractures[156]

1.8.1 BMP/TGF-β pathway

The TGF-β superfamily contains more than 30 members, including BMPs, TGF-βs, activins, and other factors[157]. The BMP/TGF-β signalling pathway is widely involved in cell proliferation, differentiation, and apoptosis. It also has a dual role in regulating cell differentiation. For example, BMP-2 has been identified as a regulator of both osteogenic and adipogenic differentiation of MSCs and ESCs[147, 158]. Similarly, a study analysing 14 types of BMPs demonstrated that most BMPs exhibited distinct abilities to regulate expression of makers of four common lineages derived from MSCs[16].

The BMP/TGF-β pathway transmits signals into the cytoplasm *via* the activation of two types of serine/threonine kinase receptors. BMPs start signalling through the receptors BMPRI and BMPRII, which consist of a short extracellular domain, a single transmembrane domain, and an intracellular domain with serine/threonine kinase activity. There are seven BMPRIs for the TGF-β ligands, three of which bind BMPs: BMPRIA, BMPRIB, and type IA activin receptor. There are also four BMPRIIs for the TGF-β ligands, three of which interact with BMPs: BMPRIIB, ACTRIIA, and ACTIIB receptors[159]. Initially,

ligands bind with high affinity to BMPRI followed by heterodimerisation with BMPRII. This allows BMPRII to phosphorylate and activate the kinase activity of BMPRI[160]. The way the heteromeric complex is formed may vary and depends on the type of BMP. BMPRI organises into a receptor complex with BMPRII or recruits BMPRII. For example, either BMP2 or BMP4 preferentially interacts with BMPRI receptors and recruit the BMPRII receptors[161]. However, BMP6 and BMP7 bind BMPRII receptors and recruit type I receptors[162]. Depending on the oligomerisation pattern for signal transduction, a different pathways might be activated[163].The signal transduction is mediated *via* both the canonical mothers against decapentaplegic homolog (Smad)-dependent pathways and non-canonical Smad-independent signaling pathways (Figure 1.5).

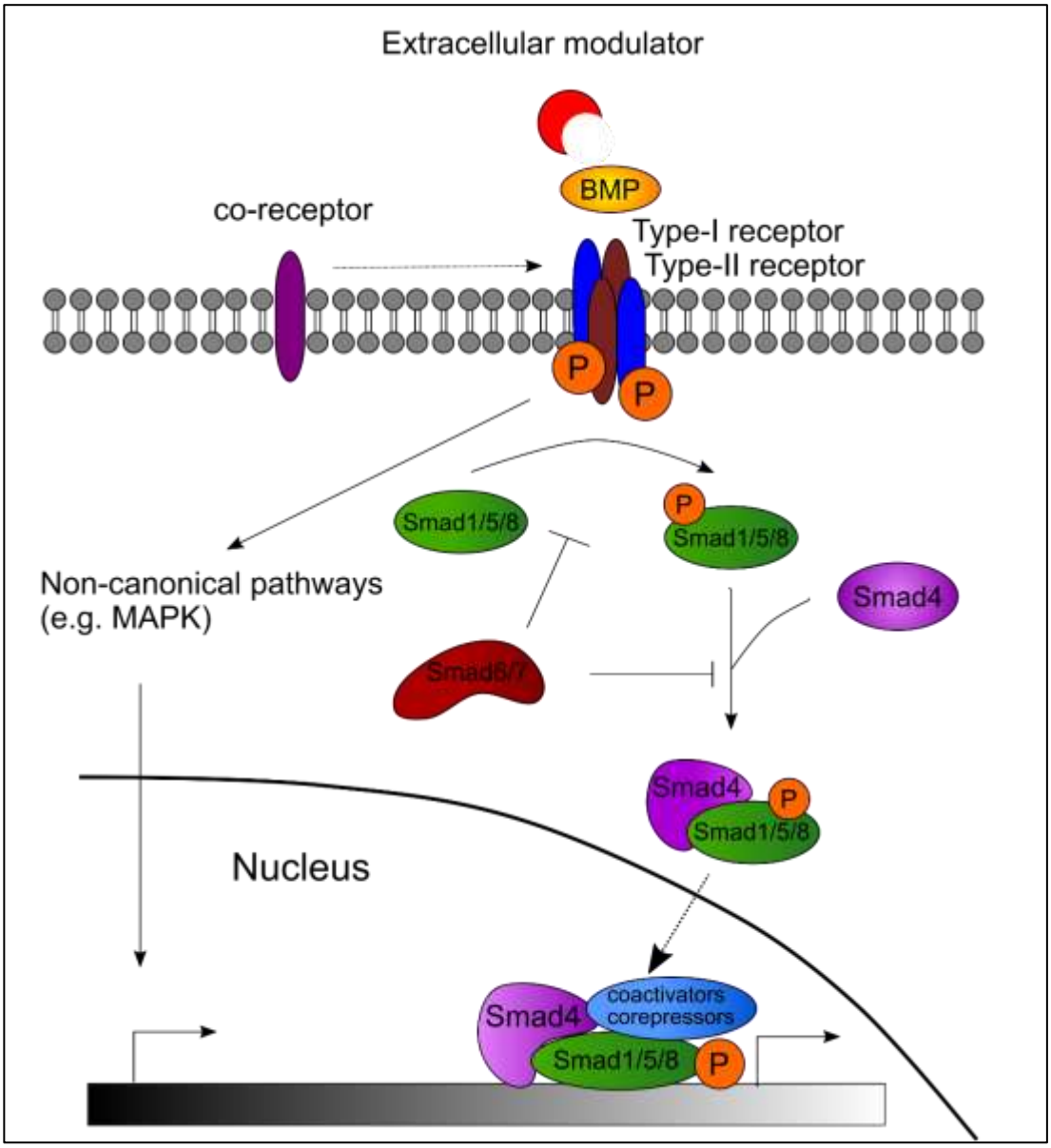

Figure 1.5. TGF-β canonical and non-canonical signalling pathway. Redrawn and adapted[157].

1.8.2 Canonical pathway

The canonical pathway is triggered when BMP/TGF-βs bind to the corresponding surface receptor kinase which is activated through oligomerisaition and phosphorylation. Signals are transmitted *via* the human Smad proteins. Smads are intracellular proteins and they generally consist of three distinct domains: an N-terminal mad-homology 1 (MH1) domain that carries nuclear localization signal and a DNA-binding region, a C-terminal MH2 domain that binds to BMPRI to mediate Smad-dependent transcriptional activity, and a proline-rich linker domain that separates the MH1 and MH2 domains[164, 165]. Activation of the type I receptor results in the phosphorylation

of the receptor-regulated cytoplasmic Smads proteins (R-Smad) at the C-terminal serine residues. R-Smads regulate TGF-β signalling in a pathway-specific manner. SMAD 2 and 3 are phosphorylated by TGF-β whereas Smad 1, 5 and 8 are usually activated by BMPs[166, 167]. This event is followed by disassociation of phosphorylated R-Smad from the BMPRs and it subsequently interacts with the co-mediator Smad (C-Smad), Smad4 forming a complex. The complex translocates to the nucleus where it binds to specific promoters and regulates the transcription of target gene expression[168]. Smads can control cell response in various ways. For example, FN coated surfaces immobilised with BMP-2 triggered the phosphorylation of Smad1/5 resulting in increased cell migration[169].

1.8.3 Noncanonical pathway

Besides Smad-mediated transcription, TFG-β/BMP-2 pathway activates other non-canonical signalling pathways. The non-canonical pathway includes mainly molecules which belong to MAPK family; ERK, JNK and p38 MAPK kinase pathways[170]. For example, rapid activation of ERK through TFG-β was reported in epithelial[171] and in breast cancer cells[172]. Noncanonical pathways have been shown to transmit signals in a Smad-dependent way[173]. However, other studies suggest a Smad-independent signalling as well. For example, Smad-independent JNK activation has been documented[174].

BMP/TGF-β pathway is involved in RUNX2 regulation. More specifically, BMP-2 has been shown to upregulate RUNX2 *via* Smads 1,3, and 5[175, 176]. By introducing mutations on RUNX2, it was found that the activated SMAD complex interacts with the C-terminal of RUNX2 inducing the expression of osteogenic genes[177]. Similar results were found in other studies suggesting that the formation of RUNX2-SMAD interactions are essential in signal transduction that modulate osteogenic differentiation[175, 178].

1.9 Biomaterials

TE attempts to mimic the physical, chemical and topographical properties of the ECM in order to direct a desired cell response in a controlled environment. A myriad of biomaterials has been used *in vivo* for biomedical applications.

Biomaterials are designed not only to interact with the surrounding environment but also to provide informative signals and allow cells to interact with them, thus guiding their fate[179]. Despite their diversity, they have to fulfil certain requirements. Biomaterials are designed to be biocompatible and biodegradable and their properties are specific to the tissue of interest[180].

There is a wide range of biomaterials depending on the applications they are used for and the cell type. Broadly, they can be classified as synthetic (such as poly(L-lactic acid (PLLA), poly(glycolic acid) (PGA), poly(caprolactone) (PCL)), and natural (such as collagen, gelatin, fibrin, chitosan)[181, 182]. They can be also classified based on their structure and function, for example they can be porous scaffolds or they might be used for drug delivery[183, 184]. Natural polymers were the first biodegradable materials to be used in clinical applications due to their improved interactions with cells. Common synthetic polymers present advantages too due to their manufacturing process and their reproducibility. However, they might lack the chemical or topographical cues which cells recognise and respond to.

Even though the ECM is a highly complex structure, several strategies, such as surface modification, are implemented to recapitulate its characteristics. For example, the RGD and GFOGER (Gly-Phe-Hyp-Gly-Glu-Arg) adhesion motif have been used extensively to coat biomaterial surfaces and enhance their bioactivity[185]. In such systems, the ligand type, its concentration and spatial distribution are highly defined and can control cell response. For example, varying the spacing of the RGD ligand affects integrin clustering and cell spreading[186] as well as lineage commitment of MSCs[187].

1.9.1 Surface properties

In order to further investigate the clinical potential of stem cells, a plethora of biomaterials has been used. Based on their composition and structure, biomaterials can provide physical and chemical signals to recreate a physiological niche. It is well established that manipulation of the topography, chemistry, stiffness and dimensionality of the substrate can instruct stem cell fate decisions. Using microfabrication technologies, surfaces with various topographies in terms of size, type and distribution, have been produced to

induce specific cell responses *in vitro*. It is well documented that micro- and nanoscale feature can affect cell adhesion and differentiation. For example, substrates with micrometre-scale islands of ECM with defined shape and size induced cells to selectively adhere on these regions and adopt their geometry[188]. Moreover, the use of nanopits at a specific arrangement was shown to maintain multipotency of MSC[189] or to induce an increase in the expression of osteogenic markers in MSCs indicating osteogenic differentiation[190, 191]. In another study, MSC differentiation towards specific lineages depended on the size of groove/ridge structures[192]. It has been also demonstrated that MSC differentiation can be influenced by the mechanical properties of the underlying matrix. Engler *et al*. showed that hMSCs undergo osteogenic differentiation when plated onto stiff matrices whereas softer matrices generated neuronal and myogenic differentiation[193]. Similarly, MSC commitment towards chondrogenic or adipogenic differentiation could be controlled by varying the stiffness of polymer surfaces without exogenous growth factor[194].

Taking into consideration that stem cells reside in a 3D environment *in vivo*, studies have explored their behaviour in a more physiological-like context. For example, MSCs were embedded into synthetic 3D matrices in order to characterise their osteogenic commitment in relation to various stiffness. Such variations however were not followed by changes in cell morphology as observed in 2D studies[195]. Chemical modification of biomaterials has been investigated as well. Self-assembled monolayers (SAMs) with well-defined chemistries changed the structure and activity of adsorbed FN[196] and induced osteogenic differentiation of immature osteoblast-like cells[197]. In addition, control of MSCs towards adipogenic and osteogenic differentiation has been achieved by using small-molecule chemical groups tethered to polyethylene glycol (PEG) hydrogels[198].

1.9.2 Protein adsorption

The first event that rapidly occurs upon contact of a biomaterial with biological fluids *in vivo* or *in vitro* is protein adsorption on the surface. Initial protein adsorption occurs spotnaneously[199] and is driven by short- and long-range forces including electrostatic, hydrophobic, hydrogen bonding and van der

Waals interactions[200]. The composition of the adsorbed protein layer changes over time due to the competitive displacement of faster diffusing molecules by proteins with higher affinity proteins for the surface[201].

For most cell types, adhesion to the ECM is essential for survival[202] and cell morphology[203, 204]. Therefore, the ability of biomaterials to adsorb proteins determines whether they can support cell adhesion and spread. For example, FN coatings of titanium disks and glass supported the growth and spread of osteoblasts[205] while it enhanced bone-derived cell adhesion on tissue culture polystyrene[206]. In addition, the structure and distribution of the adsorbed protein can facilitate the availability of integrin binding sites which affects protein activity[207] and cell attachment, differentiation and migration[208-210]. Cell processes depend on adsorbed proteins as well. The expression of osteogenic markers in MSCs has been found to be dependent on the density of adsorbed FN on PCL[211]. Beyond initial attachment, cell-biomaterials interactions are dynamic. As cells spread, forces are generated in the actin cytoskeleton and are transmitted to the ECM. On biomaterial surfaces, these forces might be sufficient to reorganise and remove adsorbed proteins that cells are anchored to[212].

The characteristics of the substrate (wettability, surface energy, charge, topography), the protein (affinity, size, charge, concentration) and the environment (solvent, pH, temperature) influence protein adsorption on the biomaterial interface[200, 213-217]. For example, FN and VN were reported to adsorbed at a higher rate on hydroxyapatite, compared to titanium and stainless steel, resulting in an increase in osteoblast attachment[218]. Generally, hydrophobic surfaces tend to adsorb more protein than hydrophilic surfaces[219]. However, protein adsorption also depends on the surface charge. Higher plasma protein adsorption was observed with higher surface charge density of nanoparticles[214].

1.9.3 Biomaterials and growth factors

ECM controls cell behaviour through the ability to locally bind and release soluble macromolecules, such as GFs which have a strong effect in regulating cell responses. GFs display some limitations due to their low protein stability,

short circulating half-life, rapid rate of cellular internalization, and localized tissue activity as a mechanism for spatial and temporal control[220]. However, due to their potential as therapeutic tools, a lot of effort has been dedicated to design biomaterials that bind and release GFs using ECM components. The focus of such approaches is to locally deliver controlled and sustained low doses of GF[220, 221]. GF delivery can be designed by both encapsulation and surface immobilisation approaches[222, 223]. Another approach is to functionalise the material surface with specific GF binding sites. For example, biomaterials have been modified with heparin which contain multiple GF binding domains[224].

1.9.3.1 Bone tissue engineering

During bone formation, BMPs are involved in the recruitment and differentiation of stem cells into bone tissue. Bone TE (BTE) combines the use of osteoinductive scaffolds, osteogenic cells which either initiate bone formation or induce resident cells to do so and osteoinductive GFs to trigger bone formation. In a GF-based treatment, the balance between release and retention of such GFs is critical as they can trigger adverse clinical effects such as inflammation[225, 226]. A common, less invasive, strategy is to use injectable GFs. However, several days of stimulation and high doses are required due to BMP short half-life and rapid clearance. This can cause side effects such as ectopic ossification[220].

Incorporation of GFs in synthetic materials include covalent[227] or non-covalent[228] binding. For example, physical or chemical entrapment in biomaterials provides a way to present GFs in a controlled spatiotemporal manner[229]. In this approach, release of GFs can be achieved through diffusion, scaffold degradation or through the affinity of biomolecules to the surface[230]. Different types of ECM proteins have also the potential to be used in TBE. Such proteins or peptides do not only induce osteogenesis, but they are also involved in cell adhesion and proliferation. For example, enhanced osteogenic expression in MSC was observed when RGD was immobilised on titanium oxide nanotubes[231]. Although the RGD motif can promote cell adhesion through $\alpha_5\beta_1$, the PHSRN is required for stable binding. In line with this, osteogenic differentiation of osteoblasts was increased in alginates which combined both RGD and PHSRN sequences[232].

1.9.4 Project aims

Stem cells reside *in vivo* in the niche where they receive and integrate multiple cues which ultimately regulate cell behaviour. However, cells lose the expression of their markers outside of their niche compromising their differentiation potential[233]. Engineering biomaterials with defined properties is essential in recapitulating to a degree the physiological properties of the cell microenvironment and direct stem cell fate outside of their niche. A common approach for surface functionalization is coating with adhesive peptides such as the RGD motif[186, 187, 234]. Despite the versatility of such surfaces, they display limited biological activity. For example, they have a lower adhesion potential than full-length ECM proteins due to lack of synergistic domains. The use of ECM molecules provides an alternative way to mimic the complexity of cell-ECM interactions. Apart from integrin binding sites, they also contain sites for protein-protein interactions and GF binding.

Among the ECM proteins, FN is an interesting protein to study. It undergoes structural changes and can be stretched by several folds *via* cell-generated traction forces leading to the unfolding of cryptic binding sites[235, 236]. Ellipsometric measurements showed a more extended FN organization on hydrophobic than on hydrophilic titanium alloy[237]. Atomic force microscopy has also demonstrated a more rigid and elongated FN conformation on hydrophobic surfaces[238, 239]. Roughness and nanoscale surface topography have been shown to influence FN adsorption too[240, 241].

Past studies have investigated how the polymer surfaces poly(ethyl acrylate), PEA and poly(methyl acrylate), PMA affect FN conformation. PEA differs from PMA in methyl group in the side chain. Although these polymers are chemically similar, two distinct conformation of FN are observed upon adsorption. FN adopts a network-like conformation on PEA. In contrast, globular aggregates are formed on PMA (Figure 1.6). The differential distribution of FN leads to changes in its biological activity for example in the availability of the integrin binding domain (FNIII9–10)[242], the PHSRN domain[243] and the heparin II binding domain (FNIII12-14)[244].

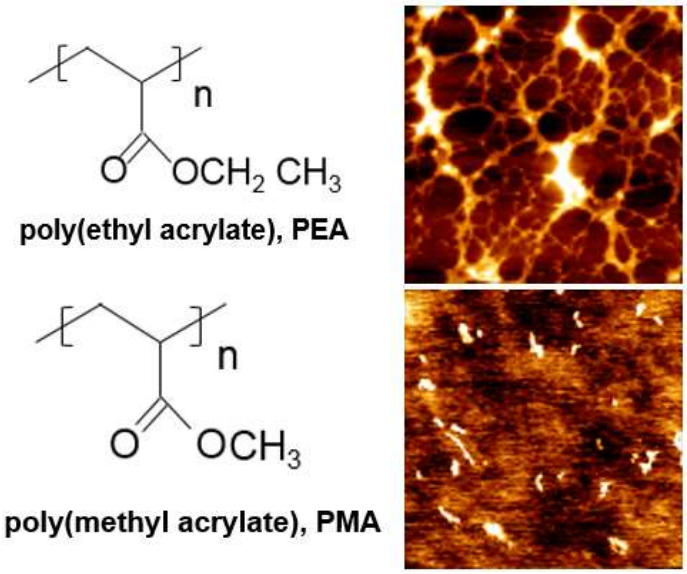

Figure 1.6. Chemical structure of PEA and PMA. AFM height images showing FN distribution on PEA and PMA.

The main objectives of this thesis is:

- To explore how a differential conformation of FN can be achieved by using a series of copolymers with specific ratios of EA/MA (100/0, 70/30, 50/50, 30/70, 0/100).
- To assess whether such conformation changes affect the availability of binding domains and BMP-2 binding.
- To use this system in order to study hMSCs fate including adhesion, morphology and osteogenic differentiation.
- To develop a method in order to isolate focal adhesions on PEA and PMA and to further analyse their protein composition.
- To characterise the cell migratory behaviour on FN-coated PEA and PMA.

2. Surface characterisation

2.1 Introduction

This chapter describes how the degree of FN fibrillogenesis can be modulated by the series of copolymers. Fluorescence microscopy and FRET spectroscopy showed that FN structure changes from a compact form when initially bound to cells to an extended conformation. Distinct degrees of FN extension were also observed during this process[245]. Time-lapse AFM with fluorescence microscopy demonstrated a step-like pattern of early FN extension which was divided into three stages depending on the fibril length[246]. In addition, FN conformation has been shown to affect growth factor binding[244].

We seek to understand how the EA/MA ratio impacts FN organisation and whether intermediate degrees of FN fibrillogenesis are obtained. We also explore whether such conformation changes affect the exposure of important binding domains of FN. To do so, surfaces were characterised in terms of wettability as well as FN adsorption. AFM was used to investigate FN conformation and domain availability was documented by carrying out antibody-based methods. As part of surface characterisation, the BMP-2 adsorption on the FN-coated copolymers was investigated too.

2.2 Materials and methods

2.2.1 Materials

List of reagents	
Toluene……	Alfa Aesar
Ethyl acrylate……..	Sigma-Aldrich
Methyl acrylate……	Sigma-Aldrich
Benzoin……...	Sigma
Absolute ethanol…….	VWR Chemical
Dulbecco's phosphate buffered saline (DPBS)…….	Life Technologies
Formaldehyde……..	Fisher Scientific
Tween 20®…….	Sigma
Bovine serum albumin (BSA)…….....	Roche/Sigma
Human plasma fibronectin……	Sigma-Aldrich
Mouse monoclonal HFN7.1 antibody……..	DSHB
Mouse monoclonal P5F3 antibody……..	Santa Cruz Biotechnology
Mouse monoclonal mAb1937 antibody……..	Merck-Millipore
Horseradish peroxidase (HRP) anti-mouse antibody……...	Invitrogen
Substrate solution…….....	R&D Systems
Stop solution……...	R&D Systems
Odyssey blocking solution……	LI-COR®
IRDye® 800CW anti-mouse antibody…….	LI-COR®
Micro BCA™ protein assay kit…….	ThermoFisher Scientific
Human BMP-2 produced in CHO……	R&D Systems
Human BMP-2 DuoSet ELISA…….	R&D Systems
Anti-BMP-2/BMP-4 antibody……	Santa Cruz Biotechnology
Gold particle–conjugated anti-rabbit antibody…….....	Aurion

2.2.2 Samples preparation

PEA, PMA bulk polymers as well as bulk copolymers (70%EA/30%MA, 50%EA/50%MA, 30%EA/70%PMA) were synthesised by radical polymerisation of ethyl acrylate and methyl acrylate initiated by benzoin as the photoinitiator at 1 wt%. Polymer solutions were prepared by dissolving using toluene with 4% w/v PEA, 4.5% w/v EA70/MA30, 5% w/v EA50/MA50, 5.5% w/v EA30/MA70 and 6% w/v PMA. Glass coverslips (12 mm diameter) were sonicated in ethanol for 30 min. Next, they were rinsed with ethanol and dried at 60 ^{o}C. Solutions (100 µl) were deposited onto the glass coverslips and were spin

coated at a velocity of 3000 rpm with an acceleration of 3000 rpm/sec for 30 sec. Samples were dried at 60^{o}C in vacuum for 2 h.

2.2.3 Protein coating

Human plasma FN solutions were prepared in Dulbecco's phosphate buffered saline (DPBS) at 20 µg/ml. Unless otherwise stated, samples were coated with FN solutions for 1h. For BMP-2 coating, FN-coated surfaces as well as samples without adsorbed FN were incubated with 1% w/v BSA/PBS for 30 minutes. Next, samples were incubated with BMP-2 for 1 h at 25 ng/mL or 100 ng/mL in DPBS. Coating at 25 ng/mL was carried out in ELISA for the quantification of BMP-2 adsorption and for characterising ALP expression. Coating at 100 ng/mL was carried out to characterise RUNX2 and OCN expression.

2.2.4 Water contact angle

Water contact angle (WCA, θ) measurements on the surfaces were carried out before and after FN adsorption. Static contact angle (SCA), advancing contact angle (ACA) and receding contact angle (RCA) were measured (Figure 2.1).

Figure 2.1. Representative pictures of SCA, ACA and RCA on FN-coated PEA.

For the SCA, a 3 µl water drop was deposited onto the surface and images were recorded for 30 sec at 20 frames/sec while measuring the angle of the drop with the polymer surface. SCA was then defined by fitting Young-Laplace equation around the droplet. The ACA was determined when the SCA expanded in volume by adding 10 µl of water at a rate of 0.1 µl/sec resulting in increase of the baseline. Images were recorded for 80 sec at 5 frames/sec. RCA was determined by removing 13 µl of water at a rate of 0.1 µl/sec resulting in the contraction of the water drop until all water was removed. Images were

recorded for 130 sec at 5 frames/sec. RCA was defined at the point at which the baseline decreased. Measurements were carried out using a Theta optical tensiometer (Biolin Scientific). Three samples were used and three different measurements were recorded on each sample. High contrast images of water droplets were recorded and the OneAttension software was used to determine droplet shape.

2.2.5 Atomic force microscopy

2.2.5.1 Tapping mode

Samples were coated with FN at 20 μg/ml for 10 minutes. They were washed twice with PBS and then with milliQ water and they were dried with N_2 flow. To visualise FN distribution and conformation, several areas on the samples were scanned. Atomic force microscopy (AFM; Nanowizard 3 from JPK) was conducted in tapping mode using cantilevers with force constant of 3 N/m, a resonance frequency of 75 kHz and a pyramidal tip with an 8 nm radius (MPP-21220, Bruker). To quantitatively assess FN distribution, images were exported to Fiji and the skeletonize plugin was applied. Next, the fractal dimension (F_D) was measured using the FracLac plugin.

2.2.5.2 Force spectroscopy

Samples were incubated with milliQ water overnight. For force spectroscopy measurements, 5 μm silica beads were attached on a tipless silicon cantilever with a force constant of about 3 N/m. To do so, a solution containing the beads was mixed with ethanol (1:50). Next, the solution was sonicated for 10 min and it was deposited onto a glass slide. Beads were spread using N_2 flow. Epoxy glue was deposited onto the other side of the slide. To embed the beads, the cantilever was moved manually until its end was dipped into the glue. The cantilever was then lifted and a bead was attached to its glued end.

For the force spectroscopy measurements, the cantilever deflection was calibrated. The first step involved converting a certain measured change in photodetector voltage to the distance in nanometres (nm) the cantilever deflects. This conversion factor is usually called the sensitivity. To do so, a force-distance curve on a clean glass slide was performed. The repulsive

contact region of the curve was linear and it was used to determine the sensitivity. The spring constant was then measured using the thermal noise method and used to convert the cantilever deflection into a force using Hooke's law. Force spectroscopy measurements were then carried out using a set-point of 100 nN, a zeta length of 10 µm, and a velocity of 2.5 µm/s at room temperature. Force mapping was carried out. Four areas (50 µm x 50 µm) were chosen on each surface. In every map, 25 force curves were generated. Results were analyzed using the JPK processing software and force curves were fitted with a Hertz model at 50 nm indentation.

2.2.6 Micro-bicinchoninic acid protein quantification

BCA assay was performed for the colorimetric detection and quantification of the protein. Samples were coated with FN at 20 µg/ml for 1 h. Next, 150 µl of supernatant was collected and it was loaded in a 96-well plate. A set of protein standards was prepared by using albumin (diluted in PBS) starting at 40 µg/mL and a 4-point serial dilution in duplicate was prepared including a blank standard (PBS). FN solution used for the coating was used as internal standard. Standards together with the FN solution used for coating were also loaded in the 96-well plate. In addition, the working reagent was prepared by mixing 25 parts of reagent A, 24 parts of reagent B and 1 part of reagent C. Next, BCA working reagent was added and the plate was incubated at 37°C for 2 hours. BCA is used as the detection reagent for Cu^{+1} which is formed when Cu^{+2} is reduced by protein in an alkaline environment. After that, the absorbance was measured at 562 nm on a plate reader (Tecan NanoQuant Infinite M200 Pro).

To analyse the results, the average of the adsorption reading (at 562 nm) of the blank standard was subtracted from the readings (at 562 nm) of all the other individual standards and unknown sample replicates. Next, a standard curve was prepared by plotting the average of each albumin standard (after correction) against its concentration in µg/ml. The best-fit curve generated by regression analysis was used to determine the protein concentration of each unknown sample and of the FN solution used for substrate coating. To quantify the amount of FN remained on the surface, the amount of protein of the

unknown samples was subtracted from the amount of FN contained in the initial coating solution.

2.2.7 Enzyme-linked immunosorbent assay

FN coated samples were incubated with 1% v/v BSA/PBS for 30 minutes. Primary antibody was prepared in 1% v/v BSA/PBS with HFN7.1. Samples were incubated for 1 hour followed by washes with 0.5% v/v Tween20/PBS in agitation. Anti-mouse HRP conjugated secondary antibody was prepared in 1% v/v BSA/PBS. Samples were incubated for 1 hour. After the washing steps, samples were transferred to a new plate and incubated with substrate in dark. After 20 minutes, a stop solution was added to the wells. The solution was transferred to a 96 well-plate and the absorbance was measured at 450 nm and 540 nm on a plate reader (Tecan NanoQuant Infinite M200 Pro). For results analysis, the 540-nm readings were subtracted from the respective 450-nm readings to correct for optical imperfections; next, the average of each sample was plotted.

2.2.8 Quantification of BMP-2 adsorption

A 96-well plate was incubated with capture antibody specific for BMP-2 overnight. Next, antibody solution was removed and the wells were washed with wash buffer (0.05% Tween20/PBS) three times. The plate was blocked with blocking buffer (1% v/v reagent diluent/milliQ water) for 30 minutes coated with BMP2. After 1 h, the supernatant was collected and transferred in low-protein binding tubes. Samples were washed with PBS which was also collected in the tubes. BMP2 standards were prepared in PBS starting at 48 µg/mL and followed by an 11-point serial dilution. A blank standard (PBS) was included too. Apart for the external standards, BMP2 solution used for coating and 1% v/v BMP-2 solution (in PBS) were used as internal standards.

The collected supernatants (100 µl) and standards were added to a 96-well plate. After 2 hours, solution was removed and the wells were washed. Detection antibody was prepared in reagent diluent and 100 µl were added to the wells. After 2 hours, solution was removed followed by washing steps. Streptavidin-HRP was added at a working dilution (in reagent diluent) and the plate was incubated for 20 minutes in dark. Washing steps were repeated and

the plate was incubated with substrate solution for 20 minutes in dark. Stop solution was added in the wells and absorbance was measured at 450 nm and 540 nm on a plate reader.

For analysis, the 540-nm readings were subtracted from the 450-nm readings to correct for the optical imperfections. Then, the BMP-2 concentration (in ng/ml) of each standard and the corresponding absorbance value was logged and a standard-curve was generated. Next, the BMP-2 concentration (in ng/ml) was plotted against the absorbance. The best-fit curve generated by regression analysis was used to determine the concentration of each unknown sample and of the internal standards (BMP-2 solution used for coating). Next, the amount of BMP-2 in the supernatant was estimated. The amount of BMP-2 adsorbed on the surfaces was quantified by subtracting the amount of BMP-2 in supernatant from the amount of BMP-2 in the solution used for coating.

2.2.9 In-cell Western™ assay

FN-coated samples were incubated with blocking solution (Odyssey blocking buffer) for 2 h. Next, primary antibodies were prepared in blocking solution containing rabbit polyclonal anti-FN (1:400), mouse mAb1937 (1:2000) and mouse P5F3 (1:300) antibodies. Samples were incubated with antibody solutions and after 1 h they were washed (0.1% v/v Tween20/PBS) five times for 5 min with gentle shaking. Secondary antibodies were prepared in blocking solution containing infrared labelled anti-rabbit or anti-mouse IRDye® 800CW antibody (1:800) for 1 h in dark. Samples were washed again and transferred to a new plate. Next, samples were scanned with detection in 800 nm channel using an Odyssey® system. To analyse the results, the average readings of each sample was plotted.

2.2.10 Immunogold staining

Samples were coated with FN at 20 μg/ml for 10 min. After they were washed twice with PBS, they were coated with BMP-2 at 100 ng/ml for 1 h. Next, samples were fixed (4% formaldehyde/PBS) for 30 min. Another set of fixed FN-coated samples were included too. All samples were washed three times with PBS. Next, a primary antibody solution was prepared containing anti–rabbit BMP-2/BMP-4 antibody in PBS (1:50). Samples were incubated with

antibody solution for 1 h. Next, samples were washed (0.5% v/v Tween 20/PBS) three times for 1 min. Secondary antibody was prepared containing 15-nm gold particle–conjugated anti-rabbit immunoglobulin G (1:20). Samples were incubated with antibody solution for 1 h. Next, samples were washed and fixed. Finally, samples were washed with milliQ water and were dried with N_2 flow.

2.2.11 Statistical analysis

Data are represented as mean ± standard deviation (SD) and were analysed using GraphPad Prism 5. Statistically significant differences were assessed by t-test using a Tukey's post-test. A two-way ANOVA using a Bonferroni post hoc test was applied for multiple comparisons at a 0.05 significance level, with *$p < 0.05$, **$p < 0.01$, ***$p < 0.0001$.

2.3 Results

2.3.1 Water Contact Angle

WCA measurements were carried out to characterise the wettability of the surfaces. SCA as well as ACA and RCA were characterised before and after FN adsorption (Table 2.1, Table 2.2).

Substrate	SCA	ACA	RCA	Hysteresis
PEA100	67.58 ± 5.18	105.70 ± 1.04	36.45 ± 1.32	69.25 ± 1.22
PEA70	64.91 ± 2.11	102.45 ± 1.72	32.37 ± 5.3	70.07 ± 6.63
PEA50	70.77 ± 4.99	96.76 ± 2.04	31.05 ± 1.17	65.64 ± 2.98
PEA30	67.76 ± 1.49	96.76 ± 3.32	38.85 ± 11.83	57.91 ± 11.05
PMA100	68.87 ± 5.25	92.26 ± 4.72	30.61 ± 5.71	61.66 ± 6.09

Table 2.1. WCA measurements. Measurements were carried out prior FN coating. Error values are standard deviation (n=3 per sample, 3 samples tested).

Substrate	SCA	ACA	RCA	Hysteresis
PEA100	66.67 ± 1.71	96.26 ± 5.67	8.62 ± 0.67	87.64 ± 5.81
PEA70	66.01 ± 1.87	97.00 ± 2.43	13.96 ± 2.82	83.03 ± 3.38
PEA50	69.11 ± 7.97	79.08 ± 10.45	18.51 ± 2.35	60.57 ± 9.29
PEA30	60.31 ± 0.74	71.40 ± 3.49	14.22 ± 1.96	57.17 ± 3.95
PMA100	57.65 ± 1.84	70.02 ± 4.49	11.99 ± 6.38	58.03 ± 7.98

Table 2.2. WCA measurements. Measurements were carried out after FN coating. Error values are standard deviation. (n=3 per sample, 3 samples tested).

No differences were found in the SCA (from ~ 67^{o} on PEA to ~ 68^{o} on PMA) of the surfaces before FN coating indicating similar wettability (Figure 2.2). SCA of the surfaces ranged from ~65^{o} to ~70^{o} indicating that surfaces are hydrophobic. Contrary, SCA decreased linearly with decreased EA units (from ~66^{o} on PEA to ~57^{o} on PMA) after FN coating. In particular, SCA was significantly higher on FN-coated PEA and PEA70 than on FN-coated PEA30 and PMA. In addition, SCA on PEA30 and PMA decreased when samples were coated with FN.

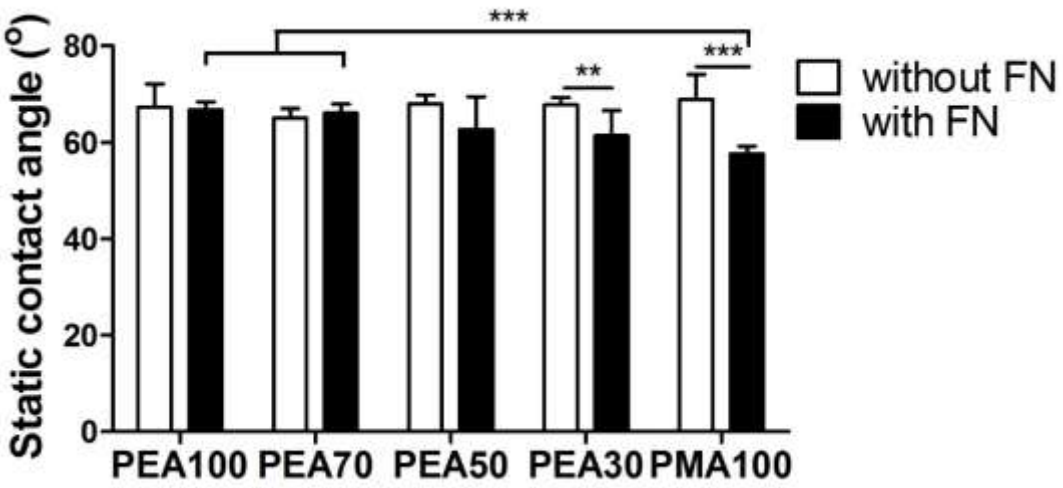

Figure 2.2. Static contact angle. Graphs represent the SCA of the surfaces before and after FN coating.

Surface wettability affects phenomena such as protein adsorption[247], and is indicative of surface properties, such as chemistry[248]. However, the measurement of the SCS alone is not sufficient to fully assess surface wettability. Characterising the dynamic angles (ACA and RCA) were required too. ACA decreased with decreased concentration of EA (Figure 2.3).

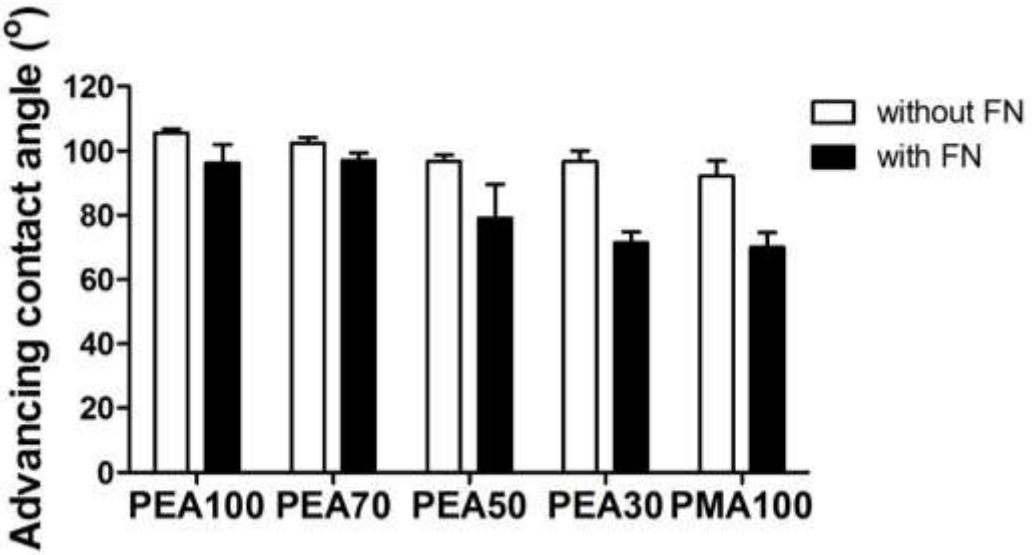

Figure 2.3. Advancing contact angle. Graphs represent the ACA of the surfaces before and after FN coating.

Substrate	P value
Without FN	
PEA100 vs. PEA50……..	**
PEA100 vs. PEA30……	***
PEA100 vs. PMA100…….	***
PEA70 vs. PEA50 …….	*
PEA70 vs. PEA30 …….	*
PMA70 vs. PMA100……..	***
With FN	
PEA100 vs. PEA50……	***
PEA100 vs. PEA30……	***
PEA100 vs. PMA100 …….....	***
PEA70 vs. PEA30 (with FN) ……	***
PMA70 vs. PMA100 …….....	***
PEA50 vs. PEA30……..	**
PEA50 vs. PMA100……..	**
Without FN vs. with FN	
PEA100……..	**
PEA50…….	***
PEA30…….	***
PMA100……..	***

Table 2.3. List of statistically differences for ACAs. P values represent the degree of significance. Stars are **P<0.1 and ***P<0.01. (n=3 per sample, 3 samples tested).

In particular, ACA was higher on PEA100 and PEA70 than on PEA50, PEA30 and PMA. ACA followed a similar trend when samples were coated FN. However, the decrease was more pronounced with decreased ratio of EA which is indicated by the lower ACA on the FN-coated PEA50, PEA30 and PMA (Table 2.3).

RCA was lower on all samples after FN adsorption compared to samples prior coating suggesting that the protein coated surfaces become more hydrophilic (Figure 2.4, Table 2.4).

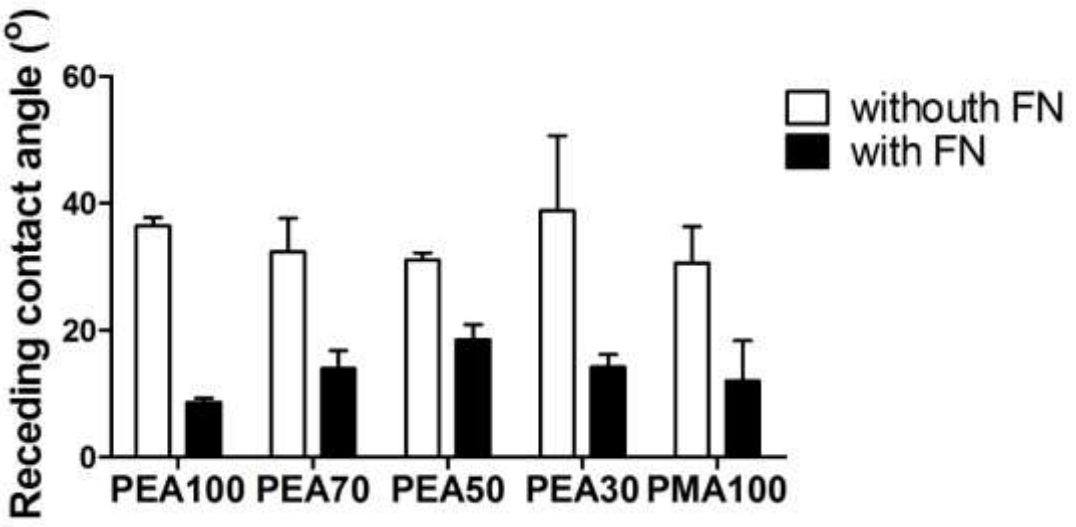

Figure 2.4. Receding contact angle. Graphs represent the RCA of the surfaces before and after FN coating.

Substrate	P value
Without FN	
PEA70 vs. PEA30……..	*
PEA50 vs. PEA30……..	*
With FN	
PEA100 vs. PEA50……...	**
PEA30 vs. PMA100 ……..	**
Without FN vs. with FN	
PEA100 ……...	***
PEA70 …….....	***
PEA50……..	***
PEA30 …….	***
PMA100……	***

Table 2.4. A list of significant differences for ACAs. P values represent the degree of significance. Stars are *P<0.5 **P<0.1 and ***P<0.01. (n=3 per sample, 3 samples tested).

Hysteresis was estimated too and represents the difference between ACA and RCA. Hysteresis was similar on samples prior FN coating. After FN coating, it decreased significantly with decreased concentration of EA. More specifically, hysteresis on PEA and PEA70 was higher compared to the rest of the samples. In addition, hysteresis of FN-coated PEA and PEA70 was higher than the

hysteresis of those samples without protein adsorption. This can be explained by the decrease of RCA after FN adsorption (Figure 2.5).

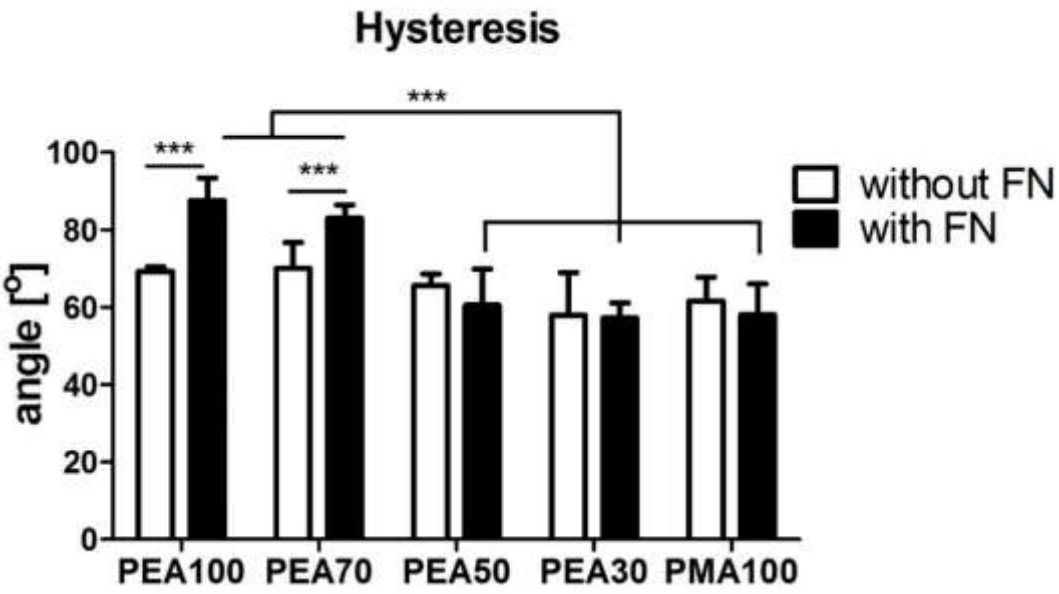

Figure 2.5. Hysteresis. Graphs represent the hysteresis of the surfaces without (white bars) and with (black bars).

without FN	with FN
• SCA remains constant • ACA decreases with increased MA concentration • PEA30 with highest RCA • Hysteresis remains constant	• SCA decreases with increased MA concentration • ACA decreases with increased MA concentration • PEA50 with highest RCA • Hysteresis decreases with increased MA concentration
without VS with FN	
• SCA is higher on FN-coated PEA30 and PMA100 compared to PEA30 and PMA100 without protein coating • ACA is lower on FN coated PEA100, PEA50, PEA30 and PMA100 compared to PEA100, PEA50, PEA30 and PMA100 without protein coating • RCA decreases significantly on FN-coated samples compared to samples without protein coating • Higher hysteresis on FN-coated PEA100 and PEA70 compared to PEA100 and PEA70 without protein	

Table 2.5. Summary of WCA results.

2.3.2 Force spectroscopy

The elastic modulus of the surfaces was analysed by atomic force spectroscopy measurements. To do so, samples were immersed in milliQ water overnight and a 5 μm bead was attached to a silicon cantilever in order to ident the surfaces. Analysis of the force curves showed that the young's modulus of the surfaces was in the range of hundreds of kPa (Figure 2.6). It should be noted though that that large variation in stiffness was observed. This was because the areas on the surfaces with high Young's modulus affecting the error bars. Despite the variation observed in the elastic modulus, no statistical differences were found.

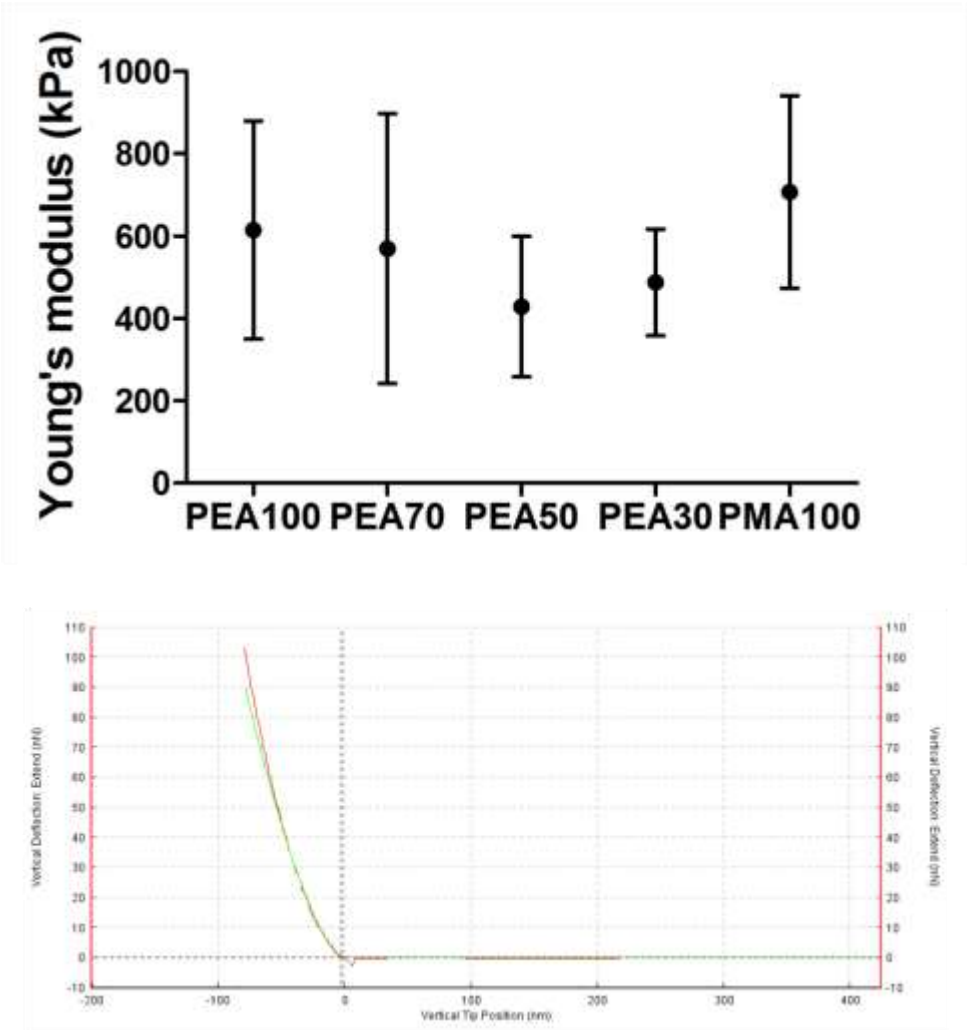

Figure 2.6. Stiffness characterisation. Young's modulus of surfaces (top). Example of force curve obtained from measurements. The Hertz model was applied to calculate the Young's modulus (bottom). (n=100 per sample, 1 samples tested).

2.3.3 FN conformation

AFM images in tapping mode were taken to assess how the EA/MA ratio affects FN distribution on the surfaces upon adsorption and whether different degrees of FN fibrillogenesis can be obtained.

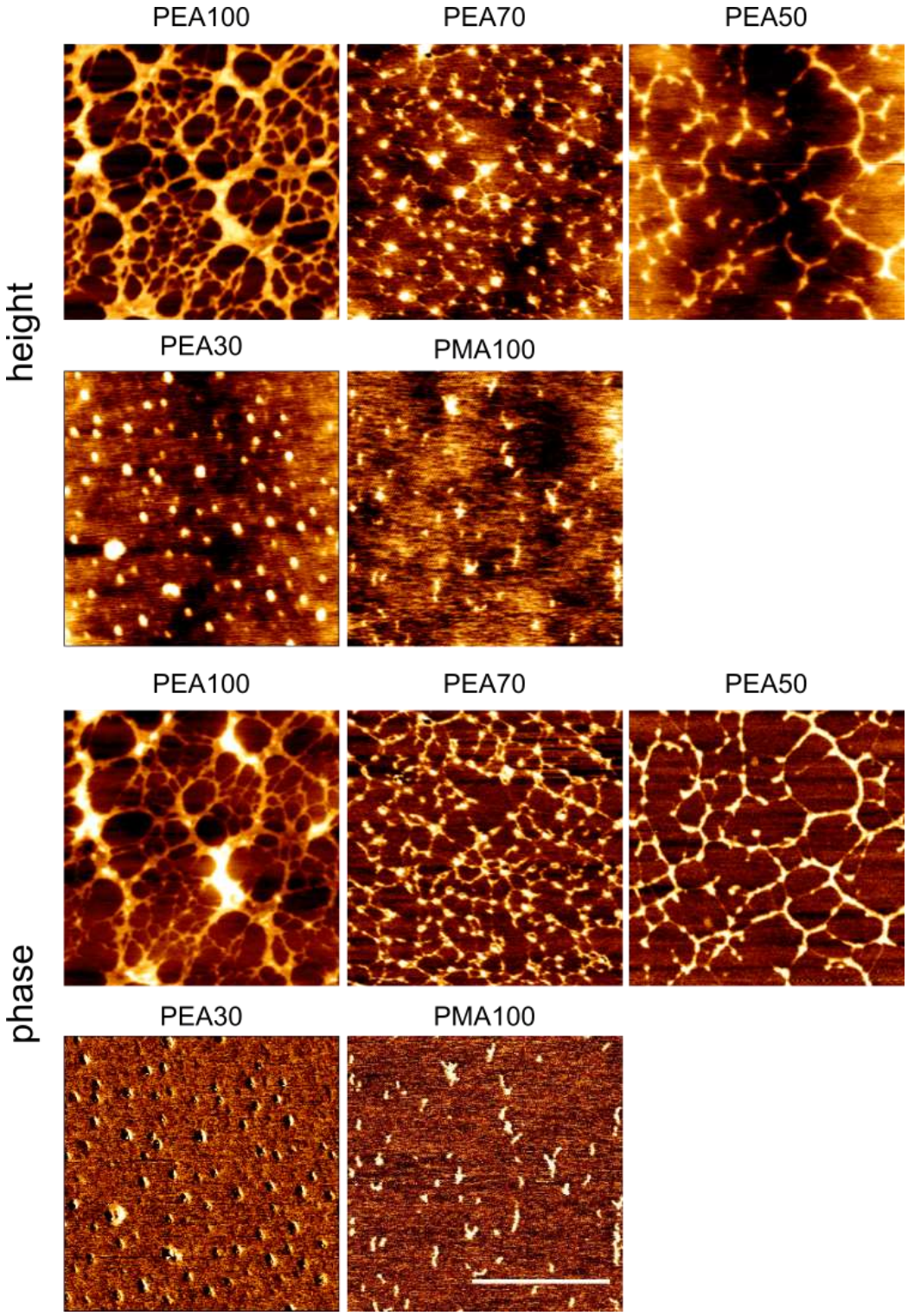

Figure 2.7. FN fibrillogenesis. Height and phase AFM images. Samples were coated with a FN solution at a concentration of 20 µg/ml for 10 min. Scale bar is 500 nm.

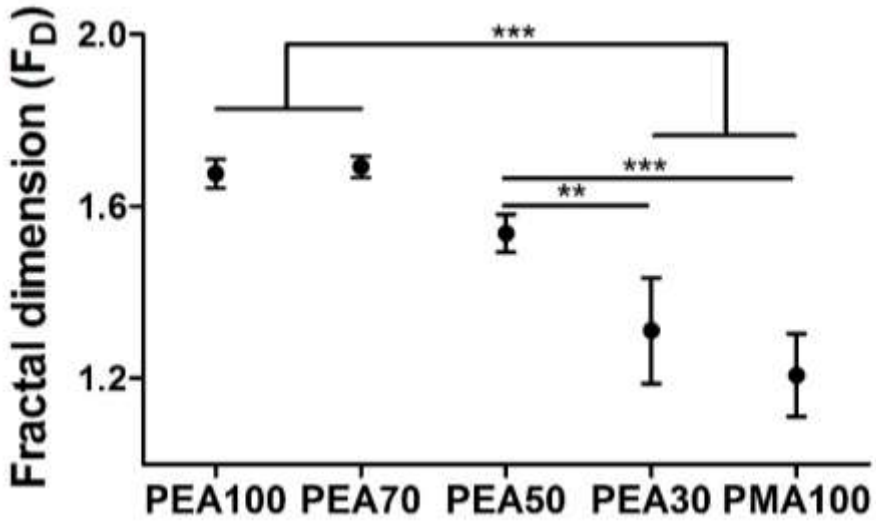

Figure 2.8. Fractal dimension (FD) calculated from AFM images. (4 images/sample were analysed).

AFM height and phase images (Figure 2.7) demonstrate the distribution and conformation of adsorbed FN on the surfaces. It is shown that the degree of FN fibrillogenesis depends on the EA/MA ratio. As described previously, PEA triggers the formation of a well-connected network of FN fibrils. With decreased concentration of EA, the density of the interconnected network decreases as well. This conformation is lost with decreased EA/MA ratio resulting in a globular conformation of FN on PMA. To quantitatively assess the density of the FN network, AFM images were analysed using ImageJ and the plugin FracLac. The Fractal dimension decreased with decreased concertation of EA units indicating that a well-connected network is adopted on PEA (Figure 2.8).

2.3.4 FN surface density

The surface density of FN adsorbed on the surfaces was indirectly quantified by measuring the depletion of FN from solution. For a direct way to assess the level of adsorbed FN, an ICW™ assay was performed. The surface density of FN was similar on all the surfaces (Figure 2.9, a). Similarly, ICW™ assay using a polyclonal anti-FN antibody did not reveal any statistical differences in the relative availability of adsorbed FN (Figure 2.9, b).

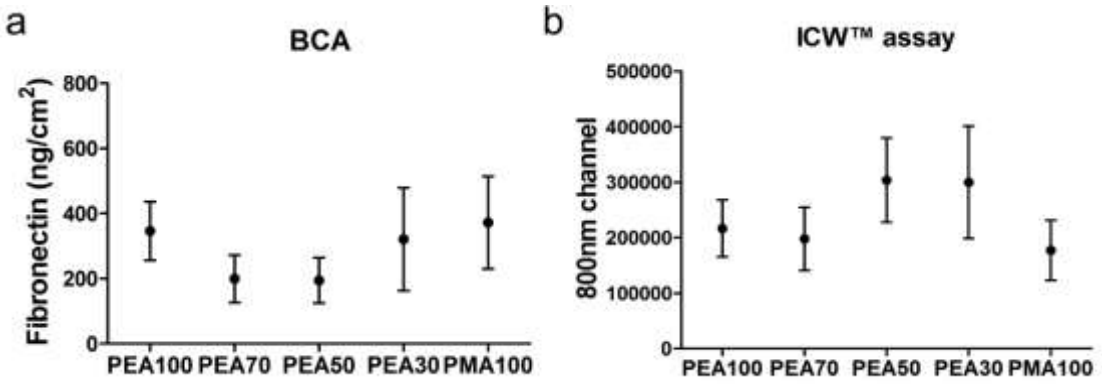

Figure 2.9. Surface density of FN adsorbed on the copolymers for 1 h. (a) BCA assay to indirectly quantify the amount of adsorbed FN (n=3 per sample, 3 biological replicates). (b) ICW™ assay using a polyclonal anti-FN antibody to assess FN availability. (n=3 per sample, 1 biological replicates).

2.3.5 Availability of FN domains

To evaluate how the EA/MA ratio of the materials affects the availability of important binding domains of FN after adsorption, ELISA and ICW™ assay were performed. Monoclonal antibodies used were the HFN7.1, mAb1937 and P5F3. HFN7.1 is directed against the $FNIII_{9\text{-}10}$ repeat of FN which is involved in integrin binding and cell adhesion. The mAb1937 is directed against the $FNIII_{8}$ repeat which is near the synergy domain. The P5F3 is directed against the $FNIII_{12\text{-}14}$ repeat which contributes to growth factor binding.

The availability of the $FNIII_{9\text{-}10}$ repeat (integrin binding domain) increases linearly with increased ratio of EA/MA. PEA and PEA70 displayed the higher availability of $FNIII_{9\text{-}10}$ repeat compared to the rest of the samples. Also, higher availability is found on PEA50 and PEA30 compared to PMA (Figure 2.10).

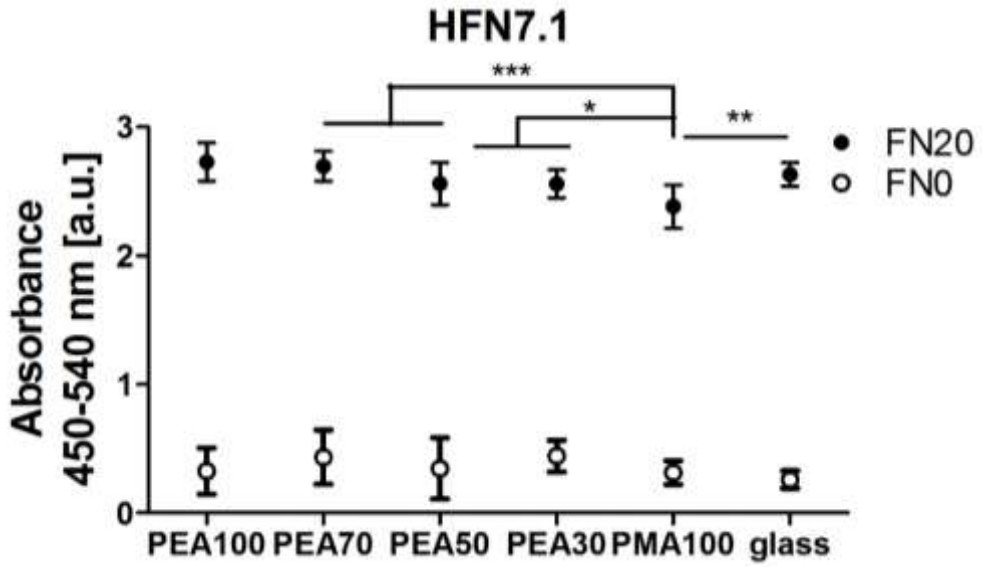

Figure 2.10. ELISA to probe for structural differences of FN conformation dependent on EA/MA ratio. Availability of the $FNIII_{9-10}$ (HFN7.1 antibody) on FN-coated surfaces and non-protein coated surfaces. (n=3 per sample, 3 biological replicates)

An ICW™ assay was carried out as well. In this case, the antibodies P5F3 (against $FNIII_{12-14}$ repeat) and mab1937 (against the FNI_{II8} repeat) were used.

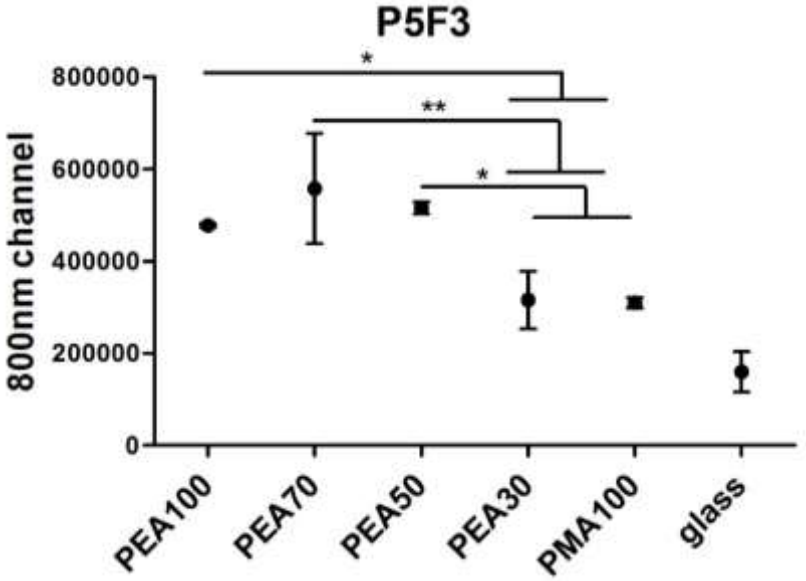

Figure 2.11. ICW™ assay to probe for structural differences of FN conformation dependent on EA/MA ratio. Availability of the $FNIII_{12-14}$ (P5F3 antibody) on FN-coated surfaces and non-protein coated surfaces. (n=3 per sample, 3 biological replicates)

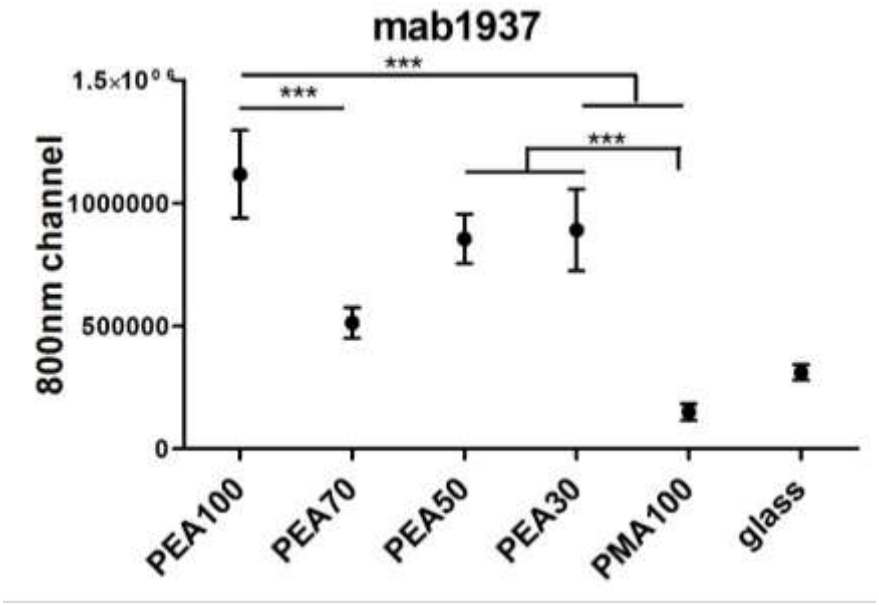

Figure 2.12. ICW™ assay to probe for structural differences of FN conformation dependent on EA/MA ratio. Availability of the $FNIII_8$ repeat (mab1937 antibody) on FN-coated surfaces and non-protein coated surfaces. (n=3 per sample, 3 biological replicates)

The $FNIII_{12\text{-}14}$ repeat is less available with decreased ratio of EA/MA. Particularly, the $FNIII_{12\text{-}14}$ repeat is less available on PEA30 and PMA compared to the rest of the samples (Figure 2.11). In addition, the availability of $FNIII_8$ repeat is higher with increased EA units. PEA, PEA50 and PEA30 demonstrated higher availability of this repeat compared to PEA70 and PMA (Figure 2.12).

2.3.6 BMP2 adsorption

A sandwich ELISA was performed to assess whether the differential conformation of FN affects the surface density of BMP-2 bound on FN-coated surfaces. To do so, FN and next BMP-2 (at 25 ng/ml) were adsorbed on the materials.

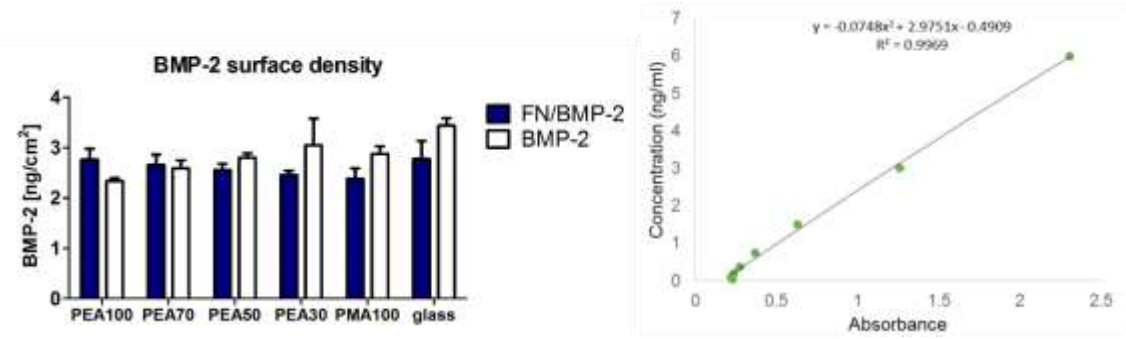

Figure 2.13. Quantification of BMP-2 adsorption. Standard curve used to quantify the amount of BMP-2 (top). Surface density of BMP-2 adsorbed on FN-coated surfaces (left, blue bars) and on surfaces without protein (right, white bars).

No statistically significant differences were found in the surfaces density of BMP-2 among the FN-coated surfaces indicating that FN conformation does not alter BMP-2 adsorption (Figure 2.13).

Substrate	P value
BMP-2	
PEA100 vs. PEA50……	*
PEA100 vs. PEA30……..	**
PEA100 vs. PMA100……....	*
PEA100 vs. glass ……..	***
PEA70 vs. PEA30……..	**
PEA70 vs glass……	***
PEA50 vs. glass……	**
PMA100 vs. glass……	*

Table 2.6. Statistically significant differences for the BMP-2 coated surfaces. P values represent the degree of significance. Stars are *P<0.5 **P<0.1 and ***P<0.01. (n=3 per sample, 3 biological replicates),

2.3.7 BMP-2 binding

To examine how BMP-2 binds to FN-coated surfaces, an anti-BMP-2 antibody and then a secondary antibody labelled with a gold particle were used. Next, AFM was performed to localise BMP-2 molecules.

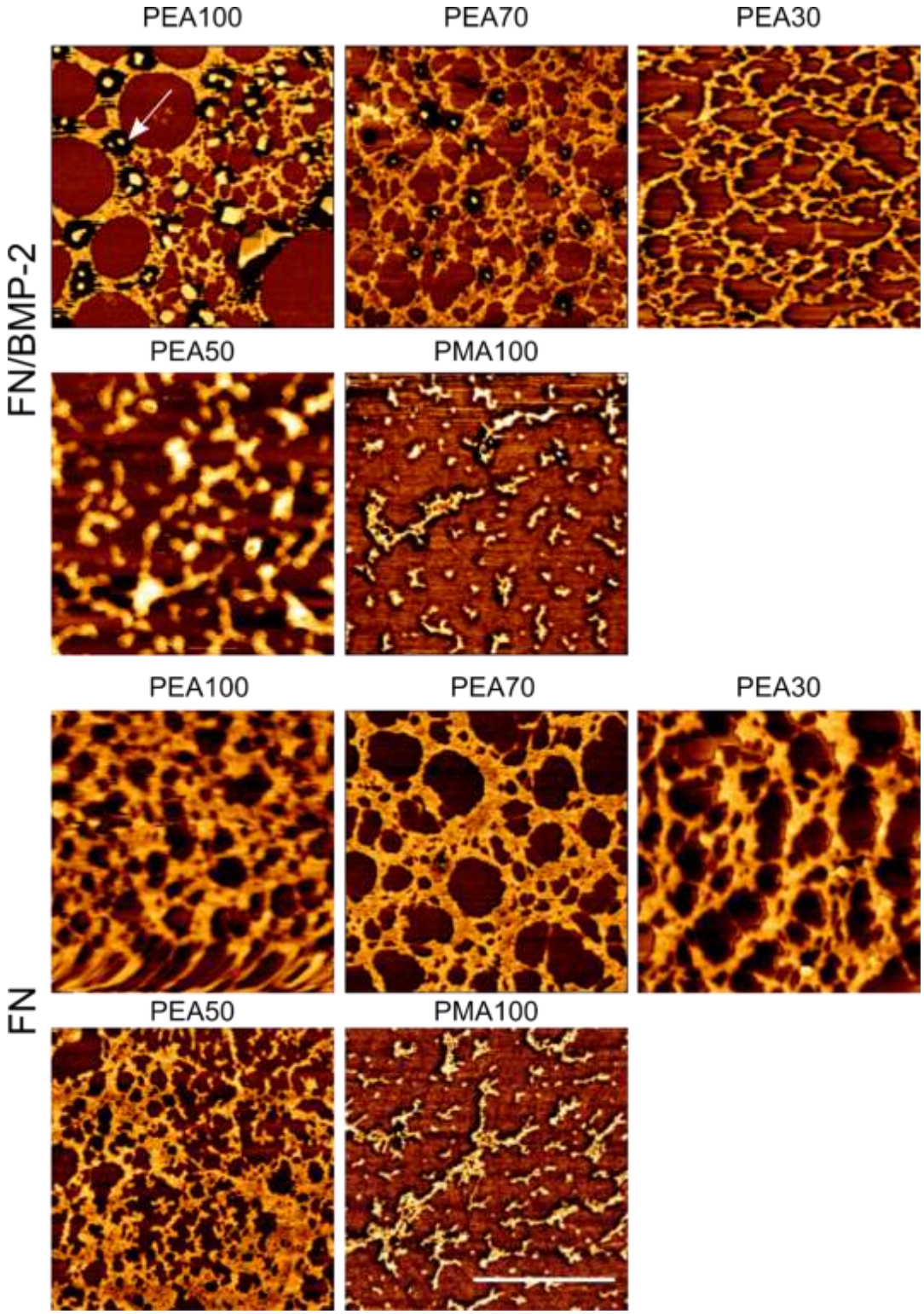

Figure 2.14. BMP-2 adsorption on FN-coated surfaces. Phase AFM images after adsorption of FN (20 µg/ml) and BMP-2 (100 ng/ml) and after adsorption of FN. Scale bar is 500 nm.

Phase AFM pictures showed that BMP-2 is adsorbed on the on top of open network of FN molecules (Figure 2.14). Particles were mostly seen on FN network formed on PEA and PEA70 (indicated by the white arrows). However, just few particles were seen on surfaces with decreased concentration of EA. In addition, on surfaces where BMP-2 was not adsorbed no gold nanoparticles were observed. Phase AFM images of FN/BMP-2 coated PEA at different magnifications (5 µm, 1 µm and 500 nm) demonstrate that BMP-2 is bound only on the extended FN molecules. A section of one gold nanoparticle bound on adsorbed FN show a height profile of ~ 7 nm (Figure 2.15).

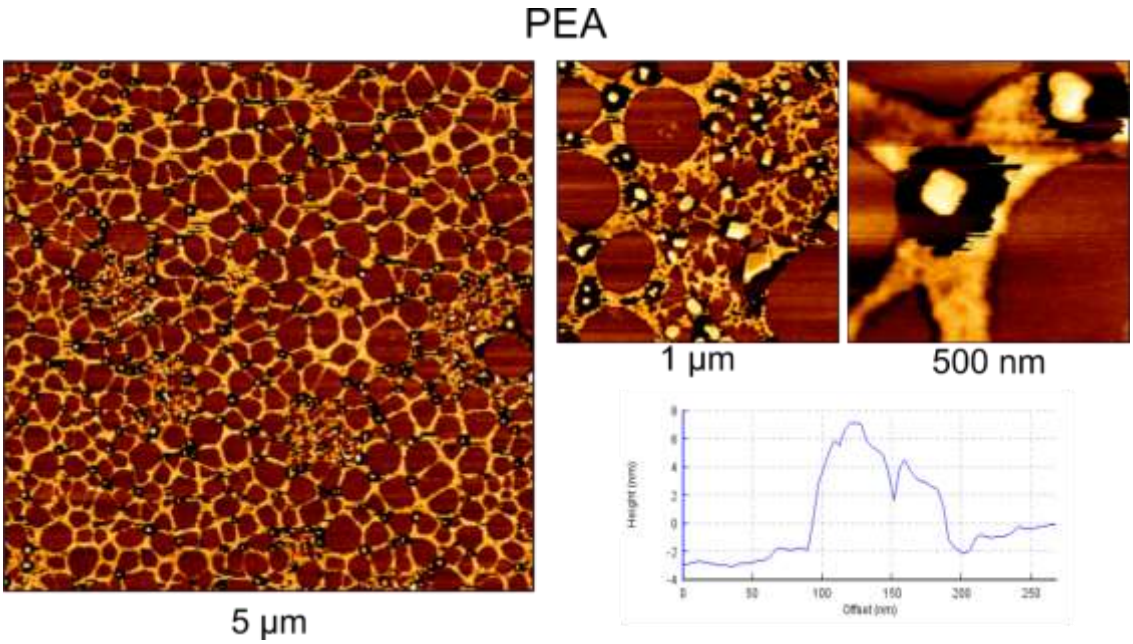

Figure 2.15. Phase AFM images at different magnifications showing BMP-2 interaction with FN network formed on PEA. PEA was coated with FN (20 µg/ml) and BMP-2 (100 ng/ml) and an immunogold staining was carried out.

2.4 Discussion

This chapter describes the characterisation of material properties and, particularly, how the EA/MA ratio alters the interactions of FN with the surface and the biological activity of the protein. Surfaces were assessed in terms of wettability, stiffness, FN conformation as well as surface density upon adsorption. In addition, the availability of important binding sites of FN was investigated. BMP-2 adsorption on FN-coated surfaces was studied too.

Characterising material wettability is a common approach to measure the hydrophobicity of a solid surface. Differences found in wettability depend on the surface properties such as surface roughness, topography, homogeneity or molecular mobility[249]. In this work, the wettability of the surface was characterised by measuring the SCA, ACA, RCA and the hysteresis. SCA was similar through the series of copolymers before FN coating. After FN adsorption, SCA decreased with decreased ratio of EA/MA indicating that the surfaces become more hydrophilic with decreased EA concentration (Figure 2.2). ACA decreased with decreased ratio of EA/MA prior or after FN coating. Generally, ACA was higher on PEA and PEA70 than on PEA50, PEA30 and PMA. Interestingly, this difference was more pronounced on FN-coated samples because of the lower ACA in PEA50, PEA30 and PMA (Figure 2.3). It can be postulated that FN-coated surfaces become more homogeneous with decreased EA units therefore they facilitate the spreading of the contact line. RCA was similar among the samples before and after protein coating. However, it was lower on the FN-coated surfaces compared to the non-protein coated samples (Figure 2.4). This suggests that the liquid molecules resist the flow on the surfaces coated with FN. Additionally, hysteresis significantly decreases with decreased concentration of EA units after FN adsorption which can be explained by the drastic decrease of RCA (Figure 2.5). These results support that FN-coated samples are smoother after FN coating with decreased concentration of EA indicating that FN is more homogenously distributed with increased EA/MA ratio.

AFM was carried out to explore how the different ratio of EA/MA units affects the conformation of adsorbed FN. Height and phase images showed that FN organises into a network-like conformation on PEA. This network becomes less

connected with decreased EA/MA ratio. Eventually, the connection is lost and globular aggregates are formed on PMA (Figure 2.7). Analysis of the images confirms the results demonstrating that different degrees of FN fibrillogenesis are obtained by changing the EA/MA ratio (Figure 2.8). It can be therefore suggested that the specific material-protein interactions result in a different degree of FN fibrillogenesis dependent on the EA/MA ratio. Force spectroscopy measurements in liquid were carried out to characterise the stiffness of the surfaces. The Young's modulus of the surfaces exhibits a wide variation on all the surfaces and ranges from about 0.2 MPa to 0.9 MPa. Tissue elasticity ranges in stiffness from soft (0.1 kPa in brain) to rigid (100 kPa in collagenous bone)[193]. Difference in substrate stiffness affect MSC response in vitro too. Engler *et al*. showed that MSCs respond to material stiffness ranging from 0.1-40 kPa with osteogenic phenotype at high elastic modulus[193]. Given that the stiffness of the copolymers is higher than what cells can sense, the surfaces are considered stiff. Therefore, any differences observed in cell behaviour can be attributed to FN conformation and not to the mechanical properties of the surfaces.

The surface density of FN and the available adsorbed FN were quantified by BCA and ICW™ assay respectively. Even though no changes in the amount of adsorbed FN were found (Figure 2.9), FN conformation is different as observed *via* AFM. FRET analysis has indicated that FN fibrils are highly elastic and cell-generated contractile forces are sufficient to stretch them by several folds[250]. Consequently, some cryptic binding domains, and particularly the FN type III domains, might be exposed [236]. Such conformational changes influence FN-FN interactions[235], integrin binding and cell behaviour[66]. Taking this into consideration, we investigated how the different degrees of FN fibrillogenesis alter the differential availability of cell and growth factor binding domains. To investigate domain exposure, ELISA and ICW™ assays were performed. ELISAs and ICW™ assay using monoclonal antibody against the flexible linker in FNIII9-10 (integrin binding domain), FNIII8 and FNIII12^{-14} repeat (GF binding domain), showed decreased availability with decreased concentration of EA units (Figure 2.10, Figure 2.11, Figure 2.12). These results indicate that the network conformation of FN formed with increased EA concentration facilitates

the exposure of these domains. In addition, surfaces with higher EA/MA ratio promote the simultaneous availability of the integrin and GF binding domain.

ELISA showed that similar amounts of BMP-2 were adsorbed on FN-coated surfaces (Figure 2.13). However, immunogold staining and AFM imaging showed that adsorbed BMP-2 is found to preferentially bind to the open and more extended FN molecules formed on PEA and PEA70. On the contrary, a decrease in the number of bound BMP-2 was observed with decreased concentration of EA (Figure 2.14). It should be mentioned that AFM images demonstrate specific BMP-2 binding on FN after fixing. BMP-2 that was not bound to FN (for example on PMA) might have been washed away due to the several washes and thus no particles were observed. In contrast, ELISA protocol required less washes and, subsequently, adsorbed BMP-2 on the surfaces might have been quantified. Therefore, no differences were found.

These results indicate that the degree of FN fibrillogenesis and, particularly, the extended network conformation of FN on PEA and PEA70, can control specific BMP-2 binding onto the FN fibrils. Taking into consideration that the availability of FN repeats involved in cell binding changes depending on the EA/MA ratio, it can be suggested that the synergistic presentation of BMP-2 and cell binding domains can be obtained in a controlled manner.

3. MSC response

3.1 Introduction

The role of FN and its organisation in guiding stem cell differentiation has been previously demonstrated too. *In vitro* studies have shown that FN conformation can regulate the osteogenic differentiation of osteoblast-like cells[251] and MSCs[244]. Furthermore, changes in FN structure mediated by the surface chemistry of SAMs altered integrin binding and enhanced the expression of osteogenic markers[197]. Similarly, conformation changes of FN induced by sulfated hyaluronan resulted in an increase of ALP activity underlying the role of protein conformation on cell differentiation[252].

The previous chapter described the surface properties and how surface the EA/MA ratio affects FN conformation and the availability of binding domains. This chapter focuses on examining how the changes in FN activity on the material interface can tune the response of MSCs in terms of adhesion and osteogenic differentiation *via* the different degrees of FN fibrillogenesis. Taking into consideration that cell adhesion plays an important role in cell functions, FAs and cell morphology were characterised. The potential of the material interface to drive MSCs into osteogenic commitment was also investigated. To do so, osteogenic differentiation was assessed by characterising the expression of the markers RUNX2, ALP and OCN.

3.2 Materials and Methods

3.2.1 Materials

List of reagents	
Dulbecco's Modified Eagle's Medium……..	Sigma
Sodium pyruvate……..	Sigma
L-glutamine……..	Sigma
Penicillin streptomycin……	Sigma
Fungizone……..	Life Technologies
Foetal bovine serum……	Life Technologies
Trypsin/EDTA……..	Sigma
L-ascorbic acid……..	Sigma-Aldrich
Dexamethasone……..	Sigma
Sodium phosphate monobasic (NaH_2PO_4)……..	Sigma
Formaldehyde……	Fisher Scientific
Triton X-100……	Sigma
Tween®20……..	Sigma
Bovine serum albumin……..	Roche/Sigma
Saccharose……..	Fisher Chemicals
Sodium chloride……..	Fisher Chemicals
Magnesium chloride……..	VWR Chemicals
4-(2-hydroxyethyl)-1-piperazineethanesulfonic acid (HEPES)……..	Sigma
ALP kit, Leukocyte kit ……..	Sigma-Aldrich
Acetone……..	Fisher Chemicals
Mouse monoclonal vinculin antibody……	Sigma
Mouse monoclonal osteocalcin antibody……..	Santa Cruz Biotechnology
Rabbit polyclonal RUNX2 antibody……	Santa Cruz Biotechnology
Cy-3 anti-mouse antibody ……..	Jackson ImmunoResearch
Vectashied with DAPI……	Vector Laboratories
Phallacidin……..	Life Technologies
CellTag ICW700……..	LI-COR®
Anti-mouse ICW800……..	LI-COR®
Anti-rabbit ICW800……	LI-COR®

3.2.2 Human Mesenchymal Stem Cells

Human mesenchymal stem cells were purchased from PromoCell®. Cells express the markers CD73/CD90/CD105 whereas they lack expression of

CD14/CD19/CD45/HLA-DR. For expansion, cells were thawed from stock and were maintained in high glucose DMEM supplemented with 10% v/v FBS, 1% v/v antibiotic mix (2.9% v/v L-Glutamine, 1.9% v/v penicillin/streptomysin, 0.2 % v/v fungizone) and 0.1% v/v sodium pyruvate at 37°C, 5% CO_2. Media change was carried out every 3 to 4 days. For splitting or cell seeding, cells were rinsed with warm PBS followed by 2 ml of trypsin/EDTA. After removing the solution, cells were incubated at 37 °C for 60 to 120 sec until the cells were detached from the tissue culture flask. Next, complete medium (supplemented with 10% v/v FBS) was added to the flask, cell suspension was transferred to a falcon tube and centrifuged at 1300 rpm for 5 min. Afterwards, the supernatant was removed and the cell pellet was suspended in 1 ml of FBS-free medium. Cell density was measured using a Neubauer haemocytometer. Cells were used at passages P0 to P5 for cell attachment (3.2.3.1) and cell adhesion (3.2.3.2, 3.2.3.3) experiments. Cells were used at passages P0 to P3 for experiments characterising osteogenic differentiation (3.2.4.1, 3.2.4.2, 3.2.4.3, 3.2.5).

3.2.3 Adhesion of hMSCs

3.2.3.1 Cell attachment

UV-sterilised samples were coated with FN at 20 µg/ml for 1 h. According to a previously described protocol[253], cells were washed twice with PBS and blocked with heat-denatured 1% w/v BSA /PBS for 30 min. Cells were trypsinised, harvested and resuspended in complete medium and cell suspension was incubated at 37 °C, 5% CO_2 for 10 min. Next, cells were seeded onto the surfaces at a seeding density of 90000 cells/cm^2 for 20 minutes at 37 °C. Then, samples were washed twice with PBS, they were fixed (3.7% v/v formaldehyde/PBS) for 30 min at 4°C and washed again with PBS. Next, samples were incubated with permeabilisation buffer (0.5% v/v Triton X-100, 10.3% w/v saccharose, 0.292% w/v NaCl, 0.06% w/v $MgCl_2$, and 0.476% w/v HEPES adjusted to pH 7.2) for 5 min and mounted with vectashield with DAPI. Images were taken and the number of cells was quantified using the CellC total cell count analysis.

3.2.3.2 Cell adhesion

UV-sterilised samples were coated with FN at 20 μg/ml for 1 h. hMSCs were harvested by trypsinization and cell suspension was diluted in FBS-free medium to a final density of 1000 cells/cm^2. Then cells were seeded onto the surfaces and were incubated at 37°C, 5% CO_2 for 3 h and 24 h. For the early time point, cell culture was maintained in FBS-free conditions. For the later time point medium was replaced with complete medium 3 hours after seeding. After the given time, cells were washed with warm PBS and were fixed as described previously. Samples were kept in PBS at 4°C.

3.2.3.3 Cell adhesion on FN/BMP-2 coated surfaces

One day before cell harvesting, medium was changed with medium containing 1% v/v FBS. The next day, UV-sterilised samples were coated with FN at 20 μg/ml for 1 h. After they were washed twice with PBS, they were blocked with heat-denatured 1% w/v BSA/PBS for 30 minutes. Next, they were coated with BMP-2 at 100 ng/ml for 1 hour. Then, cells were harvested and cell suspension was diluted in 1 ml of FBS-free medium at a final density of 3000 cells/cm^2. Culture was maintained in FBS-free medium at 37°C, 5% CO_2 and after 2h medium was replaced with medium containing 1% v/v FBS. Three days after seeding, cells were fixed as described previously.

3.2.4 Osteogenesis of hMSCs

3.2.4.1 ALP expression at different time points

Glass samples were coated with FN. Next, they were blocked with heat-denatured 1% w/v BSA/PBS for 30 minutes and then they were coated with BMP-2 at 100 ng/ml for 1 h. Glass samples coated only with FN (20 μg/ml) were included too. hMSCs were harvested and cell suspension was diluted in 1 ml of FBS-free medium at a seeding density of 10000 cells/cm^2 and cell culture was maintained at 37°C in FBS-free conditions for 2 h. Medium was replaced with medium containing 1% v/v FBS which was also used for medium change every 3 d. For the osteogenic differentiation control, cell suspension was also diluted in complete medium at a seeding density of 10000 cells/cm^2 and cells were seeded on FN-coated glass. In this case, medium was replaced with osteogenic medium (10% v/v FBS, 0.1 μM dexamethasone, 25 μg/mL L-

ascorbic acid, 3 mM NaH_2PO_4) when cells reached confluency. Cell culture was maintained at 37°C for 1 d, 14 d and 21 d.

3.2.4.2 ALP expression on the copolymers

The same procedure was followed as described above. Samples were PEA100, PEA70, PEA50, PEA30, PMA100 and glass. FN-coated copolymers and glass samples were included too. Culture was maintained at 37°C, 5% CO_2 for 21 d.

3.2.4.3 RUNX2 and OCN expression

UV-sterilised samples were coated with FN (20 µg/mL). Next they were blocked with heat-denatured 1% w/v BSA/PBS for 30 minutes and coated with BMP-2 at 100 ng/ml for 1 h. Copolymers coated only with FN as well as FN-coated glass samples were included too. Cells were harvested and cell suspension was diluted in medium with 2.5% v/v FBS at a seeding density of 2500 cells/cm^2. Next, cells were seeded onto the surfaces. Furthermore, cell suspension was diluted in complete medium at a seeding density of 2500 cells/cm^2 and cells were seeded on FN-coated glass. Cell culture was maintained at 37°C, 5% CO_2 and medium was changed every 2 to 3 d. For the copolymers coated with FN and FN/BMP-2, medium was replaced with medium containing 2.5% v/v FBS and BMP-2 at 25 ng/ml whereas, for the FN-coated glass samples, medium was replaced with osteogenic medium when cells reached confluency. Cell culture was maintained for 5 d to characterise RUNX2 expressions and 21 d to characterise OCN expression.

3.2.5 ALP staining

Prior to the assay, a fixative and an alkaline-dye mixture were prepared. The fixative solution was prepared by mixing 25.5% v/v citrate solution, 66.3% v/v acetone and 8.2% v/v 37% formaldehyde. To prepare the alkaline-dye mixture, equal volumes of nitrite solution and FBB-alkaline solution were mixed gently (2.1% v/v nitrite solution, 2.1% v/v FBB-alkaline solution). The solution was allowed to stand for 2 min and then it was added to milliQ water. Next, 2.1% v/v naphthol AS-BI alkaline solution was added to the solution. Samples were washed with warm PBS and incubated with fixative solution for 30 sec. Next,

they were washed with milliQ water for 45 sec and they were incubated with alkaline-dye mixture for 15 min in dark. After removing the solution, samples were rinsed with milliQ water for 2 min. Next, samples were incubated with neutral red solution for 2 min for counterstain. Next, samples were rinsed thoroughly in tap water and then they were air-dried. For analysis, images were exported to Fiji. The trainable Weka segmentation was used to train a classifier to distinguish ALP aggregates from the background. After applying the classifier in all the pictures, a binary pixel segmentation was produced which was used for quantification of ALP area.

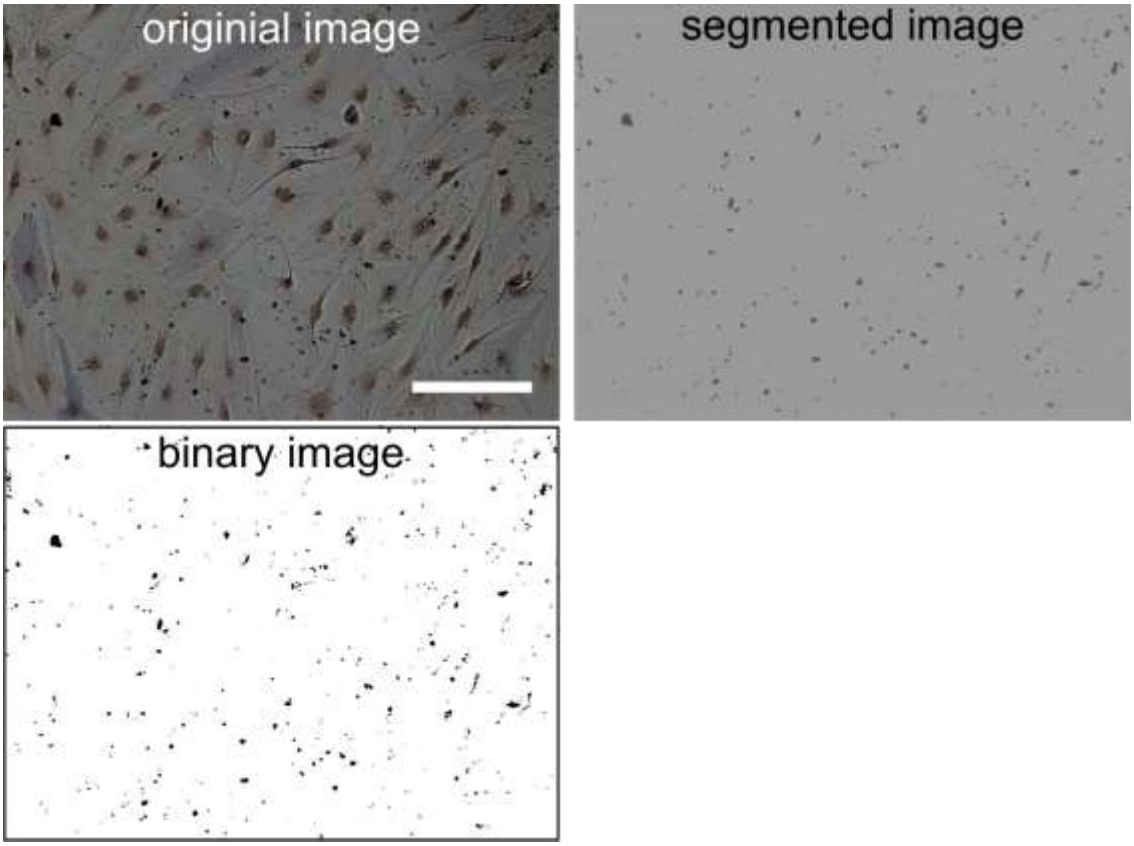

Figure 3.1. Quantification of ALP expression. A trainable Weka segmentation was applied to the original images which were next converted to binary images. Scale bar is 100 μm.

3.2.6 Immunohistochemistry

Fixed cells were washed three times with PBS and were incubated with permeablisation buffer (0.5% v/v Triton X-100, 10.3% w/v saccharose, 0.292% w/v NaCl, 0.06% w/v $MgCl_2$, and 0.476% w/v HEPES adjusted to pH 7.2) for 5 min followed by blocking with 1% v/v BSA/PBS for 30 min. Next, samples were

incubated with primary antibody containing mouse anti-vinculin antibody (1:400) or mouse anti-osteocalcin antibody (1:100) in 1% v/v BSA/PBS for 1 hour. Next, they were washed twice with 0.5% v/v Tween20/PBS. Samples were incubated with secondary Cy3 anti-mouse IgG (1:100) and BODIPY FL phallacidin (1:100) in 1% v/v BSA/PBS for 1 hour. After washing, samples were placed on glass slides and mounted with Vectashield containing DAPI.

3.2.7 In-Cell Western™ assay

An ICW™ assay was carried out to characterise RUNX2 and OCN expression. Fixed cells were washed with PBS, they were incubated with permeabilisation buffer for 5 min and were blocked with 1% w/v BSA/PBS for 30 min with gentle shaking. Primary antibodies were prepared in 1% w/v BSA/PBS containing anti-rabbit RUNX2 (1:100) or anti-mouse osteocalcin (1:100) antibodies. Samples were incubated with the primary antibody and after 1 hour they were washed three times for 5 minutes with 0.5% v/v Tween20/PBS in shaking. Secondary antibody was prepared in 1% w/v BSA/PBS containing anti-mouse or anti-rabbit IRDye 800 CW (1:800) and CellTag 700 Stain (1:500). CellTag is a near-infrared fluorescent cell stain which accumulates in both the nucleus and cytoplasm. Samples were incubated for 1 hour in dark and next the washing steps were repeated. Finally, samples were transferred to a new plate and readings were measured on Odyssey® plate reader with detection in 800 and 700 nm channels. The intensity settings were kept constant for each scan.

3.2.8 Cell imaging

Fluorescent pictures were taken using an epifluorescence microscope (Zeiss AXIO Observer Z1, Jena, Germany).

3.2.9 Image analysis of FAs and cell size and OCN quantification

To characterise FA morphology, vinculin fluorescent images were quantified using the online adhesion server[254] (Figure 3.2). For cell size quantification, actin fluorescence images were imported to ImageJ and the Otsu's method was applied to automatically threshold the images. Next, binary images were created which were used and to quantify cell area and circularity (Figure 3.3).

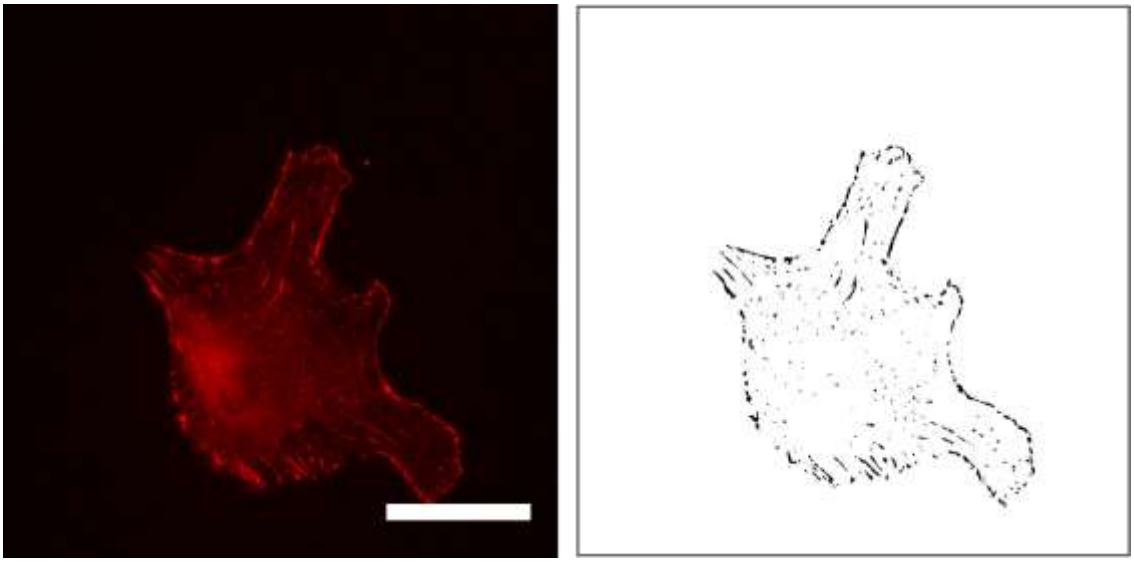

Figure 3.2. FA analysis. Vinculin immunofluorescence images were processed though the online adhesion server and binary images highlighting FAs were obtained. Scale bar is 50 μm.

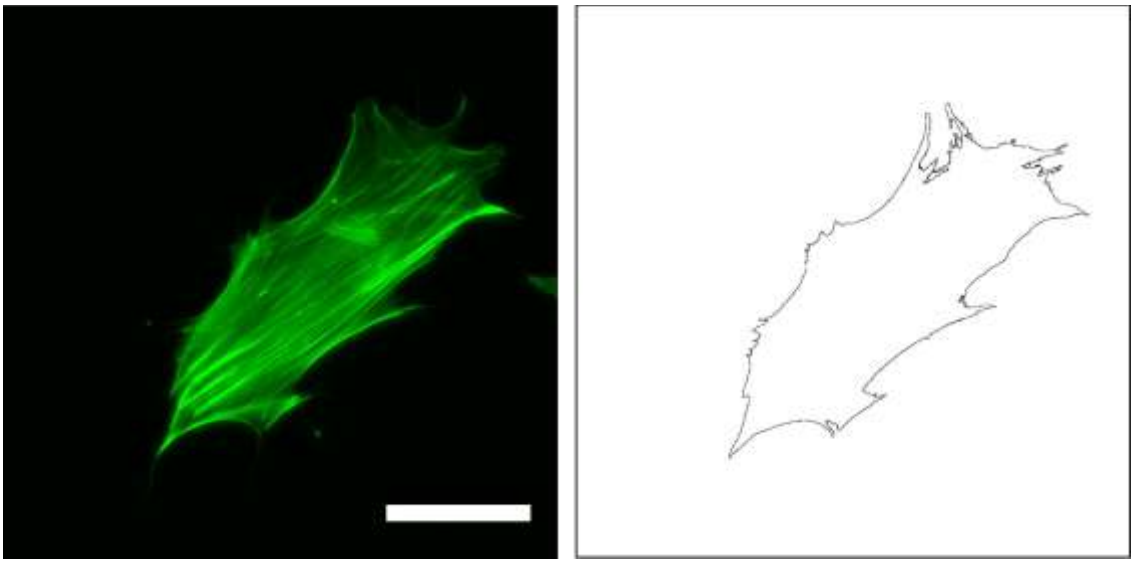

Figure 3.3. Cell area analysis. Actin immunofluorescence images were exported to ImageJ a threshold was applied to quantify total cell area. Scale bar is 50 μm.

3.2.10 Statistical analysis

Data are represented as mean ± SD and were analysed using GraphPad Prism 5. Statistically significant differences were assessed by t-test using a Tukey's post-test. A two-way ANOVA using a Bonferroni post hoc test was applied for multiple comparisons at a 0.05 significance level, with *$p < 0.05$, **$p < 0.01$, ***$p < 0.0001$.

3.3 Results

3.3.1 Attachment assay

A short cell attachment and DAPI staining were performed to assess the initial attachment of hMSCs on the protein coated copolymers. Initial adhesion was allowed for 20 min and characterisation was carried out according to a standard protocol[253]. Non-protein coated surfaces did not favour cell attachment. To measure the percentage of cells attached on the FN-coated copolymers, the nuclei number was quantified. Analysis showed that a similar percentage of cell attachment was found on the surfaces (Figure 3.4).

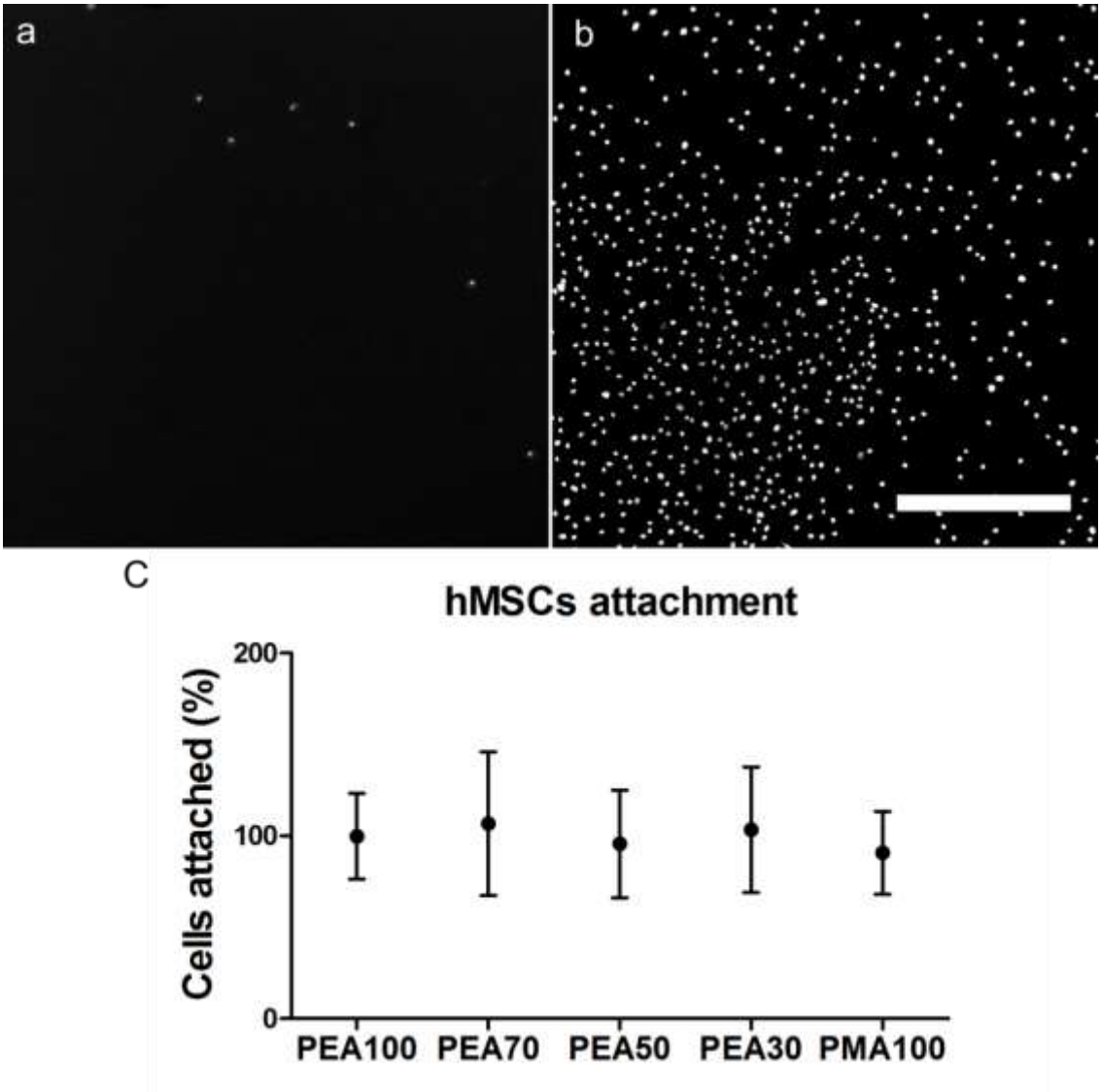

3.3.2 Figure 3.4. Cell attachment of hMSCs. DAPI staining of hMSCs cultured on surfaces without and with FN coating (a and b respectively). Scale bar is 500 μm. Quantification of cell attachment. Percentage of cells attached on the surfaces with respect to cell density (c). (n=3 per sample)**Adhesion assay**

MSC adhesion on the FN-coated copolymers was explored by performing a 3 h and 24 h adhesion experiment. For the earlier time point, the culture was maintained in serum free conditions so that the initial cell-material interactions occurred through the layer of adsorbed FN. For the latter time point, medium was replaced with medium supplemented with 10% v/v FBS 3 h after seeding. Cells were seeded at a low density to avoid cell-cell contact. Immunofluorescence staining of vinculin and actin was performed to characterise the FAs and cell morphology (Figure 3.5, Figure 3.6).

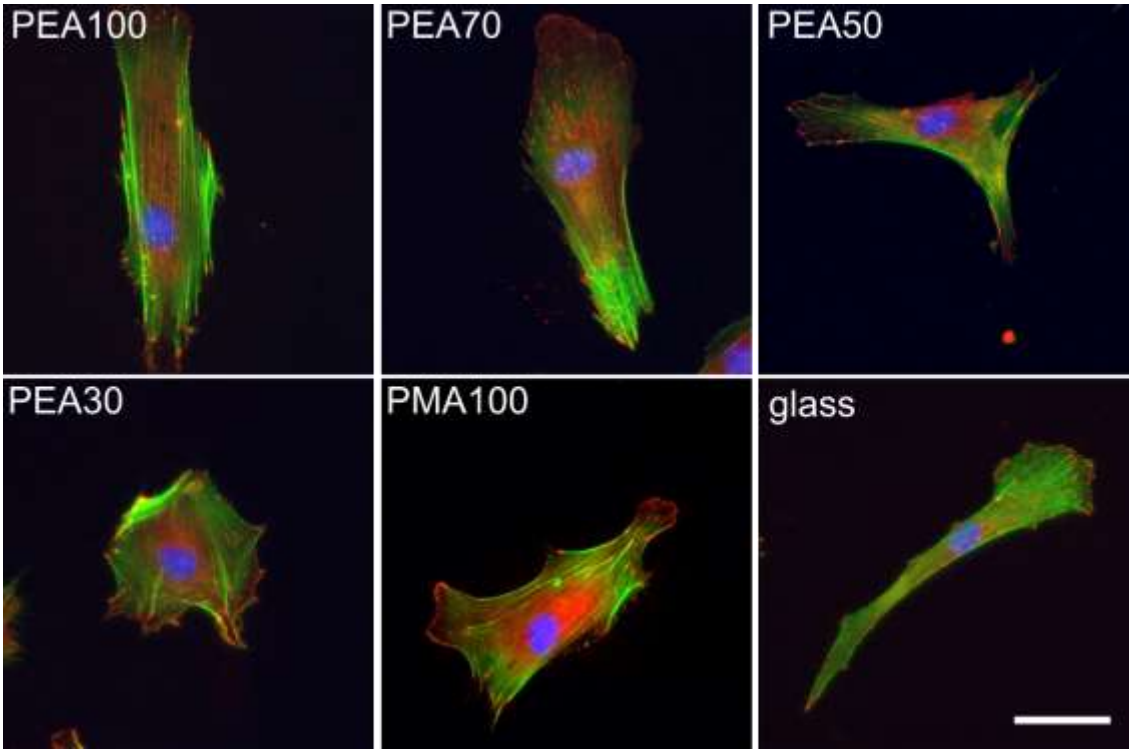

Figure 3.5. Adhesion of hMSCs. Immunofluorescent pictures of hMSCs on FN-coated surfaces 3 h after seeding in serum-free conditions. Fluorescent staining of vinculin (in red), F-actin (in green) and nucleus (in blue). Scale bar is 50 μm. (n=3 per sample, 2 biological replicates).

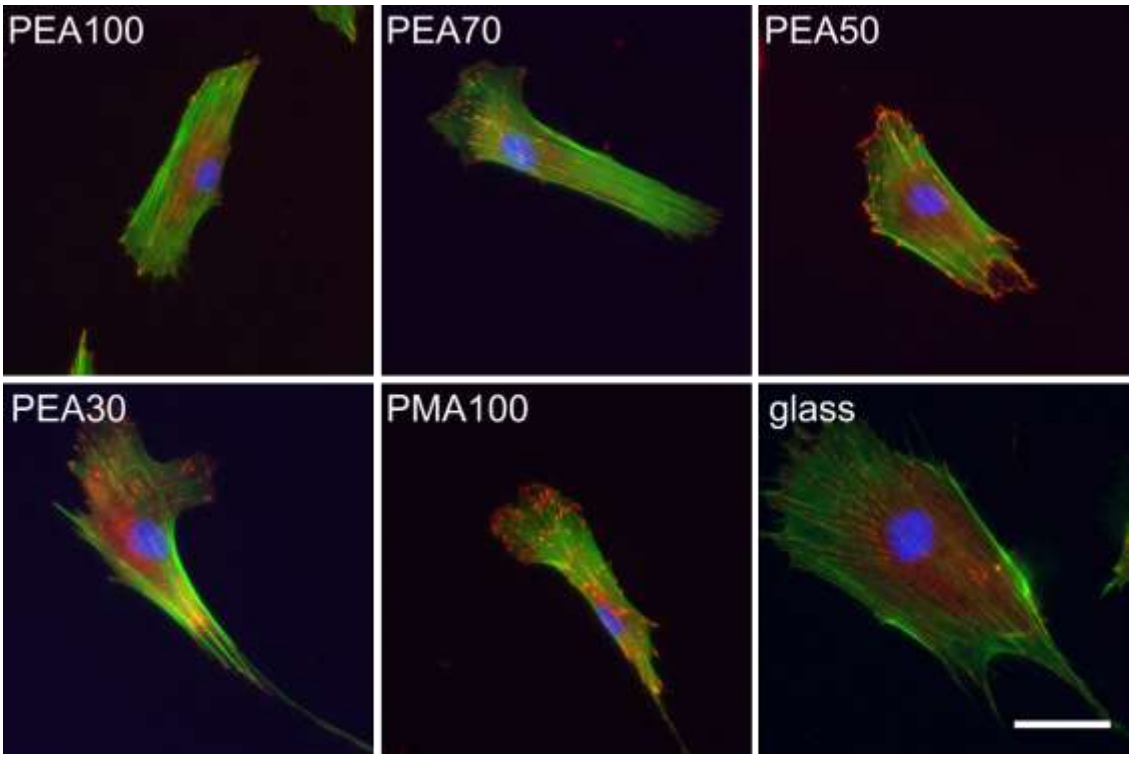

Figure 3.6. Adhesion of hMSCs. Immunofluorescent pictures of hMSCs on FN-coated surfaces 24 h after seeding. Fluorescent staining of vinculin (in red),

F-actin (in green) and nucleus (in blue). Scale bar is 50 μm. (n=3 per sample, 2 biological replicates).

FAs were developed on all the surfaces and cells appeared well spread. Image analysis of vinculin staining was carried out to quantify the area and length distribution of FAs. Focal complexes shorter than 1 μm were removed from the analysis. For quantitative analysis, FAs were classified based on the area as immature (0-1 μm^2), intermediate (1-2 μm^2) and mature (>2 μm^2) and further sub-classified by length as short (1-2 μm), intermediate (2-3 μm) and long (>3 μm)[255, 256]. Both the area and length distribution histograms of FAs showed a skewed distribution towards smaller adhesions at both time points (Figure 3.7, Figure 3.8).

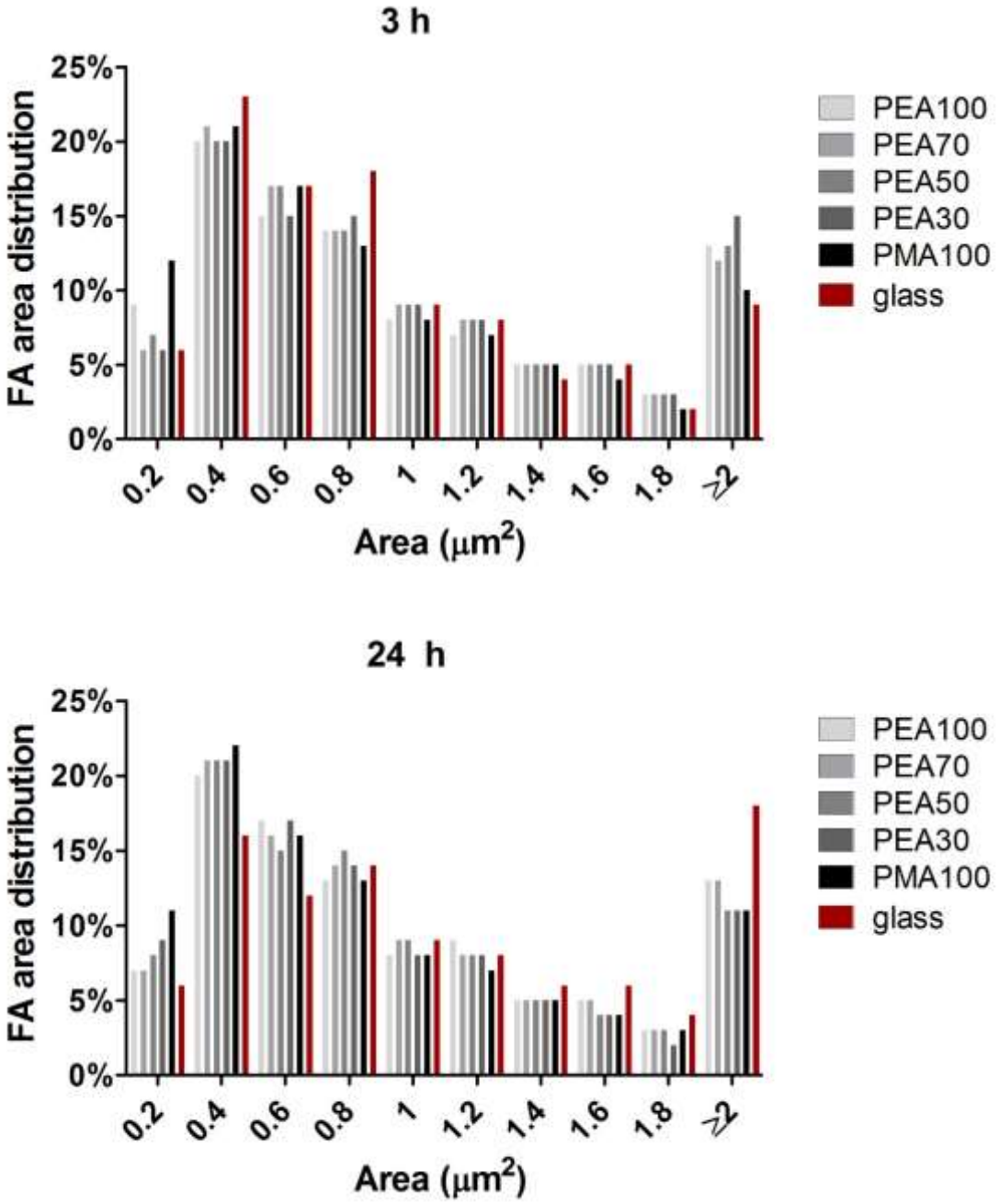

Figure 3.7. Area distribution histograms of FAs on FN-coated copolymers 3 h (top) and 24 h (bottom) after seeding. (25-30 images per condition, were analysed. n=3 per sample, 2 biological replicates)

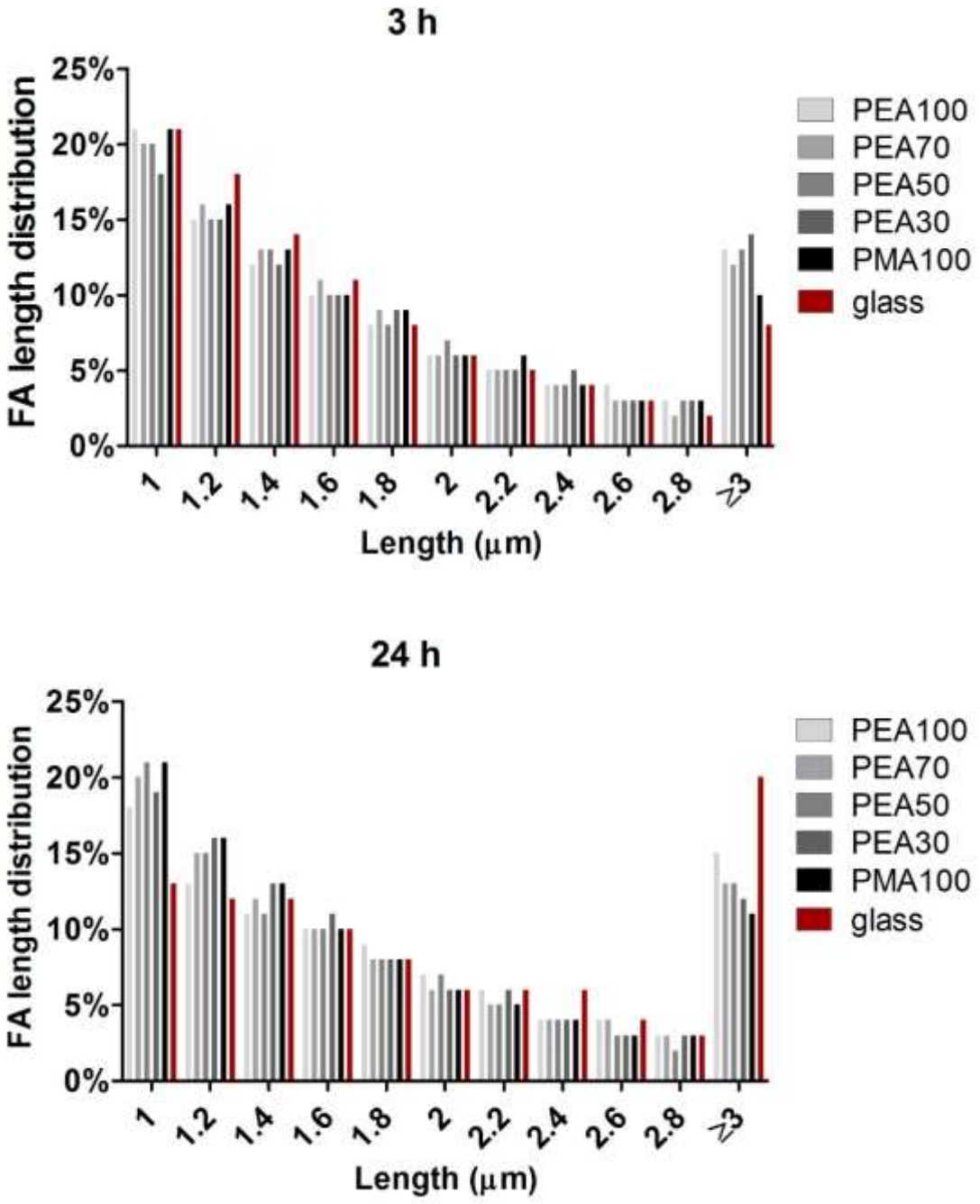

Figure 3.8. Length distribution histograms of FAs on FN-coated copolymers 3 h (top) and 24 h (bottom) after seeding. (25-30 images per condition were analysed. n=3 per sample, 2 biological replicates).

To further analyse FA morphology, the average area and length of FAs was plotted. No statistically significant differences were found in FA area among the seried of the copolymers over time (Figure 3.9). The length of FAs formed on PEA30 was found higher than on PMA100 at the early time point (Figure 3.10).

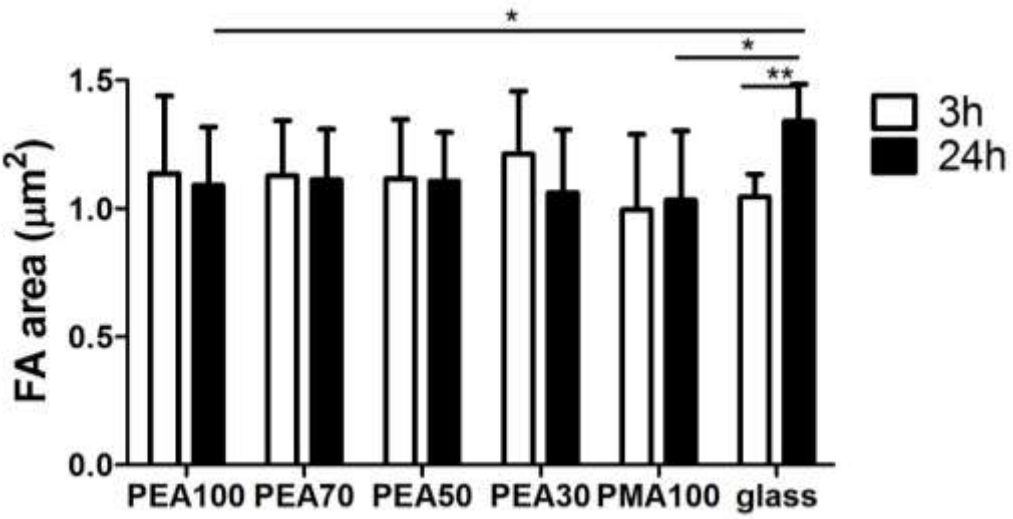

Figure 3.9. FA average area (μm^2) of hMSCs on FN-coated copolymers. FA average area (μm^2) of hMSCs on FN-coated copolymers. Culture was maintained for 3 h (white bars) and 24 h (black bars). (25-30 images per condition were analysed. n=3 per sample, 2 biological replicates).

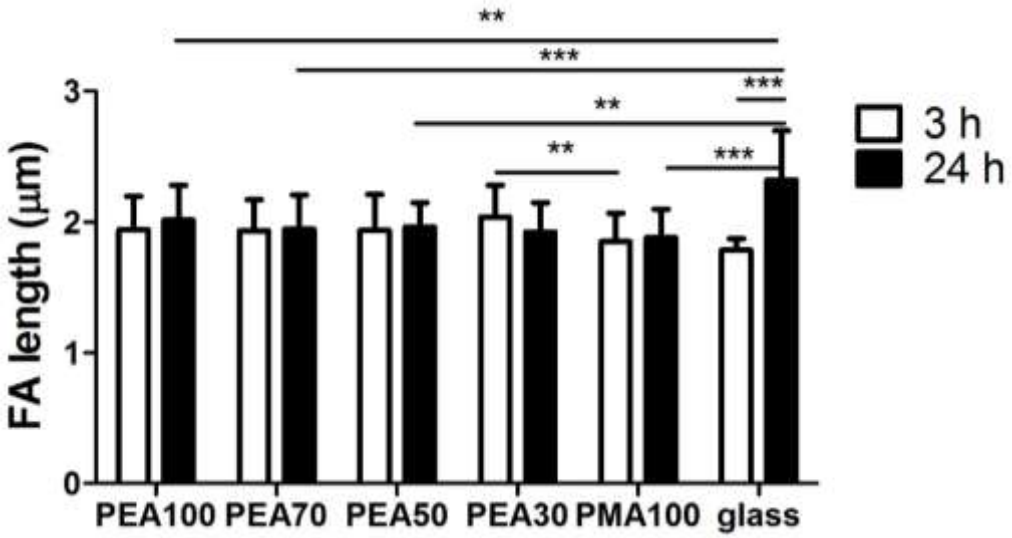

Figure 3.10. FA average length (μm) of hMSCs on FN-coated copolymers. Culture was maintained for 3 h (white bars) and 24 h (black bars). (25-30 images per condition were analysed. n=3 per sample, 2 biological replicates)

To assess whether larger FAs are formed on the FN-coated surfaces, the values of FA area and length of each cell were filtered based on their size. FAs with size greater than 2 μm^2 (for the area) and 3 μm (for the length) were averaged for each cell and plotted. No differences were revealed in the formation of larger FAs (≥ 2 μm^2 and ≥ 3 μm) through the series of FN-coated copolymers over time. The number of larger FAs ≥ 2 μm^2 was not statistically different in the series of the copolymers (Figure 3.11). However, longer and more FAs ≥ 3 μm were formed on PEA100 compared to PMA100 (Figure 3.12).

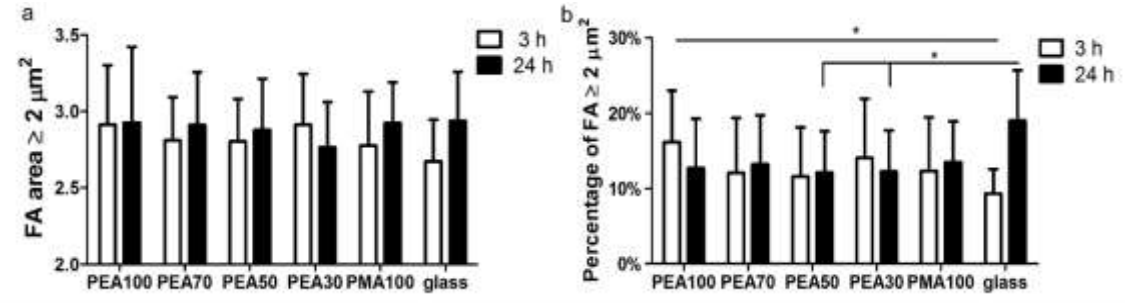

Figure 3.11. FA average area and number on FN-coated copolymers. FA average area ≥ 2 μm^2 in hMSCs (a). Percentage of FAs ≥ 2 μm^2 in hMSCs. Culture was maintained for 3 h (white bars) and 24 h (black bars). (25-30 images per condition were analysed. n=3 per sample, 2 biological replicates).

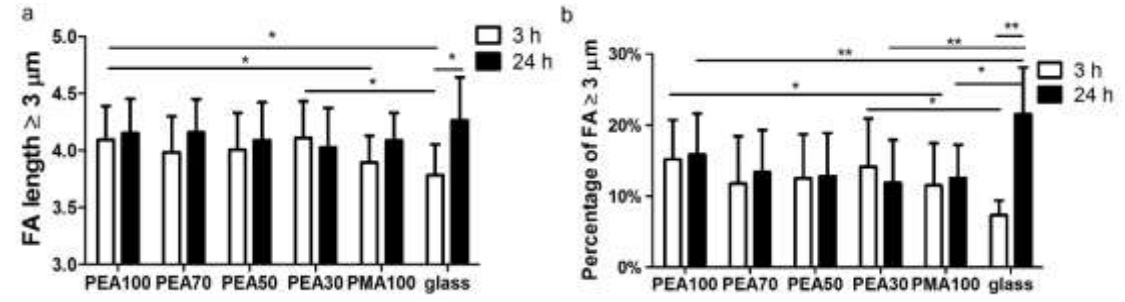

Figure 3.12. FA average length and number on FN-coated copolymers. FA average length ≥ 3 μm in hMSCs (a). Percentage of FAs ≥ 3 μm in hMSCs. Culture was maintained for 3 h (white bars) and 24 h (black bars). (25-30 images per condition were analysed. n=3 per sample, 2 biological replicates).

Cell morphology was assessed to further explore the effect of FN organisation on the copolymers. Analysis was carried out by applying a threshold on actin fluorescence images to quantify cell area and circularity. Cell area decreased with decreased concentration of EA units 3 h after seeding. Cells displayed the smaller spread area on PMA at the early time point whereas cell area was

similar on the rest of the samples. Spread area decreased over time on all surfaces apart from PMA and no differences were found (Figure 3.13).

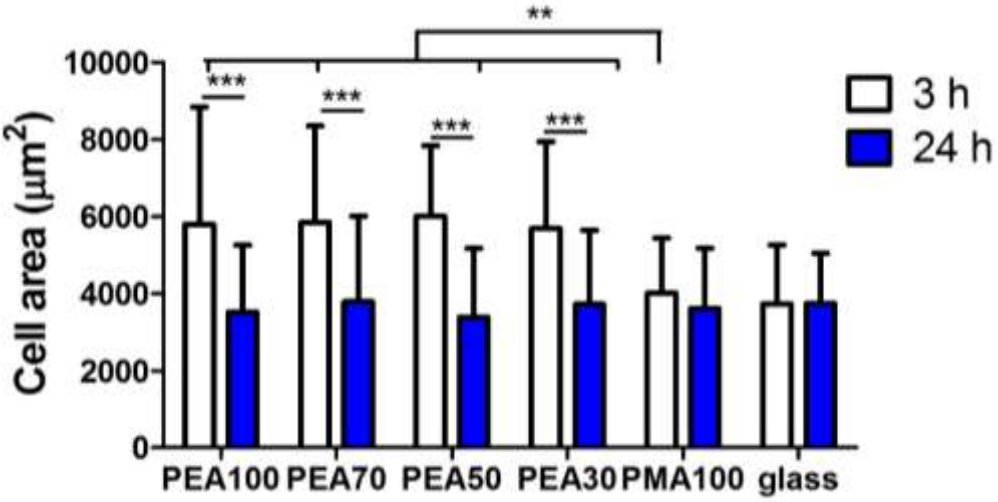

Figure 3.13. Area of hMSCs on FN-coated copolymers over time. The graph represents the cell area 3 h (white bars) and 24 h (blue bars) after seeding. (25-30 per condition images were analysed. n=3 per sample, 2 biological replicates).

Cell circularity decreased with decreased EA/MA ratio at the early time point. More specifically, it was higher on PMA than on PEA and PEA70 3 h after seeding. However, cell circularity decreased only on PMA over time whereas it was similar on the rest of the samples at both time points (Figure 3.14).

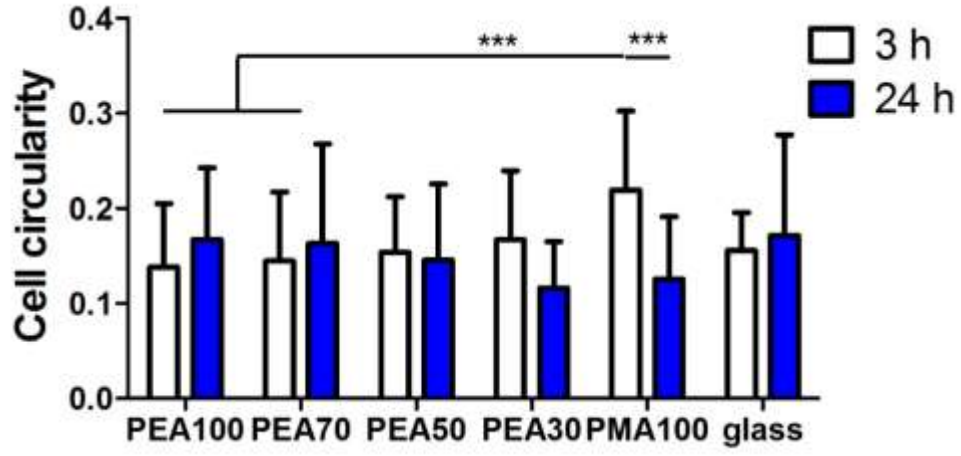

Figure 3.14. **Circularity of hMSCs on FN-coated copolymers over time.** The graph represents the cell area 3 h (white bars) and 24 h (blue bars) after seeding. (25-30 images per condition were analysed. n=3 per sample, 2 biological replicates)

3.3.3 Cell morphology on FN/BMP-2 coated surfaces

Cell adhesion depends on several factors including the ECM composition as well as on the availability of cell surface and GF receptors. To determine whether binding of BMP-2 on FN-coated surfaces influences cell morphology, MSCs were seeded at low seeding density on FN/BMP-2 coated surfaces and maintained in low-serum condition for 1 d. Next, a vinculin, actin and nuclei staining was carried out (Figure 3.15, Figure 3.16).

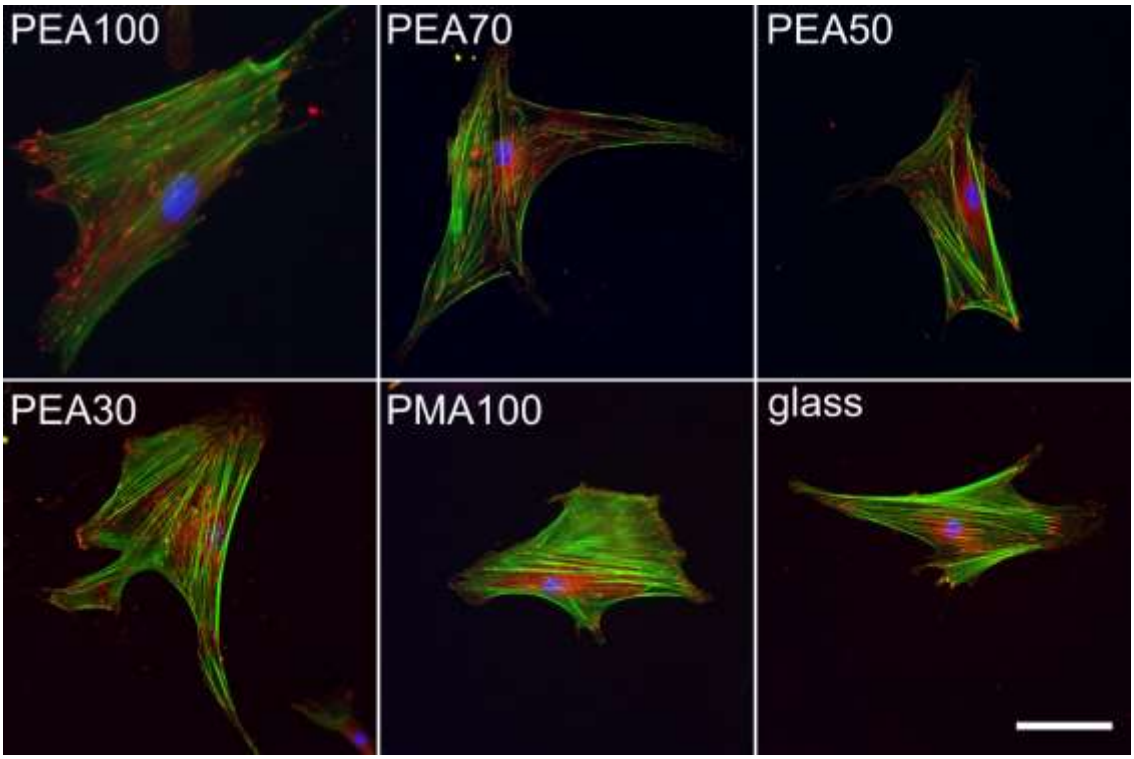

Figure 3.15. Immunofluorescent images of hMSCs seeded on FN/BMP-2 coated surfaces. Culture was maintained for 24 h. Staining of vinculin (red), F-actin (green) and nucleus (blue). Scale bar is 100 µm. (n=3 per sample, 2 biological replicates).

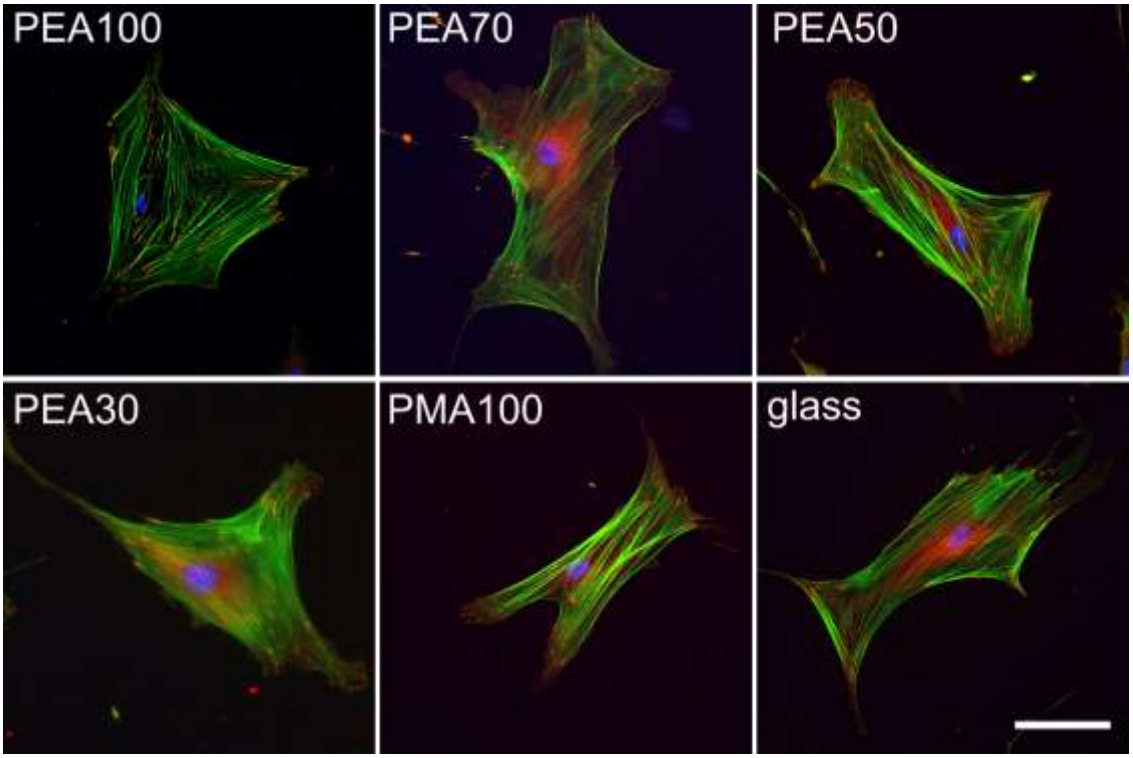

Figure 3.16. Immunofluorescent images of hMSCs seeded on FN coated surfaces. Culture was maintained for 24 h. Staining of vinculin (red), F-actin (green) and nucleus (blue). Scale bar is 100 μm. (n=3 per sample, 2 biological replicates).

Cell area and circularity were quantified by processing the actin fluorescence pictures. No statistically significant differences were found indicating that BMP-2 bound on FN-coated copolymers did not affect cell morphology (Figure 3.17, Figure 3.18).

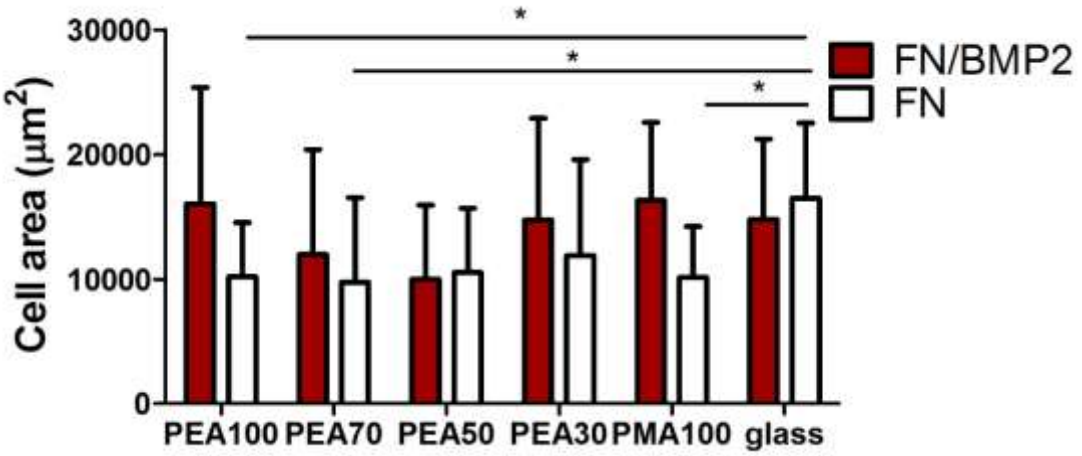

Figure 3.17. Area of hMSCs on FN/BMP-2 coated surfaces (red bars) and FN-coated bars (white bars) 24 h after culture. (25-30 images per condition were analysed. n=3 per sample, 2 biological replicates).

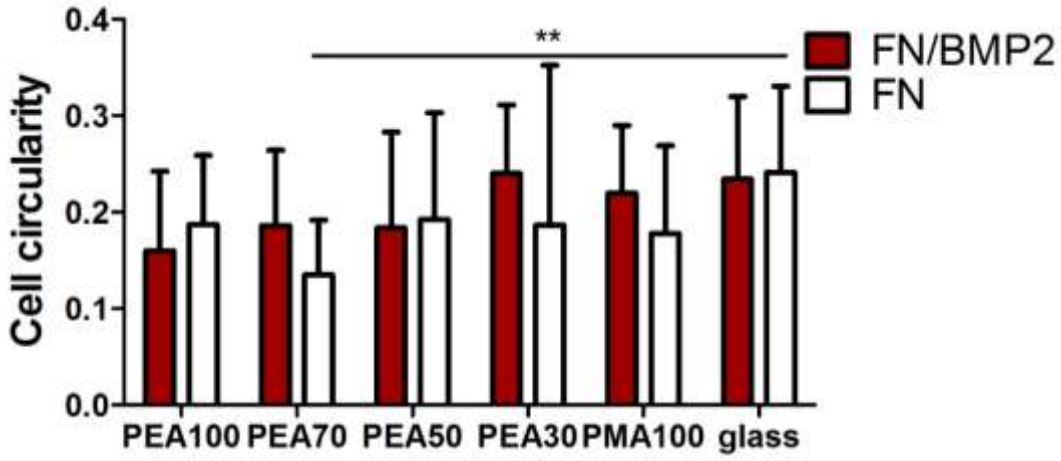

Figure 3.18. **Circularity of hMSCs on FN/BMP-2 coated surfaces (red bars) and on FN-coated bars (white bars) 24 h after culture.** (25-30 images per condition were analysed. n=3 per sample, 2 biological replicates).

3.3.4 Osteogenesis of hMSCs

3.3.4.1 RUNX2

The potential of the surfaces to guide hMSCs towards osteogenic lineage depending on the degree of FN fibrillogenesis was explored. Cells were cultured on surfaces after coating with FN and BMP-2 at low seeding density and low serum concentration. Surfaces coated only with FN were included as well. As a positive control, cells were seeded on FN-coated glass and culture was maintained in osteogenic medium. An ICW™ assay was performed 5 d after seeding to characterise RUNX2 expression normalised to the cell number.

RUNX2 expression was higher with increased EA/MA ratio on FN/BMP-2 copolymers 5 d after seeding. Higher RUNX2 expression was found on PEA where FN organises into a network-like conformation compared to PEA30 and PMA. In contrast, no difference in RUNX2 expression was found on FN-coated surfaces. Furthermore, RUNX2 expression was significantly higher on FN/BMP-2 coated PEA compared to PEA coated only with FN (Figure 3.19). Regarding the positive control, RUNX2 expression was similar compared to FN/BMP-2 coated PEA (Figure 3.19). These results demonstrate that the more extended conformation of FN has an effect on BMP-2 activity which subsequently alters RUNX2 expression.

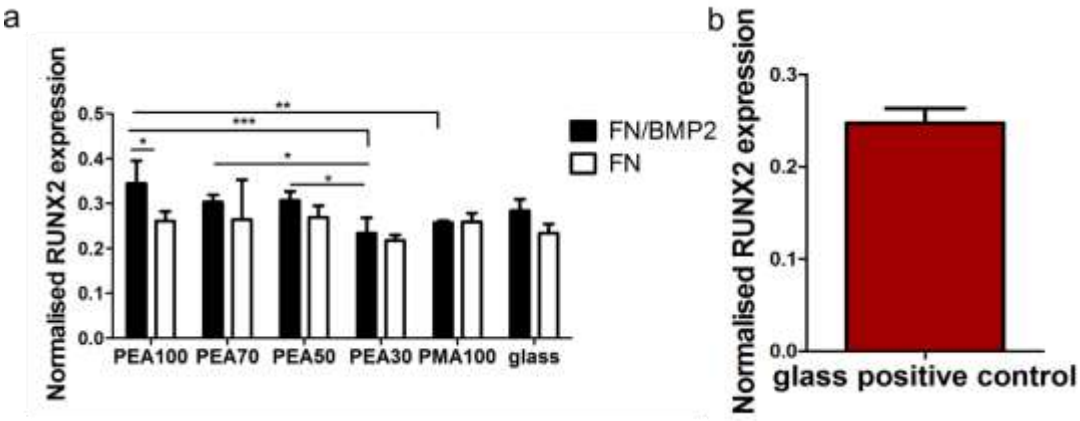

Figure 3.19. ICW™ analysis of RUNX2 expression on the copolymers at 5 d. (a) Graph shows RUNX2 expression in hMSCs seeded on FN/BMP2 coated (black bars) and FN coated (white bars) surfaces normalised to the cell number. (b) Graph shows RUNX2 expression by hMSCs seeded on FN coated glass in osteogenic medium. (n= 3 per sample, 1 biological replicate).

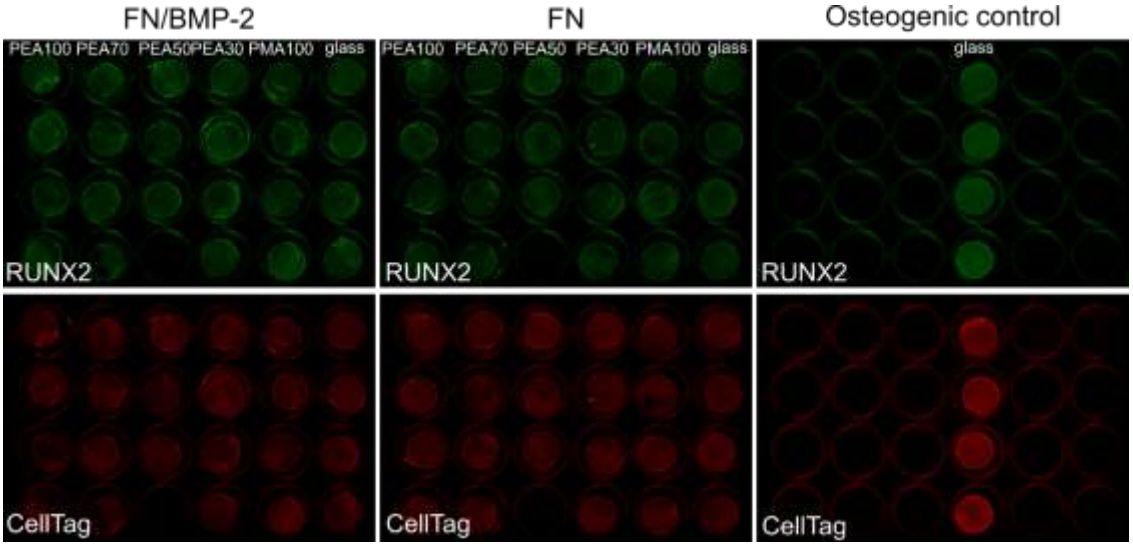

Figure 3.20. ICW™ plate image for RUNX2 expression at 5 d. hMSCs were seeded on FN/BMP2 coated (left), FN coated (middle) surfaces and on FN coated glass (right). Surfaces were incubated with an anti-RUNX2 antibody and with an infrared fluorescent dye detected at 800 nm channel (green). To normalise to the cell number, surfaces were incubated CellTag which is a near-infrared dye and is detected at 700 nm (red).

3.3.4.2 ALP expression over time

ALP expression was evaluated to further investigate hMSC osteogenic differentiation in the material interface. Initially, ALP expression was

characterised over time. Cells were cultured on glass coated with FN and BMP-2 at high seeding density. Culture was maintained in low serum concentration and ALP expression was determined by carrying out a colorimetric assay at three time points (1 d, 14 d and 21 d after seeding).

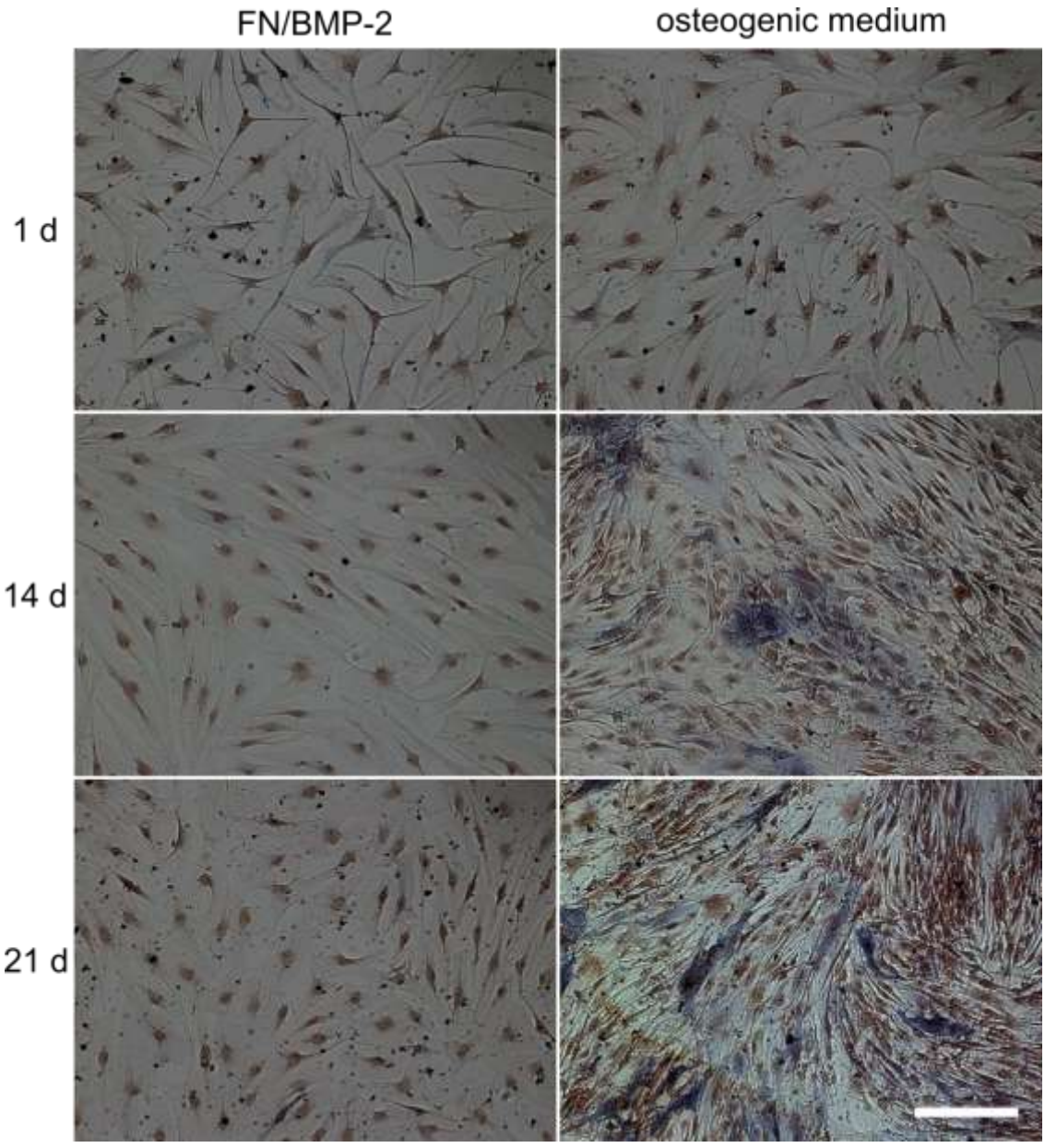

Figure 3.21. ALP expression in hMSCs. Cells were seeded on FN/BMP-2 coated glass (left column) and on FN-coated glass where osteogenic medium was used (right). Scale bae is 100 μm. (n=3 per sample).

The black aggregates on images demonstrate ALP expression (Figure 3.21). Image analysis and quantification showed that higher expression occurs 21 days after seeding. When hMSCs were cultured in osteogenic medium, increased cell proliferation and ALP expression were observed (Figure 3.22).

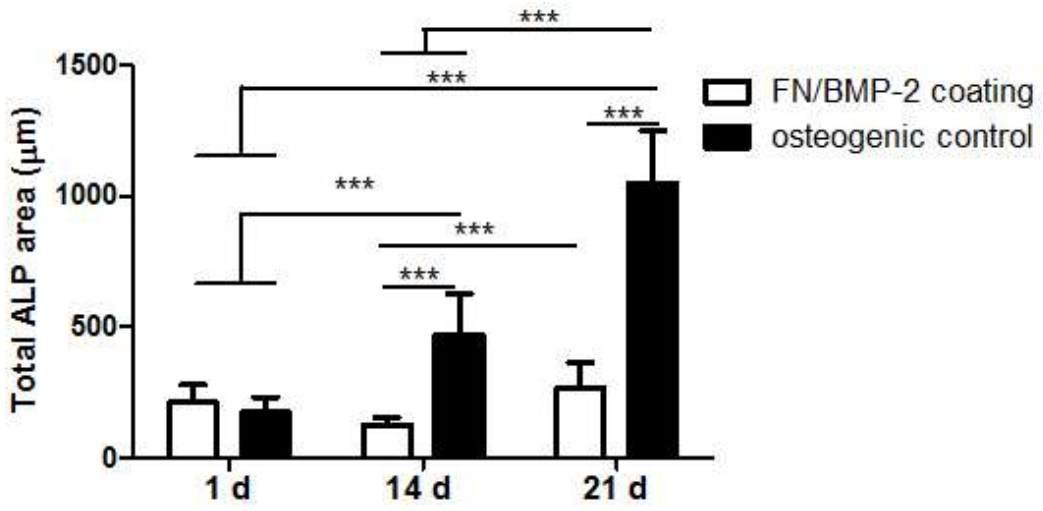

Figure 3.22. Quantification of ALP area. Cells were seeded on FN/BMP-2 coated glass (white bars) and on FN-coated glass where osteogenic medium was used (black bars). ALP staining was carried out 1 d, 14 d and 21 d after seeding. (20 pictures per condition were analysed, n=3 per sample, 1 biological replicate).

After assessing ALP expression over time, the assay was repeated including the copolymers. MSCs were seeded onto the copolymers coated with either FN/BMP-2 or FN and the culture was maintained for 21 d in low serum conditions. ALP aggregates were observed on all the FN-coated surfaces in both conditions (Figure 3.23, Figure 3.24).

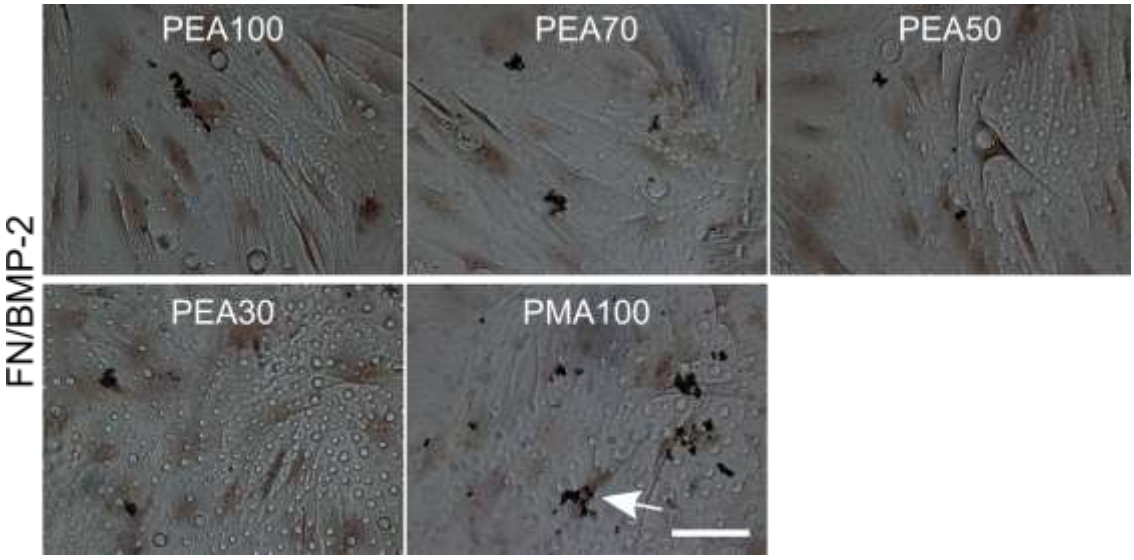

Figure 3.23. ALP expression. hMSCs were seeded on the copolymers coated with FN/BMP-2 and ALP expression was characterised 21 days after seeding. Scale bar is 100 µm. (n=3 per sample).

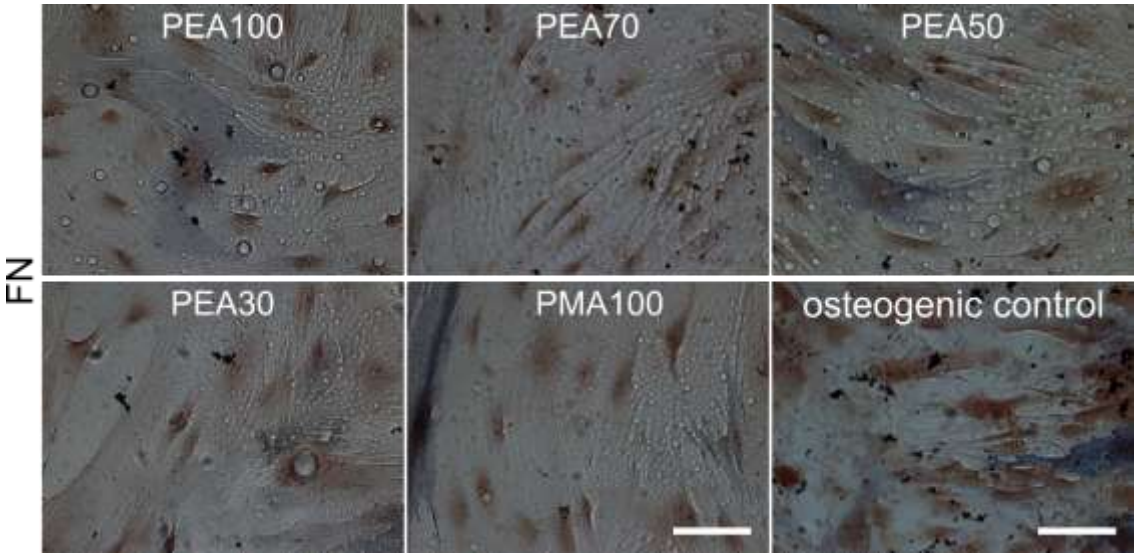

Figure 3.24. ALP expression. hMSCs were seeded on the FN-coated copolymers coated on FN-coated glass. Cells on FN-coated where incubated in osteogenic medium when they reached confluency. ALP expression was characterised 21 days after seeding. Scale bar is 100 μm.(n=3 per sample).

Segmentation of the images and quantification of ALP area showed higher ALP expression on FN/BMP-2 coated PMA where FN forms globular aggregates. ALP expression was significantly lower on the rest of the sample at both conditions (with or without BMP-2 coating) (Figure 3.25).

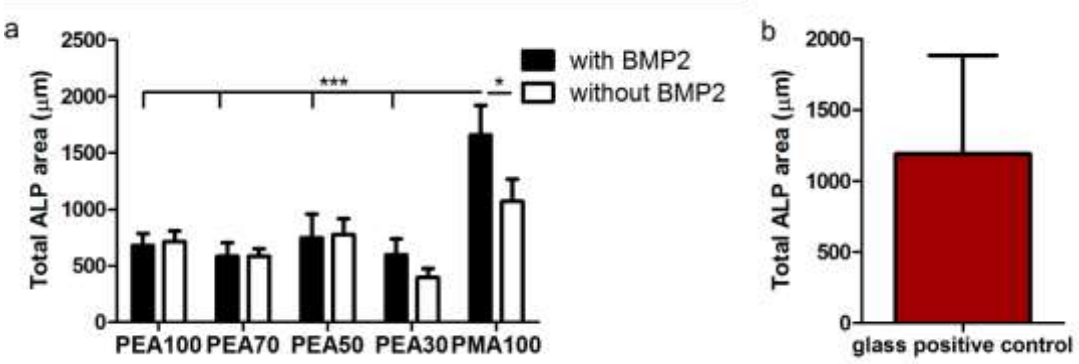

Figure 3.25. Quantification of ALP at 21 d (Figure 3.23, Figure 3.24). (a) Graph shows total ALP area on FN/BMP2 coated (black bars) and FN coated (white bars). (b) Graph shows total ALP area by FN coated glass where osteogenic medium was used. (20 images per condition were analysed, n=3 per sample, 1 biological replicate).

3.3.4.3 Osteocalcin

To further analyse osteogenic differentiation on the material interface, the expression of the late marker OCN was characterised. MSCs were cultured on FN/BMP-2 coated and on FN-coated surfaces. Cell culture was maintained for 21 d in low serum conditions. An immunofluorescence staining for OCN, actin and nuclei was carried out (Figure 3.26, Figure 3.27).

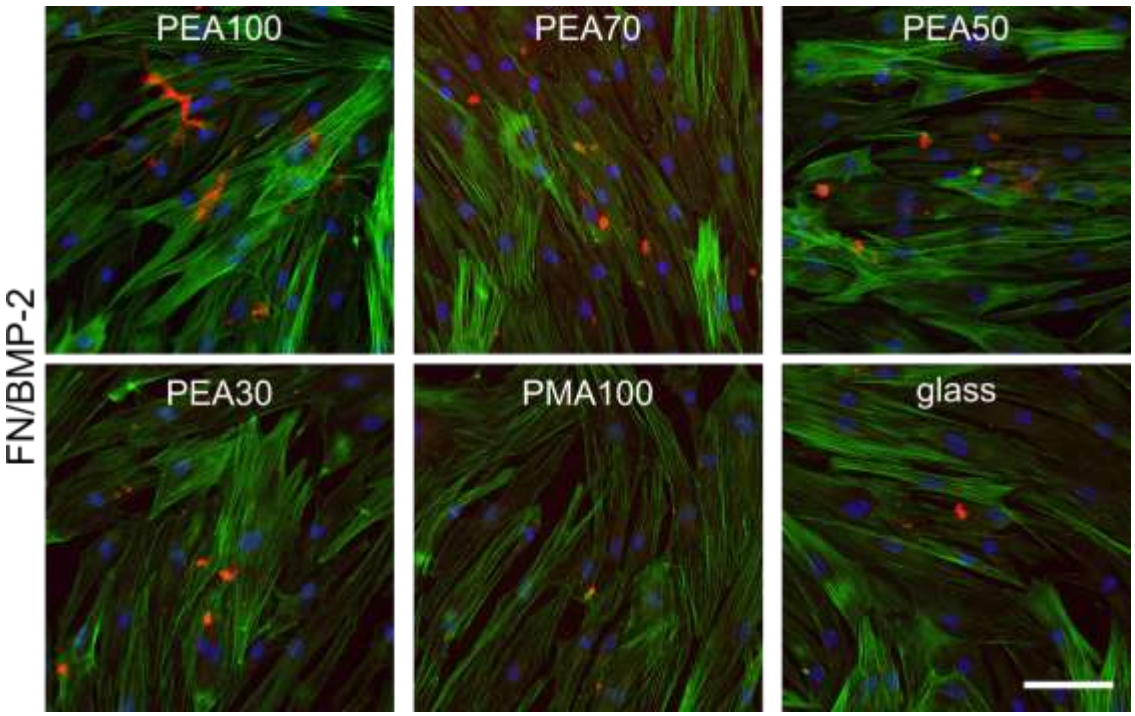

Figure 3.26. OCN expression in hMSCs at 21 d. Immunofluorescence images of hMSCs on FN/BMP-2 coated surfaces. Fluorescence staining of OCN (in red), F-actin (in green) and nucleus (in blue). Scale bar is 100 µm. (n=3 per sample).

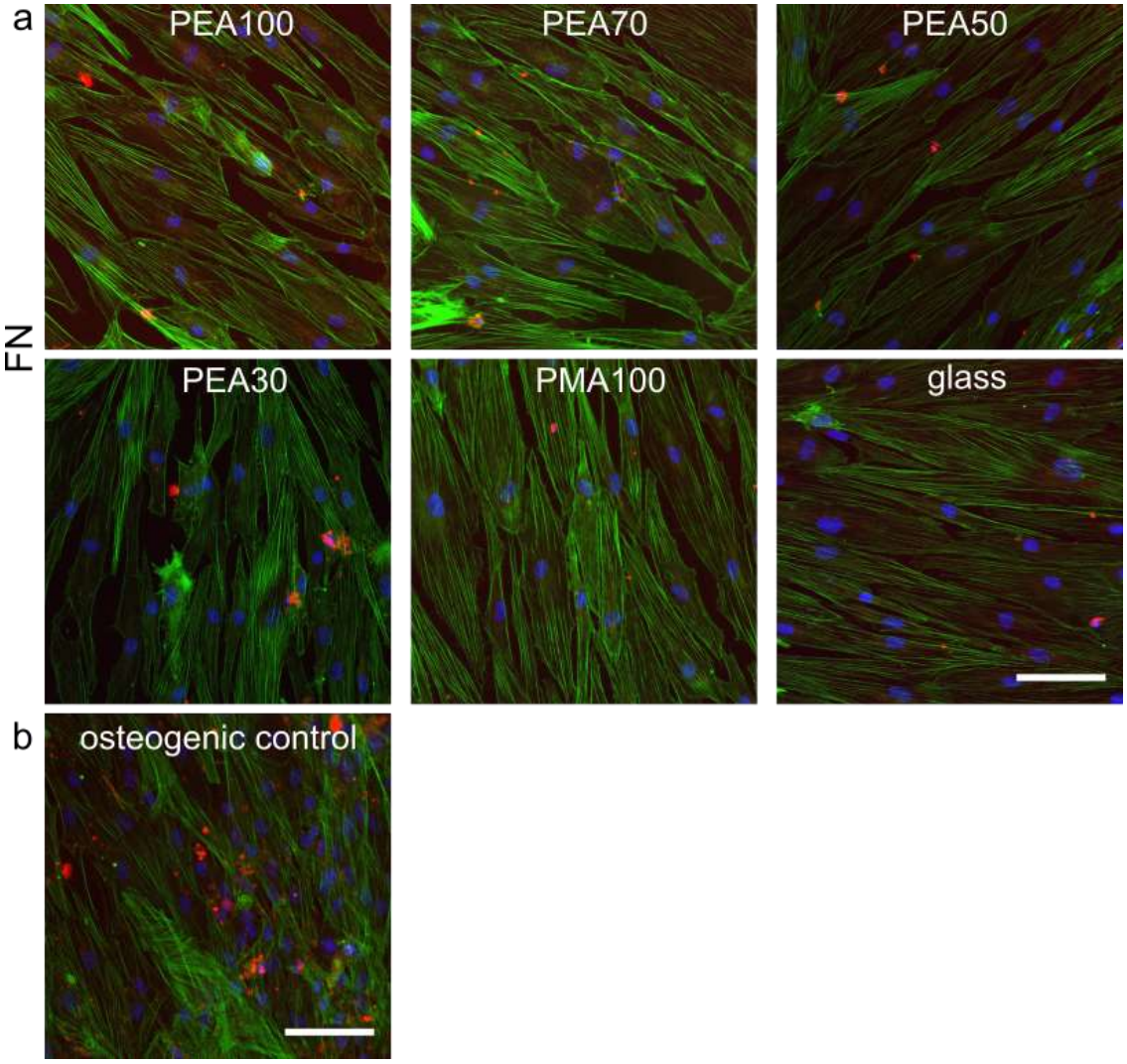

Figure 3.27. OCN expression in hMSCs at 21 d. (a) Immunofluorescence images of hMSCs on FN coated surfaces. (b) Osteogenic differentiation of hMSCs at 21 d with osteogenic medium. Fluorescence staining of OCN (in red), F-actin (in green) and nucleus (in blue). Scale bar is 100 μm. (n=3 per sample).

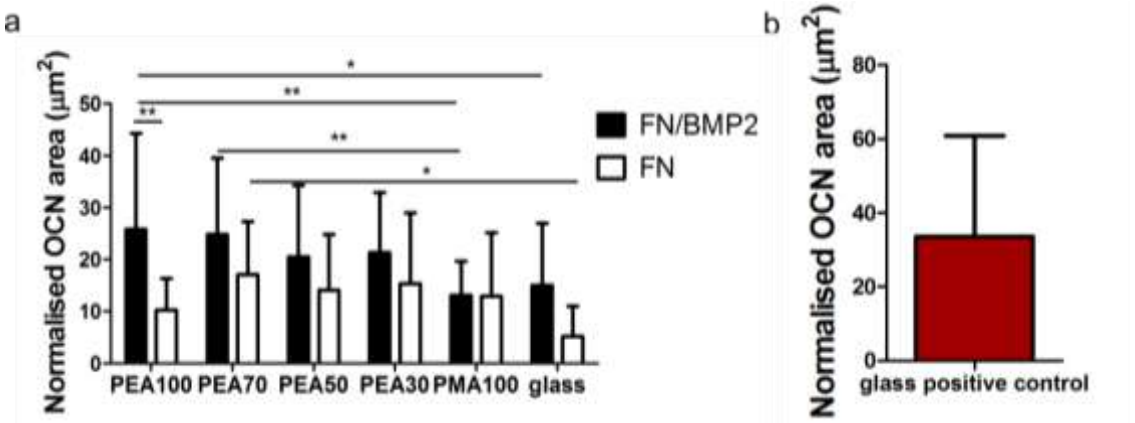

Figure 3.28. Quantification of OCN expression at 21 d (Figure 3.26, Figure 3.27). (a) Graph shows OCN expression in hMSCs seeded on FN/BMP2

coated (black bars) and FN coated (white bars) surfaces normalised to the cell number. (b) Graph shows OCN expression in hMSCs seeded on FN coated glass in osteogenic medium. (20 images per condition were analysed, n=3 per sample, 1 biological replicate).

Generally, more OCN aggregates were observed on copolymers coated with FN/BMP-2 in contrast to the FN-coated surface (Figure 3.28). Quantification of the fluorescence pictures demonstrated that OCN expression decreased with decreased EA/MA ratio when copolymers were coated with FN/BMP-2. PEA and PEA70, where FN adopts a more extended conformation, showed higher levels of OCN expression compared to PMA (Figure 3.28). In addition, PEA coated with FN/BMP2 elicited a higher OCN expression compared to control PEA. It should be noted though that the presence of BMP-2 did not have any effect on OCN expression on the copolymers. Additionally, OCN expression was higher when cells were incubated with osteogenic medium (Figure 3.28, b).

An ICW™ assay was carried out too. Cell culture was maintained for 21 d in low serum concentration and OCN expression was normalised to the cell number.

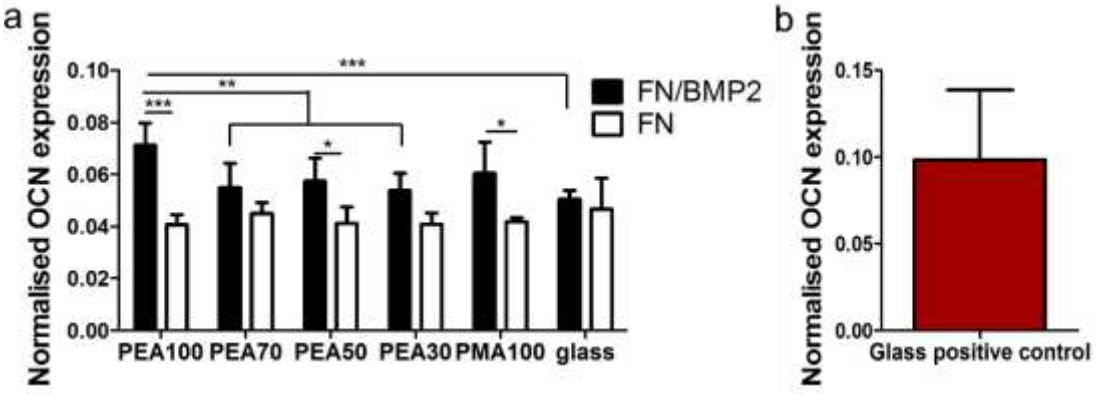

Figure 3.29. ICW™ analysis of OCN expression on the copolymers at 21 d. (a). Graph shows OCN expression in hMSCs seeded on FN/BMP2 coated (black bars) and FN coated (white bars) surfaces normalised to the cell number. (b) Graph shows OCN expression by hMSCs seeded on FN coated glass in osteogenic medium. (n=4 per sample, 1 biological replicate).

OCN expression decreased with decreased EA/MA ratio; higher on FN/BMP-2 coated PEA compared to PEA70, PEA50 and PEA30. In addition, BMP-2 coating caused an increased in OCN expression on PEA, PEA50 and PMA compared to control PEA, PEA50 and PMA (coated only with FN) (Figure 3.29, a). Furthermore, OCN expression on osteogenic control was higher than the rest of the conditions (Figure 3.29, b).

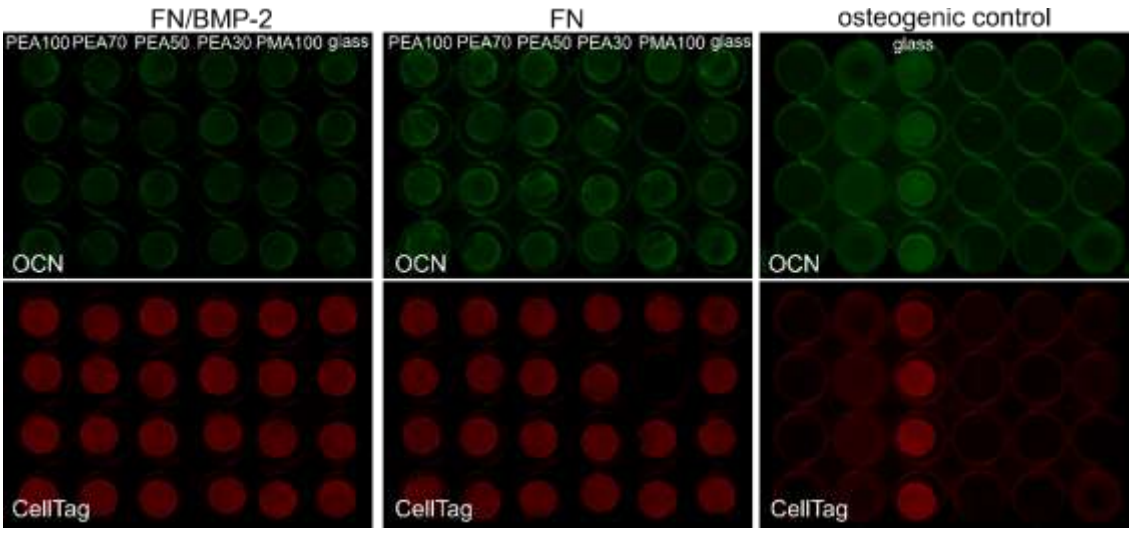

Figure 3.30. ICW™ plate image for OCN expression at 21 d. hMSCs were seeded on FN/BMP2 coated (left), FN coated (middle) surfaces and on FN coated glass (right). Surfaces were incubated with an anti-OCN antibody and with an infrared fluorescent dye detected at 800 nm channel (green). To normalise to the cell number, surfaces were incubated CellTag, which is a near-infrared dye and is detected at 700 nm (red).

3.4 Discussion

ECM is a complex three-dimensional network of non-cellular components. It provides not only a physical scaffold to cells but it also regulates a wide range of cellular processes including growth and differentiation. Understanding the cell-ECM interactions is critical in the development of material-based approaches which aim at tuning cell response. In the previous chapter, it was demonstrated that changes in the EA/MA ratio can determine the degree of FN fibrillogenesis which subsequently results in a differential availability of FN domains essential for cell attachment and growth factor binding. This chapter describes how these changes in FN activity can tune the response of hMSCs. Cell adhesion as well as osteogenic differentiation of hMSCs on the material interface were explored.

A short adhesion experiment showed that FN is required to promote cell adhesion. However, no significant differences were found in the number of hMSCs attached on the FN-coated surfaces (Figure 3.4). Another adhesion experiment was carried out at two time points (3 h and 24 h) in order to explore FA morphology as well as cell size and circularity. MSCs appeared well spread and formed FAs on all the surfaces over time (Figure 3.5, Figure 3.6). Analysis of FA area and length showed skewed distribution towards smaller FAs on all the surfaces (Figure 3.7, Figure 3.8). Analysis of the longer FAs (≥ 2 μm^2 and ≥ 3 μm) showed that longer FAs ≥ 3 μm were formed on PEA than on PMA at the early time point. The number of FAs was also higher (Figure 3.12). Quantification of cell area demonstrated higher cell spreading with increased EA/MA ratio at the early time point. Interestingly, the cell size decreased over time on all the surfaces apart from PMA where it remained constant over time (Figure 3.13). Contrary, cell circularity decreased with increased EA/MA ratio and it was higher on PMA at the early time point compared to the late time point. For the rest of the samples, cell circularity was similar at both time points (Figure 3.14). These results demonstrate that the more extended FN conformation, which corresponds to increased EA/MA ratio, promotes the spreading of MSCs at an early time point. Interestingly, cell size decreased significantly over time. In *in vitro* cell adhesion, cells initially sense their substrate *via* attachment followed by spreading of the cell body, and the organisation of actin cytoskeleton[257]. The decrease in cell size at the late time

point suggests that cells have adapted to their environment and as a result their response is different.

During cell spreading, cells interact with ECM *via* integrin receptors which contribute to signal transmission. FN, in particular, supports cell adhesion *via* binding of the integrins including $\alpha_5\beta_1$, $\alpha_v\beta_1$ and $\alpha_v\beta_3$ to the RGD and PHSRN motif[45, 59, 258]. In addition, interruption of the synergistic RGD-PHSRN interaction reduces cell attachment and influences downstream FAK signalling[259]. It was previously described that the availability of the FNIII8 and FNIII9-10 domains (Figure 2.10, Figure 2.12) in the surfaces increases with higher EA/MA ratio which indicates a more connected and extended FN network. Therefore, cells might attach and spread better on surfaces with increased EA/MA ratio because more sites for integrin binding are available therefore integrin binding with higher affinity can be achieved. Decreased cell circularity with increased EA/MA ratio also shows that cell morphology depends on the conformation of the underlying layer of adsorbed FN. Cells become rounder on surfaces where FN appears in a globular morphology further suggesting that this specific FN organisation is less favourable for integrin engagement and cell spreading.

The FNIII12-14 domain acts as a highly promiscuous growth factor binding site[70, 260]. BMP-2 has been studied extensively in order to study signalling pathways which control several aspects of cell behaviour. For example, immobilised BMP-2 has been shown to regulate cell adhesion and osteogenic differentiation as well as to control downstream signalling pathways[223, 261, 262]. This work explores the potential of the copolymers to drive hMSC osteogenesis using BMP-2 bound on FN-coated materials. To do so, the expression of known osteogenic markers was characterised at different time points. As previously described, RUNX2 is a major regulator of osteogenic differentiation[126]. In this work, hMSCs were seeded on FN/BMP-2 coated copolymers and RUNX2 expression was characterised by performing an ICW™ assay 5 d after seeding (Figure 3.19). RUNX2 expression was enhanced with increased EA/MA concentrations and, particularly, it was higher on FN/BMP-2 coated PEA compared to PEA30 and PMA. In addition, FN-bound BMP-2 on PEA induced higher RUNX2 expression compared to the control PEA (without

BMP-2). However, BMP-2 binding did not affect its expression in the rest of the samples. In a previous study, the RGD and PHSRN motifs were chemically inserted onto Ti surfaces in order to characterise how their spatial distribution affects hMSCs response. Higher RUNX2 expression was reported on surfaces presenting both domains compared to surfaces presenting the PHSRN motif alone and higher mineralization occurred when these domains were properly spaced[263]. Another study also examined the synergistic effect of RGD and BMP-2 peptides on promoting osteogenic commitment. Cells seeded on these surfaces appeared more differentiated as indicated by a decrease of the stemness marker STRO-1 and an increase in RUNX2 expression[264]. It can be postulated that the extended network of FN provides a better substrate for cell adhesion and BMP-2 presentation. Therefore, cells receive signals more efficiently in order to commit towards the osteogenic lineage.

ALP is commonly considered an early marker of osteogenesis, therefore its expression was also characterised. First, ALP expression was characterised over time. To do so, MSCs were seeded on FN/BMP-2 coated glass samples and ALP expression was measured at three time points (1 d, 14 d and 21 d after seeding). Higher ALP expression was found 21 d after seeding (Figure 3.22). Following this result, ALP expression on the copolymers was measured after 21 d (Figure 3.25). Higher ALP expression was found on FN/BMP-2 coated PMA compared to the rest of the samples. In addition, ALP expression was similar on the rest of the samples. Even though ALP is known to be involved in bone matrix mineralisation and osteogenesis, it might also indicate a less differentiated stem cell state. For example, it has been associated with the undifferentiated ESCs[148] and iPSCs[265]. In addition, ALP^+ stem cells were found to express higher levels of STRO-1. They also expressed higher levels of the stemness genes OCT4, Nanog and Sox2 compared to ALP^- stem cells[266]. Differential ALP expression of MSCs have been also reported depending on the tissue of origin[267]. It can be hypothesized that MSCs maintain their stemness when cultured on FN/BMP-2 coated PMA where FN is presented in globules. This is in line with the higher RUNX2 expression observed on FN/BMP-2 coated PEA but not PMA. These results suggest that hMSCs are already committed to osteogenic differentiation on PEA.

The matrix protein OCN is regularly a positive marker of osteogenesis and its expression was characterised 21 d after seeding. Immunofluorescent staining and image quantification showed increased OCN expression with increased EA/MA ratio (higher expression on FN/BMP-2 coated PEA and PEA70 compared to PMA) which corresponds to a more connected FN network (Figure 3.26, Figure 3.27). ICW™ assay showed similar results; higher OCN expression on FN/BMP-2 coated PEA compared to PEA70, PEA50 and PEA30 (Figure 3.29). In both cases, OCN expression remained constant on the control samples. This result show that bound BMP-2 enhanced osteogenesis on the surfaces displaying a higher degree of FN fibrillogenesis. This is in accordance with the high RUNX2 expression of hMSCs found on FN/BMP-2 coated PEA compared to PEA30 and PMA.

Based on the results, the degree of FN fibrillogenesis determined by the EA/MA ratio has an impact on FN ability to drive MSCs towards the osteogenic commitment. Higher RUNX2 and OCN expression was found on FN-coated PEA presenting BMP-2 whereas a decrease was found when FN network was less connected. A previous study showed that RUNX2 alone is not sufficient for inducing osteoblastic-specific gene expression, such as OCN, and BMP-2 is required for signal transduction[268]. In addition, several studies have associated the RGD domain with osteogenic differentiation. Garcia *et al*. reported that myogenic differentiation of C2C12 cells required binding to the RGD domain of FN[66]. Similarly, surface chemistry affected the osteogenic differentiation of osteoblast precursor cells through the binding of specific integrin receptors on RGD domain of adsorbed FN[197]. The $FNIII_{12\text{-}14}$ domain is also important in differentiation. Martino *et al*. reported enhanced morphogenesis when the integrin binding domain (FNIII9-10) and the growth factor binding domain (FNIII12-14) of FN are in close proximity suggesting synergistic signalling between the $\alpha_5\beta_1$ integrin and the growth factor receptors[269].

In chapter 2, it was also demonstrated that the FNIII12-14 domain becomes less available with increased concentration of MA units, and in particular, PEA30 and PMA displayed lower availability (Figure 2.11). It can therefore be suggested that a higher degree of FN fibrillogenesis is necessary for the MSCs to receive outside signals and display a more osteogenic phenotype. In

addition, immunogold staining showed higher BMP-2 binding on PEA and PEA70 but not on PEA50, PEA30 and PMA, demonstrating that BMP-2 is better presented on the open conformation of FN (Figure 2.14). It can be hypothesised that the well-connected network of FN on PEA allows the integrin binding domain of FN and BMP-2 to be in a closer proximity. This might lead to a more effective crosstalk resulting in enhanced osteogenic differentiation on PEA. With the introduction of MA units however, FN network appears less connected and globules are present on PEA30 and PMA. Adopting this conformation, the $FNIII_8$, $FNIII_{9-10}$ and $FNIII_{12-14}$ domains become less available which might hinder the integrin/BMP-2 interaction. Subsequently, MSCs cannot efficiently interact with their environment and their potential to differentiation is poor. It is also important to note that the whole FN protein was used for the coatings in order to recapitulate to a degree the multifunctional nature of the complex ECM protein network. This system provides increased affinity as well as domains for cell adhesion and growth factor binding. However, it also increases the complexity of FN conformation upon adsorption. It can be thus suggested that structural changes which have not been investigated might contribute to the differential cell response.

4. Integrin adhesome

4.1 Introduction

As already described, FAs are dynamic multiprotein structures which physically connect the actin cytoskeleton to the ECM. FAs serve as anchors and allow cell attachment to the surrounding environment. They also contribute to signal transduction through integrins and trigger signalling pathways which regulate a wide range of cell functions, such as migration. The diverse functions of FAs are reflected in their protein composition which changes in response to external physical and mechanical signals. For example, FAs undergo spatiotemporally cycles of assembly and disassembly during cell migration[270]. In addition, FAs composition changes in response to changes in force in order for cells to probe and respond to their mechanical environment [271, 272].

Due to the molecular heterogeneity of adhesion structures and their dynamic nature, analysis of the FA protein composition and their interactions under different biological conditions is rather challenging. Techniques aiming at isolating FAs in combination with proteomic approach have contributed to the identification of proteins involved in the formation of FAs as well as the molecular mechanism directing their interactions. Proteomics is essentially a large-scale study of a set of proteins with regard to expression, structure, function, modifications, interactions, and changes in different environments and conditions[273]. The development of new strategies for peptide sequencing using mass spectrometry (MS) has been critical to the rapid advance of proteomics[274]. In general, a mass spectrometer consists of an ion source and a mass analyser. This instrument ionises sample molecules in a gas phase and then the ions are separated based on their mass-to-charge (m/z) ratio. There are two relevant techniques for ionization: matrix assisted laser desorption/ionization (MALDI) and electrospray ionization (ESI). Both approaches are able to ionise large and polar molecules without physically destroying them. Their difference is that a peptide mixture is co-crystallised with a UV laser in MALDI whereas the peptide mixture is ionised in a liquid solvent system which can be coupled to liquid-based separation method[273].

The complex protein network which FAs form has been collectively described as the ‘integrin adhesome’[275]. Progress in proteomics has considerably increased the number of FA components. Recent attempts to explore the

adhesome composition based on immunohistochemistry and proteomic analysis have identified more than 200 proteins as components of the adhesome[276-278]. Zaidel-bar *et al*. combined data from published experimental studies and reported that FA components can be intrinsic and physically reside in adhesion sites or they can be adhesion-associated, interacting with the intrinsic proteins and regulating their function[279].

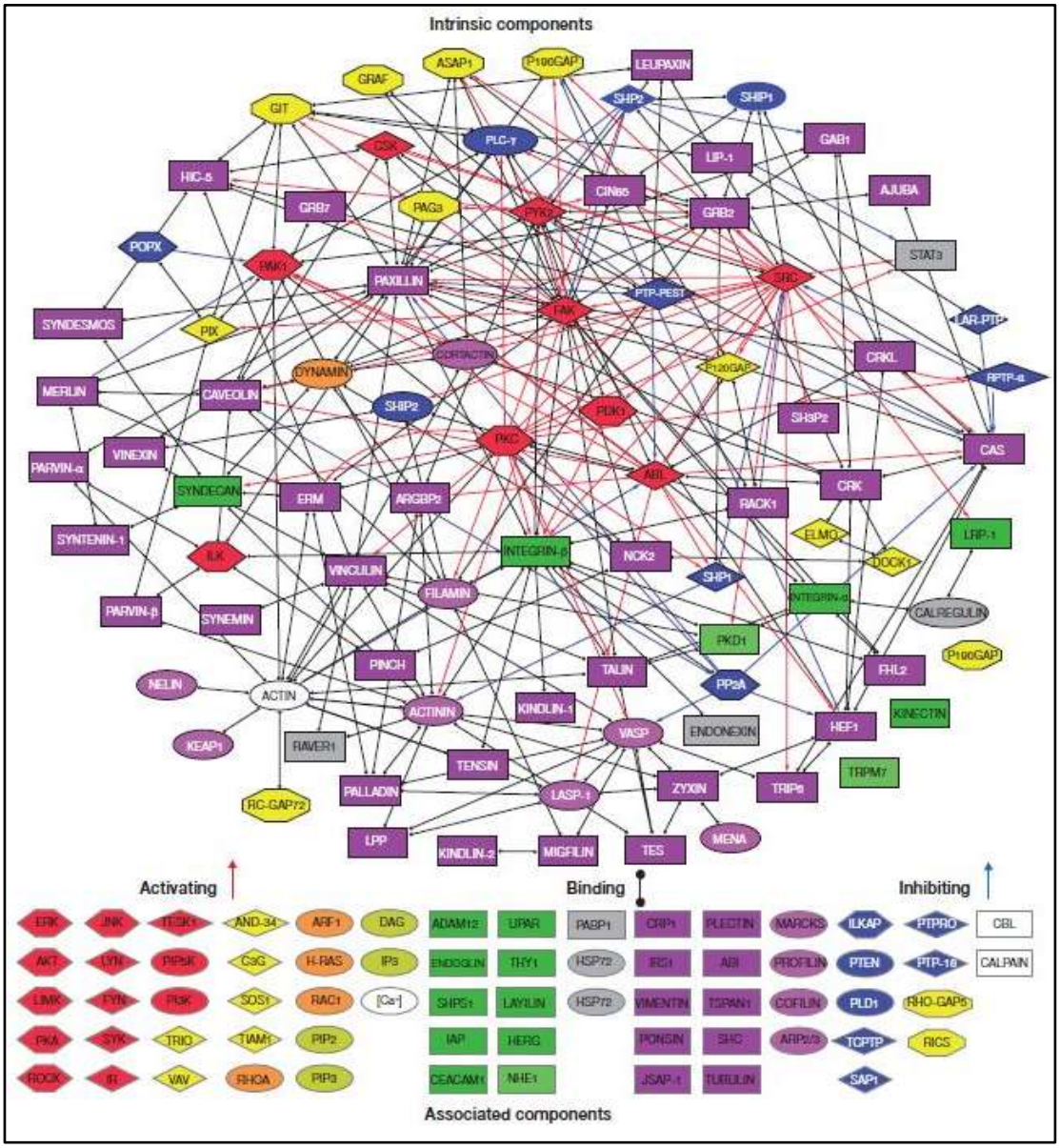

Figure 4.1. The adhesome network[279]. The network consists of 156 intrinsic and associated components and include serine/threonine protein kinases/phosphatases, tyrosine kinases/phosphatases, integrins, cytoskeletal and adaptor proteins, actin-binding proteins and adhesion proteins[279].

Proteomic studies have given important insights into the architecture of the adhesome as well as into the signals transduced across the network. The adhesome is a highly connective network and it is regulated by transient interactions between adhesome proteins and by signalling events. Methods for studying the adhesome are based on isolating these components by removing the cell body and nucleus. For example. ice-cold water to weaken the cells followed by hydrodynamic force has been used[280]. In another study, cells were treated with a hypotonic solution which contained triethanolamine (TEA) to isolate and maintain the native FA composition. This is a low ionic strength buffer which causes cell swelling and weakens the integrity of the cell membrane by inducing osmotic pressure inside the cell. After that step, membrane bound organelles, actin cytoskeleton and nuclei were washed off by hydrodynamic force using a Waterpik dental jet[281].

The aim of this work is to develop a protocol to isolate FA of MSCs cultured on PEA and PMA in order to determine substrate-dependent differences in protein composition. We hypothesise that the differential conformation of adsorbed FN might result in changes in the protein composition of FAs and we seek to identify such differences. As shown by previous studies that have isolated FA components for MS, a different set of proteins were enriched on cells cultured on FN- compared to poly-D-Lysine- coated dishes[282]. To do so, a previously outlined method was used where cells are incubated in TEA and PBS flow is used to remove the cell body and isolate FAs on the surfaces. Immunofluorescent staining of vinculin was used to validate the efficiency of the method. Finally, extracted proteins extracted from PEA, PMA and glass were analysed by MS.

4.2 Materials and methods

4.2.1 Materials

List or reagents	
Dulbecco's modified Eagle's medium (high glucose)….	PromoCell®
Dulbecco's modified Eagle's medium (low glucose)…....	Sigma
Dulbecco's phosphate buffered saline……..	Life Technologies
Glutamax……	Sigma-Aldrich
Penicillin/streptomycin…….	Sigma
Foetal bovine serum…….	Life Technologies
Trypsin/EDTA…….	Sigma
Formaldehyde……	Fischer Scientific
Human plasma fibronectin……...	R&D
Sodium dodecyl sulfate……	VWR
Mouse monoclonal anti-vinculin antibody…….	Sigma
Tween20®……...	Sigma
Triton® X 100……..	Sigma
Bovine serum albumin……..	Roche/Sigma
Biotinylated anti-mouse antibody……	Vector Laboratories
Fluorescein streptavidin……...	Vector Laboratories
Rhodamine-phalloidin……..	Invitrogen
Vectashield with DAPI……..	Vector Laboratories
Cy-3 anti-mouse antibody……	Jackson ImmunoResearch
FASP kit……..	Expedeon

4.2.2 C2C12

C2C12 cells were purchased from Sigma-Aldrich. For expansion, cells were thawed and maintained in DMEM supplemented with 20% v/v FBS 1% v/v penicillin/streptomycin at 37 °C and 5% CO_2. Cells were harvested when they reached 70%-80% confluency. They were washed with PBS followed by 2 ml of trypsin/EDTA. After removing trypsin/EDTA, cells were incubated at 37 °C until detached from the flask. Next, 4 ml of complete medium was added to the flask and cell suspension was transferred to a falcon tube. Cell density was measured using a Neubauer haemocytometer. Cells were used at passages P0 to P5.

4.2.3 Human Mesenchymal Stem Cells

MSCs were maintained in DMEM containing 10% v/v FBS and 1% v/v at 37°C and 5% CO_2. Harvesting and splitting was carried out as described in section 3.2.2. Cells were used at passages P0 to P5.

4.2.4 Cell culture

UV-sterilised PEA, PMA and glass samples were coated with FN at 20 µg/ml for 1 h. Cells were harvested by trypsinisation and cell suspension was diluted in FBS-free medium to a final density of 2500 cells/cm^2. Cells were seeded onto the surfaces and maintained in serum free conditions for 3 h. After that, medium was replaced with medium containing 20% v/v (for C2C12 cells) and 10% v/v FBS (for MSCs). Culture of C2C12 and MSCs was maintained for 1 d and 3 d respectively at 37 °C, 5% CO_2.

4.2.5 Optimisation of FA isolation using C2C12 cells

For the isolation of FAs, a TEA-containing solution was prepared (2.5 mM in PBS, pH 7.2). One day after seeding, cells were washed with warm PBS and were incubated with the TEA solution for 3 minutes. Next, cells were washed with PBS for 10 sec using a dental waterpik at its highest, medium or lowest pressure. The extension tip of the waterpik was kept perpendicular to the surface and it was manually moved from the one end of the coverslip to the other.

4.2.6 Optimisation of FAs isolation using MSCs

MSCs were seeded on PEA, PMA and glass and culture was maintained for 3 d. To isolate FAs, two approaches were carried out. In a first attempt, cells were washed with warm PBS and incubated with a 2.5 mM TEA-containing solution for 3 min. Next, a round mask fitted on top of the sample at a distance of 1 mm was used. The mask had on hole in the middle with the same diameter size as the waterpik tip. Next cells were washed with PBS for 10 sec. In a second attempt, cells were incubated with TEA for 2 min and a mask with three holes was fitted on top of the samples. Cells were washed with PBS for 5 sec by adjusting the tip in two of the holes (Figure 4.2).

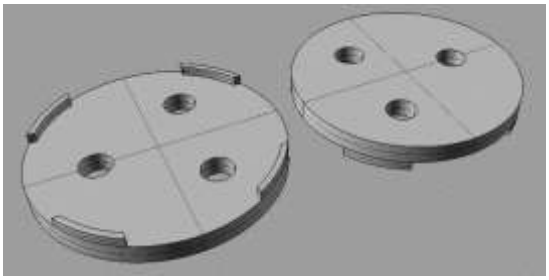

Figure 4.2. Mask used for flashing the cells with PBS. The tip of the waterpik jet was fitted in two off the holes.

4.2.7 Immunohistochemistry

After treatment of cells with TEA solution and washing with PBS, cells were fixed (3.7% v/v formaldehyde/PBS) for 30 min at 4°C. C2C12 cells were washed with PBS and were permeabilised for 5 min. Next, samples were incubated with blocking solution (1% w/v BSA/PBS) for 30 min. Primary antibody containing mouse monoclonal anti-vinculin antibody was prepared in blocking solution. Cells were incubated with the solution at 4 °C overnight. The next day, samples were washed three times (0.5% v/v Tween-20/PBS) for 5 min. Then, secondary antibody was prepared in blocking solution containing biotinylated anti-mouse antibody for 1 h at 37 °C. Samples were washed again and incubated with fluorescein streptavidin and rhodamine-phalloidin for 30 min at 37 °C in dark. Next, cells were washed and mounted with vectashield containing DAPI. The protocol for staining of MSCs is described in section 3.2.6.

4.2.8 Cell imaging

Fluorescent pictures were taken using an epifluorescence microscope (Zeiss AXIO Observer Z1, Jena, Germany).

4.2.9 Solubilising of FAs

Samples were incubated with 100 µl of 1% w/v sodium dodecyl sulfate solution for 30 sec. A cell scrapper was used to remove the remaining proteins from the surfaces. Protein solution was extracted from 5 samples per condition, transferred to a low binding protein tubes and stored at -80°C.

4.2.10 Filtered-aided sample preparation

First, a urea sample solution was prepared by adding 1 ml of Tris hydrochloride solution to one tube of urea. In addition, a 10x iodoacetamide solution was prepared by adding 100 µl urea sample solution to one tube of iodoacetamide provided with the kit. Next, 200 µl of urea solution was mixed with the protein extract. The solution was transferred in a spin filter and centrifuged at 14000 x g for 15 min. Next, 10 µl of 10x iodoacetamide solution and 90 µl of urea solution were added to the spin filter and were vortexed for 1 min and afterwards they were incubated without mixing in dark. After 20 min, the spin filter was centrifuged at 14000 x g for 10 min. Next, 100 µl of urea solution was added to the spin filter which was centrifuged at 14000 x g for 15 min. After repeating this step twice, the flow-though was discarded from the collection tube. Next, 100 µl of 50 mM ammonium bicarbonate solution were added to the filter and centrifuged at 14000 x g for 10 min. This step was repeated twice. Next, 75 µl of digestion solution was added and vortexed for 1 min. The filter was incubated at 37 °C for 4 h was transferred to a new collection tube. 40 µl of 50 mM ammonium bicarbonate solution were added and the filter was centrifuged for 10 min and this step was repeated once. Next, 50 µl of sodium solution were added and the filter was centrifuged for 10 min. Finally, the filtrate contained digested proteins and was acidified with trifluoroacetic acid.

4.2.11 Mass spectrometry

The digested peptides were analysed by ESI Fourier transform ion cycolotron resonance mass spectrometry. Data was processed using the automated Matrix Science Mascot Daemon server (v 2.6.0) allowing a mass tolerance of 0.5 Da.

4.2.12 Identification of FA proteins

In order to identify the set of proteins previously identified as adhesion components, the adhesome website (http://www.adhesome.org/) was used. The adhesome network was developed from the biomedical literature and consists of 150 components of FAs which are both intrinsic and associated proteins.

4.2.13 Protein abundance

Mascot uses the mass values and calculates the probability, P, that the observed match between the experimental data and the database sequence is a random event. The match with the lowest probability is reported as the best match. Protein score is the sum of identification scores of its peptides. There are different approaches to obtain quantitative proteomic information about protein abundance. For example, a high protein score has been used to characterise protein abundance[283]. However, scores have been considered a poor estimate of protein abundance[284]. Instead, more accurate 'protein abundance indices' have been developed and essentially represent the number of observed peptides divided by the number of observed peptides per protein[285]. Ishima *et al*. reported that the relationship between the number of peptides identified and the protein amount in a sample is logarithmic, described by the term exponentially modified protein abundance index (emPAI). emPAI offers a label-free quantitation of the proteins in a mixture based on protein coverage by the peptide matched[286]. The FA proteins were analysed based on both the emPAI and P.

4.2.14 Principal component analysis

In order to determine whether the results are variable, the protein hits were associated with the corresponding gene using the Entrez Gene database in NCBI. Next, a principal component analysis (PCA) based on the emPAI and P was carried out in R.

4.2.15 Gene ontology and enrichment analysis

The PANTHER (Protein Analysis THrough Evolutionary Relationships, v11.1) classification system[287] was used to carry out a Gene Ontology (GO) classification. Two protein lists were generated for classification. The first list contained the FA proteins and the second one contained the rest of the identified proteins. Classification was performed according to the protein class, molecular function and biological process. The DAVID (Database for Annotation, Visualization and Integrated Discovery, v6.1) bioinformatics resource[288] was used to characterise gene abundance.

4.3 Results

4.3.1 Optimisation using C2C12

Initially, C2C12 cells were used to optimise the protocol. Cells were cultured on FN-coated PEA, PMA and glass in serum free conditions for the first 3 h and, next, in complete medium. After 24 h, cells were treated with TEA solution for 3 min. In order to assess the effect of PBS pressure, waterpik was set at the highest, intermediate and lowest setting and the tip was moved manually over the surfaces. To evaluate the results, a vinculin, actin and nucleus staining was carried out.

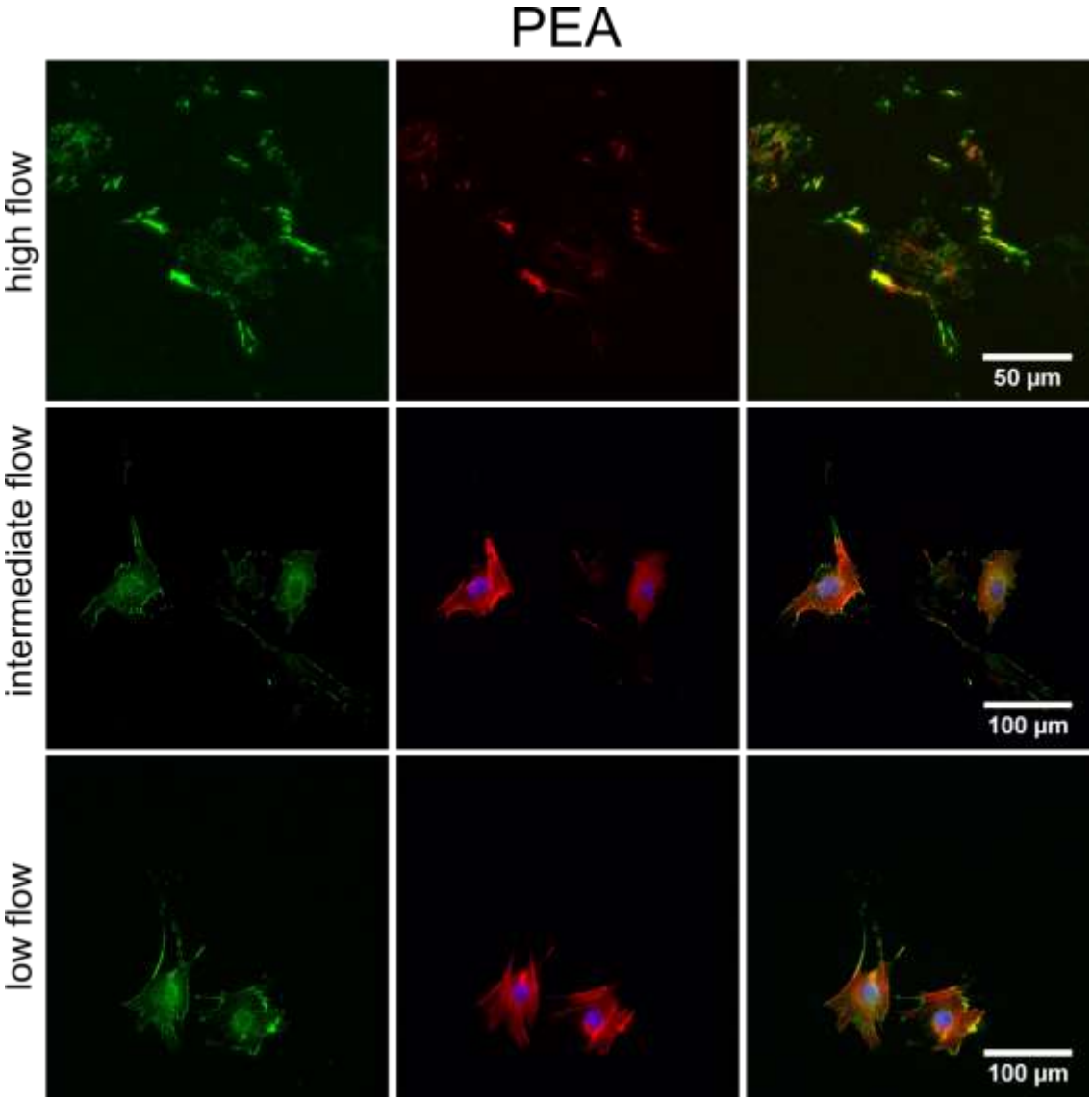

Figure 4.3. Immunofluorescence images of C2C12 cells on FN-coated PEA 1 d after seeding. Cells were treated with TEA for 3 min and washed with PBS at the highest (top row), intermediate (middle row) or low pressure (bottom

row). Staining of vinculin (green) actin (red) and nuclei (blue). Scale bar is 50 µm (top row) and 100 µm (middle and bottom row). (n=1 per sample).

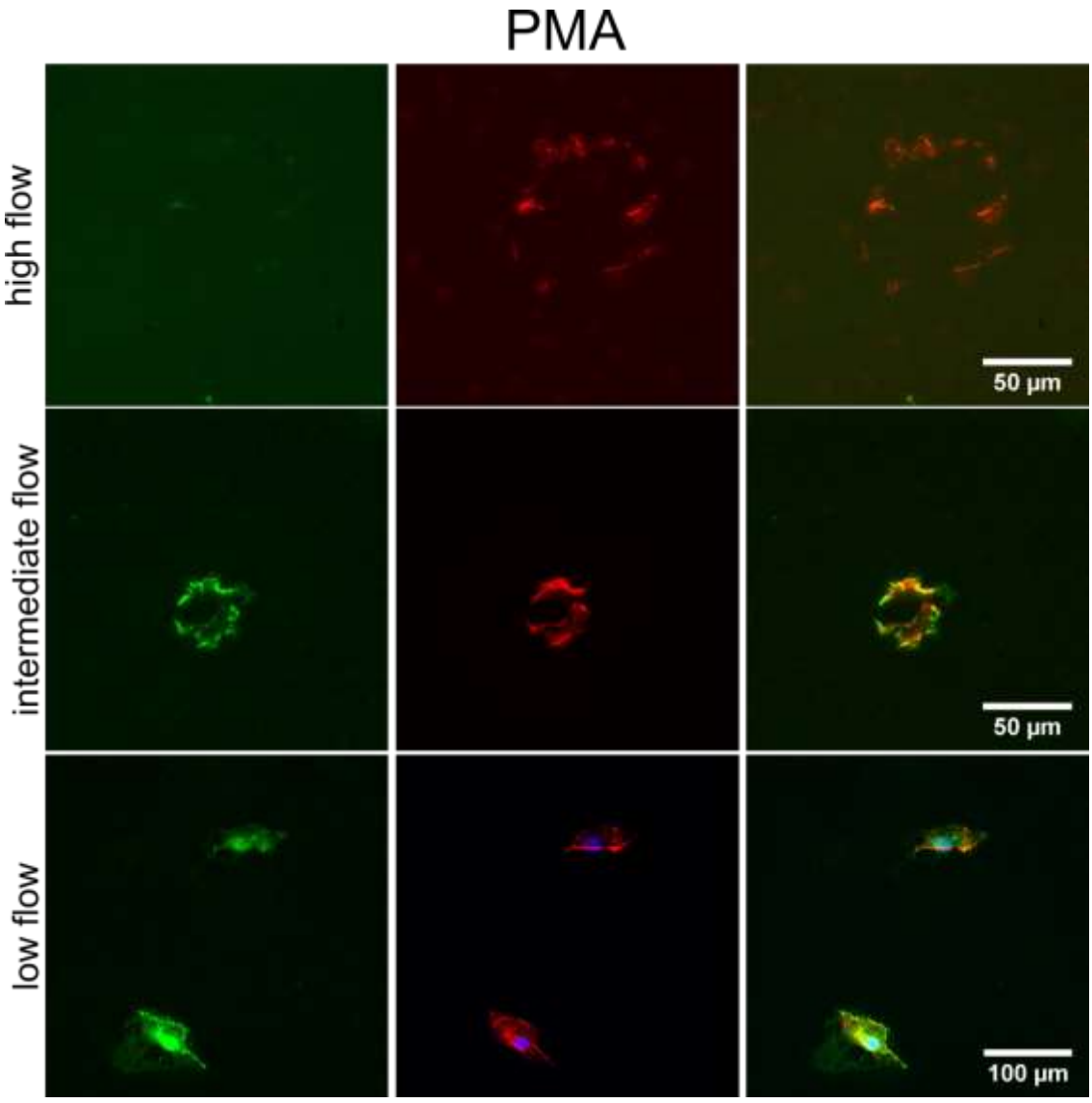

Figure 4.4. Immunofluorescence images of C2C12 cells on FN-coated PMA 1 d after seeding. Cells were treated with TEA for 3 min and washed with PBS at the highest (top row), intermediate (middle row) or low pressure (bottom row). Staining of vinculin (green), F-actin (red) and nuclei (blue). Scale bar is 50 µm (top and middle row) and 100 µm (bottom row). (n=1 per sample).

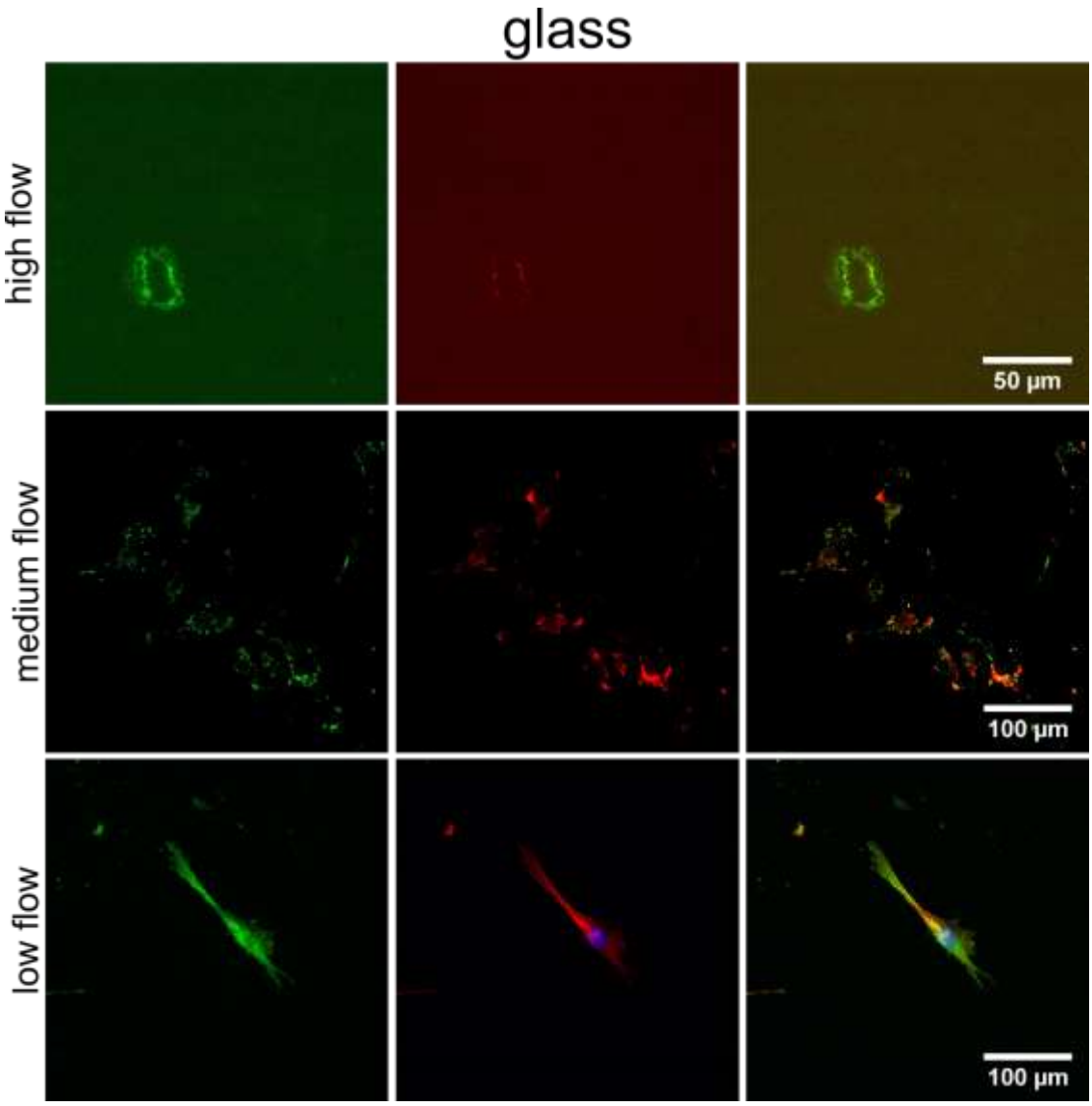

Figure 4.5. Immunofluorescence images of C2C12 cells on FN-coated glass 1 d after seeding. Cells were treated with TEA for 3 min and washed with PBS at the highest (top row), intermediate (middle row) or low pressure (bottom row). Staining of vinculin (green), F-actin (red) and nuclei (blue). Scale bar is 50 µm (top row) and 100 µm (middle and bottom row). (n=1 per sample).

Washing off the cells at the highest waterpik pressure resulted in the removal of cell body and nuclei in all the surfaces while vinculin and actin remained on the samples. High pressure had a stronger effect on cells seeded on PMA and glass where vinculin and actin were sparse (Figure 4.4, Figure 4.5, top row). In contrast, more vinculin was observed on PEA (Figure 4.3, top row). The same procedure was followed using intermediate waterpik pressure. Similarly, cell body and nucleus were removed from some cells on PEA. However, isolation was not efficient since intact cells were observed as well (Figure 4.3, middle

row). For PMA and glass, intermediate pressure was sufficient to remove the cell body and nuclei while vinculin and actin remained attached to the surfaces (Figure 4.4, Figure 4.5, middle row). As expected, washing the cells at the lowest waterpik setting did not remove the cell body efficiently from the surfaces (Figure 4.3, Figure 4.4, Figure 4.5, bottom row). Based on these results, isolation of FAs is surface-dependent since PBS flow at the same setting did not give similar results. Highest flow was more efficient for isolating FAs on PEA whereas intermediate pressure was better for washing off cells on PMA and glass.

4.3.2 Isolation of FAs using hMSCs

MSCs were seeded on FN coated PEA, PMA and glass and culture was maintained for 3 d. Next, cells were incubated with TEA solution for 3 min and they were washed with PBS for 10 sec using a waterpik jet. A mask with a hole in the middle was placed on top of the samples at a distance of 1 mm. To determine the effect of fluid flow on the removal of cell body, the waterpik jet was set at its lowest, intermediate and highest pressure setting.

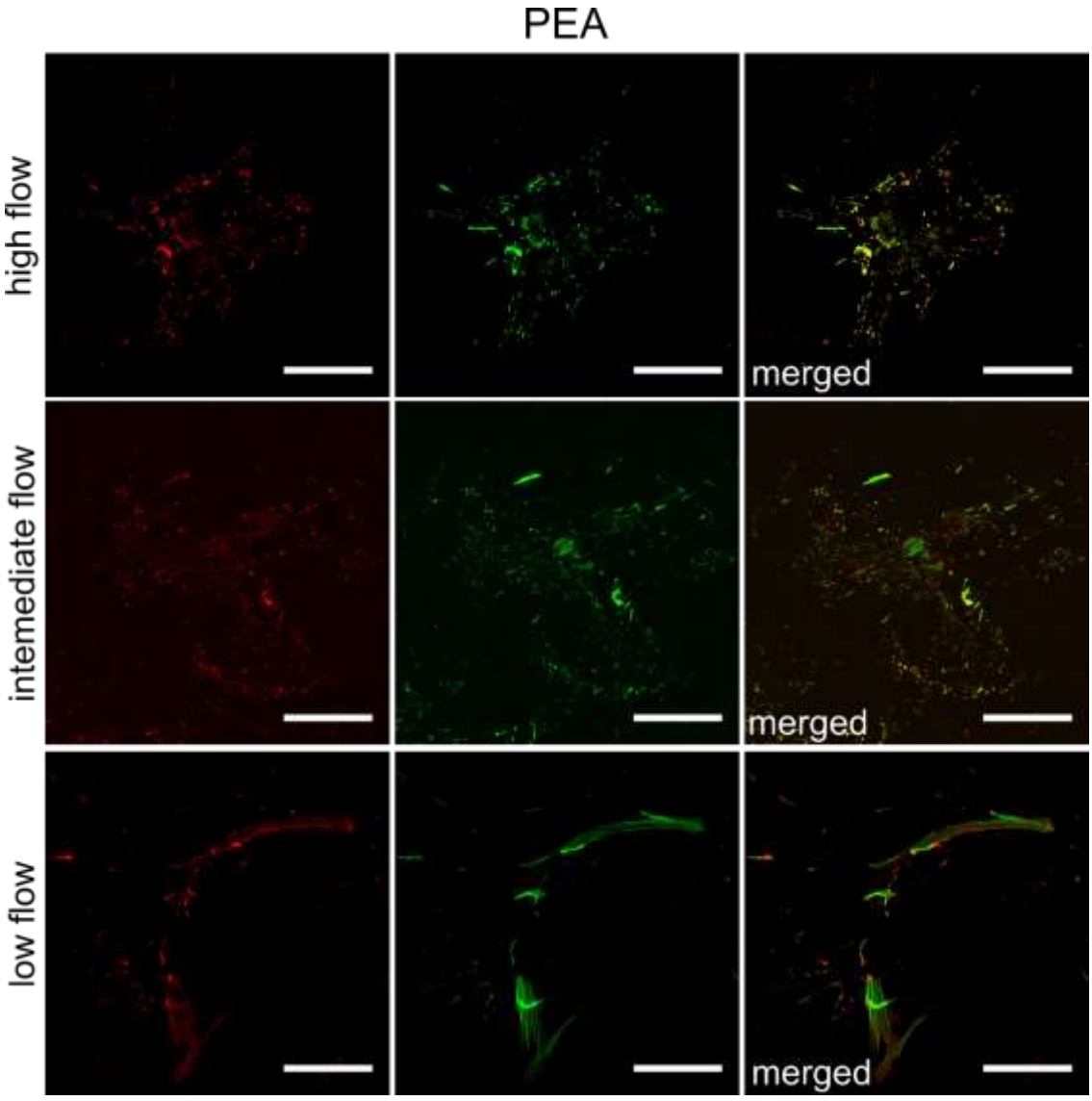

Figure 4.6. **Isolation of FAs on FN-coated PEA at high, intermediate and low flow fluid.** Immunofluorescent pictures of hMSCs 3 d after seeding. Cells were incubated with TEA for 3 min and were washed with PBS at the highest (top row), intermediate (middle row) or low pressure (bottom row). Fluorescent staining of vinculin (red), F-actin (green) and nuclei (blue). Scale bar is 50 μm (top row) and 100 μm (middle and bottom row). (n=1 per sample).

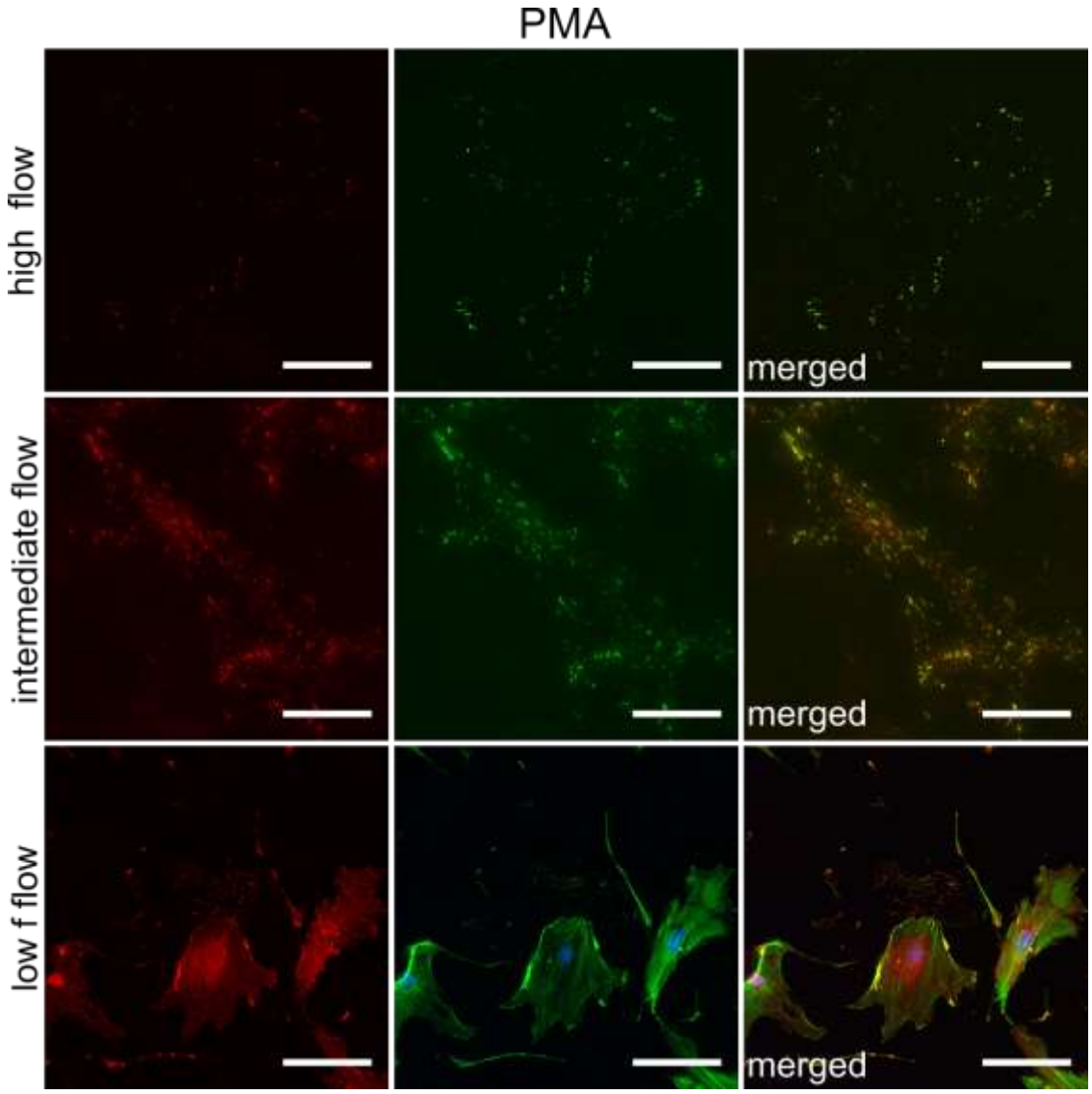

Figure 4.7. Isolation of FAs on FN-coated PMA at high, intermediate and low flow fluid. Immunofluorescent pictures of hMSCs 3 d after seeding. Cells were incubated with TEA for 3 min and were washed with PBS at the highest (top row), intermediate (middle row) or low pressure (bottom row). Fluorescent staining of vinculin (red), F-actin (green) and nuclei (blue). Scale bar is 100 µm. (n=1 per sample).

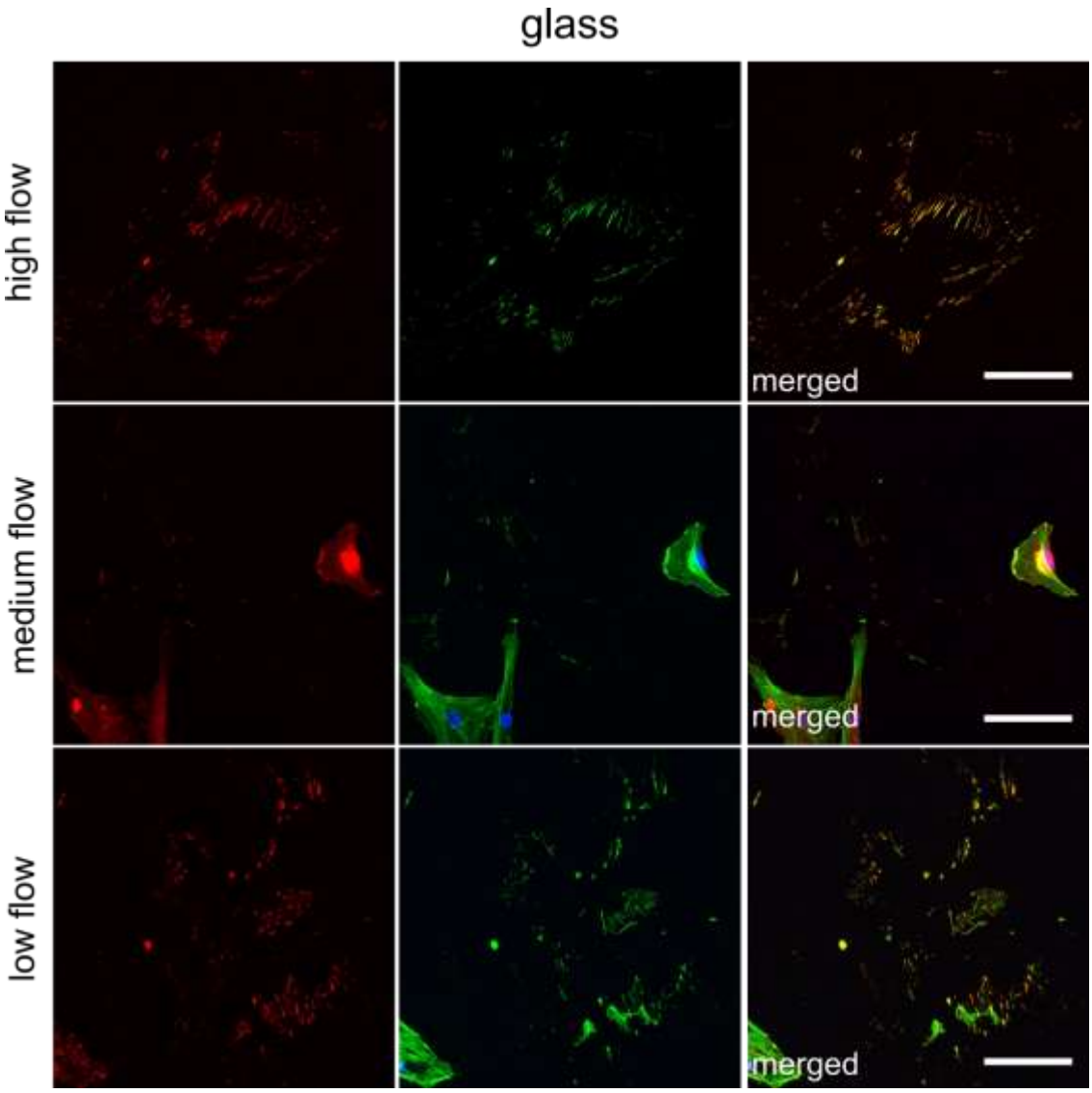

Figure 4.8. Isolation of FAs on FN-coated glass at intermediate and low flow fluid. Immunofluorescent pictures of hMSCs 3 d after seeding. Cells were incubated with TEA for 3 min and were washed with PBS at the highest (top row), intermediate (middle row) or low pressure (bottom row). Fluorescent staining of vinculin (red), F-actin (green) and nuclei (blue). Scale bar is 100 µm. (n=1 per sample).

At high and intermediate waterpik pressure, fluid flow removed the cell body and nuclei from PEA leaving vinculin and actin. However, high flow resulted in sparse amount of vinculin left on PMA (Figure 4.7, top row). Contrary, cell body and DNA were more efficiently removed with intermediate flow pressure. Fluid flow at the lowest setting gave poor results on all surfaces. Even though the nucleus was removed from some cells, intact cells were found on the surfaces (Figure 4.6, Figure 4.7, Figure 4.8, bottom row).

Based on these observations, isolation of FAs was improved with increased PBS flow, the results were not homogenous over the surface. Intact cells that have maintained their cell body and nucleus were observed, particularly towards the edge of the samples, irrespective of the flow pressure (Figure 4.9, Figure 4.10, Figure 4.11).

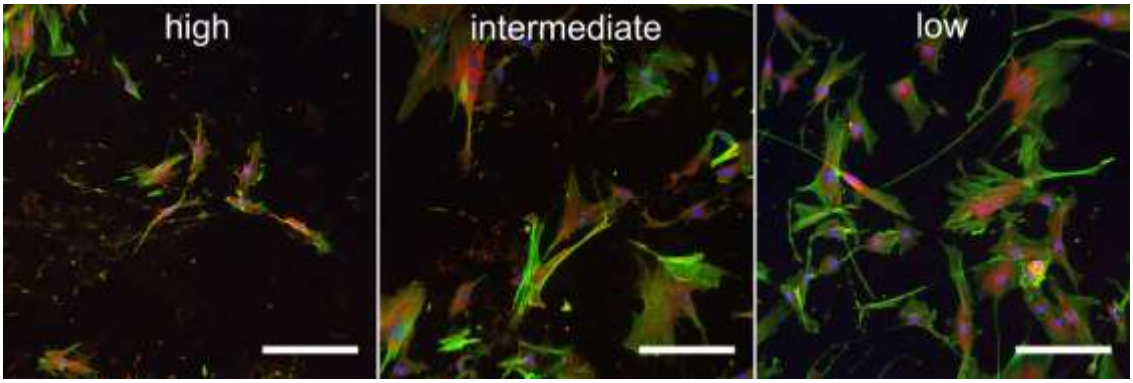

Figure 4.9. Isolation of FAs on FN-coated PEA at high, intermediate and low flow pressure. Immunofluorescent pictures of hMSCs 3 d after seeding at the edge of the sample. Cells were incubated with TEA for 3 min and were washed with PBS. Fluorescent staining of vinculin (red), actin (green) and nuclei (blue). Scale bar is 200 µm.

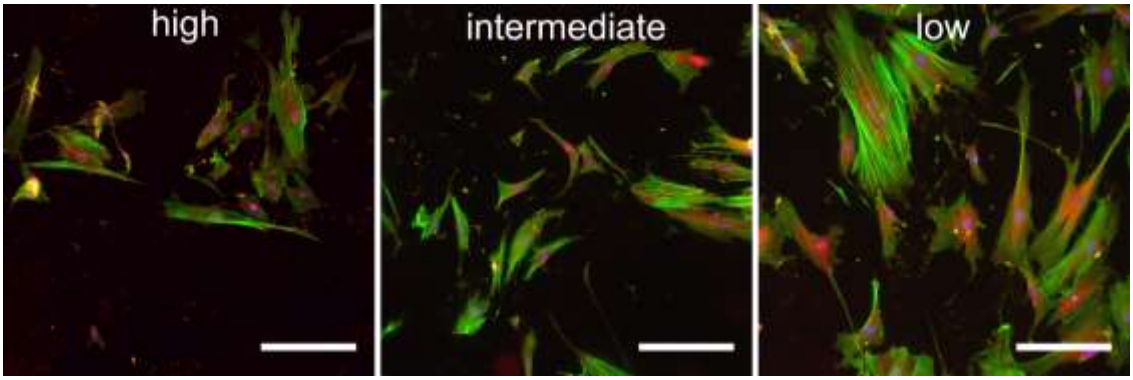

Figure 4.10. Isolation of FAs on FN-coated PMA at high, intermediate and low flow pressure. Immunofluorescent pictures of hMSCs 3 d after seeding at the edge of the sample. Cells were incubated with TEA for 3 min and were washed with PBS. Fluorescent staining of vinculin (red), actin (green) and nuclei (blue). Scale bar is 200 µm.

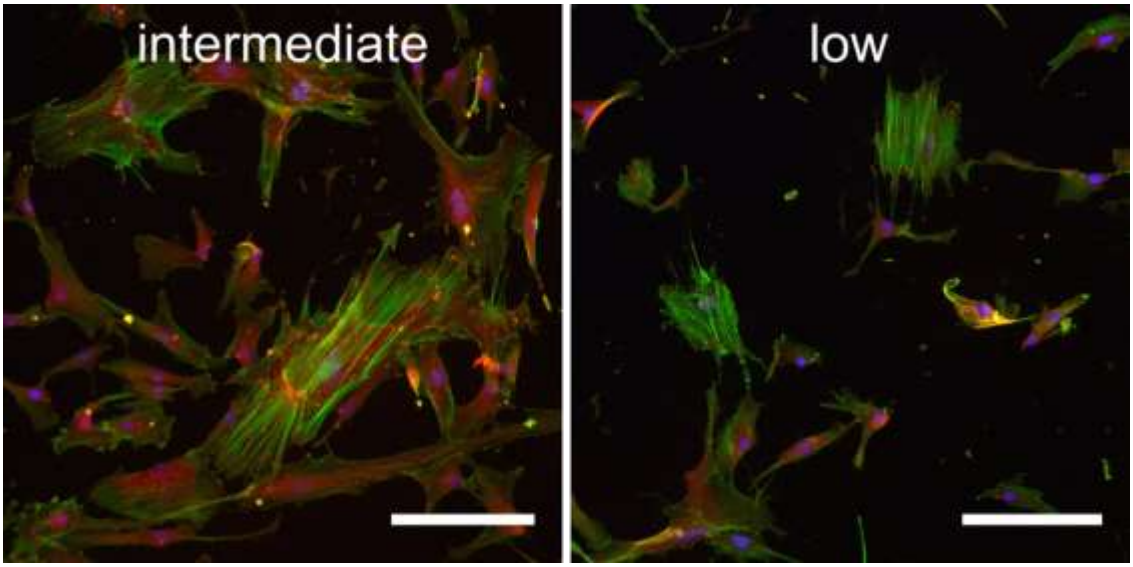

Figure 4.11. Isolation of FAs on FN-coated glass at medium and low flow pressure. Fluorescent pictures of hMSCs 3 d after seeding at the edge of the sample. Cells were incubated with TEA for 3 min and were washed with PBS. Fluorescent staining of vinculin (red), actin (green) and nuclei (blue). Scale bar is 200 μm.

Based on these results, a mask with one hole in the middle was not sufficient to remove the cell body and nucleus in the majority of cells. As expected, the efficiency of the method was surface-dependent. More specifically, fluid flow at the highest setting was required for PEA whereas fluid flow at intermediate setting was required for PMA and glass.

4.3.3 Isolation of hMSCs using a mask

To remove the cell body and nuclei from the majority of cells, a mask with two holes was used. Similarly to the previous method, culture was maintained for 3 d. However, cells were incubated with TEA for 2 min and they were washed using a waterpik jet for 5 sec from each hole. Based on the previous optimisation, the fluid flow was the highest setting for PEA and intermediate setting for PMA. Treating the cells with TEA for 2 min followed by two washes for 5 sec removed cell bodies and nuclei from most of the cells while FAs remained intact (Figure 4.12).

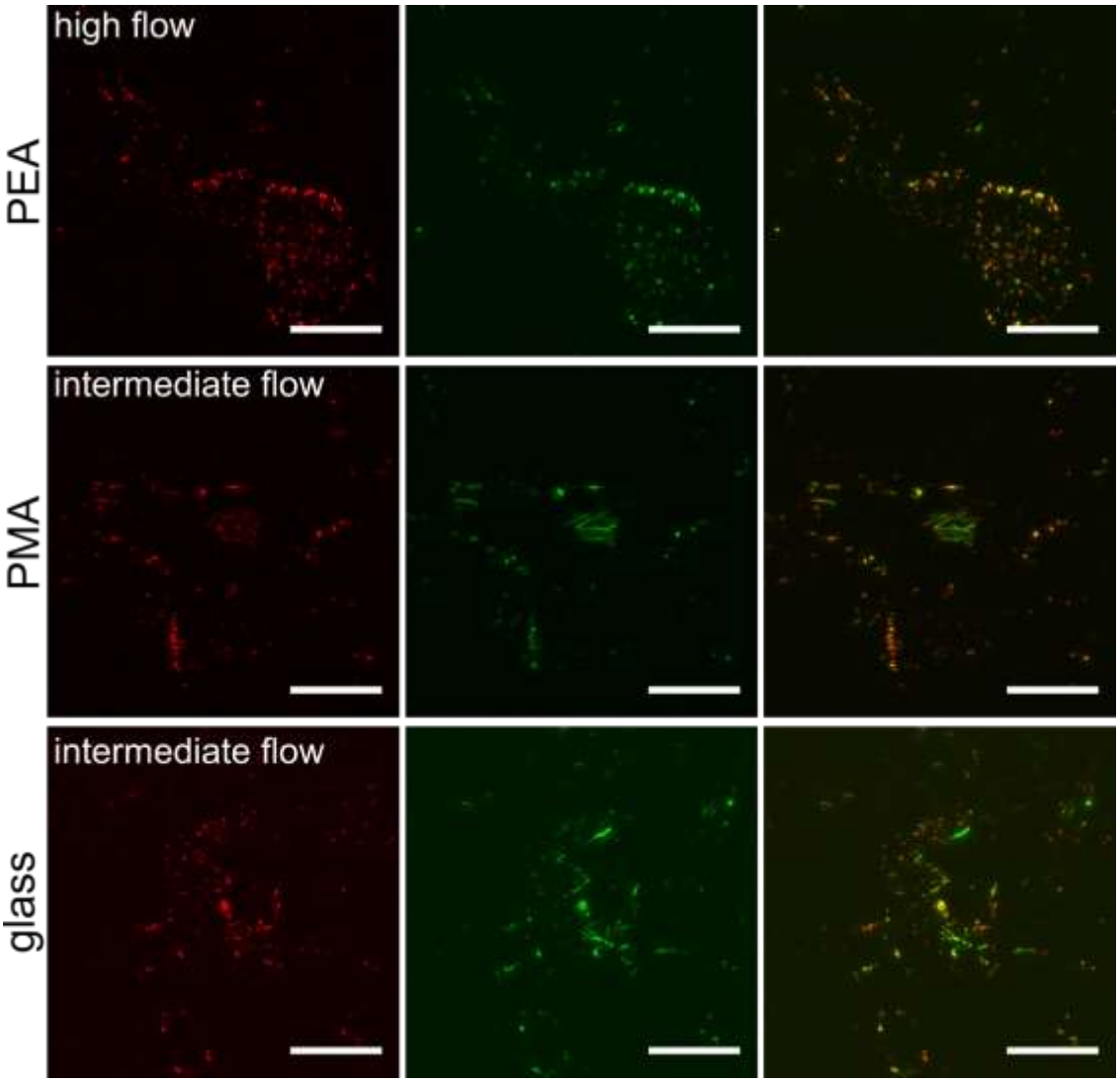

Figure 4.12. Isolation of FAs in hMSCs. Immunofluorescent pictures of hMSCs on FN-coated PEA, PMA and glass 3 d after seeding. Cells were incubated with TEA for 2 min and were washed with PBS using a mask and high (PEA) or intermediate flow (PMA, glass). Fluorescent staining of vinculin (red) and F-actin (green). Scale bar is 50 μm. (n=1 per sample).

4.3.4 Proteomics

4.3.4.1 PCA

To identify the protein composition of FAs, the SDS solution was digested using FASP and protein identification was carried out using the Mascot search engine. Regarding the proteins identified in the mixture, 377 proteins were found on PEA, 548 on PMA and 469 on glass. As expected, the identified proteins covered a wide variety including cytoskeletal, cytosolic and nuclear proteins. There were also proteins because of contamination such as keratin. It should be noted that some of the common FA proteins such as paxilin were not identified. This might be because the peptides were below the threshold of detection. To analyse the results, the proteins were connected to the corresponding gene. In order to assess whether the results were variable, a PCA based on the emPAI was performed to determine the variability of the results. According to the analysis, results are variable (Figure 4.13). The proportion of variance expressed in each PC is: PC1 = 71% and PC2 = 28.9%.

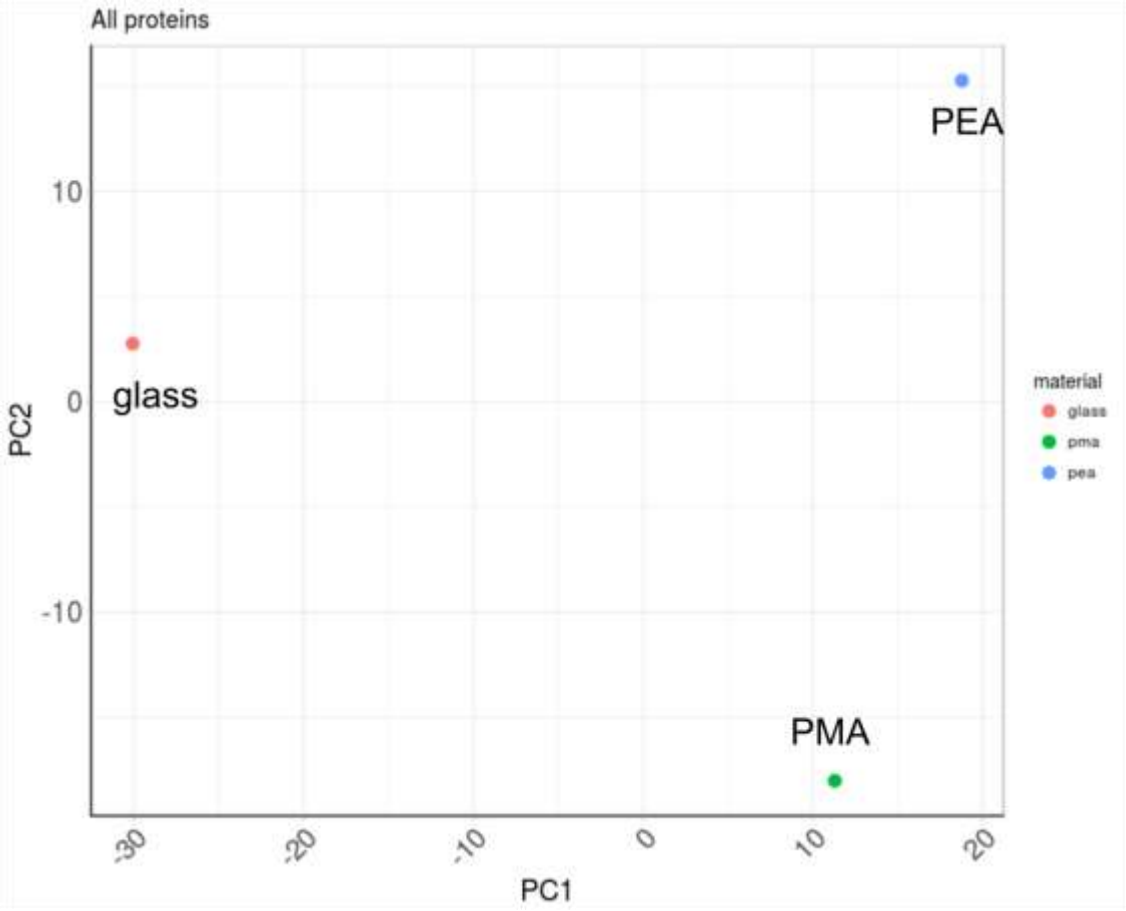

Figure 4.13. PCA based on the emPAI. All the proteins hits in the solubilised solution of PEA, PMA and glass were processed in R. (n=5 per sample, 1 biological replicate).

To identify the proteins previously associated with the formation of FAs, a list in the adhesome network was used. It was found that 26 proteins were common between the list and the search results (Table 4.1). To determine whether the identified FA-proteins are variable on PEA, PMA and glass, a second PCA was carried out using this protein set. Simialy, the results were variable (Figure 4.14). The proportion of variance epxressed in each PC is: PC1 = 92.1% and PC2 = 7.8%.

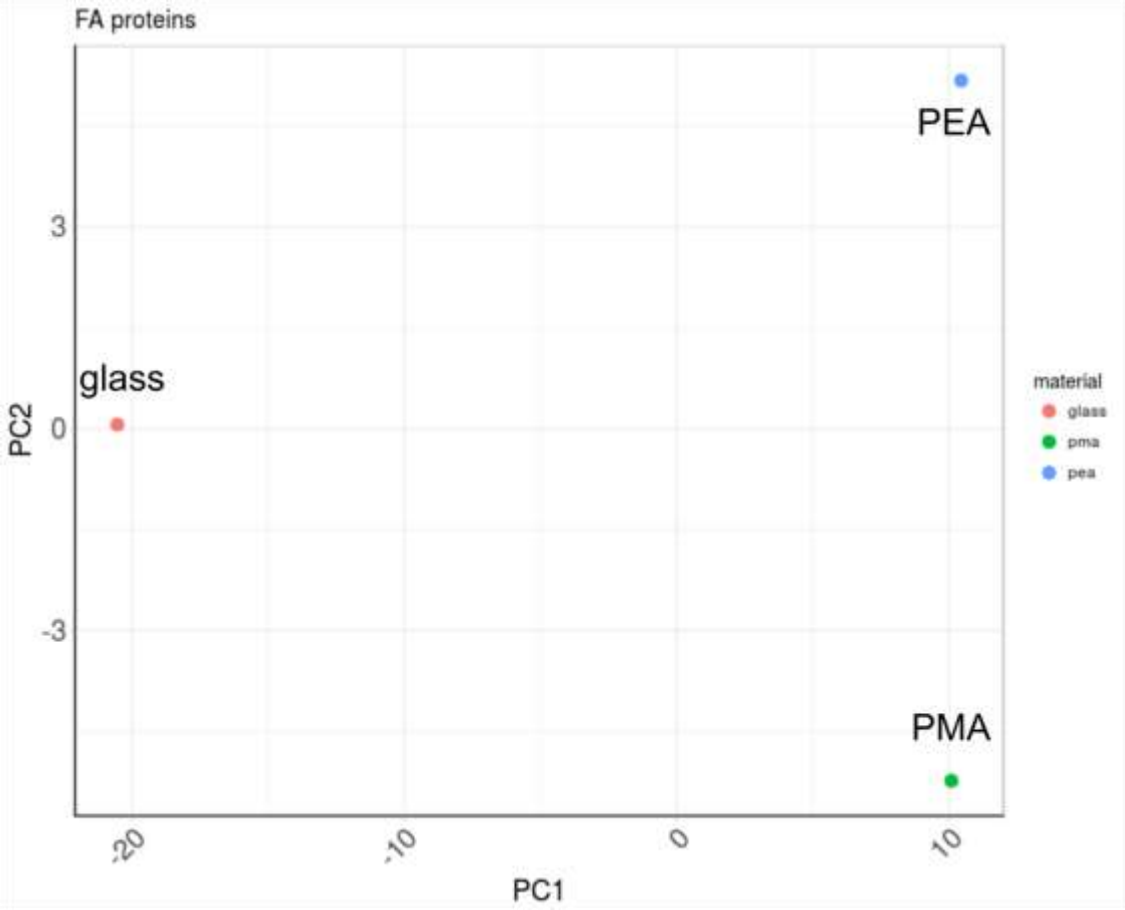

Figure 4.14. PCA based on the emPAI. The protein hits in the solubilised solution of PEA, PMA and glass previously identified as components of FAs were processed in R. (n=5 per sample, 1 biological replicate).

4.3.4.2 Analysis based on the emPAI and probability score

Further analysis revealed that 15 proteins were common in PEA, PMA and glass (Figure 4.15), 6 we shared between PMA and glass and 1 was shared between PEA and PMA (Figure 4.16). In addition, 1 protein was found only in PEA whereas 2 only in PMA and glass (Figure 4.17). In order to extract quantitative information about the abundance of FA proteins, the emPAI was used for plotting.

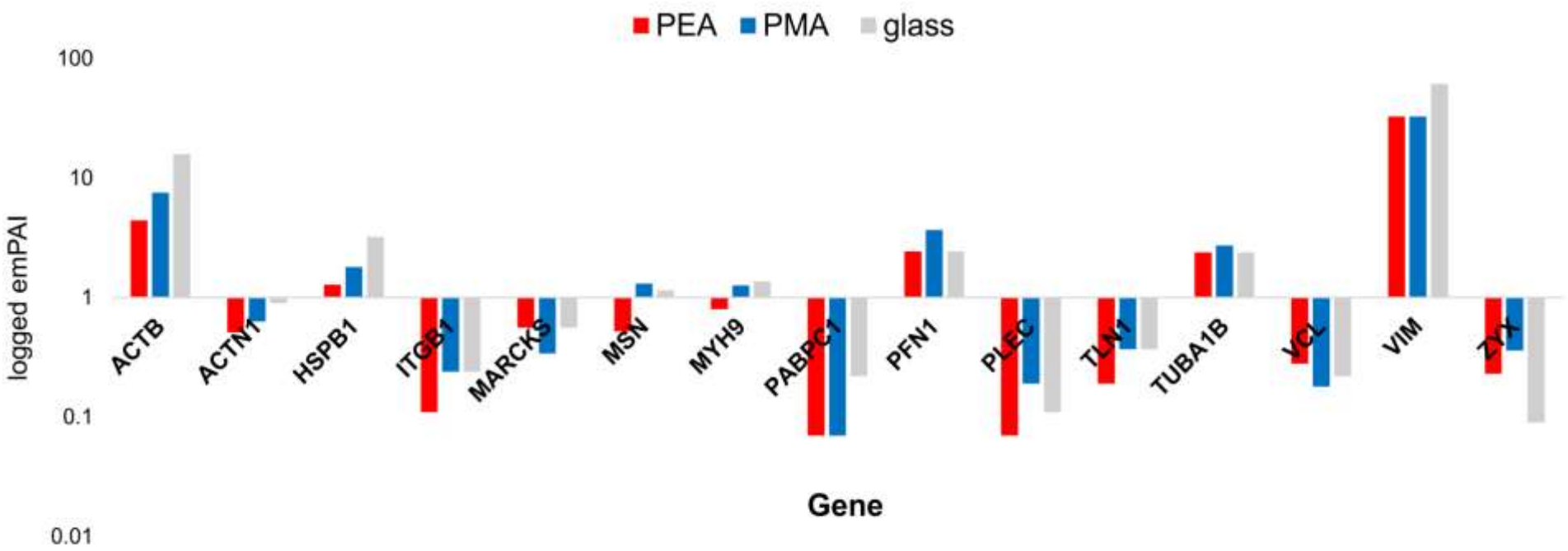

Figure 4.15. Logged emPAI of the FA-associated protein hits common in PEA, PMA and glass. (n=5 per sample, 1 biological replicate).

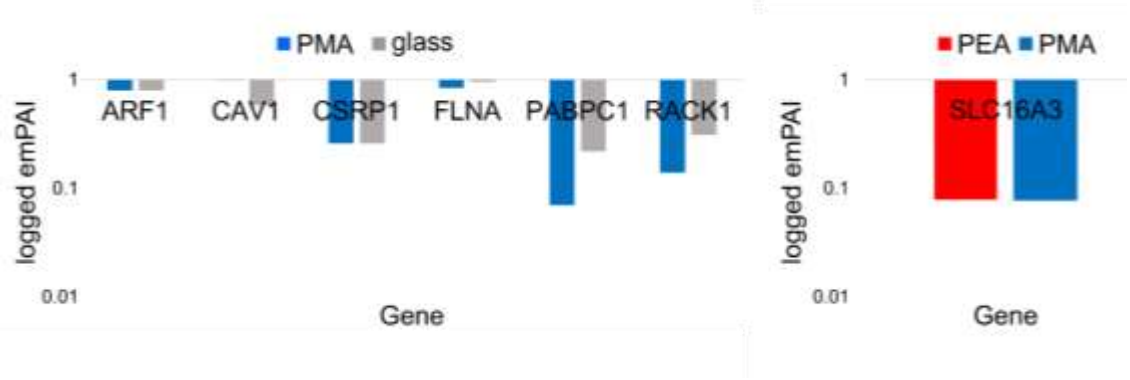

Figure 4.16. Logged emPAI of FA-associated genes shared between PMA and glass (left) and between PEA and PMA (right). (n=5 per sample, 1 biological replicate).

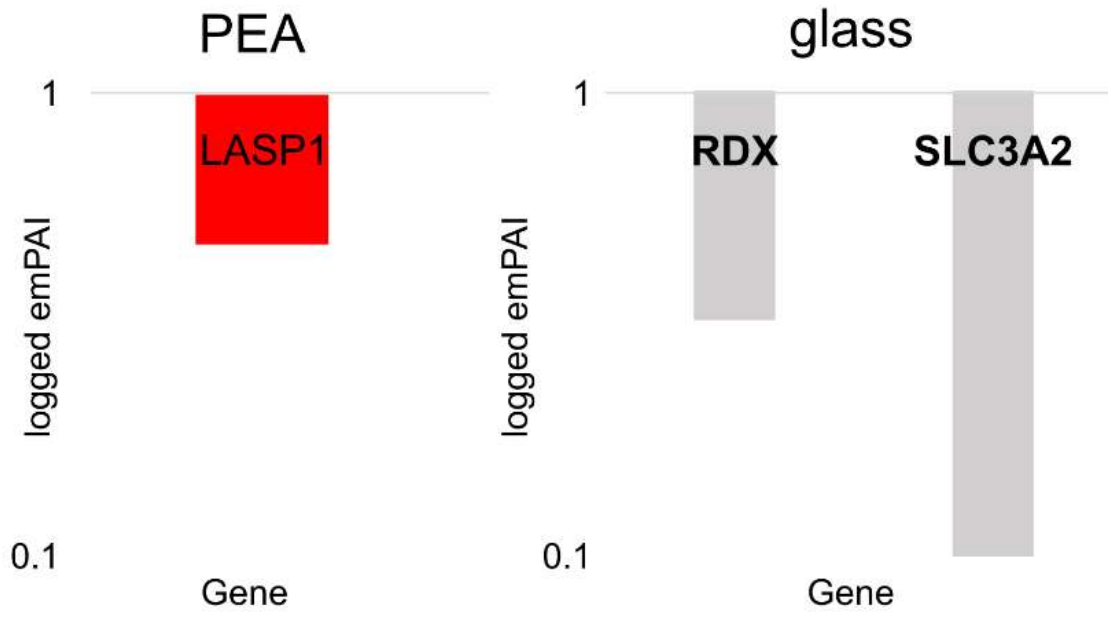

Figure 4.17. Logged emPAI of FA-associated genes unique in PEA (left) and glass (right). (n=5 per sample, 1 biological replicate).

To assess whether the proteins matches were significant, FA proteins were analysed based on the P.

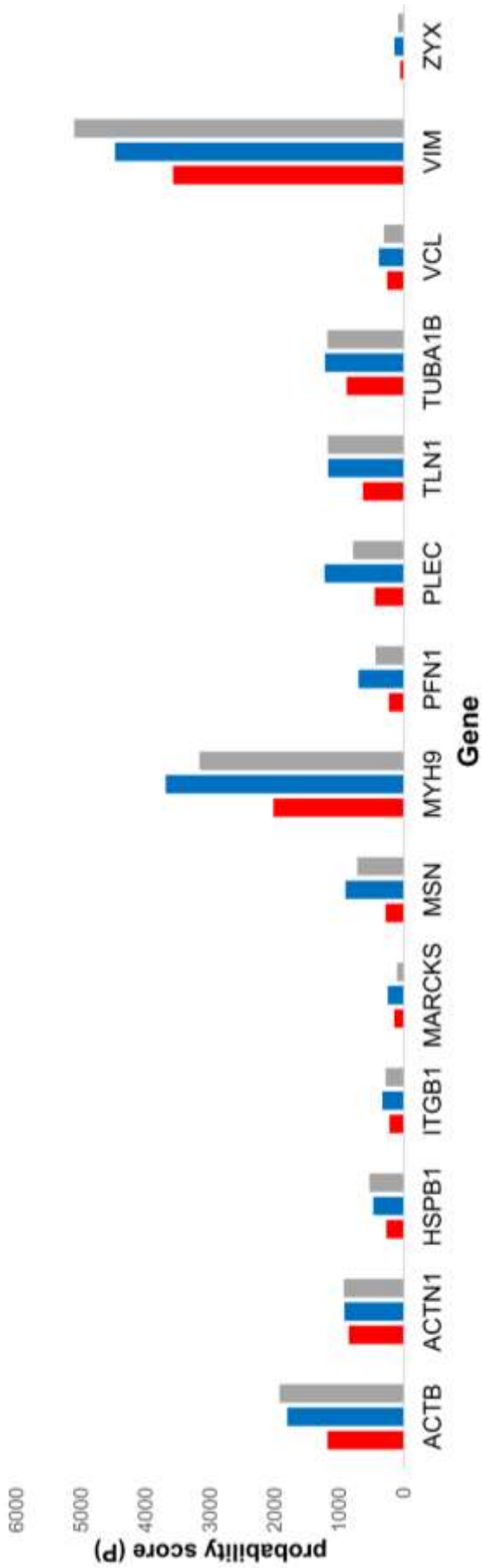

Figure 4.18. Provability score (P) of the FA-associated genes common in PEA, PMA and glass. (n=5 per sample, 1 biological replicate).

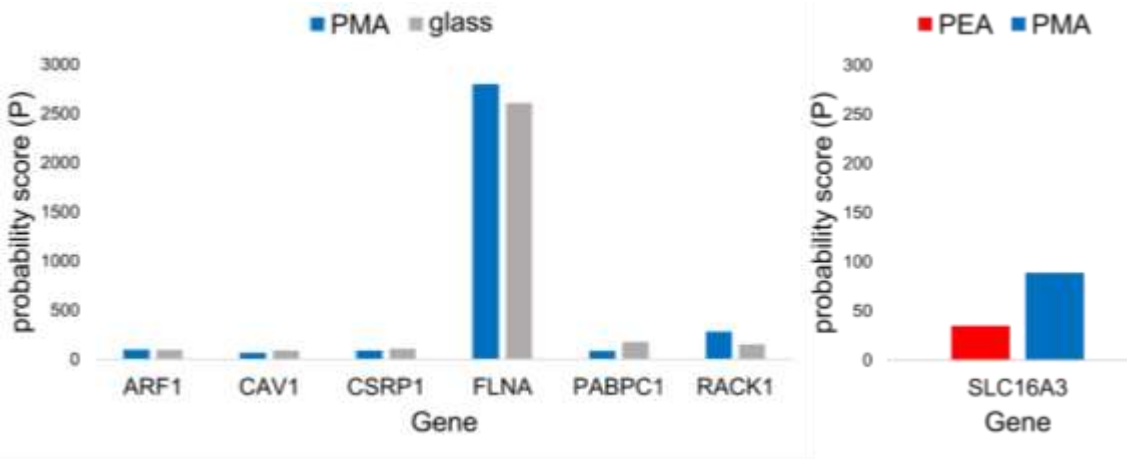

Figure 4.19. Probability score (P) of FA-associated genes shared between on PMA and glass (left graph) and between PEA and PMA (right graph). (n=5 per sample, 1 biological replicate).

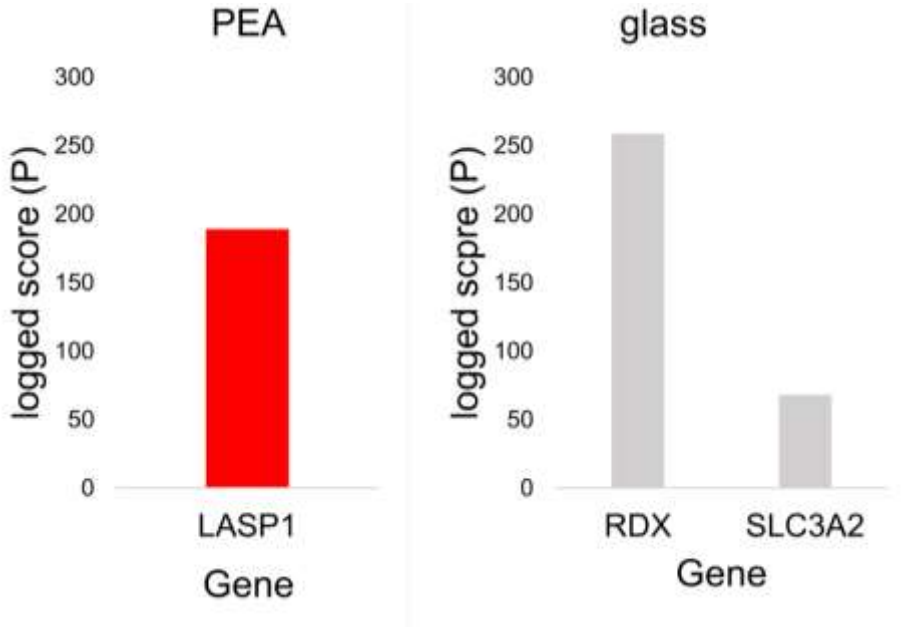

Figure 4.20. Probability score (P) of FA-associated genes unique on PEA, PMA and glass. (n=5 per sample, 1 biological replicate).

Gene	material	emPAI	score (P)
ACTB actin beta	PEA	4.43	1188
	PMA	7.53	1808
	glass	15.79	1929
ACTN1 actinin alpha 1	PEA	0.51	857
	PMA	0.63	926
	glass	0.9	932
ARF1 ADP ribosylation factor 1	PEA	-	-
	PMA	0.8	99
	glass	0.8	95
CALR calreticulin	PEA	-	-
	PMA	-	-
	glass	0.34	283
CAPN2 calpain 2	PEA	-	-
	PMA	-	-
	glass	0.13	62
CAV1 caveolin 1	PEA	-	-
	PMA	0.99	67
	glass	0.58	91
CSRP1 cysteine and glycine rich protein 1	PEA	-	-
	PMA	0.26	90
	glass	0.26	107
FLNA filamin A	PEA	-	-
	PMA	0.1	2800
	glass	0.34	2609
HSPB1 heat shock protein family B (small) member 1	PEA	1.28	272
	PMA	1.8	477
	glass	3.22	536
ITGB1 integrin subunit beta 1	PEA	0.11	224
	PMA	0.24	335
	glass	0.24	283
LASP1 LIM and SH3 protein 1	PEA	0.48	189
	PMA	-	-
	glass	-	-
MARCKS myristoylated alanine rich protein kinase C substrate	PEA	0.56	152
	PMA	0.34	252
	glass	0.56	107
MSN moesin	PEA	0.52	285
	PMA	1.31	907
	glass	1.15	722
MYH9 myosin heavy chain 9	PEA	0.8	2024
	PMA	1.26	3692
	glass	1.36	3170
PABPC1 poly(A) binding protein cytoplasmic 1	PEA	-	-
	PMA	0.07	86
	glass	0.22	178
PFN1 profilin 1	PEA	2.43	234
	PMA	3.67	703

	glass	2.43	443
PLEC plectin	PEA	0.07	451
	PMA	0.19	1232
	glass	0.11	791
RACK1 receptor for activated C kinase 1	PEA	-	-
	PMA	0.31	283
	glass	0.14	152
RDX radixin	PEA	-	-
	PMA	-	-
	glass	0.32	259
SLC16A3 solute carrier family 16 member 3	PEA	0.1	35
	PMA	0.1	89
	glass	-	-
SLC3A2 solute carrier family 3 member 2	PEA	-	-
	PMA	-	-
	glass	0.08	68
TLN1 talin 1	PEA	0.19	636
	PMA	0.37	1177
	glass	0.37	1180
TUBA1B tubulin alpha 1b	PEA	2.39	886
	PMA	2.73	1226
	glass	2.39	1188
VCL vinculin	PEA	0.28	263
	PMA	0.18	389
	glass	0.22	310
VIM vimentin	PEA	32.73	3579
	PMA	32.73	32.74
	glass	61.43	5110
ZYX zyxin	PEA	0.23	56
	PMA	0.36	148
	glass	0.09	95

Table 4.1. The table shows the FA-associated genes together the emPAI and P in each material (PEA. PMA and glass).

Protein	Function
ACTB	Highly conserved proteins involved in cell motility, structure and intercellular signalling. Major component of the contractile apparatus.
ACTN1	Represents cytoskeletal proteins. Actin-binding with diverse functions dependent on the cell type.
ARF1	Expresses small guanine nucleotide-binding. Involved in protein trafficking among different compartments.
CALR	Major Ca^{2+}-binding protein in endoplasmatic reticulum.

CAPN2	Intracellular cysteine proteases.
CAV1	Scaffolding protein. Main component of the caveolae plasma membranes found in most cell types. Involved in the interactions of integrins to the tyrosine kinase FYN, an initiating step in coupling integrins to the Ras-ERK pathway.
CSRP1	Involved in processes important for differentiation and development.
FLNA	Non-muscle F-actin-binding protein. Contributes to the elastic properties of F-actin networks and to the recruitment of F-actin into extended networks.
HSPB1	Translocates to the nucleus from the cytoplasm in response to stress. Acts as a molecular chaperone that promotes the correct folding of other proteins.
ITGB1	Receptor of ECM proteins, such as FN and collagen.
LASP1	Plays a role in the function of cytoskeleton. Localised to multiple sites of dynamic actin assembly, such as FAs and lamellipodia membrane.
MARCKS	Actin filament crosslinking protein localised to the plasma membrane.
MSN	Belongs to the ERM family. Mediates interactions between cytoskeletal structures and plasma membrane,
MYH9	Non-muscle myosin. Involved in multiple functions, including cytokinesis, cell motility and maintenance of cell shape.
PABPC1	Binds to poly(A) tail of mRNA. Shuttles between cytoplasm and nucleus. Binding of PABPC1 to poly(A) promotes ribosome recruitment and initiates translation.
PFN1	Actin-binding protein. Involved in the structure of the cytoskeleton by regulating actin polymerisation.
PLEC	interlinks intermediate filaments with microtubules and microfilaments.
RACK1	Guanine nucleotide-binding protein. Acts as a scaffolding/anchoring protein, regulates diverse cell activities and the expression of binding proteins.
RDX	Cytoskeletal protein that belongs to the ERM family. Involved in the interaction between membrane proteins and cytoskeleton.
SLC16A3	Mediated lactic acid and pyruvate transport across plasma membrane.

SLC3A2	Cell surface, transmembrane protein. Involved in the regulation of intracellular Ca^{2+} and transports of L-type amino acids.
TLN1	Contributes to connecting cytoskeletal structures to the plasma membrane.
TUBA1B	Major components of microtubules. Binds to GTP.
VCL	Cytoplasmic actin-binding protein found in FAs. Involved in protein-protein interactions and regulates cell-ECM interactions.
VIM	Intermediate filament protein. Together with actin microfilaments, they are involved in cytoskeleton structure. Contributes to cell morphology and integrity.
ZYX	FA protein. Binds to ACTN1. Involved in the formation of actin-rich structures and contributes to cell adhesion to the ECM.

Table 4.2. Summury of the function of the identified FA proteins.

The intermediate filament vimentin had the higher emPAI followed by actin and profilin on the three substrates. Other proteins with high emPAI were tubulin and heat shock protein family B (small) member 1 (Table 4.1). It should be noted though that a high emPAI does not always corresponds to a high score. For example, the emPAI of plectin is 0.19 on PMA and the score is 1232. This might be because peptides are scored so that they best match the data rather than by their absolute intensities.

4.3.4.3 Gene ontology analysis

The next step was to connect these FA proteins with its associated GO terms using PANTHER. The proteins identified in isolated FAs were classified according to their protein class, biological process and molecular function using the PANTHER classification system.

Protein class	PEA	PMA	glass
calcium-binding protein	-	6.70%	6.50%
cell adhesion molecule	9.50%	6.70%	6.50%
cell junction protein	9.50%	6.70%	6.50%
chaperone	4.80%	3.30%	3.20%
cytoskeletal protein	47.60%	36.70%	38.70%
enzyme modulator	9.50%	13.30%	12.90%
extracellular matrix protein	4.80%	3.30%	3.20%
hydrolase	-	3.30%	6.50%
membrane traffic protein	-	3.30%	3.20%
receptor	4.80%	3.30%	3.20%
structural protein	4.80%	6.70%	6.50%
transmembrane receptor protein	-	3.30%	3.20%
transporter	4.80%	3.30%	-

Figure 4.21. Classification of FA proteins based on their protein class. The pie charts describe the protein class of the FA proteins identified in PEA, PMA and glass and the percentage of genes involved in each protein class. (n=5 per sample, 1 biological replicate).

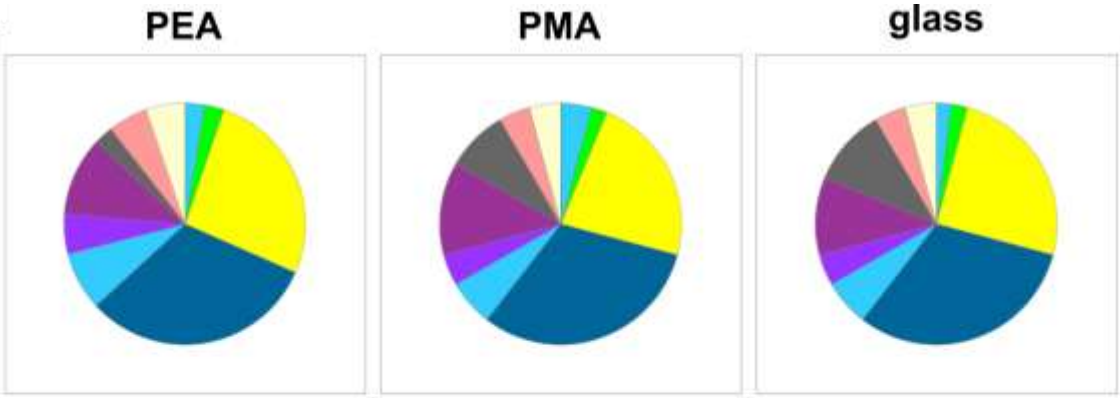

Biological process	PEA	PMA	glass
biological adhesion	2.60%	4.20%	2.10%
biological regulation	2.60%	2.10%	2.10%
cellular component organisation	26.30%	22.90%	25.00%
cellular response	31.60%	31.30%	31.30%
developmental process	7.90%	6.30%	6.30%
immune system process	5.30%	4.20%	4.20%
localisation	10.50%	12.50%	10.40%
metabolic process	2.60%	8.30%	10.40%
multicellular organismal process	5.30%	4.20%	4.20%
response to stimulus	5.30%	4.20%	4.20%

Figure 4.22. Classification of FA proteins based on their biological process. The pie charts describe the biological process of the FA proteins identified in PEA, PMA and glass and the percentage of genes involved in each biological process. (n=5 per sample, 1 biological replicate).

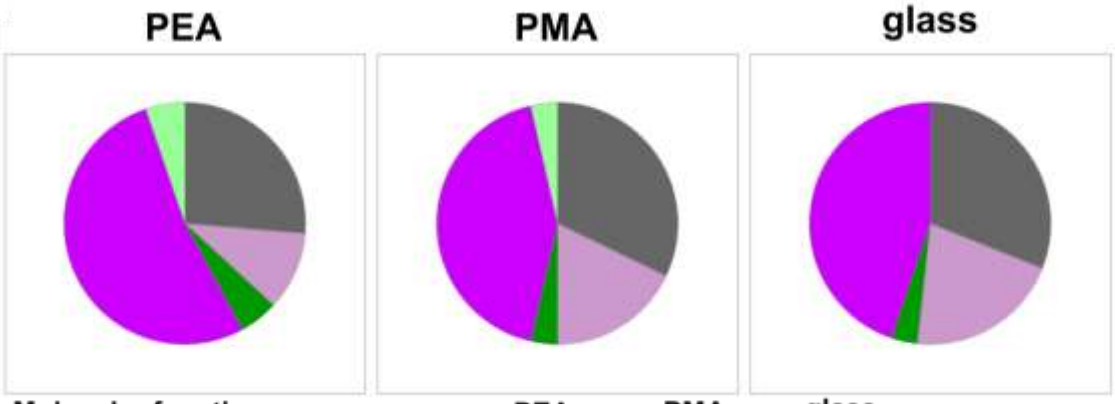

Molecular function	PEA	PMA	glass
binding	26.30%	32.10%	31.00%
catalytic activity	10.50%	17.90%	20.70%
receptor activity	5.30%	3.60%	3.40%
structural molecule activity	52.60%	42.90%	44.80%
transporter activity	5.30%	3.60%	-

Figure 4.23. Classification of FA proteins based on their molecular function. The pie charts describe the molecular functions of the FA-associated genes identified in PEA, PMA and glass and the percentage of genes involved in each molecular process. (n=5 per sample, 1 biological replicate).

According to classification, most of the identified proteins are cytoskeletal proteins, such as actin, and intermediate filament proteins such as plectin, moesin, filamin-A, vimentin (Figure 4.21). They are mainly involved in cellular component organization (Figure 4.22) and they have structural activity as well as binding activity, for example Ca^{2+} ion binding activity (e.g. calreticulin) and protein binding (e.g. zyzin and myosin-9) (Figure 4.23).

4.3.4.4 Gene enrichment analysis

Next, a gene enrichment analysis was carried out using DAVID. Gene enrichment analysis is a computational method which compares the abundance of specific GO-terms in a dataset. Statistical significance is determined by calculating a modified Fisher P-value exact test. The threshold of P-value was set at 0.05 and a smaller P-value shows more enrichment. The fold enrichment was estimated as well and is a measure of the magnitude of enrichment. The majority of genes in PEA, PMA and glass encode phosphoproteins (e.g. vinculin, talin, zyxin, vimentin). Moreover, they are post-translationally modified by the attachment of at least one acetyl group. They are found in the plasma membrane and in cytoplasm and are mainly cytoskeletal-related and actin-binding proteins. The group with the highest gene enrichment are cytoskeletal-related protein and FA proteins (Table 4.3, Table 4.4,Table 4.5).

PEA			
Term	**%**	**P Value**	**Fold Enrichment**
phosphoprotein	92.3	2.24E-08	2.44
acetylation	80.7	1.35E-13	5.89
plasma membrane	76.9	6.98E-07	2.7
cytoplasm	65.3	2.66E-07	3.77
non-membrane-bounded organelle	61.5	7.94E-06	3.15
cytoskeleton	50	5.41E-12	15.12
plasma membrane part	46.1	0.001074	2.78
cytoskeletal protein binding	46.1	7.37E-10	11.88
cytosol	42.3	7.17E-05	4.22
actin binding	42.3	2.03E-10	16.84
cytoskeleton organization	38.4	7.20E-09	14.1
cell membrane	38.4	0.00119	3.37
focal adhesion	34.6	9.29E-08	12.64

Table 4.3. Gene enrichment analysis of FA proteins found on PEA. The table describes enriched terms associated with the gene list, the percentage of involved genes/total genes, the P-value and the fold enrichment.

PMA			
Term	**%**	**P Value**	**Fold Enrichment**
phosphoprotein	100	3.42E-09	2.64
acetylation	80.9	4.14E-11	5.9
plasma membrane	71.4	8.91E-05	2.53
non-membrane-bounded organelle	66.6	7.64E-06	3.44
cytoplasm	61.9	2.27E-05	3.57
cytoskeleton	52.3	2.00E-10	15.84
cytosol	47.6	4.88E-05	4.8
actin binding	42.8	1.41E-08	17.06
cytoskeletal protein binding	42.8	4.07E-07	11.03
plasma membrane part	42.8	0.00963	2.61
cytoskeleton organization	38.1	3.06E-07	14.6
focal adhesion	38.1	3.69E-07	13.49
cell motion	38.1	5.47E-07	13.4
structural molecule activity	38.1	2.84E-05	7.8

Table 4.4. Gene enrichment analysis of FA proteins found on PMA. The table describes enriched terms associated with the gene list, the percentage of involved genes/total genes, the P-value and the fold enrichment.

glass			
Term	**%**	**P Value**	**Fold Enrichment**
phosphoprotein	91.6	1.34E-07	2.42
acetylation	83.3	1.90E-13	6.08
plasma membrane	75	5.04E-06	2.64
cytoplasm	66.6	4.43E-07	3.84
non-membrane-bounded organelle	62.5	1.19E-05	3.21
cytoskeleton	50	4.47E-11	15.12
cytoskeletal protein binding	45.8	5.16E-09	11.8
cytosol	45.8	2.87E-05	4.59
actin binding	41.6	2.13E-09	16.59
plasma membrane part	41.6	0.007632199	2.52
cytoskeleton organization	37.5	6.04E-08	13.96
focal adhesion	37.5	9.29E-08	12.64
cell membrane	37.5	0.002858998	3.28
actin-binding	33.3	1.09E-08	25.95
cell motion	33.3	2.20E-06	11.39
regulation of actin cytoskeleton	33.3	2.97E-06	10.51
structural molecule activity	33.3	7.91E-05	6.82
cell projection	33.3	1.15E-04	6.37
disease mutation	33.3	0.001961124	4.02

Table 4.5. Gene enrichment analysis of FA proteins found on glass. The table describes enriched terms associated with the gene list, the percentage of involved genes/total genes, the P-value and the fold enrichment.

The FA pathway (generated by Kyoto Encyclopedia of Genes and Genomes (KEGG)[289]. It represented the interactions of the identified proteins and how they are involved in the regulation of cell motility, regulation and survival (Figure 4.24).

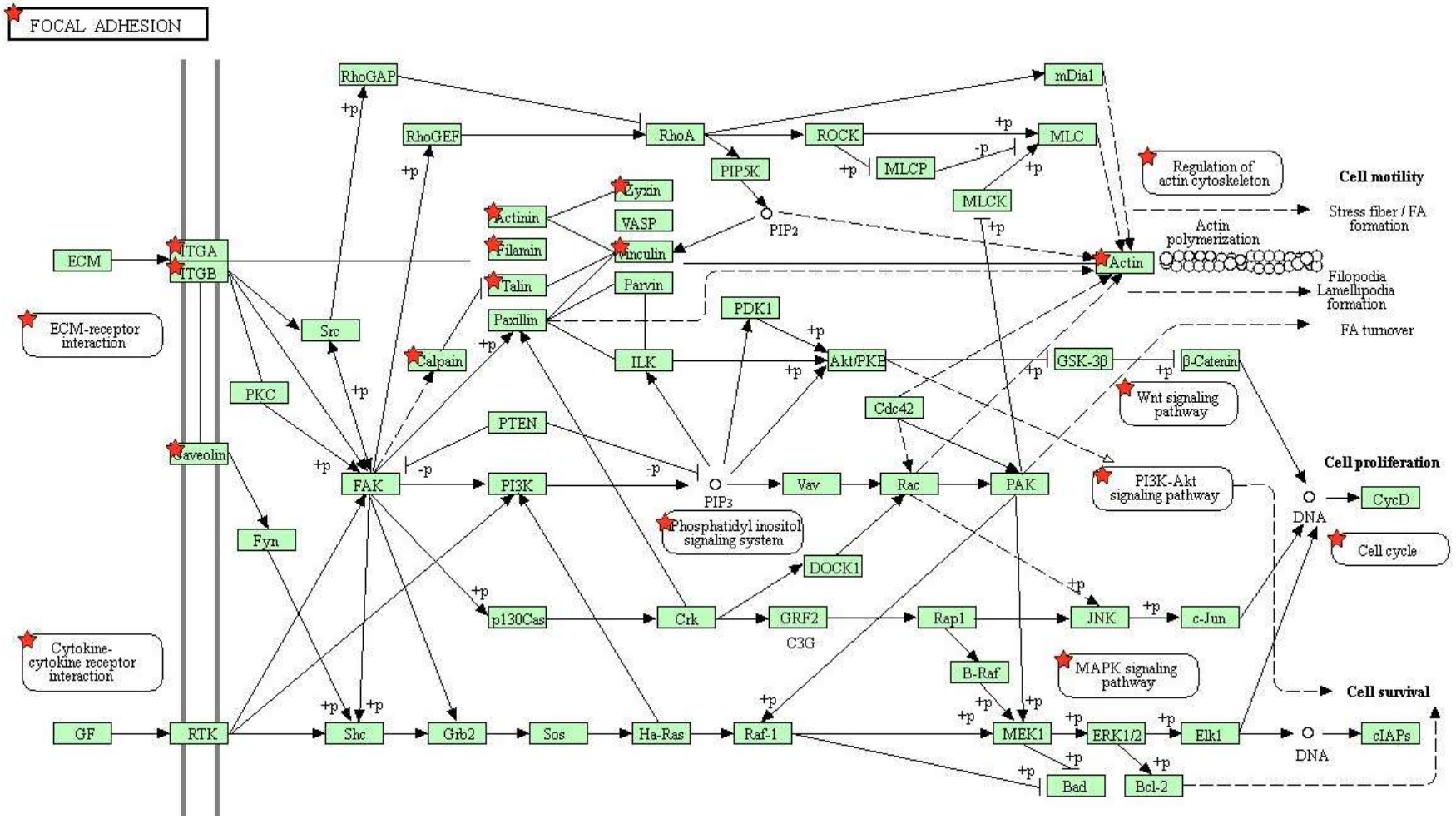

Figure 4.24. Focal adhesion pathway. The pathway was obtained using DAVID. The red stars show the identified FA-associated proteins involved in the pathway.

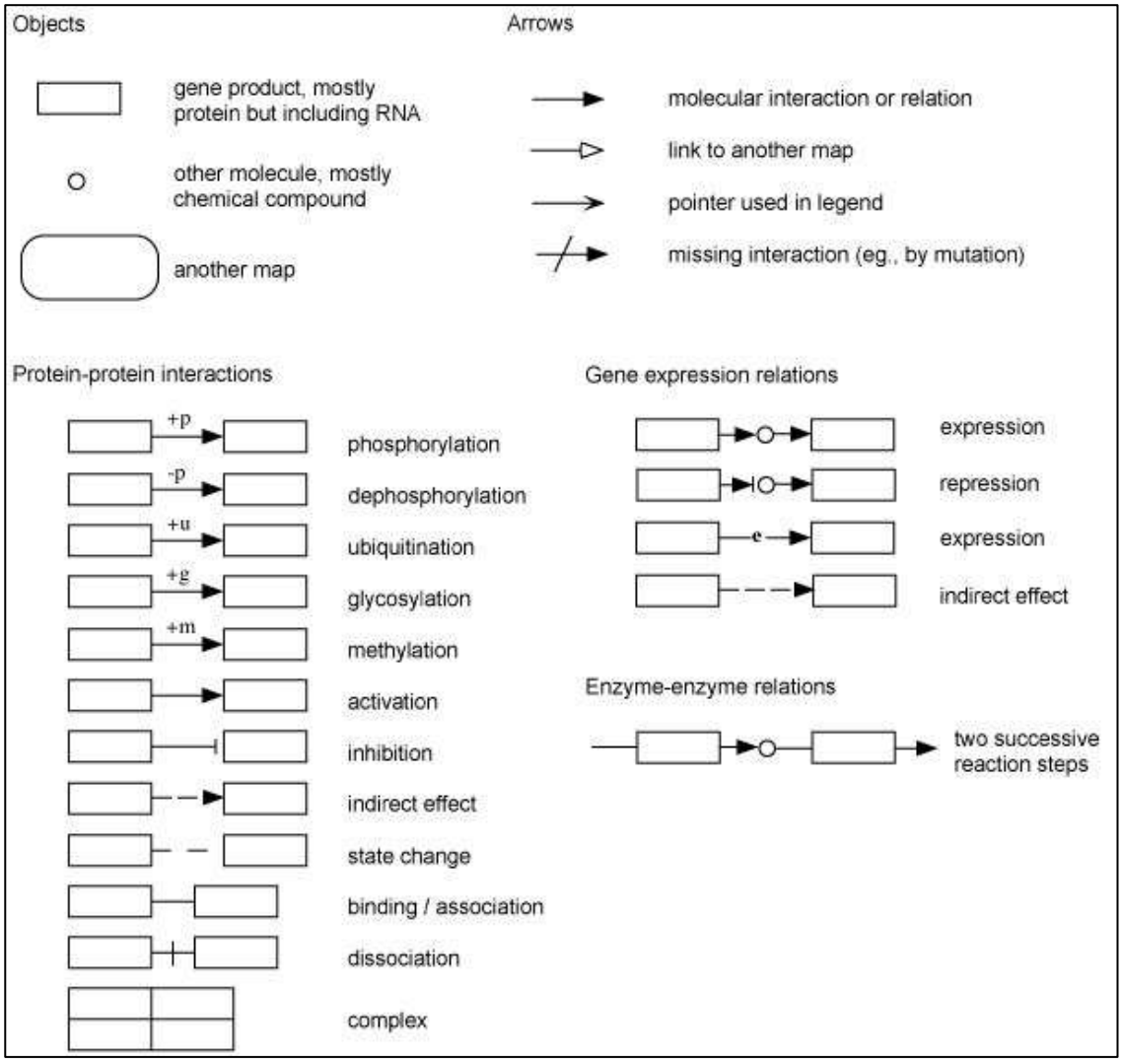

Figure 4.25. Complete list of symbols in KEGG pathway.

4.3.4.5 Analysis of non FA proteins

The remaining proteins detected in the solubilised mixture have not been previously associated with the regulation and function of FAs. In order to get insights into their function and the processes they are involved in, all the proteins found on PEA, PMA and glass were classified according to their protein class, molecular function and biological process using PANTHER.

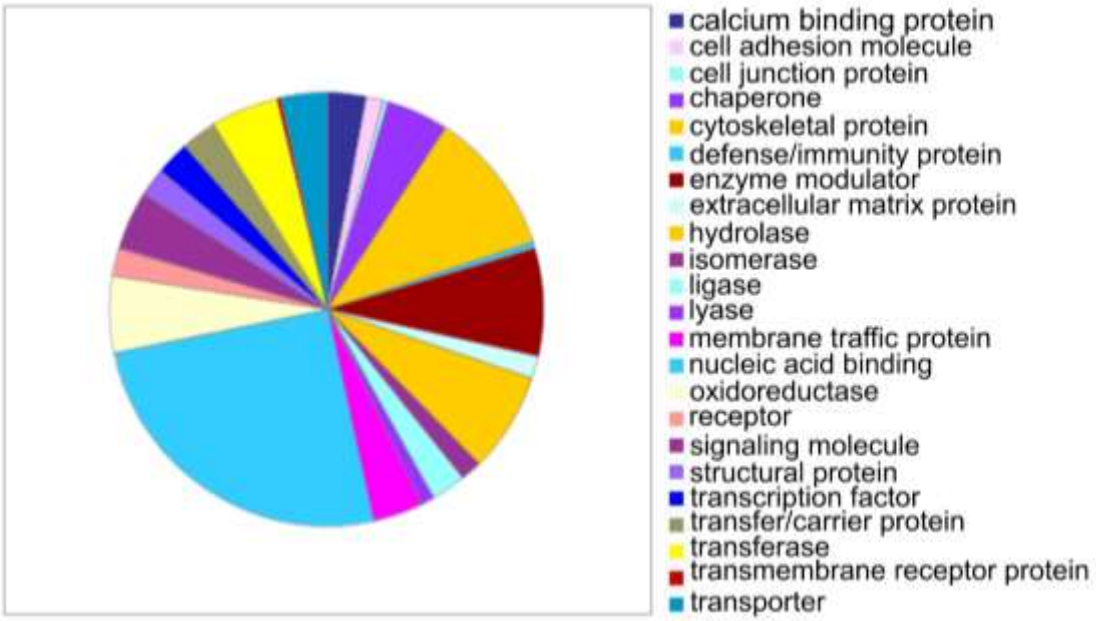

Figure 4.26. Classification of non-FA associated proteins based on their protein class. (n=5 per sample, 1 biological replicate).

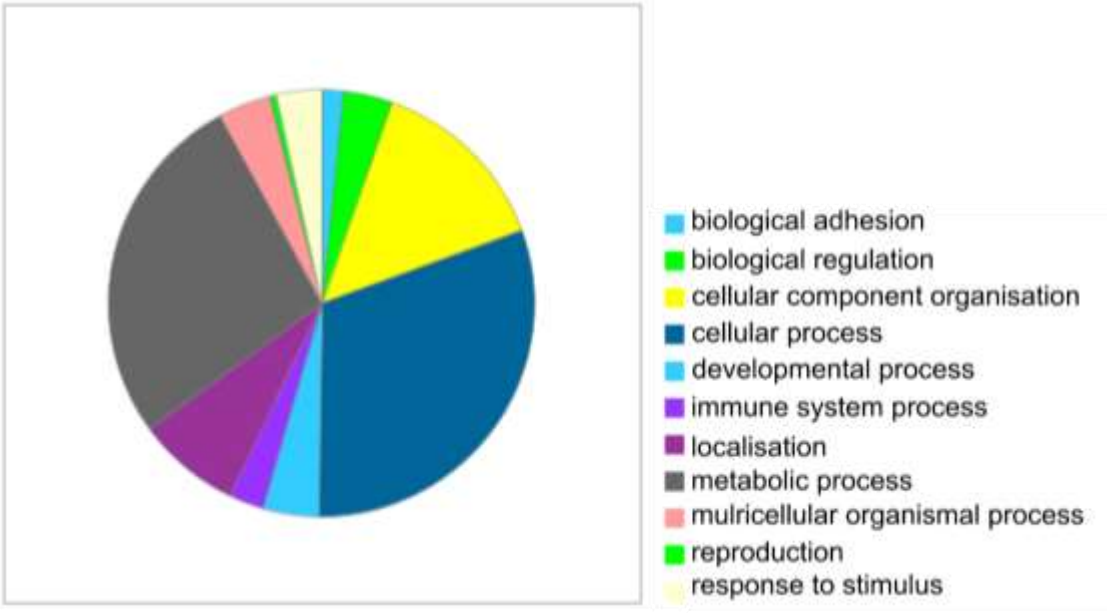

Figure 4.27. Classification of non-FA associated proteins based on their biological process. (n=5 per sample, 1 biological replicate).

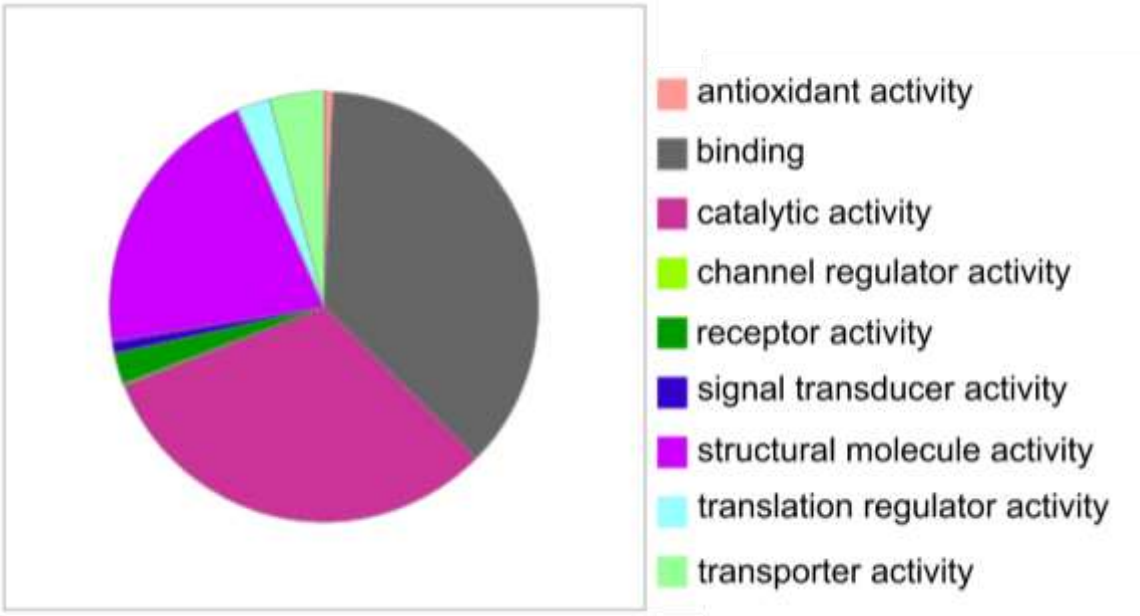

Figure 4.28. Classification of non-FAs associated proteins based on their molecular function. (n=5 per sample, 1 biological replicate).

Based on the protein class, the majority of the proteins are nucleic acid binding protein such as histones, nuclear ribonucleoproteins, and ribosomal proteins. Enzyme modulators such as G-proteins as well as cytoskeletal proteins were also identified (Figure 4.26). The proteins have mainly binding activity (protein, lipid and nucleic acid binding), catalytic activity (hydrolase and transferase activity) and structural activity (Figure 4.28). As expected, the majority of proteins are involved in a wide range of biological processes such as cell cycle and communication as well as in metabolic processes (Figure 4.27). The wide variety of proteins detected indicate that some cells remained intact thus proteins in cell body and nucleus were contained in the solubilised mixture.

4.4 Discussion

FAs are multiprotein adhesion structures involved in cell fate by incorporating external cues to signaling pathways. In order to underastand how the underlying layer of FN guides the formation of FA structures, it is essential to investigate the FA protein compostion. Previous studies have described methods for isolating FAs and cells were bound to FN-coated magnetic beads[290, 291] or FN-coated dishes[278]. This chapter focuses in the development of a method for the isolation of FAs from hMSCs seeded on PEA and PMA. After the protocol was optimised, protein composition of isolated FAs were characterised by proteomic analysis.

To optimise the protocol, C2C12 cells and hMSCs were seeded on FN-coated PEA, PMA and glass. Following a mehod developed by Kuo *et al*[281], cells were incubated with TEA solution to weaken the cell body and next they were removed with PBS using a waterpik dental jet. A vinculin, actin and nuclei staining was then performed to evaluate the efficiency of the method. In a first attempt, the waterpik tip was moved manually over the surfaces and the PBS pressure was adjusted at three settings (high, intermediate, low). It was found that the efficiency of the flow in isolating FAs depends on the substrate. More specifically, higher flow is required to wash off the cell body and nuclei from cells attached on PEA (Figure 4.3) whereas intermediate flow was required for PMA and glass (Figure 4.4, Figure 4.5). Although FAs remained attached on the surfaces while cell body and nuclei were removed, it was challenging to keep all conditions consistent (e.g. distance of the tip from the surface) leading to variable results. In addition, PBS flow often resulted in breaking the samples.

To improve the process, a mask with one hole in the middle was used and was placed on top of the surfaces. In this case, hMSCs were seeded onto FN-coated PEA, PMA and glass. Results were more consistent, however this method was not sufficient enough since intact cells, particulary at the edge of the surface, were observed (Figure 4.9, Figure 4.10, Figure 4.11). Another mask having two holes was used next. Cell body and nuclei were sufficiently removed from the surfaces. Similarly, better results were observed at high PBS flow in PEA and at intermediate flow in PMA and glass (Figure 4.12). After the protocol was optimised, FAs attached on the FN-coated surfaces were

solubilised using an SDS solution and a cell scraper. Peptide mixture was digested with FASP and analysed by ESI. It should be mentioned that FA fractions contain actin. However, this is unavoidable since FAs and actin cytoskeleton are interdependent structurers.

A wide variety of proteins were identified including FA proteins as well as cytoskeletal and nuclear proteins. ECM proteins were identified too, including fibronectin, laminin, collagen and tenascin. A literature-based list containing FA-related protein was obtained from the adhesome network and was used to identify a subset of proteins which have been previously described as FA components[279]. The identified protein were characterised based on the emPAI which provides a way to obtain quantitative information about protein abundance, and the probability score. Two lists of identified proteins were used for analysis: a list containing the FA proteins and a list with the remained identified proteins. Analysing both lists by PCA based on the emPAI showed the three different protein mixtures are variable (Figure 4.13, Figure 4.14). Comparing the adhesome network list and the identified proteins, it was found that 26 proteins were shared. As expected, most of the proteins were common in PEA, PMA and glass (Figure 4.15). In addition, LASP1 was uninque on PEA, and RDX and SLC3A2 were only detected in glass (Figure 4.17). LASP1 is a signaling molecule[292] and can bind to actin[293] and zyxin[294]. The expression of LASP1 have been associated with changes in FAs, migration and proliferation[295, 296]. RDX belongs to the ezrin/radixin/moesin (ERM) protein family and facilitates the interactions between actin filaments and focal adhesion proteins[297]. RDX is also involved in integrin activation[298]. SLC3A2 is a type II transmembrane glyocoprotein and it has been found to associate with β 1 integrin[299, 300].

Based on the protein class classification (Figure 4.21), the percentage of cytoskeletal proteins is similar on PMA and glass (36.70% and 38.70%), whereas it is higher on PEA (47.60%). The same trend is observed on most of protein class subcategories, such as cell adhesion molecule and cell junction protein. In line with this, the classification based on the molecular functon (Figure 4.23) reveales more similarities between PMA and glass. For example, similar percentag of proteins with binding and catalytic/receptor binding activity

are found on PMA and glass. It can thus be postulated that PEA triggers a distinct cell behaviour in terms of substrate adhesion, whereas cells on PMA and glass exhibit a similar behaviour. These results might explain the differences observed on cell area and circularity, with cells being more well spread with increased EA concentration (Figure 3.13, Figure 3.14). It should be noted though that these results might not be representative due to the lack of replicates.

The output of the proteomic analysis is a long list of identified proteins characterised by a probability score and the quantitative value emPAI. In order to interpret these data and understand the proteome function, a Gene Ontology analysis was carried out using the PANTHER classifier and the DAVID bioinformatics resources. PANTHER and DAVID facilitates the high-throughput analysis by combining gene function, ontology, pathways and statistical analysis tools and aim at extracting biological meaning from large data set. Classification according to the protein class, molecular function and biological process showed that the identified FA proteins are mainly cytoskeletal and actin-binding proteins. Gene enrichment analysis showed that this group together with FA proteins have the highest enrichment.

Based on the emPAI and P, vimentin was the most abudant protein identified in the solubilised solution extracted from PEA, PMA and glass. Vimentin is a one of the most widely expressed intermidiate filament proteins and is mainly found in cells of mesenchymal origin[301, 302]. Generally, vimentin plays a functional and structural role in regulatin the cytoskeleton. There is also evidence that it associates with integrins. For example, vimentin interacts with $\alpha_2\beta_1$-eriched FAs[303], with $\alpha_6\beta_4$ integrin when cells were attached to either laminin 5 or FN[304] and with $\alpha_5\beta_1$ integrin[305]. The second most abundant protein was actin. Actin is central in FA regulation and mechanotransduction. It interacts with numerous proteins such as talin[306], filamin[307], and actinin[308]. Other proteins were identidied and can provide a direct link to actin cytoskeleton. For example, plectin can provide a direct link to vimentin[309, 310].

Ovarall, this chapter describes the optimisation of a method to isolate MSC FAs. Regarding the mass spectrometry data, further replicates are required in

order to statistically determine whether there are differences in protein compostion depending on the material interface. Furthermore, well known FA proteins were not identified or they were characterised by low abundance. This may be due to the presence of significant amounts of actin and FN in FA fractions. Subsequently, further steps are required in order to remove actin, for example by immunodepletion[311].

5. Cell migration

5.1 Introduction

Cell migration is a highly integrated process and plays an important role in both physiological and pathological cell processes, for example morphogenesis during development, immune response, wound repair and tumour metastasis[312]. There are different modes of cell migration, such as single-cell migration (amoeboid or mesenchymal) or collective migration, and they depend on the cell type[313]. For example, epithelial cells move along a basement membrane[314] whereas leukocytes migrate along and through any membrane in the body[315]. Cells exerting mesenchymal migration are characterised by high levels of adhesion to the ECM and cytoskeleton contractility. Contrary, amoeboid migration describes the migration of highly motile, rounded or ellipsoidal cells which do not form FAs and exert weak traction forces on the surrounding environment[316]. Collective cell migration is involved in tissue formation, organ development and wound healing and refers to the coordinated migration of a group of cells in the same direction at a similar speed [317].

Cell migration is tightly controlled and requires rapid changes in cell adhesion and actomyosin cytoskeleton. Generally, during cell migration cells appear polarised having a leading edge which points in the cell direction and a trailing edge (Figure 5.1). Dynamic control of intracellular signals including GFs and ECM interactions is essential for the maintenance of cell polarity[318]. The leading edge is characterised by actin polymerisation followed by the formation of protrusions and membrane extension which mediates cell attachment and traction forces to the substrate. Stronger cell attachment caused by the contraction of the cytoskeleton filaments is observed at the cell front and the cell body is being pulled towards the leading edge. In contrast, adhesions are disassembled and released at the cell rear to allow the tail to retract. All these steps result in coordinated cell translocation[270, 319].

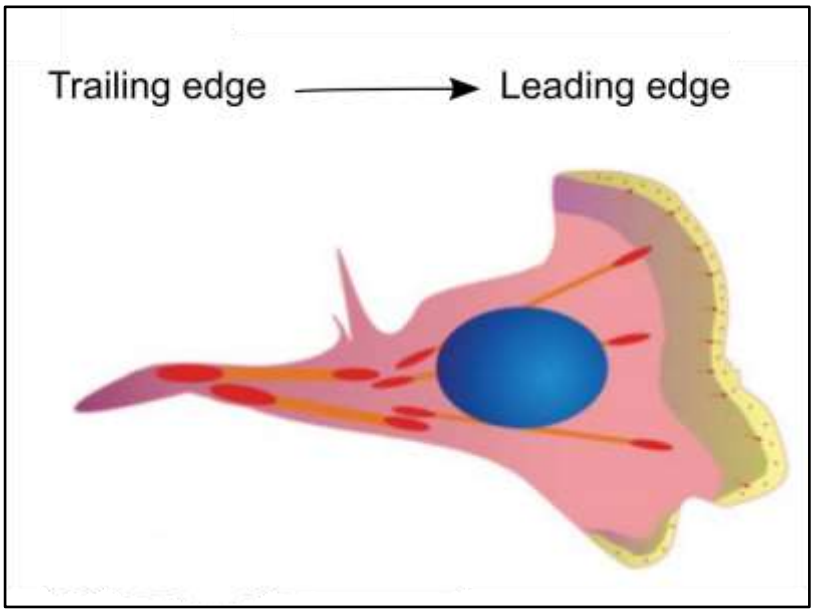

Figure 5.1. Polarity in migrating cell. Polarisation requires dynamic reorganisation of actin cytoskeleton and is characterised by the development of a protruding front which is closer to the direction of migration, and a retracting rear[319].

Diverse physical and chemical signals coming from the ECM strongly affect cell migration. For example, it has been demonstrated that stiffer and more rigid matrices support enhanced cell migration[320-323]. Furthermore, cell adhesion to the ECM, mainly *via* integrins, is fundamental in migratory behaviour. As previously described, integrins link the cell to the substratum and regulate signalling pathways, such as FAK[324, 325], essential for cell migration. Different integrins have distinct roles in cell migration. For example, $\alpha_5\beta_1$ has been shown to assemble nascent adhesions and promote cell protrusions whereas $\alpha_v\beta_3$ reinforces the development of large FAs and accumulates in areas subjected to high tension[326]. In addition, β_1 promotes random migration while β_3 induces persistent migration[327]. During migration FAs undergo repeated cycles of assembly and disassembly followed by a change in their protein composition[319, 328]. Their role in cell migration is well documented. For example, it has been shown that nascent FAs transmit sufficient forces to pull the cell forward[329]. In addition, varying the size of FAs using nanopatterned surfaces correlates with a specific cell migratory behaviour[330].

It is well established that cell motility is influenced by the ligand density presented on the substrate, the integrin expression levels of the cells and the

integrin-ligand affinity[331, 332]. Changes in cell migration on protein coated surfaces can be also due to changes in the protein conformation which result in changes in protein bioactivity[332]. It has become evident that cell speed exhibits a biphasic behaviour and maximum cell speed occurs at intermediate levels of cell-substratum adhesiveness where both adhesion formation and release are efficient [331-334].

Studying cell migration behaviour in the presence of physichochemical cues is of great importance in order to design instructive biomaterials. This chapter focuses on the characterising the migratory behaviour of human fibroblasts and hMSCs on PEA and PMA coated with FN. Particularly, this work explores whether the differential conformation of adsorbed FN on PEA and PMA affects cell motility. To do so, migration assays were carried out over the course of 24 h and cell speed was characterised. FA morphology was analysed as well to explore whether there is a functional relationship with FN conformation. Matrix secretion and matrix reorganisation were studied as well.

5.2 Materials and methods

5.2.1 Materials

List of reagents	
Dulbecco's modified eagle's medium……	Sigma
Glutamax……	Invitrogen
Penicillin/streptomycin……	Biochrom
Dulbecco's phosphate buffered saline……	Life Technologies
Foetal bovine serum……	Biochrom/ Life Technologies
Human plasma fibronectin……	Sigma-Aldrich
Trypsin/EDTA……..	Sigma
Hoechst® 33342……	ThermoFisher Scientific
Formalheyde…….....	Fischer Chemicals
Tween20®……	Sigma-Aldrich
Bovine serum albumin……	Roche/Sigma
Mouse monoclonal anti-vinculin antibody……	Sigma
Mouse monoclonal anti-cellular FN antibody.....	Abcam
Cy-3 anti-mouse antibody…….....	Jackson ImmunoResearch
Alexa fluor 660 phalloidin…….....	Invitrogen
Alexa fluor 350 phalloidin	Invitrogen
Rhodamine phalloidin……	Life Technologies
Vectashield with DAPI……...	Vector Laboratories
FluoroTag FITC conjugation kit…….....	Sigma-Aldrich

5.2.2 Cell culture

Primary human dermal fibroblasts (from a 25-year old male) and hMSCs (from a 77-year old female) were used. Fibroblasts and hMSCs were maintained at 37°C and 5% CO_2 in DMEM (with glucose, 1% v/v P/S, and 10% v/v FBS) and in DMEM (low glucose, 1% v/v P/S, 10% v/v FBS and 1% v/v Glutamax) respectively. Media change was carried out every 3 days. For splitting or cell seeding, cells were rinsed twice with warm PBS followed by 2.5 ml of trypsin/EDTA. Cells were incubated at 37°C for 60 to 120 sec until the cells were detached from the tissue culture flask. Next, 7.5 ml of complete medium (supplemented with 10% v/v FBS) was added to the flask, cell suspension was transferred to a falcon tube and cell density was measured using a cell counter (CASY model TT system). Next, cell solution was centrifuged at (fibroblasts: 1500 rpm for 6 min or for 8 min, hMSCs: 1300 rpm for 8 min). Afterwards, the

supernatant was removed and the cell pellet was suspended in 1 ml of medium. Primary fibroblasts and MSCs were used at passages P0 to P5.

5.2.3 Optimisation of migration assay

TCP was coated with FN at 20 µg/ml for 1 h. Human fibroblasts were harvested, cell solution was diluted in medium at a density of 5000 cells/cm^2 and cells were seeded on the samples. For diluting the cell solution, medium containing 10% v/v FBS or FBS-free was used. Cell cultured was maintained at 37°C, 5% CO_2 for 3 h. In order to assess the effect of nuclear staining on cell migration, cells were incubated with Hoechst® 33342 nucleic acid dye for 10-15 min at 37 °C. Next, medium was replaced by fresh cell culture medium. For this optimisation, cells without nuclear staining were included too. The plate was mounted in the motorised staged of a Leica DMI6000 time-lapse microscope to record cell migration. Four ROIs in each sample were selected and images were recorded every 15 min for 24 h. Four time-lapse videos were analysed per condition. To characterise cell velocity, automatic tracking the nucleus was carried out, whereas manual tracking of nucleus was carried out for cells without nuclear staining. The software Volocity was used to quantify cell velocity.

Conditions:

1. without FN-coating, without FBS, without DNA staining
2. with FN-coating, without FBS, without DNA staining
3. without FN-coating, with FBS, without DNA staining
4. with FN-coating, with FBS, without DNA staining
5. without FN-coating, without FBS, with DNA staining
6. with FN-coating, without FBS, with DNA staining
7. without FN-coating, with FBS, with DNA staining
8. with FN-coating, with FBS, with DNA staining

5.2.4 Cell seeding on surfaces

UV sterilised PEA and PMA cover slips were coated with FN at 20 µg/ml for 1 h. After cells were harvested by trypsinisation, they were seeded at a density of 5000 cells/cm^2. Medium supplemented with 10% v/v FBS was used. Cells were maintained at 37 °C for 3 h. Next, nuclear staining was carried out by

incubating the cells with Hoechst® 33342 nucleic acid dye for 10-15 min at 37°C. Next, the medium was replaced by fresh cell culture medium and the plate was mounted in the motorised staged of a Leica DMI6000 time-lapse microscope to record cell migration. Four ROIs in each sample were selected and images were recorded every 10 min for 24 h. Four time-lapse videos were analysed per condition and velocity was assessed by automatically tracking the cell nucleus using the software Volocity. To characterise FA formation, FN secretion and FN remodelling, PMA and PEA cover slips were coated with FN at 20 µg/ml for 1 h. Human fibroblasts and hMSCs were seeded at a density of 5000 cells/cm^2 and incubated at 37°C for 6 h and 22 h. Medium supplemented with 10% v/v FBS was used. Next, samples were fixed (3.7% v/v formaldehyde/PBS) at 4°C and washed with PBS.

5.2.5 FITC-labelled FN

FN solution was prepared at 1 mg/ml in milliQ water. Next, two solutions of sodium carbonate were prepared: (1) 1 M sodium carbonate in milliQ water and (2) 0.1 M sodium carbonate in milliQ water. Next, solution (1) was added to FN solution (1:10). Next, one vial of FITC was reconstituted with 2 ml of solution (2) until all FICT was dissolved. Next FITC solution was mixed with FN solution (1:25). The tube was covered with aluminium foil to protect from light and it was incubated for 2 h at room temperature. Next, the cap of a Sephadex G-25M column was removed and the lower tip was cut to let excess of liquid flow through. After the column was equilibrated with PBS, the FITC-mixture was added to the top to separate labelled FN from unconjugated molecules. Next, PBS was used to elute the column and 0.25 ml fractions were collected. The absorbance of each fraction was measured at 280 nm and at 495 nm using a nanodrop (Nanodrop100 spectrophotometer, ThermoScientific) to calculate the FITC/Protein molar ratio (F/P) according to the equation:

$$\frac{MW}{389} \times \frac{A495/195}{A280\ -[(0.35 \times A495)/E_{280}^{0.1\%}} = \frac{A495 \times C}{A280\ -[(0.35 \times A495)}$$

Where: $C = \frac{MW \times E_{280}^{0.1\%}}{389 \times 195}$

MW is the molecular weight of the protein and 389 is the molecular weight of FITC. 195 is the absorption $E_{280}^{0.1\%}$ of bound FITC at 490 nm at pH 13.0. $E_{280}^{0.1\%}$ is the absorption at 280 nm of a protein at 1.0 mg/ml. $0.35 \times A495$ is the correction factor due to the absorbanve of FITC at 280 nm. C is a constant value for FITC conjugation of a given protein.

5.2.6 Immunohistochemistry

5.2.7 Focal adhesions

The protocol for vinculin, actin and nuclei staining is described in section 4.2.7.

5.2.8 Fibronectin secretion

Fixed cells were incubated with permeabilisation buffer for 5 min followed by blocking (1% v/v BSA/PBS) for 30 min. Next, samples were incubated with mouse monoclonal anti-cellular FN antibody (1:400) in blocking solution for 1h. After they were washed twice (0.5% v/v Tween20/PBS), they were incubated with secondary Cy-3 anti-mouse antibody (1:200) and Alexa fluor 488 phalloidin (1:100) in blocking solution for 1 h. Next, samples were washed again and they were mounted using Vectashield with DAPI. For analysis, fluorescent images of endogenous FN were exported ImageJ and the integrated density was measured.

5.2.9 Fibronectin reorganisation

Fixed cells were incubated with permeabilisation buffer for 5 min followed by blocking (1% v/v BSA/PBS) for 30 min. Next, fibroblasts were incubated with mouse monoclonal anti-cellular FN antibody (1:400) in blocking solution for 1h. After samples were washed (0.5 % v/v Tween20/PBS), they were incubated with secondary Cy-3 anti-mouse antibody for 1h and Alexa fluor 350 phalloidin (1:100) in blocking solution for 1 h. MSCs were incubated with rhodamine phalloidin (1:100) in blocking solution for 1 h. Finally, fibroblasts and MSCs were mounted with Vectashield without DAPI and with DAPI respectively. To quantify FN reorganisation, images were exported to ImageJ and actin was used as a mask for FITC-FN reorganisation. The mean intensity of FITC-FN underneath each cell as measured and normalised to the mean intensity of area outside the cell.

5.2.10 Cell imaging

Fluorescent pictures were taken using an epifluorescence microscope (Zeiss AXIO Observer Z1, Jena, Germany).

5.2.11 Statistical analysis

Data are represented are mean ± SD and were analysed using GraphPad Prism 6. Statistically significant differences were assessed by two-way ANOVA using a Bonferroni post hoc test at a 0.05 significance level, with *$p < 0.05$, **$p < 0.01$, ***$p < 0.0001$.

5.3 Results

5.3.1 Optimisation

In order to characterise the effect of FBS and DNA staining on cell migration, human fibroblasts were initially cultured on TCP coated with FN. Culture media was either FBS-free or contained 10% v/v FBS. Culture was maintained for 3 h and a live-cell fluorescent staining of nuclei was carried out. Cells without DNA staining were included too. For cells without DNA staining, velocity was characterised by manually tracking of nucleus. For cells with DNA staining, velocity was characterised by automatic tracking.

Cell speed was higher when complete medium was used and cells were not DNA-stained (black bars). Cell speed however decreased when DNA staining was carried out (blue bars). FBS also played a role in velocity. When media was not supplemented with FBS and cells were not DNA stained, cell speed decreased over time (white bars). Velocity decreased more when DNA staining was carried out (light blue bars) (Figure 5.2). Based on these observations, the following migrations assays were carried out in complete medium since it was more favourable to the cells. In addition, although DNA staining compromised cell migration, it was carried out in order the cell tracking to be possible.

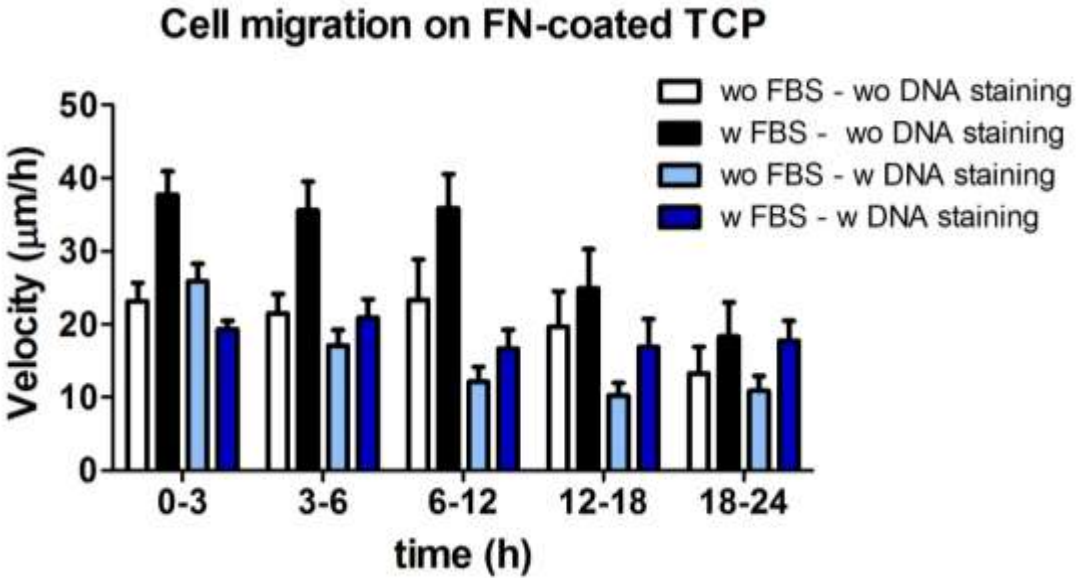

Figure 5.2. Migration of human fibroblasts on FN-coated TCP over 24 h. Graphs shows the velocity of human fibroblasts and demonstrates how FBS and nucleus staining affects cell speed. (n=3 per sample, 1 biological replicate).

5.3.2 Velocity

PEA and PMA are chemically similar with PEA containing one more methyl group than PMA. However, while similar, a different conformation of FN is adopted upon adsorption on PEA and PMA. To study whether such changes in organisation affect cell migration, a 24 h migration assay was carried out. Fibroblasts and hMSCs were seeded on FN-coated PEA and PMA and maintained at 37°C for 3 h to allow for initial attachment. Cell velocity (μm/h) was characterised over the course of 24 h.

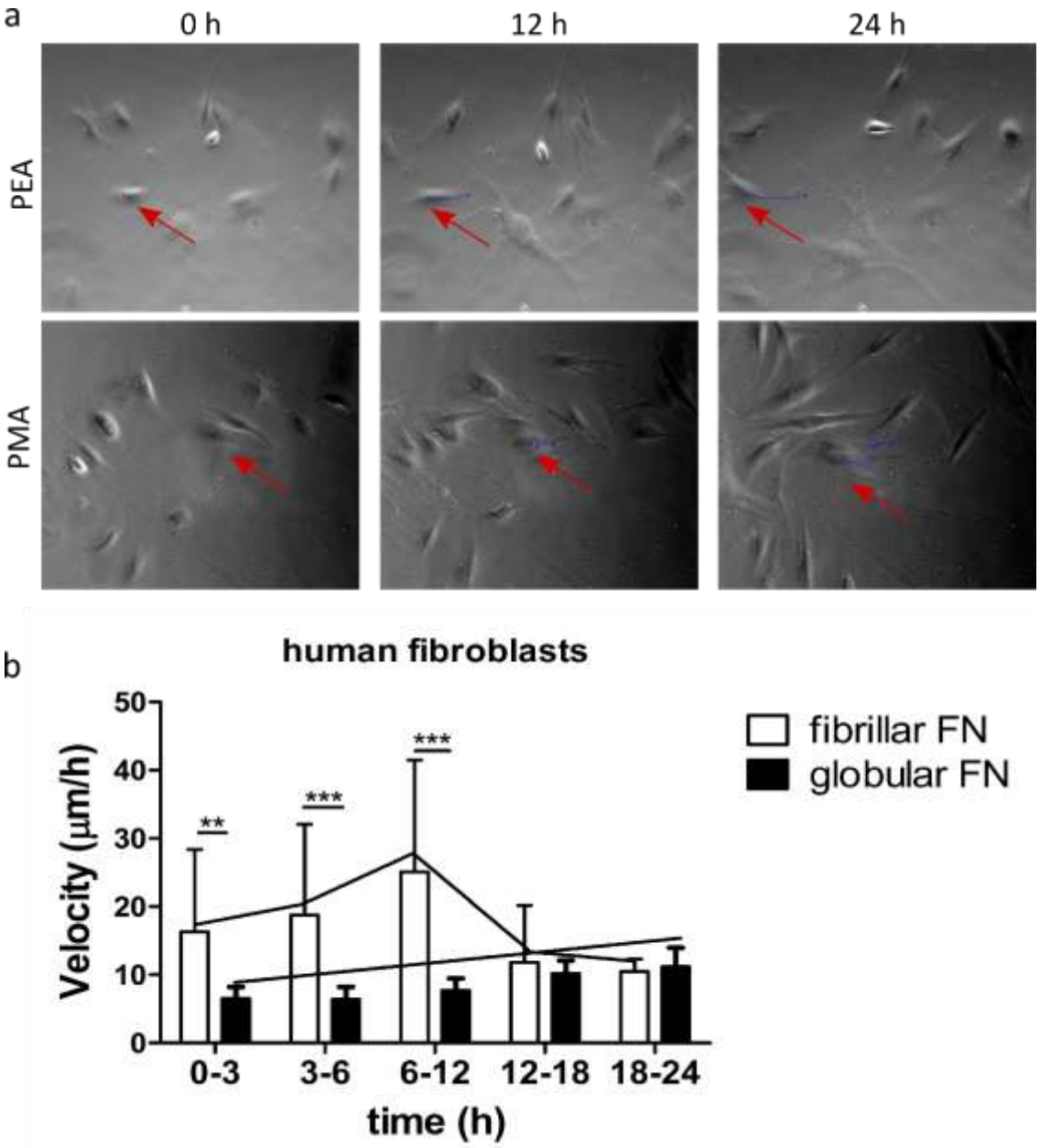

Figure 5.3 Migration of human fibroblasts on fibronectin-coated PEA and PMA over the course of 24h. (a) Phase contrast pictures of human fibroblasts on PEA and PMA 0h, 12h, 24h after attachment. Red arrows indicate the

migration of single cells over time. (b) Velocity (μm/h) of human fibroblasts. (n=3 per sample, 3 biological replicates).

Human fibroblasts moved rapidly on PEA for the first 12 h and after this cell speed decreased. In contrast, no such initial rapid cell movement was observed on PMA, on which fibroblasts only slightly increased their speed over time. Fibroblast speed was highly significantly ($p<0.001$) greater on PEA than on PMA during the first 12 h, achieving up to ~ 25 μm/hour on PEA compared to ~10 μm/hour on PMA (Figure 5.3).

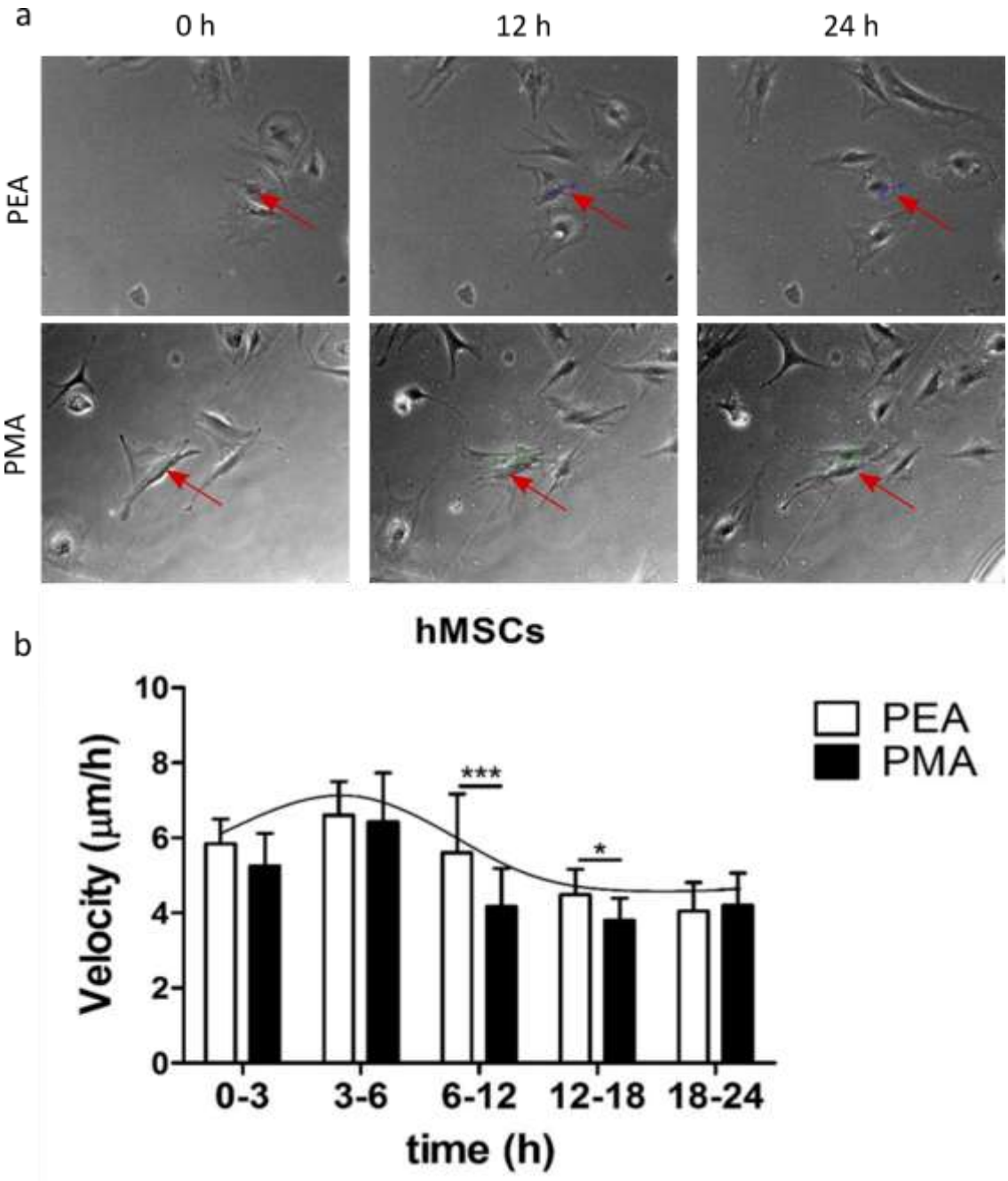

Figure 5.4. Migration of hMSCs on fibronectin-coated PEA and PMA over the course of 24h. (a) Phase contrast pictures of hMSCs on PEA and PMA 0h,

12h, 24h after attachment. Red arrows indicate the migration of single cells over time. (b) Velocity (μm/h) of hMSCs. (n=3 per sample, 3 biological replicates).

For MSCs, cell velocity followed a similar trend on both polymers. As shown in the graph (Figure 5.4, b), cells increased their speed within the first 6 h and then it slowed down reaching an average speed of ~4.2 μm/h

5.3.3 Focal adhesion analysis

The morphology of FAs was characterised on the material interface in order to elucidate whether there is a functional relationship between cell motility and FA morphology. Cells were seeded on FN coated PEA and PMA and a vinculin staining was carried out after 6 h and 22 h. Area and length distribution of FAs were analysed by quantifying the fluorescent pictures (Figure 5.5, Figure 5.6).

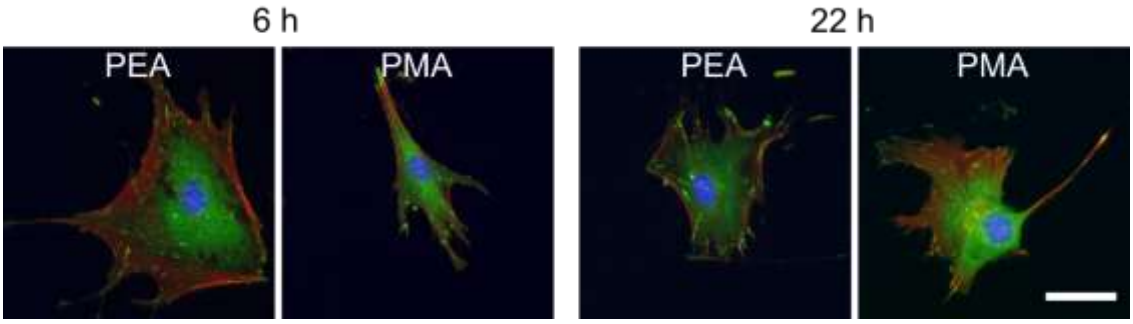

Figure 5.5. Immunofluorescence images of human fibroblasts on FN-coated PEA and PMA 6 h and 22 h after seeding. Fluorescent staining of vinculin (green), F-actin (red) and nuclei (blue). Scale bar is 50 μm. (n=3 per sample, 1 biological replicate).

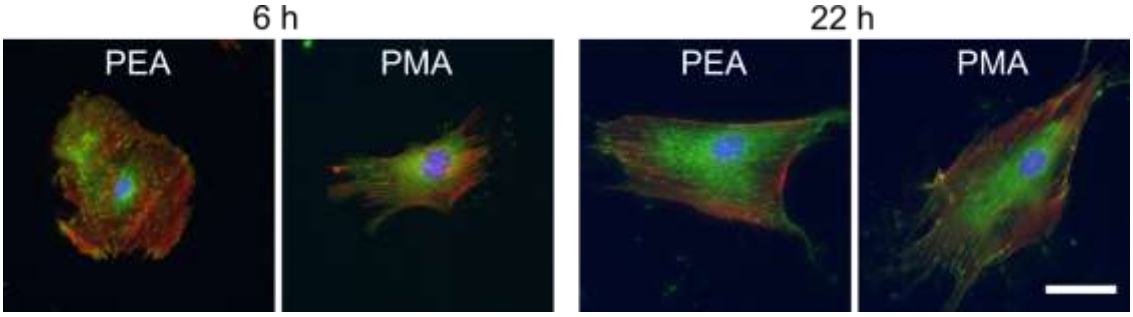

Figure 5.6. Immunofluorescent images of hMSCs on FN-coated PEA and PMA 6 h and 22 h after seeding. Fluorescent staining of vinculin (green), F-actin (red) and nuclei (blue). Scale bar is 50 μm. (n=3 per sample, 1 biological replicate).

Gross cell morphological differences were not observed between PEA and PMA. Cells looked similarly well spread and well-formed FAs were observed (Figure 5.5, Figure 5.6). For quantitative analysis of FAs, they were classified by area as immature (0-1 μm^2), intermediate (1-2 μm^2) and mature (>2 μm^2) and further sub-classifed by length as short (1-2 μm), intermediate (2-3 μm) and long (>3 μm). Analysis of the adhesions revealed skewed distribution (towards smaller adhesion as expected) on both PEA and PMA. For human fibroblasts, the fraction of mature FAs (≥ 2μm^2) remained constant with time on PEA (from 14% to 16%) and PMA (from 15% to 14%) (Figure 5.7). Similarly, no differences were found in the fraction of mature FA over time for hMSCs (Figure 5.8).

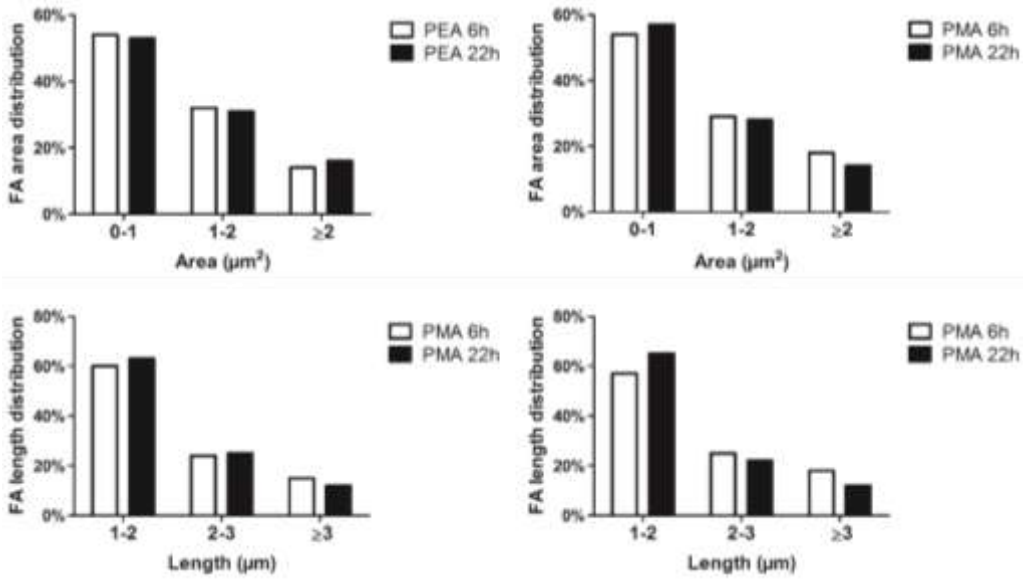

Figure 5.7. Area amd length distribution of FAs of human fibroblasts on FN-coated PEA and PMA 6 h and 22 h after seeding. (20 images per condition were analysed, n=3 per sample, 1 biological replicate).

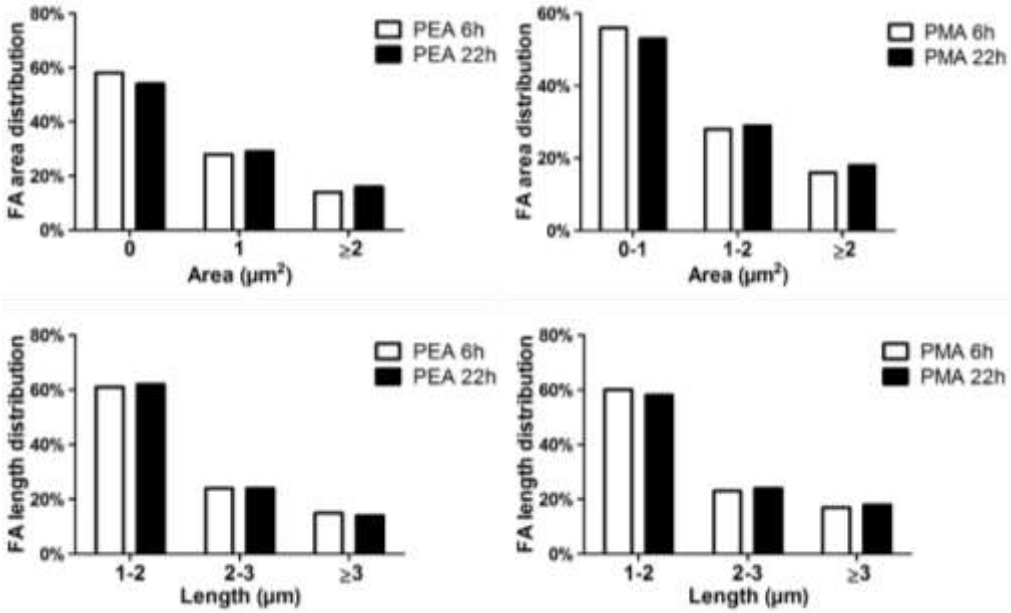

Figure 5.8. Area amd length distribution of FAs of hMSCs on FN-coated PEA and PMA 6 h and 22 h after seeding. (20 images per condition were analysed, n=3 per sample, 1 biological replicate).

5.3.4 Endogenous FN

The effect of FN conformation on PEA and PMA on cell secreted, endogenous FN was explored. Cells were seeded on FN coated PEA and PMA and staining of endogenous FN was performed 6 h and 22 h after seeding. Immunofluorescent staining of fibroblasts and hMSCs showed an increase of deposited endogenous FN over time confirmed by quantification of the images (Figure 5.9, Figure 5.10).

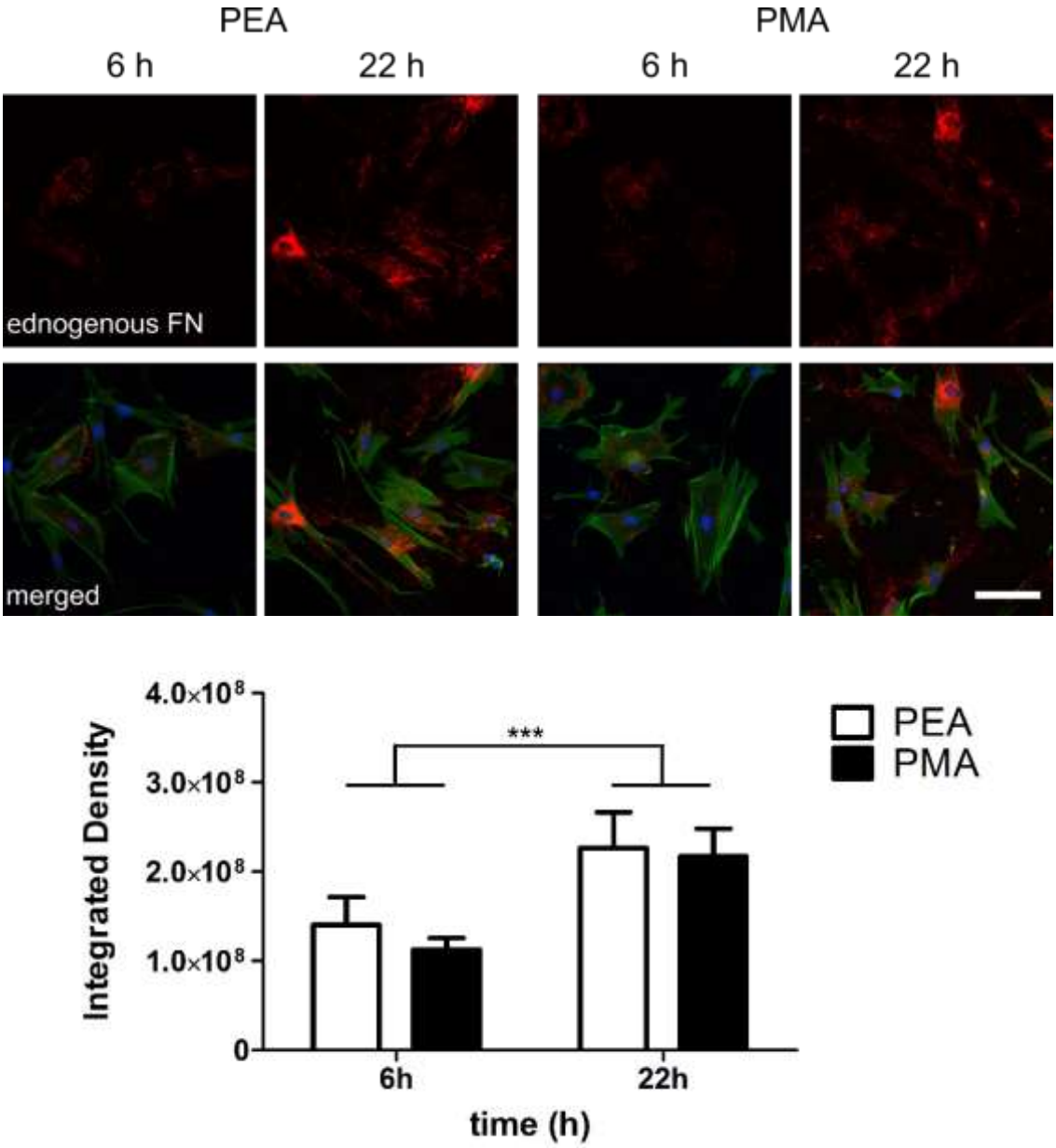

Figure 5.9. Endogenous FN. Immunofluorescent images of human fibroblasts on FN-coated PEA and PMA 6h and 22h after seeding. Staining of endogenous FN (red), actin (green) and nuclei (blue). Scale bar is 100 μm (top). Quantification of FN secreted by human fibroblasts on PEA and PMA (white

and black bars respectively) 6h and 22h after seeding (bottom). (20 images per condition were analysed, n=3 per sample, 1 biological replicate).

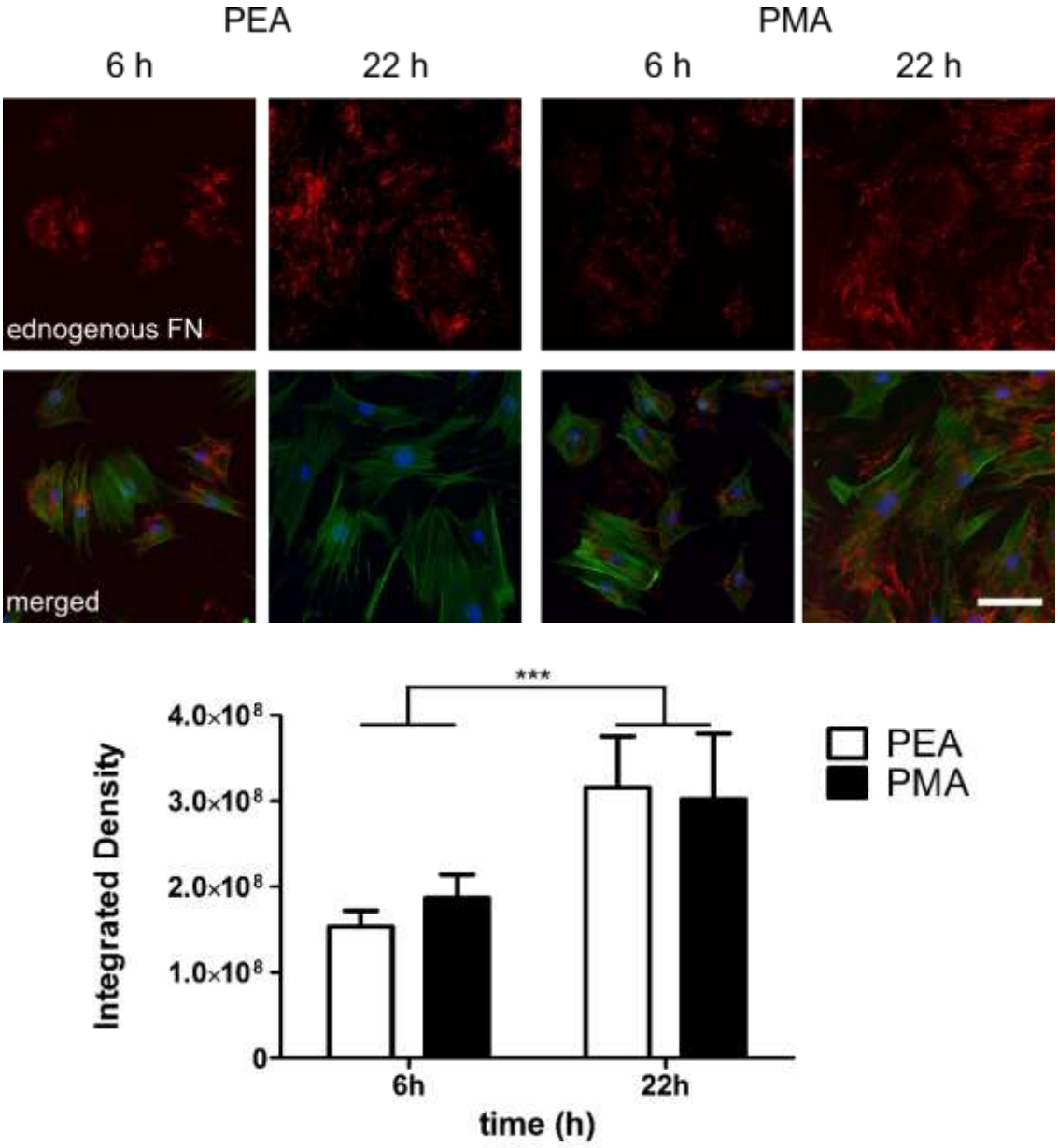

Figure 5.10. Endogenous FN. Immunofluorescent images of hMSCs on FN-coated PEA and PMA 6h and 22h after seeding. Staining of endogenous FN (red), actin (green) and nuclei (blue). Scale bar is 100 μm (top). Quantification of FN secreted by human fibroblasts on PEA and PMA (white and black bars respectively) 6h and 22h after seeding (bottom). (20 images per condition were analysed, n=3 per sample, 1 biological replicate).

5.3.5 Fibronectin remodelling

In order to study how cells reorganise the pre-adsorbed layer of FN on PEA and PMA, FITC-labelled FN was used. FN reorganisation appears as dark areas against the fluorescent background surrounded by brighter fibrils. Human fibroblasts appeared to reorganise FN more effectively on PMA over time whereas poor reorganisation was found on PEA (Figure 5.11). Contrary, no differences in FN reorganisation by hMSCs were observed over time on both polymers (Figure 5.12).

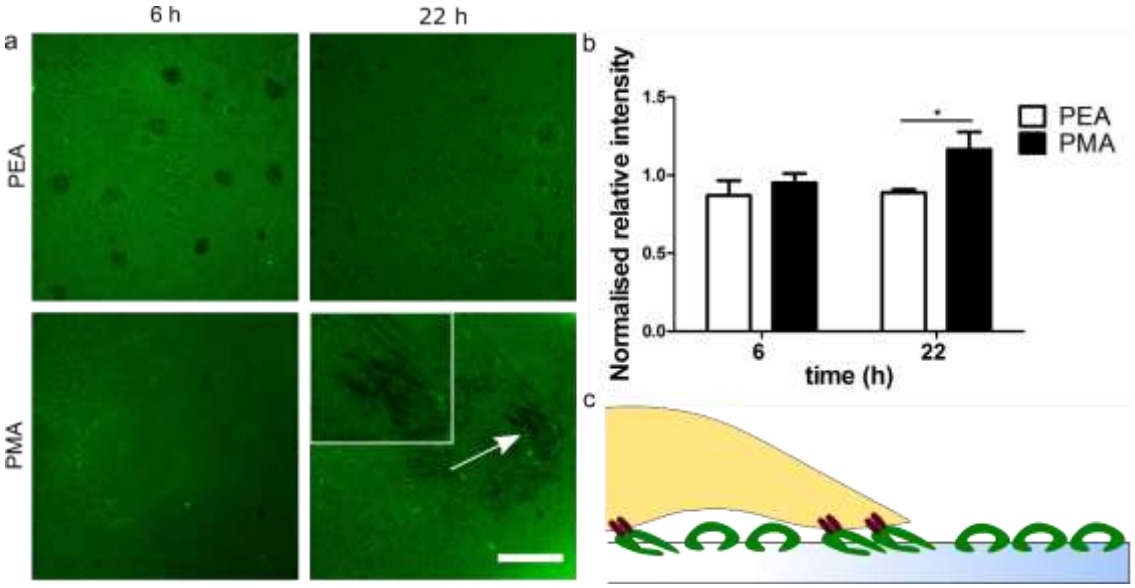

Figure 5.11. FN reorganisation by human fibroblasts. (a) Fluorescence pictures of FITC-labelled FN on PEA and PMA reorganised by human fibroblasts at 6h and 22h after seeding. Scale bar is 30 μm. (b) Normalised fluorescence intensity of FN within the cell compared with the intensity outside the cell area. (10 images per condition were analysed, n=3 per sample, 1 biological replicate).

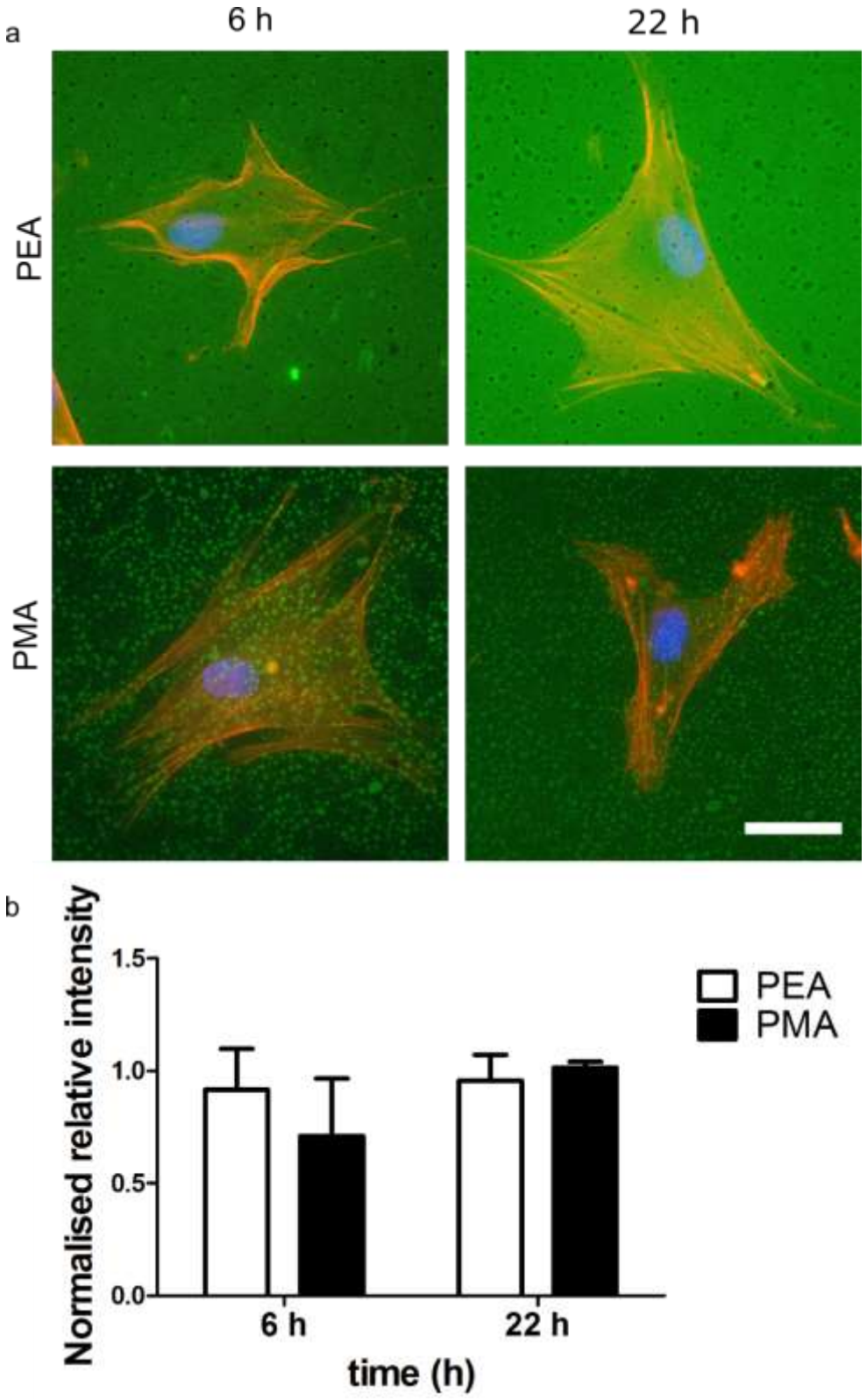

Figure 5.12. FN reorganisation by hMSCs. (a) Fluorescence pictures of FITC-labelled FN on PEA and PMA reorganised by hMSCs at 6h and 22h after seeding. Staining of actin (red) and nucleus (blue) Scale bar is 30 μm. (b) Normalised fluorescence intensity of FN within the cell compared with the intensity outside the cell area. (10 images per condition were analysed, n=3 per sample, 1 biological replicate).

5.4 Discussion

This chapter focuses on characterising the migratory characteristics of human fibroblasts and hMSCs on FN-coated PEA and PMA. These polymers have similar chemical properties and, when coated with FN, similar amount of the adsorbed protein have been measured (Figure 2.9). However, FN undergoes different structural changes upon passive adsorption on PEA and PMA triggered by the chemical properties of the substrate resulting in changes in protein and the availability of important binding domains (Figure 2.10, Figure 2.11, Figure 2.12)[196, 335, 336].

It is well established that cell migration is highly controlled by the ligand density, the ligand-integrin binding affinity and the integrin level[337]. With this in mind, FN conformation and its effect on cell migration was explored. Migration assays revealed that the initial speed of fibroblasts was higher the first 6 h on the FN network adopted on PEA followed by a decrease. Contrary, cells maintained their speed on globular FN on PMA over time (Figure 5.3). In the case of hMSCs, cell speed followed a similar trend on both surfaces; it increased within the first 6 h and then it decreased. However, higher speed was found on the FN networks on PEA over the 6th to 18th hours of migration, similarly to the higher speed of fibroblasts on this surface (Figure 5.4). Such biphasic behaviour in cell migration speed has been extensively described in previous studies which have cited that intermediate levels of cell adhesion were required for this enhanced migration to be seen[331, 332, 338]. It is also known that multiple domains of FN contribute to cell migration e.g. RGD and PHSRN synergy sequence[339-341], thus different structural patterns might result in changes in cell motility. The availability of the PHSRN site located in a loop region of $FNIII_9$ was found higher on PEA than on PMA (Figure 2.12). In addition, other studies have associated the PHSRN with enhanced cell migration *in vitro* and accelerated wound healing *in vivo*[342, 343]. We thus postulate that the network-like conformation of FN on PEA provides a sufficient level of adhesiveness for enhanced fibroblasts motility. In contrast, the globular organisation on PMA might alter the extent to which important binding domains are displayed, resulting in decreased cell motility compared to PEA.

FAs formation was examined in order to gain further insights into cell migration. Previous work has correlated FA size and cell speed[344]. However, in this study FA distribution was not dramatically different in fibroblasts or hMSCs on either PEA or PMA (Figure 5.5, Figure 5.6, Figure 5.7, Figure 5.8). Thus, it appears that size, per se, was not responsible for cell migration on the substrates and that other cell functions, such as the secretion or cell driven re-organisation of ECM proteins might affect and regulate cellular migration beside the initial microenvironment available to cells.

ECM synthesised and secreted by cells can have an impact on cell migration[345]. To further explore migratory characteristics, we investigated whether cell migration was associated with cell-mediated FN remodelling, including its reorganisation and deposition. An increase in FN secreted by both fibroblasts and hMSCs was found over the course of 24 hours. However, no significant changes were observed between substrates (Figure 5.9, Figure 5.10). Interestingly, MSCs were shown to secrete more FN compared to fibroblasts on both PEA and PMA. We thus postulate that a more abundant matrix secretion might affect cell migration, hindering a differential migratory response of hMSCs to FN conformation.

Remodelling of the ECM induced by cell-generated traction forces is a highly regulated process and is essential for important cellular functions including cell migration. Previous work using 3D collagen matrices has, for example, reported that higher invasiveness of breast cancer cells on areas that were not reorganised[346]. Similarly, enhanced invasion and migration of breast cancer cells was found when ECM acquired a specific alignment[347]. In order to gain further insights into this process, the reorganisation of adsorbed FN by fibroblasts and hMSCs was assessed. FN remodelling by fibroblasts was higher on PMA over time whereas no changes were seen on PEA (Figure 5.11). It can be suggested that cells might have to reorganise the layer of FN to be able to use the RGD and PHSRN groups efficiently on PMA, while on PEA the FN is presented to the cells in a more immediately usable conformation. This lack of having to reorganise the adsorbed FN might lead to the higher speed of fibroblasts observed on PEA. It could be further postulated that, as cells tend to modify their surrounding environment before they secrete their

own matrix[212, 348], the strong interaction of FN with PEA inhibits this matrix remodelling, resulting in a decrease in cell speed after the initial rapid migration phase. On the other hand, FN reorganisation by hMSCs was similar on both PEA and PMA over time (Figure 5.12); cell speed was similar on both PEA and PMA (it was higher on PEA only from the 6th to 18th h of the migration assay). It can be postulated that, due to the high matrix secretion, the layer of adsorbed FN on both PEA and PMA might not be easily available for the cells to reorganise it. Therefore, cell binding domains might not become available and subsequently efficient cell attachment might be hindered. It can be hypothesized that this might be associated with the similar trend of cell speed exhibited on PEA and PMA by hMSCs.

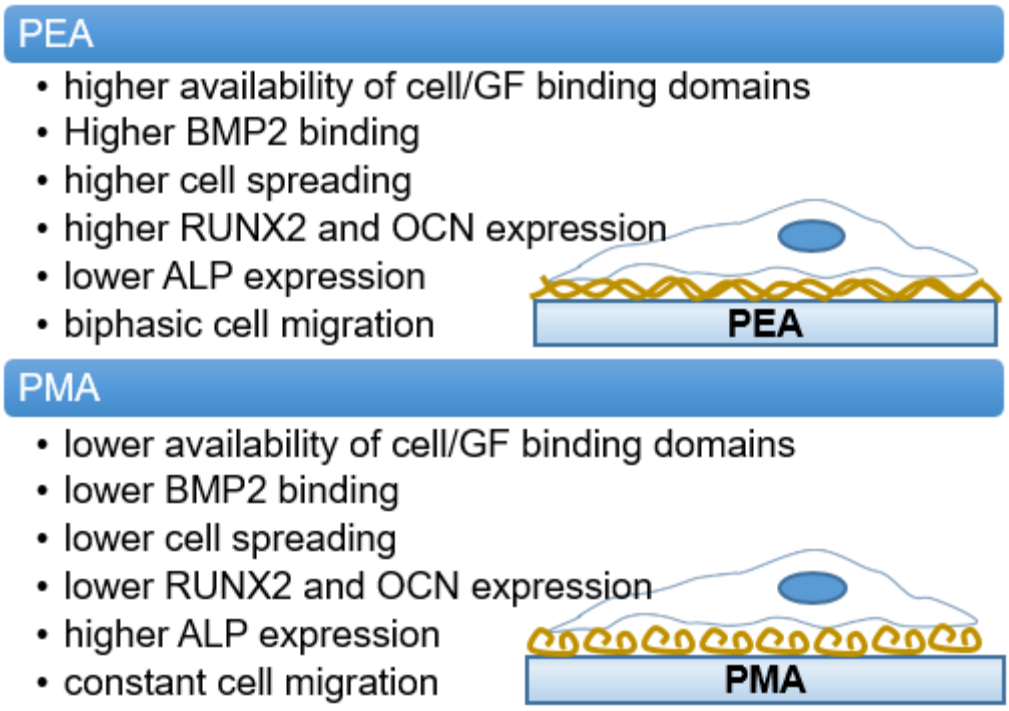

Figure 5.13. Summary of results obtained for PEA and PMA. Schematic summarises the main results in terms of domain availability, BMP2 binding, cell adhesion, osteogenic differentiation and migration.

6. Discussion and Conclusions

6.1 Discussion

Stem cells hold a position of great importance for maintaining proper tissue function and replacing damaged cells after injury. They reside in a multipotent and quiescent state in a specialised microenvironment, the niche, which is found in most adult issues. This niche provides spatial and temporal exogenous cues which promote quiescence or coordinate stem cell activation for example in response to injury[349]. Due to their diverse differentiation potential, stem cells represent a promising source for TE and therapeutic strategies. Among adult stem cells, MSCs can be isolated from several adult tissues including bone marrow, adipose tissues, liver and pancreas, and can differentiate into diverse lineages. Because of their properties, they show great potential in clinical applications. For example, Horwitz *et al*. demonstrated the potential of mesenchymal progenitors in transplanted marrow in treating children with osteogenic imperfecta[350]. However, the development of cell-based approaches is hindered by the inability to manipulate stem cells while maintaining their potency *in vitro*[351].

Stem cells are in constant and dynamic interactions with the ECM, which is required for the regulation of cell processes. Deciphering the mechanisms that control cellular processes has therefore become an area of great interest. TE thus aims at engineering novel biomaterials which not only provide a scaffold for cells, but also sustain their function by providing physicochemical signals in a controlled environment. A plethora of biomaterials has been used over the years attempting to recapitulate the physiological ECM. Numerous studies have identified important parameters for a controlled cell response; it is now well established that surface topography, chemistry, stiffness and dimensionality are of critical significance[64, 193, 352, 353]. Among the biomaterials, polymers have been extensively used due to their diversity and their advantages in terms of their manufacturing process and reproducibility[354]. However, biomaterials might fail to efficiently mimic the cell native environment. This can be due to the lack of fine cues which cells can recognise and respond to. Surface modification, such as coating of polymeric surfaces with protein components or peptides, is a common approach to address this issue and ensure surface functionality and activity[185].

As already described, the ECM is a natural 3D network composed of fibre-forming proteins, such as laminin, collagen, FN, and other proteins such as glycosaminoglycans and soluble factors[3]. It is a reservoir of biochemical signals and it constantly remodelled through cell-mediated forces. Several studies have used ECM proteins for surface coating in order to generate interfaces which cells can interact with[64, 196, 244]. In addition to the physical properties of the ECM, biochemical components, such as growth factors, can regulate cell behaviour. For example, attempts have been made to incorporate growth factors into polymeric substrates in order to induce stem cell differentiation[260]. More specifically, BMP-2 has been associated with osteogenic differentiation and bone formation and recombinant BMP-2 is approved by the U.S. Food and Drug Administration and already used for certain clinical applications[355]. However, a supraphysiologic dose of BMP-2 (1.5 mg/ml) is required and can induce adverse clinical effects such as inflammation and extopic bone formation[356].

Among the ECM proteins, FN has been used in several TE studies. FN is a large glycoprotein and contains multiple domains for cell adhesion, protein interactions and growth factor binding. It has attracted significant attention because it undergoes fibrillogenesis *in vivo via* integrin binding and application of mechanical forces which eventually results in the formation of a fibrillar meshwork. This in turn can alter FN bioactivity though the exposure of binding domains. A number of studies have demonstrated that $FNIII_{12\text{-}14}$ strongly interacts with growth factors[70], while $FNIII_{9\text{-}10}$ favours integrin engagement and cell binding[66]. It is now also known that fibrillogenesis can occur in cell-free systems for example by using chemical agents such as polyamines[357]. These systems that induce a specific FN organisation can be used to get better insights into the regulatory role of the ECM in cell behaviour.

The effect of intrinsic polymer properties with respect to FN organisation has been investigated in several studies. Two synthetic polymers, poly(ethyl acrylate), PEA and poly(methyl acrylate), PMA have been shown to trigger two distinct FN conformations upon adsorption[353]. A network-like conformation is observed on PEA whereas FN is maintained in a globular state on PMA. Several studies have demonstrated the effect of these two material interfaces

in cell response. For example, the network organised on PEA enhances myoblast differentiation *via* cell contractility[353]. It is also shown that PEA favours the synergistic interactions of growth factor receptors and integrins[244, 358].

The overall aim of this work was to investigate whether polymeric surfaces with defined chemistries of EA/MA can trigger distinct FN conformations and to characterize the effect of the material interface in MSC behaviour in terms of adhesion and osteogenic differentiation. Moreover, a method was developed in order to isolate focal adhesions from MSCs cultured on PEA and PMA. The adhesive structures were further characterised by proteomic analysis in order to investigate how the network-like and globular FN might affect their protein composition. Finally, the effect of FN organisation on cell migration was studied too.

6.2 Thesis conclusions

- **FN conformation depends on the EA/MA ratio.**
  A well connected and extended network is formed on PEA. The network becomes less connected when MA is introduced and FN globular aggregates are formed on PMA.

- **Differential FN conformation affects domain availability and BMP-2 adsorption.**
  The availability of the $FNIII_8$, $FNIII_{9\text{-}10}$ and $FNIII_{12\text{-}14}$ domains is higher with increased EA concentration. Also, more BMP-2 particles are adsorbed on PEA100 and PEA70. Consequently, the integrin binding domain of FN is presented in synergy with BMP-2 on the surfaces where FN forms a more extended network.

- **Cell morphology and osteogenic differentiation are affected by the underlying surfaces**.
  hMSC size is higher and spreading is better with increased EA concentration. When the surfaces are coated with FN/BMP-2, higher expression of RUNX2 and OCN is induced on PEA. In contrast, higher expression of ALP is induced on PMA. It is important to note that low dosed of BMP-2 drive the osteogenic differentiation of cells.

- **FA protein composition is different on FN coated PEA and PMA.** Proteomic analysis of the FAs isolated on PEA and PMA followed by PCA shows that their protein composition differs on PEA and PMA.

- **FN organization on PEA and PMA causes cell to migrate differently.** Human fibroblast have to reorganise FN adsorbed on PMA before they can fully exploit it and by the time they have reorganised it they have changed from migratory/proliferative activity to a more matrix-secreting, differentiating activity; thus their speed is always slow. On PEA, however, they can immediately exploit the networks for movement and growth causing an initial speedy migration followed by a slow migration.

6.3 Further work

The potential of the copolymers to drive the osteogenic differentiation of MSCs was investigated by characterising the expression of osteogenic markers. As part of this work, it was intended that signaling pathways triggered by BMP-2 were studied. Previous work showed enhanced FAK phosphorylation in C2C12 cells with increased EA concentration[359]. It is therefore particularly interesting to study whether the degree of FN fibrillogenesis affect FAK signaling and other important pathways for osteogenic differentiation, including Smad and ERK signaling. Besides investigating signaling pathways, it is also essential to explore how BMP-2 receptors interact with integrins. Previous studies suggest that colocalisation and synergistic interaction of growth factors and integrins influence cell response. For example, integrin α_v has been found to colocalise with VEGFR-2 on the extended FN network on PEA[358], and coimmunoprecipitation of integrin β1 and BMPRI occurred on this surface[244]. Exploring whether gradual loss in network connection influences signaling events and receptor-integrin interactions will give better insights into the molecular mechanisms guiding MSC response to the external environment. Elucidating these mechanisms is critical in order to use stem cells as therapeutic tools.

In terms of proteomics, attempts were made to develop and establish a protocol to isolate FAs from MSCs grown on PEA and PMA. Analysis and

classification of the proteins previously associated with the integrin adhesome gave interesting results. However, more replicates are needed in order to efficiently characterise FA formation and composition. It should be noted that in this study PEA and PMA were included. In addition to these surfaces, examining whether the different degrees of FN fibrillogenesis adopted on the copolymers induce changes in the adhesome is interesting. This will allow us to further understand the role of FN conformation in cell response. Proteomic analysis can be also performed to assess whether BMP-2 binding on FN triggers changes in the protein composition. Given that the protein interactions within FAs are transient and are characterised by a continuous 'on' and 'off' state, it is also important to evaluate changes over time. Moreover, it is interesting to evaluate changes in FA composition when cell contractility is inhibited. Regarding cell migration, further experiments could be performed to analyse the different cell speed exhibited on PEA and PMA. For example, analysis of cell directionality and persistence could further elucidate migratory behaviour. Investigating whether there are differences in the type of integrins required for cell migration on the two materials could also be an important aspect.

Overall, materials that modulate FN conformation upon simple adsorption can be incorporated into novel approaches to study the response of other cell types. These series of copolymers can also be used to coat other type of scaffolds, such as 3D scaffolds, and create mimic more efficiently the natural ECM in order to gain further insights into how ECM interacts with cells.

7. References

1. Narayanan, K.; Mishra, S.; Singh, S.; Pei, M.; Gulyas, B.; Padmanabhan, P., Engineering Concepts in Stem Cell Research. *Biotechnology Journal*, 1700066-n/a.
2. Brown, P. T.; Handorf, A. M.; Jeon, W. B.; Li, W.-J., Stem Cell-based Tissue Engineering Approaches for Musculoskeletal Regeneration. *Current pharmaceutical design* **2013,** *19* (19), 3429-3445.
3. Theocharis, A. D.; Skandalis, S. S.; Gialeli, C.; Karamanos, N. K., Extracellular matrix structure. *Advanced Drug Delivery Reviews*.
4. Moser, M.; Nieswandt, B.; Ussar, S.; Pozgajova, M.; Fassler, R., Kindlin-3 is essential for integrin activation and platelet aggregation. *Nat Med* **2008,** *14* (3), 325-330.
5. Järveläinen, H.; Sainio, A.; Koulu, M.; Wight, T. N.; Penttinen, R., Extracellular Matrix Molecules: Potential Targets in Pharmacotherapy. *Pharmacological Reviews* **2009,** *61* (2), 198-223.
6. Mouw, J. K.; Ou, G.; Weaver, V. M., Extracellular matrix assembly: a multiscale deconstruction. *Nat Rev Mol Cell Biol* **2014,** *15* (12), 771-785.
7. Hynes, R. O., Integrins: Bidirectional, Allosteric Signaling Machines. *Cell* **2002,** *110* (6), 673-687.
8. Geiger, B.; Spatz, J. P.; Bershadsky, A. D., Environmental sensing through focal adhesions. *Nat Rev Mol Cell Biol* **2009,** *10* (1), 21-33.
9. Hynes, R. O., Integrins: A family of cell surface receptors. *Cell* **1987,** *48* (4), 549-554.
10. Xiong, J.-P.; Stehle, T.; Diefenbach, B.; Zhang, R.; Dunker, R.; Scott, D. L.; Joachimiak, A.; Goodman, S. L.; Arnaout, M. A., Crystal Structure of the Extracellular Segment of Integrin αVβ3. *Science (New York, N.Y.)* **2001,** *294* (5541), 339-345.
11. Campbell, I. D.; Humphries, M. J., Integrin Structure, Activation, and Interactions. *Cold Spring Harbor Perspectives in Biology* **2011,** *3* (3), a004994.
12. Springer, T. A.; Dustin, M. L., Integrin inside-out signaling and the immunological synapse. *Current Opinion in Cell Biology* **2012,** *24* (1), 107-115.
13. Calderwood, D. A., Integrin activation. *Journal of Cell Science* **2004,** *117* (5), 657.
14. Kim, C.; Ye, F.; Ginsberg, M. H., Regulation of Integrin Activation. *Annual Review of Cell and Developmental Biology* **2011,** *27* (1), 321-345.
15. Luo, B.-H.; Carman, C. V.; Springer, T. A., Structural Basis of Integrin Regulation and Signaling. *Annual review of immunology* **2007,** *25*, 619-647.
16. Kang, Q.; Song, W.-X.; Luo, Q.; Tang, N.; Luo, J.; Luo, X.; Chen, J.; Bi, Y.; He, B.-C.; Park, J. K.; Jiang, W.; Tang, Y.; Huang, J.; Su, Y.; Zhu, G.-H.; He, Y.; Yin, H.; Hu, Z.; Wang, Y.; Chen, L.; Zuo, G.-W.; Pan, X.; Shen, J.; Vokes, T.; Reid, R. R.; Haydon, R. C.; Luu, H. H.; He, T.-C., A Comprehensive Analysis of the Dual Roles of BMPs in Regulating Adipogenic and Osteogenic Differentiation of Mesenchymal Progenitor Cells. *Stem Cells and Development* **2009,** *18* (4), 545-558.
17. Wang, W.; Zhu, J.; Springer, T. A.; Luo, B.-H., Tests of Integrin Transmembrane Domain Homo-oligomerization during Integrin Ligand Binding and Signaling. *Journal of Biological Chemistry* **2011,** *286* (3), 1860-1867.
18. Hohenester, E., Signalling complexes at the cell-matrix interface. *Current Opinion in Structural Biology* **2014,** *29*, 10-16.
19. Anthis, N. J.; Campbell, I. D., The tail of integrin activation. *Trends in biochemical sciences* **2011,** *36* (4), 191-198.
20. Atherton, P.; Stutchbury, B.; Wang, D.-Y.; Jethwa, D.; Tsang, R.; Meiler-Rodriguez, E.; Wang, P.; Bate, N.; Zent, R.; Barsukov, I. L.; Goult, B. T.; Critchley, D. R.; Ballestrem, C., Vinculin controls talin engagement with the actomyosin machinery. *Nature Communications* **2015,** *6*, 10038.
21. Monkley, S. J.; Kostourou, V.; Spence, L.; Petrich, B.; Coleman, S.; Ginsberg, M. H.; Pritchard, C. A.; Critchley, D. R., Endothelial cell talin1 is essential for embryonic angiogenesis. *Developmental Biology* **2011,** *349* (2), 494-502.

22. Theodosiou, M.; Widmaier, M.; Böttcher, R. T.; Rognoni, E.; Veelders, M.; Bharadwaj, M.; Lambacher, A.; Austen, K.; Müller, D. J.; Zent, R.; Fässler, R., Kindlin-2 cooperates with talin to activate integrins and induces cell spreading by directly binding paxillin. *eLife* **2016,** *5*, e10130.
23. Humphries, J. D.; Wang, P.; Streuli, C.; Geiger, B.; Humphries, M. J.; Ballestrem, C., Vinculin controls focal adhesion formation by direct interactions with talin and actin. *The Journal of Cell Biology* **2007,** *179* (5), 1043-1057.
24. Wolfenson, H.; Bershadsky, A.; Henis, Y. I.; Geiger, B., Actomyosin-generated tension controls the molecular kinetics of focal adhesions. *Journal of Cell Science* **2011,** *124* (9), 1425-1432.
25. Galbraith, C. G.; Yamada, K. M.; Sheetz, M. P., The relationship between force and focal complex development. *The Journal of Cell Biology* **2002,** *159* (4), 695-705.
26. Small, J. V.; Auinger, S.; Nemethova, M.; Koestler, S.; Goldie, K. N.; Hoenger, A.; Resch, G. P., Unravelling the structure of the lamellipodium. *Journal of Microscopy* **2008,** *231* (3), 479-485.
27. Izzard, C. S., A precursor of the focal contact in cultured fibroblasts. *Cell Motility and the Cytoskeleton* **1988,** *10* (1-2), 137-142.
28. Prager-Khoutorsky, M.; Lichtenstein, A.; Krishnan, R.; Rajendran, K.; Mayo, A.; Kam, Z.; Geiger, B.; Bershadsky, A. D., Fibroblast polarization is a matrix-rigidity-dependent process controlled by focal adhesion mechanosensing. *Nat Cell Biol* **2011,** *13* (12), 1457-1465.
29. Guo, W.-h.; Frey, M. T.; Burnham, N. A.; Wang, Y.-l., Substrate Rigidity Regulates the Formation and Maintenance of Tissues. *Biophysical Journal* **2006,** *90* (6), 2213-2220.
30. Brown, M. C.; Cary, L. A.; Jamieson, J. S.; Cooper, J. A.; Turner, C. E., Src and FAK Kinases Cooperate to Phosphorylate Paxillin Kinase Linker, Stimulate Its Focal Adhesion Localization, and Regulate Cell Spreading and Protrusiveness. *Molecular Biology of the Cell* **2005,** *16* (9), 4316-4328.
31. Calalb, M. B.; Polte, T. R.; Hanks, S. K., Tyrosine phosphorylation of focal adhesion kinase at sites in the catalytic domain regulates kinase activity: a role for Src family kinases. *Molecular and Cellular Biology* **1995,** *15* (2), 954-963.
32. Westhoff, M. A.; Serrels, B.; Fincham, V. J.; Frame, M. C.; Carragher, N. O., Src-Mediated Phosphorylation of Focal Adhesion Kinase Couples Actin and Adhesion Dynamics to Survival Signaling. *Molecular and Cellular Biology* **2004,** *24* (18), 8113-8133.
33. George, E. L.; Georges-Labouesse, E. N.; Patel-King, R. S.; Rayburn, H.; Hynes, R. O., Defects in mesoderm, neural tube and vascular development in mouse embryos lacking fibronectin. *Development* **1993,** *119* (4), 1079.
34. Sponziello, M.; Rosignolo, F.; Celano, M.; Maggisano, V.; Pecce, V.; De Rose, R. F.; Lombardo, G. E.; Durante, C.; Filetti, S.; Damante, G.; Russo, D.; Bulotta, S., Fibronectin-1 expression is increased in aggressive thyroid cancer and favors the migration and invasion of cancer cells. *Molecular and Cellular Endocrinology*.
35. Vogel, V., Mechanotransduction involving multimodular proteins: converting force into biochemical signals. Annual Review of Biophysics and Biomolecular Structure 2006; Vol. 35, pp 459–88.
36. Pankov, R.; Yamada, K., Fibronectin at a glance. Journal of Cell Science 2002; Vol. 115, pp 3861-3863.
37. Ingham, K. C.; Brew, S. A.; Migliorini, M. M., Further localization of the gelatin-binding determinants within fibronectin. Active fragments devoid of type II homologous repeat modules. *Journal of Biological Chemistry* **1989,** *264* (29), 16977-16980.
38. Singh, P.; Carraher, C.; Schwarzbauer, E. J., Assembly of Fibronectin Extracellular Matrix. Annu Rev Cell Dev Biol: 2010; Vol. 26, pp 397-419.
39. Mao, Y. M.; Schwarzbauer, E. J., Fibronectin fibrillogenesis, a cell-mediated matrix assembly process. Matrix Biology: 2005; Vol. 24, pp 389-99.
40. Baron, M.; Kingsman, A. J.; Kingsman, S. M.; Campbell, I. D., Protein Production in Biotechnology. 1990.

41. Main, A. L.; Harvey, T. S.; Baron, M.; Boyd, J.; Campbell, I. D., The three-dimensional structure of the tenth type III module of fibronectin: An insight into RGD-mediated interactions. *Cell* **1992,** *71* (4), 671-678.
42. Sottile, J.; Hocking, D. C., Fibronectin Polymerization Regulates the Composition and Stability of Extracellular Matrix Fibrils and Cell-Matrix Adhesions. *Molecular Biology of the Cell* **2002,** *13* (10), 3546-3559.
43. Kubow, K. E.; Vukmirovic, R.; Zhe, L.; Klotzsch, E.; Smith, M. L.; Gourdon, D.; Luna, S.; Vogel, V., Mechanical forces regulate the interactions of fibronectin and collagen I in extracellular matrix. *Nature Communications* **2015,** *6*, 8026.
44. Wierzbicka-Patynowski, I.; Schwarzbauer, J. E., The ins and outs of fibronectin matrix assembly. *Journal of Cell Science* **2003,** *116* (16), 3269.
45. Pierschbacher, M. D.; Ruoslahti, E., Cell attachment activity of fibronectin can be duplicated by small synthetic fragments of the molecule. *Nature* **1984,** *309* (5963), 30-33.
46. Hynes, R. O., Integrins: Versatility, modulation, and signaling in cell adhesion. *Cell* **1992,** *69* (1), 11-25.
47. Sechler, J. L.; Cumiskey, A. M.; Gazzola, D. M.; Schwarzbauer, J. E., A novel RGD-independent fibronectin assembly pathway initiated by alpha4beta1 integrin binding to the alternatively spliced V region. *Journal of Cell Science* **2000,** *113* (8), 1491.
48. Hotchin, N. A.; Hall, A., The assembly of integrin adhesion complexes requires both extracellular matrix and intracellular rho/rac GTPases. *The Journal of Cell Biology* **1995,** *131* (6), 1857.
49. Gee, E. P. S.; Yüksel, D.; Stultz, C. M.; Ingber, D. E., SLLISWD Sequence in the 10FNIII Domain Initiates Fibronectin Fibrillogenesis. *The Journal of Biological Chemistry* **2013,** *288* (29), 21329-21340.
50. Johnson, K. J.; Sage, H.; Briscoe, G.; Erickson, H. P., The Compact Conformation of Fibronectin Is Determined by Intramolecular Ionic Interactions. *Journal of Biological Chemistry* **1999,** *274* (22), 15473-15479.
51. Erickson, H. P., Reversible unfolding of fibronectin type III and immunoglobulin domains provides the structural basis for stretch and elasticity of titin and fibronectin. *Proceedings of the National Academy of Sciences of the United States of America* **1994,** *91* (21), 10114-10118.
52. Hocking, D. C.; Smith, R. K.; McKeown-Longo, P. J., A novel role for the integrin-binding III-10 module in fibronectin matrix assembly. *The Journal of Cell Biology* **1996,** *133* (2), 431.
53. Sechler, J. L.; Rao, H.; Cumiskey, A. M.; Vega-Colón, I.; Smith, M. S.; Murata, T.; Schwarzbauer, J. E., A novel fibronectin binding site required for fibronectin fibril growth during matrix assembly. *The Journal of Cell Biology* **2001,** *154* (5), 1081.
54. Schwarzbauer, J. E.; DeSimone, D. W., Fibronectins, Their Fibrillogenesis, and In Vivo Functions. *Cold Spring Harbor Perspectives in Biology* **2011,** *3* (7), a005041.
55. Ruoslahti, E.; Pierschbacher, M. D., New perspectives in cell adhesion: RGD and integrins. *Science* **1987,** *238* (4826), 491.
56. Humphries, J. D.; Byron, A.; Humphries, M. J., Integrin ligands at a glance. *Journal of Cell Science* **2006,** *119* (19), 3901.
57. Bowditch, R. D.; Hariharan, M.; Tominna, E. F.; Smith, J. W.; Yamada, K. M.; Getzoff, E. D.; Ginsberg, M. H., Identification of a novel integrin binding site in fibronectin. Differential utilization by beta 3 integrins. *Journal of Biological Chemistry* **1994,** *269* (14), 10856-10863.
58. Benito-Jardón, M.; Klapproth, S.; Gimeno-Lluch, I.; Petzold, T.; Bharadwaj, M.; Müller, D. J.; Zuchtriegel, G.; Reichel, C. A.; Costell, M., The fibronectin synergy site re-enforces cell adhesion and mediates a crosstalk between integrin classes. *eLife* **2017,** *6*, e22264.
59. Aota, S.; Nomizu, M.; Yamada, K. M., The short amino acid sequence Pro-His-Ser-Arg-Asn in human fibronectin enhances cell-adhesive function. *Journal of Biological Chemistry* **1994,** *269* (40), 24756-24761.

60. Mardon, H. J.; Grant, K. E., The role of the ninth and tenth type III domains of human fibronectin in cell adhesion. *FEBS Letters* **1994,** *340* (3), 197-201.
61. Takagi, J.; Strokovich, K.; Springer, T. A.; Walz, T., Structure of integrin α5β1 in complex with fibronectin. *The EMBO Journal* **2003,** *22* (18), 4607-4615.
62. Humphries, J. D.; Byron, A.; Humphries, M. J., INTEGRIN LIGANDS. *Journal of cell science* **2006,** *119* (Pt 19), 3901-3903.
63. Krammer, A.; Craig, D.; Thomas, W. E.; Schulten, K.; Vogel, V., A structural model for force regulated integrin binding to fibronectin's RGD-synergy site. *Matrix Biology* **2002,** *21* (2), 139-147.
64. Martino, M. M.; Mochizuki, M.; Rothenfluh, D. A.; Rempel, S. A.; Hubbell, J. A.; Barker, T. H., Controlling integrin specificity and stem cell differentiation in 2D and 3D environments through regulation of fibronectin domain stability. *Biomaterials* **2009,** *30* (6), 1089-1097.
65. Brown, A. C.; Rowe, J. A.; Barker, T. H., Guiding Epithelial Cell Phenotypes with Engineered Integrin-Specific Recombinant Fibronectin Fragments. *Tissue Engineering. Part A* **2011,** *17* (1-2), 139-150.
66. García, A. J.; Vega, M. D.; Boettiger, D., Modulation of Cell Proliferation and Differentiation through Substrate-dependent Changes in Fibronectin Conformation. *Molecular Biology of the Cell* **1999,** *10* (3), 785-798.
67. Rossier, O.; Octeau, V.; Sibarita, J.-B.; Leduc, C.; Tessier, B.; Nair, D.; Gatterdam, V.; Destaing, O.; Albigès-Rizo, C.; Tampé, R.; Cognet, L.; Choquet, D.; Lounis, B.; Giannone, G., Integrins β1 and β3 exhibit distinct dynamic nanoscale organizations inside focal adhesions. *Nat Cell Biol* **2012,** *14* (10), 1057-1067.
68. Mooradian, D. L.; Lucas, R. C.; Weatherbee, J. A.; Furcht, L. T., Transforming growth factor-β1 binds to immobilized fibronectin. *Journal of Cellular Biochemistry* **1989,** *41* (4), 189-200.
69. Rahman, S.; Patel, Y.; Murray, J.; Patel, K. V.; Sumathipala, R.; Sobel, M.; Wijelath, E. S., Novel hepatocyte growth factor (HGF) binding domains on fibronectin and vitronectin coordinate a distinct and amplified Met-integrin induced signalling pathway in endothelial cells. *BMC Cell Biology* **2005,** *6* (1), 8.
70. Martino, M. M.; Hubbell, A. J., The 12th–14th type III repeats of fibronectin function as a highly promiscuous growth factor-binding domain. FASEB J.: 2010; Vol. 24, pp 4711-21.
71. Wijelath, E. S.; Rahman, S.; Namekata, M.; Murray, J.; Nishimura, T.; Mostafavi-Pour, Z.; Patel, Y.; Suda, Y.; Humphries, M. J.; Sobel, M., Heparin-II Domain of Fibronectin Is a Vascular Endothelial Growth Factor–Binding Domain: Enhancement of VEGF Biological Activity by a Singular Growth Factor/Matrix Protein Synergism. *Circulation research* **2006,** *99* (8), 853-860.
72. Mahla, R. S., Stem Cells Applications in Regenerative Medicine and Disease Therapeutics. *International Journal of Cell Biology* **2016,** *2016*, 6940283.
73. Scadden, D. T., The stem-cell niche as an entity of action. *Nature* **2006,** *441* (7097), 1075-1079.
74. Evans, M. J.; Kaufman, M. H., Establishment in culture of pluripotential cells from mouse embryos. *Nature* **1981,** *292* (5819), 154-156.
75. Martin, G. R., Isolation of a pluripotent cell line from early mouse embryos cultured in medium conditioned by teratocarcinoma stem cells. *Proceedings of the National Academy of Sciences of the United States of America* **1981,** *78* (12), 7634-7638.
76. Rippon, H. J.; Bishop, A. E., Embryonic stem cells. *Cell Proliferation* **2004,** *37* (1), 23-34.
77. Ulloa-Montoya, F.; Verfaillie, C. M.; Hu, W.-S., Culture systems for pluripotent stem cells. *Journal of Bioscience and Bioengineering* **2005,** *100* (1), 12-27.
78. Goodell, M. A.; Nguyen, H.; Shroyer, N., Somatic stem cell heterogeneity: diversity in the blood, skin and intestinal stem cell compartments. *Nat Rev Mol Cell Biol* **2015,** *16* (5), 299-309.

79. Takahashi, K.; Yamanaka, S., Induction of Pluripotent Stem Cells from Mouse Embryonic and Adult Fibroblast Cultures by Defined Factors. *Cell* **2006,** *126* (4), 663-676.
80. Hernigou, P., Bone transplantation and tissue engineering, part IV. Mesenchymal stem cells: history in orthopedic surgery from Cohnheim and Goujon to the Nobel Prize of Yamanaka. *International Orthopaedics* **2015,** *39* (4), 807-817.
81. Pittenger, M. F.; Mackay, A. M.; Beck, S. C.; Jaiswal, R. K.; Douglas, R.; Mosca, J. D.; Moorman, M. A.; Simonetti, D. W.; Craig, S.; Marshak, D. R., Multilineage Potential of Adult Human Mesenchymal Stem Cells. *Science* **1999,** *284* (5411), 143-147.
82. Dominici, M.; Le Blanc, K.; Mueller, I.; Slaper-Cortenbach, I.; Marini, F. C.; Krause, D. S.; Deans, R. J.; Keating, A.; Prockop, D. J.; Horwitz, E. M., Minimal criteria for defining multipotent mesenchymal stromal cells. The International Society for Cellular Therapy position statement. *Cytotherapy* **2006,** *8* (4), 315-317.
83. Galipeau, J.; Krampera, M.; Barrett, J.; Dazzi, F.; Deans, R. J.; Debruijn, J.; Dominici, M.; Fibbe, W. E.; Gee, A. P.; Gimble, J. M.; Hematti, P.; Koh, M. B. C.; Leblanc, K.; Martin, I.; McNiece, I. K.; Mendicino, M.; Oh, S.; Ortiz, L.; Phinney, D. G.; Planat, V.; Shi, Y.; Stroncek, D. F.; Viswanathan, S.; Weiss, D. J.; Sensebe, L., International Society for Cellular Therapy perspective on immune functional assays for mesenchymal stromal cells as potency release criterion for advanced phase clinical trials. *Cytotherapy* **2016,** *18* (2), 151-159.
84. Ren, G.; Zhang, L.; Zhao, X.; Xu, G.; Zhang, Y.; Roberts, A. I.; Zhao, R. C.; Shi, Y., Mesenchymal Stem Cell-Mediated Immunosuppression Occurs via Concerted Action of Chemokines and Nitric Oxide. *Cell Stem Cell* **2008,** *2* (2), 141-150.
85. Uccelli, A.; Moretta, L.; Pistoia, V., Mesenchymal stem cells in health and disease. *Nat Rev Immunol* **2008,** *8* (9), 726-736.
86. Discher, D. E.; Mooney, D. J.; Zandstra, P. W., Growth factors, matrices, and forces combine and control stem cells. *Science (New York, N.Y.)* **2009,** *324* (5935), 1673-1677.
87. Zhu, A. J.; Haase, I.; Watt, F. M., Signaling via β1 integrins and mitogen-activated protein kinase determines human epidermal stem cell fate in vitro. *Proceedings of the National Academy of Sciences* **1999,** *96* (12), 6728-6733.
88. Cargnello, M.; Roux, P. P., Activation and Function of the MAPKs and Their Substrates, the MAPK-Activated Protein Kinases. *Microbiology and Molecular Biology Reviews : MMBR* **2011,** *75* (1), 50-83.
89. Kyosseva, S. V., Targeting MAPK Signaling in Age-Related Macular Degeneration. *Ophthalmology and Eye Diseases* **2016,** *8*, 23-30.
90. Humphreys, J. M.; Piala, A. T.; Akella, R.; He, H.; Goldsmith, E. J., Precisely Ordered Phosphorylation Reactions in the p38 Mitogen-activated Protein (MAP) Kinase Cascade. *The Journal of Biological Chemistry* **2013,** *288* (32), 23322-23330.
91. Huang, C. Y.; Ferrell, J. E., Ultrasensitivity in the mitogen-activated protein kinase cascade. *Proceedings of the National Academy of Sciences of the United States of America* **1996,** *93* (19), 10078-10083.
92. Mansour, S. J.; Matten, W. T.; Hermann, A. S.; Candia, J. M.; Rong, S.; Fukasawa, K.; Vande Woude, G. F.; Ahn, N. G., Transformation of mammalian cells by constitutively active MAP kinase kinase. *Science* **1994,** *265* (5174), 966.
93. McKay, M. M.; Morrison, D. K., Integrating signals from RTKs to ERK//MAPK. *Oncogene* **0000,** *26* (22), 3113-3121.
94. Moodie, S. A.; Willumsen, B. M.; Weber, M. J.; Wolfman, A., Complexes of Ras.GTP with Raf-1 and mitogen-activated protein kinase kinase. *Science* **1993,** *260* (5114), 1658.
95. Geyer, M.; Wittinghofer, A., GEFs, GAPs, GDIs and effectors: taking a closer (3D) look at the regulation of Ras-related GTP-binding proteins. *Current Opinion in Structural Biology* **1997,** *7* (6), 786-792.
96. Lake, D.; Corrêa, S. A. L.; Müller, J., Negative feedback regulation of the ERK1/2 MAPK pathway. *Cellular and Molecular Life Sciences* **2016,** *73* (23), 4397-4413.

97. Yoon, S.; Seger, R., The extracellular signal-regulated kinase: Multiple substrates regulate diverse cellular functions. *Growth Factors* **2006,** *24* (1), 21-44.
98. Traverse, S.; Gomez, N.; Paterson, H.; Marshall, C.; Cohen, P., Sustained activation of the mitogen-activated protein (MAP) kinase cascade may be required for differentiation of PC12 cells. Comparison of the effects of nerve growth factor and epidermal growth factor. *Biochemical Journal* **1992,** *288* (Pt 2), 351-355.
99. Zehorai, E.; Yao, Z.; Plotnikov, A.; Seger, R., The subcellular localization of MEK and ERK—A novel nuclear translocation signal (NTS) paves a way to the nucleus. *Molecular and Cellular Endocrinology* **2010,** *314* (2), 213-220.
100. Boulton, T. G.; Yancopoulos, G. D.; Gregory, J. S.; Slaughter, C.; Moomaw, C.; Hsu, J.; Cobb, M. H., An insulin-stimulated protein kinase similar to yeast kinases involved in cell cycle control. *Science* **1990,** *249* (4964), 64.
101. Yamamoto, T.; Ebisuya, M.; Ashida, F.; Okamoto, K.; Yonehara, S.; Nishida, E., Continuous ERK Activation Downregulates Antiproliferative Genes throughout G1 Phase to Allow Cell-Cycle Progression. *Current Biology* **2006,** *16* (12), 1171-1182.
102. Bernhard, E. J.; Stanbridge, E. J.; Gupta, S.; Gupta, A. K.; Soto, D.; Bakanauskas, V. J.; Cerniglia, G. J.; Muschel, R. J.; McKenna, W. G., Direct Evidence for the Contribution of Activated N-ras and K-ras Oncogenes to Increased Intrinsic Radiation Resistance in Human Tumor Cell Lines. *Cancer Research* **2000,** *60* (23), 6597.
103. Schulze, A.; Lehmann, K.; Jefferies, H. B. J.; McMahon, M.; Downward, J., Analysis of the transcriptional program induced by Raf in epithelial cells. *Genes & Development* **2001,** *15* (8), 981-994.
104. Schlaepfer, D. D.; Broome, M. A.; Hunter, T., Fibronectin-stimulated signaling from a focal adhesion kinase-c-Src complex: involvement of the Grb2, p130cas, and Nck adaptor proteins. *Molecular and Cellular Biology* **1997,** *17* (3), 1702-1713.
105. Eliceiri, B. P.; Klemke, R.; Strömblad, S.; Cheresh, D. A., Integrin αvβ3 Requirement for Sustained Mitogen-activated Protein Kinase Activity during Angiogenesis. *The Journal of Cell Biology* **1998,** *140* (5), 1255-1263.
106. Kunath, T.; Saba-El-Leil, M. K.; Almousailleakh, M.; Wray, J.; Meloche, S.; Smith, A., FGF stimulation of the Erk1/2 signalling cascade triggers transition of pluripotent embryonic stem cells from self-renewal to lineage commitment. *Development* **2007,** *134* (16), 2895.
107. Burdon, T.; Stracey, C.; Chambers, I.; Nichols, J.; Smith, A., Suppression of SHP-2 and ERK Signalling Promotes Self-Renewal of Mouse Embryonic Stem Cells. *Developmental Biology* **1999,** *210* (1), 30-43.
108. Chen, Q.; Shou, P.; Zheng, C.; Jiang, M.; Cao, G.; Yang, Q.; Cao, J.; Xie, N.; Velletri, T.; Zhang, X.; Xu, C.; Zhang, L.; Yang, H.; Hou, J.; Wang, Y.; Shi, Y., Fate decision of mesenchymal stem cells: adipocytes or osteoblasts? *Cell Death and Differentiation* **2016,** *23* (7), 1128-1139.
109. Born, A.-K.; Lischer, S.; Maniura-Weber, K., Watching osteogenesis: Life monitoring of osteogenic differentiation using an osteocalcin reporter. *Journal of Cellular Biochemistry* **2012,** *113* (1), 313-321.
110. Torii, Y.; Hitomi, K.; Yamagishi, Y.; Tsukagoshi, N., DEMONSTRATION OF ALKALINE PHOSPHATASE PARTICIPATION IN THE MINERALIZATION OF OSTEOBLASTS BY ANTISENSE RNA APPROACH. *Cell Biology International* **1996,** *20* (7), 459-464.
111. Wennberg, C.; Hessle, L.; Lundberg, P.; Mauro, S.; Narisawa, S.; Lerner, U. H.; Millán, J. L., Functional Characterization of Osteoblasts and Osteoclasts from Alkaline Phosphatase Knockout Mice. *Journal of Bone and Mineral Research* **2000,** *15* (10), 1879-1888.
112. Kotobuki, N.; Matsushima, A.; Kato, Y.; Kubo, Y.; Hirose, M.; Ohgushi, H., Small interfering RNA of alkaline phosphatase inhibits matrix mineralization. *Cell and Tissue Research* **2008,** *332* (2), 279-288.
113. Hoang, Q. Q.; Sicheri, F.; Howard, A. J.; Yang, D. S. C., Bone recognition mechanism of porcine osteocalcin from crystal structure. *Nature* **2003,** *425* (6961), 977-980.

114. Chen, Q.; Shou, P.; Zhang, L.; Xu, C.; Zheng, C.; Han, Y.; Li, W.; Huang, Y.; Zhang, X.; Shao, C.; Roberts, A. I.; Rabson, A. B.; Ren, G.; Zhang, Y.; Wang, Y.; Denhardt, D. T.; Shi, Y., An Osteopontin-Integrin Interaction Plays a Critical Role in Directing Adipogenesis and Osteogenesis by Mesenchymal Stem Cells. *Stem cells (Dayton, Ohio)* **2014,** *32* (2), 327-337.
115. Di Benedetto, A.; Brunetti, G.; Posa, F.; Ballini, A.; Grassi, F. R.; Colaianni, G.; Colucci, S.; Rossi, E.; Cavalcanti-Adam, E. A.; Lo Muzio, L.; Grano, M.; Mori, G., Osteogenic differentiation of mesenchymal stem cells from dental bud: Role of integrins and cadherins. *Stem Cell Research* **2015,** *15* (3), 618-628.
116. Takarada, T.; Hinoi, E.; Nakazato, R.; Ochi, H.; Xu, C.; Tsuchikane, A.; Takeda, S.; Karsenty, G.; Abe, T.; Kiyonari, H.; Yoneda, Y., An analysis of skeletal development in osteoblast-specific and chondrocyte-specific runt-related transcription factor-2 (Runx2) knockout mice. *Journal of Bone and Mineral Research* **2013,** *28* (10), 2064-2069.
117. Tu, Q.; Zhang, J.; Paz, J.; Wade, K.; Yang, P.; Chen, J., Haploinsufficiency of Runx2 results in bone formation decrease and different BSP expression pattern changes in two transgenic mouse models. *Journal of Cellular Physiology* **2008,** *217* (1), 40-47.
118. Wojtowicz, A. M.; Templeman, K. L.; Hutmacher, D. W.; Guldberg, R. E.; García, A. J., Runx2 Overexpression in Bone Marrow Stromal Cells Accelerates Bone Formation in Critical-Sized Femoral Defects. *Tissue Engineering. Part A* **2010,** *16* (9), 2795-2808.
119. Ge, C.; Xiao, G.; Jiang, D.; Franceschi, R. T., Critical role of the extracellular signal–regulated kinase–MAPK pathway in osteoblast differentiation and skeletal development. *The Journal of Cell Biology* **2007,** *176* (5), 709-718.
120. Komori, T., Regulation of bone development and extracellular matrix protein genes by RUNX2. *Cell and Tissue Research* **2009,** *339* (1), 189.
121. Xiao, G.; Jiang, D.; Thomas, P.; Benson, M. D.; Guan, K.; Karsenty, G.; Franceschi, R. T., MAPK Pathways Activate and Phosphorylate the Osteoblast-specific Transcription Factor, Cbfa1. *Journal of Biological Chemistry* **2000,** *275* (6), 4453-4459.
122. Ge, C.; Xiao, G.; Jiang, D.; Yang, Q.; Hatch, N. E.; Roca, H.; Franceschi, R. T., Identification and Functional Characterization of ERK/MAPK Phosphorylation Sites in the Runx2 Transcription Factor. *The Journal of Biological Chemistry* **2009,** *284* (47), 32533-32543.
123. Jun, J. H.; Yoon, W.-J.; Seo, S.-B.; Woo, K.-M.; Kim, G.-S.; Ryoo, H.-M.; Baek, J.-H., BMP2-activated Erk/MAP Kinase Stabilizes Runx2 by Increasing p300 Levels and Histone Acetyltransferase Activity. *The Journal of Biological Chemistry* **2010,** *285* (47), 36410-36419.
124. Ge, C.; Yang, Q.; Zhao, G.; Yu, H.; Kirkwood, K. L.; Franceschi, R. T., INTERACTIONS BETWEEN EXTRACELLULAR SIGNAL-REGULATED KINASE 1/2 AND P38 MAP KINASE PATHWAYS IN THE CONTROL OF RUNX2 PHOSPHORYLATION AND TRANSCRIPTIONAL ACTIVITY. *Journal of bone and mineral research : the official journal of the American Society for Bone and Mineral Research* **2012,** *27* (3), 538-551.
125. Shui, C.; Spelsberg, T. C.; Riggs, B. L.; Khosla, S., Changes in Runx2/Cbfa1 Expression and Activity During Osteoblastic Differentiation of Human Bone Marrow Stromal Cells. *Journal of Bone and Mineral Research* **2003,** *18* (2), 213-221.
126. Komori, T., Regulation of Osteoblast Differentiation by Runx2. In *Osteoimmunology: Interactions of the Immune and skeletal systems II*, Choi, Y., Ed. Springer US: Boston, MA, 2010; pp 43-49.
127. Kim, J.-B.; Leucht, P.; Luppen, C. A.; Park, Y. J.; Beggs, H. E.; Damsky, C. H.; Helms, J. A., Reconciling the roles of FAK in osteoblast differentiation, osteoclast remodeling, and bone regeneration. *Bone* **2007,** *41* (1), 39-51.
128. Hu, J.; Liao, H.; Ma, Z.; Chen, H.; Huang, Z.; Zhang, Y.; Yu, M.; Chen, Y.; Xu, J., Focal Adhesion Kinase Signaling Mediated the Enhancement of Osteogenesis of

Human Mesenchymal Stem Cells Induced by Extracorporeal Shockwave. *Scientific Reports* **2016,** *6*, 20875.
129. Salasznyk, R. M.; Klees, R. F.; Williams, W. A.; Boskey, A.; Plopper, G. E., Focal adhesion kinase signaling pathways regulate the osteogenic differentiation of human mesenchymal stem cells. *Experimental Cell Research* **2007,** *313* (1), 22-37.
130. Hughes, D. E.; Salter, D. M.; Dedhar, S.; Simpson, R., Integrin expression in human bone. *Journal of Bone and Mineral Research* **1993,** *8* (5), 527-533.
131. Grzesik, W. J.; Robey, P. G., Bone matrix RGD glycoproteins: Immunolocalization and interaction with human primary osteoblastic bone cells in vitro. *Journal of Bone and Mineral Research* **1994,** *9* (4), 487-496.
132. Hamidouche, Z.; Fromigué, O.; Ringe, J.; Häupl, T.; Vaudin, P.; Pagès, J.-C.; Srouji, S.; Livne, E.; Marie, P. J., Priming integrin α5 promotes human mesenchymal stromal cell osteoblast differentiation and osteogenesis. *Proceedings of the National Academy of Sciences* **2009,** *106* (44), 18587-18591.
133. Petrie, T. A.; Raynor, J. E.; Reyes, C. D.; Burns, K. L.; Collard, D. M.; García, A. J., The effect of integrin-specific bioactive coatings on tissue healing and implant osseointegration. *Biomaterials* **2008,** *29* (19), 2849-2857.
134. Mas-Moruno, C.; Fraioli, R.; Rechenmacher, F.; Neubauer, S.; Kapp, T. G.; Kessler, H., αvβ3- or α5β1-Integrin-Selective Peptidomimetics for Surface Coating. *Angewandte Chemie International Edition* **2016,** *55* (25), 7048-7067.
135. Sato, M.; Sardana, M. K.; Grasser, W. A.; Garsky, V. M.; Murray, J. M.; Gould, R. J., Echistatin is a potent inhibitor of bone resorption in culture. *The Journal of Cell Biology* **1990,** *111* (4), 1713.
136. Horton, M. A.; Taylor, M. L.; Arnett, T. R.; Helfrich, M. H., Arg · Gly · Asp (RGD) peptides and the anti-vitronectin receptor antibody 23C6 inhibit dentine resorption and cell spreading by osteoclasts. *Experimental Cell Research* **1991,** *195* (2), 368-375.
137. Kilian, K. A.; Mrksich, M., Directing Stem Cell Fate by Controlling the Affinity and Density of Ligand-Receptor Interactions at the Biomaterials Interface. *Angewandte Chemie (International ed. in English)* **2012,** *51* (20), 4891-4895.
138. Cheng, S.-L.; Lai, C.-F.; Blystone, S. D.; Avioli, L. V., Bone Mineralization and Osteoblast Differentiation Are Negatively Modulated by Integrin αvβ3. *Journal of Bone and Mineral Research* **2001,** *16* (2), 277-288.
139. Li, B.; Moshfegh, C.; Lin, Z.; Albuschies, J.; Vogel, V., Mesenchymal stem cells exploit extracellular matrix as mechanotransducer Sci. Rep.: 2013; Vol. 3.
140. Guan, M.; Yao, W.; Liu, R.; Lam, K. S.; Nolta, J.; Jia, J.; Panganiban, B.; Meng, L.; Zhou, P.; Shahnazari, M.; Ritchie, R. O.; Lane, N. E., Directing mesenchymal stem cells to bone to augment bone formation and increase bone mass. *Nature medicine* **2012,** *18* (3), 456-462.
141. Kumar, S.; Ponnazhagan, S., Bone homing of mesenchymal stem cells by ectopic α4 integrin expression. *The FASEB Journal* **2007,** *21* (14), 3917-3927.
142. Popov, C.; Radic, T.; Haasters, F.; Prall, W. C.; Aszodi, A.; Gullberg, D.; Schieker, M.; Docheva, D., Integrins α2β1 and α11β1 regulate the survival of mesenchymal stem cells on collagen I. *Cell Death & Disease* **2011,** *2* (7), e186.
143. Sotobori, T.; Ueda, T.; Myoui, A.; Yoshioka, K.; Nakasaki, M.; Yoshikawa, H.; Itoh, K., Bone morphogenetic protein-2 promotes the haptotactic migration of murine osteoblastic and osteosarcoma cells by enhancing incorporation of integrin β1 into lipid rafts. *Experimental Cell Research* **2006,** *312* (19), 3927-3938.
144. Lai, T.-H.; Fong, Y.-C.; Fu, W.-M.; Yang, R.-S.; Tang, C.-H., Osteoblasts-derived BMP-2 enhances the motility of prostate cancer cells via activation of integrins. *The Prostate* **2008,** *68* (12), 1341-1353.
145. Carreira, A. C.; Alves, G. G.; Zambuzzi, W. F.; Sogayar, M. C.; Granjeiro, J. M., Bone Morphogenetic Proteins: Structure, biological function and therapeutic applications. *Archives of Biochemistry and Biophysics* **2014,** *561*, 64-73.
146. Sánchez-Duffhues, G.; Hiepen, C.; Knaus, P.; ten Dijke, P., Bone morphogenetic protein signaling in bone homeostasis. *Bone* **2015,** *80*, 43-59.

147. zur Nieden, N. I.; Kempka, G.; Rancourt, D. E.; Ahr, H.-J., Induction of chondro-, osteo- and adipogenesis in embryonic stem cells by bone morphogenetic protein-2: Effect of cofactors on differentiating lineages. *BMC Developmental Biology* **2005,** *5*, 1-1.
148. Thomson, J. A.; Itskovitz-Eldor, J.; Shapiro, S. S.; Waknitz, M. A.; Swiergiel, J. J.; Marshall, V. S.; Jones, J. M., Embryonic Stem Cell Lines Derived from Human Blastocysts. *Science* **1998,** *282* (5391), 1145.
149. Daluiski, A.; Engstrand, T.; Bahamonde, M. E.; Gamer, L. W.; Agius, E.; Stevenson, S. L.; Cox, K.; Rosen, V.; Lyons, K. M., Bone morphogenetic protein-3 is a negative regulator of bone density. *Nat Genet* **2001,** *27* (1), 84-88.
150. Tseng, Y.-H.; Kokkotou, E.; Schulz, T. J.; Huang, T. L.; Winnay, J. N.; Taniguchi, C. M.; Tran, T. T.; Suzuki, R.; Espinoza, D. O.; Yamamoto, Y.; Ahrens, M. J.; Dudley, A. T.; Norris, A. W.; Kulkarni, R. N.; Kahn, C. R., New role of bone morphogenetic protein 7 in brown adipogenesis and energy expenditure. *Nature* **2008,** *454* (7207), 1000-1004.
151. Elsen, M.; Raschke, S.; Tennagels, N.; Schwahn, U.; Jelenik, T.; Roden, M.; Romacho, T.; Eckel, J., BMP4 and BMP7 induce the white-to-brown transition of primary human adipose stem cells. *American Journal of Physiology - Cell Physiology* **2014,** *306* (5), C431.
152. Sampath, T. K.; Maliakal, J. C.; Hauschka, P. V.; Jones, W. K.; Sasak, H.; Tucker, R. F.; White, K. H.; Coughlin, J. E.; Tucker, M. M.; Pang, R. H., Recombinant human osteogenic protein-1 (hOP-1) induces new bone formation in vivo with a specific activity comparable with natural bovine osteogenic protein and stimulates osteoblast proliferation and differentiation in vitro. *Journal of Biological Chemistry* **1992,** *267* (28), 20352-20362.
153. Wolfman, N. M.; Hattersley, G.; Cox, K.; Celeste, A. J.; Nelson, R.; Yamaji, N.; Dube, J. L.; DiBlasio-Smith, E.; Nove, J.; Song, J. J.; Wozney, J. M.; Rosen, V., Ectopic induction of tendon and ligament in rats by growth and differentiation factors 5, 6, and 7, members of the TGF-beta gene family. *Journal of Clinical Investigation* **1997,** *100* (2), 321-330.
154. Bone morphogenetic protein-2 converts the differentiation pathway of C2C12 myoblasts into the osteoblast lineage [published erratum appears in J Cell Biol 1995 Feb;128(4):following 713]. *The Journal of Cell Biology* **1994,** *127* (6), 1755-1766.
155. Zachos, T. A.; Shields, K. M.; Bertone, A. L., Gene-mediated osteogenic differentiation of stem cells by bone morphogenetic proteins-2 or -6. *Journal of Orthopaedic Research* **2006,** *24* (6), 1279-1291.
156. Carragee, E. J.; Hurwitz, E. L.; Weiner, B. K., A critical review of recombinant human bone morphogenetic protein-2 trials in spinal surgery: emerging safety concerns and lessons learned. *The Spine Journal* **2011,** *11* (6), 471-491.
157. Wang, R. N.; Green, J.; Wang, Z.; Deng, Y.; Qiao, M.; Peabody, M.; Zhang, Q.; Ye, J.; Yan, Z.; Denduluri, S.; Idowu, O.; Li, M.; Shen, C.; Hu, A.; Haydon, R. C.; Kang, R.; Mok, J.; Lee, M. J.; Luu, H. L.; Shi, L. L., Bone Morphogenetic Protein (BMP) signaling in development and human diseases. *Genes & Diseases* **2014,** *1* (1), 87-105.
158. Zhou, N.; Li, Q.; Lin, X.; Hu, N.; Liao, J.-Y.; Lin, L.-B.; Zhao, C.; Hu, Z.-M.; Liang, X.; Xu, W.; Chen, H.; Huang, W., BMP2 induces chondrogenic differentiation, osteogenic differentiation and endochondral ossification in stem cells. *Cell and Tissue Research* **2016,** *366* (1), 101-111.
159. Wu, M.; Chen, G.; Li, Y.-P., TGF-β and BMP signaling in osteoblast, skeletal development, and bone formation, homeostasis and disease. *Bone Research* **2016,** *4*, 16009.
160. Hayrapetyan, A.; Jansen, J. A.; van den Beucken, J. J. J. P., Signaling Pathways Involved in Osteogenesis and Their Application for Bone Regenerative Medicine. *Tissue Engineering Part B: Reviews* **2014,** *21* (1), 75-87.
161. ten Dijke, P.; Yamashita, H.; Sampath, T. K.; Reddi, A. H.; Estevez, M.; Riddle, D. L.; Ichijo, H.; Heldin, C. H.; Miyazono, K., Identification of type I receptors for

osteogenic protein-1 and bone morphogenetic protein-4. *Journal of Biological Chemistry* **1994,** *269* (25), 16985-16988.
162. Ebisawa, T.; Tada, K.; Kitajima, I.; Tojo, K.; Sampath, T. K.; Kawabata, M.; Miyazono, K.; Imamura, T., Characterization of bone morphogenetic protein-6 signaling pathways in osteoblast differentiation. *Journal of Cell Science* **1999,** *112* (20), 3519.
163. Nohe, A.; Hassel, S.; Ehrlich, M.; Neubauer, F.; Sebald, W.; Henis, Y. I.; Knaus, P., The Mode of Bone Morphogenetic Protein (BMP) Receptor Oligomerization Determines Different BMP-2 Signaling Pathways. *Journal of Biological Chemistry* **2002,** *277* (7), 5330-5338.
164. Makkar, P.; Metpally, R. P. R.; Sangadala, S.; Reddy, B. V. B., Modeling and analysis of MH1 domain of Smads and their interaction with promoter DNA sequence motif. *Journal of Molecular Graphics and Modelling* **2009,** *27* (7), 803-812.
165. Chacko, B. M.; Qin, B. Y.; Tiwari, A.; Shi, G.; Lam, S.; Hayward, L. J.; de Caestecker, M.; Lin, K., Structural Basis of Heteromeric Smad Protein Assembly in TGF-β Signaling. *Molecular Cell* **2004,** *15* (5), 813-823.
166. Heldin, C.-H.; Moustakas, A., Role of Smads in TGFβ signaling. *Cell and Tissue Research* **2012,** *347* (1), 21-36.
167. Rahman, M. S.; Akhtar, N.; Jamil, H. M.; Banik, R. S.; Asaduzzaman, S. M., TGF-β/BMP signaling and other molecular events: regulation of osteoblastogenesis and bone formation. *Bone Research* **2015,** *3*, 15005.
168. ten Dijke, P.; Miyazono, K.; Heldin, C.-H., Signaling inputs converge on nuclear effectors in TGF-β signaling. *Trends in Biochemical Sciences* **2000,** *25* (2), 64-70.
169. Hauff, K.; Zambarda, C.; Dietrich, M.; Halbig, M.; Grab, A. L.; Medda, R.; Cavalcanti-Adam, E. A., Matrix-Immobilized BMP-2 on Microcontact Printed Fibronectin as an in vitro Tool to Study BMP-Mediated Signaling and Cell Migration. *Frontiers in Bioengineering and Biotechnology* **2015,** *3*, 62.
170. Derynck, R.; Zhang, Y. E., Smad-dependent and Smad-independent pathways in TGF-[beta] family signalling. *Nature* **2003,** *425* (6958), 577-584.
171. Hartsough, M. T.; Mulder, K. M., Transforming Growth Factor β Activation of p44mapk in Proliferating Cultures of Epithelial Cells. *Journal of Biological Chemistry* **1995,** *270* (13), 7117-7124.
172. Frey, R. S.; Mulder, K. M., TGFβ regulation of mitogen-activated protein kinases in human breast cancer cells. *Cancer Letters* **1997,** *117* (1), 41-50.
173. Kretzschmar, M.; Doody, J.; Timokhina, I.; Massagué, J., A mechanism of repression of TGFβ/ Smad signaling by oncogenic Ras. *Genes & Development* **1999,** *13* (7), 804-816.
174. Engel, M. E.; McDonnell, M. A.; Law, B. K.; Moses, H. L., Interdependent SMAD and JNK Signaling in Transforming Growth Factor-β-mediated Transcription. *Journal of Biological Chemistry* **1999,** *274* (52), 37413-37420.
175. Afzal, F.; Pratap, J.; Ito, K.; Ito, Y.; Stein, J. L.; van Wijnen, A. J.; Stein, G. S.; Lian, J. B.; Javed, A., Smad function and intranuclear targeting share a Runx2 motif required for osteogenic lineage induction and BMP2 responsive transcription. *Journal of Cellular Physiology* **2005,** *204* (1), 63-72.
176. Franceschi, R. T.; Xiao, G., Regulation of the osteoblast-specific transcription factor, Runx2: Responsiveness to multiple signal transduction pathways. *Journal of Cellular Biochemistry* **2003,** *88* (3), 446-454.
177. Javed, A.; Bae, J.-S.; Afzal, F.; Gutierrez, S.; Pratap, J.; Zaidi, S. K.; Lou, Y.; van Wijnen, A. J.; Stein, J. L.; Stein, G. S.; Lian, J. B., Structural Coupling of Smad and Runx2 for Execution of the BMP2 Osteogenic Signal. *The Journal of Biological Chemistry* **2008,** *283* (13), 8412-8422.
178. Javed, A.; Afzal, F.; Bae, J.-S.; Gutierrez, S.; Zaidi, K.; Pratap, J.; van Wijnen, A. J.; Stein, J. L.; Stein, G. S.; Lian, J. B., Specific Residues of RUNX2 Are Obligatory for Formation of BMP2-Induced RUNX2-SMAD Complex to Promote Osteoblast Differentiation. *Cells, Tissues, Organs* **2008,** *189* (1-4), 133-137.
179. Williams, D. F., On the nature of biomaterials. *Biomaterials* **2009,** *30* (30), 5897-5909.

180. Williams, D. F., Regulatory biocompatibility requirements for biomaterials used in regenerative medicine. *Journal of Materials Science: Materials in Medicine* **2015,** *26* (2), 89.
181. Li, Q.; Ma, L.; Gao, C., Biomaterials for in situ tissue regeneration: development and perspectives. *Journal of Materials Chemistry B* **2015,** *3* (46), 8921-8938.
182. Abbott, R. D.; Kaplan, D. L., Strategies for improving the physiological relevance of human engineered tissues. *Trends in Biotechnology* **2015,** *33* (7), 401-407.
183. Furth, M. E.; Atala, A.; Van Dyke, M. E., Smart biomaterials design for tissue engineering and regenerative medicine. *Biomaterials* **2007,** *28* (34), 5068-5073.
184. Que, R. A.; Chan, S. W. P.; Jabaiah, A. M.; Lathrop, R. H.; Da Silva, N. A.; Wang, S.-W., Tuning cellular response by modular design of bioactive domains in collagen. *Biomaterials* **2015,** *53*, 309-317.
185. Wojtowicz, A. M.; Shekaran, A.; Oest, M. E.; Dupont, K. M.; Templeman, K. L.; Hutmacher, D. W.; Guldberg, R. E.; García, A. J., Coating of Biomaterial Scaffolds with the Collagen-Mimetic Peptide GFOGER for Bone Defect Repair. *Biomaterials* **2010,** *31* (9), 2574.
186. Cavalcanti-Adam, E. A.; Volberg, T.; Micoulet, A.; Kessler, H.; Geiger, B.; Spatz, J. P., Cell Spreading and Focal Adhesion Dynamics Are Regulated by Spacing of Integrin Ligands. *Biophysical Journal* **2007,** *92* (8), 2964-2974.
187. Wang, X.; Yan, C.; Ye, K.; He, Y.; Li, Z.; Ding, J., Effect of RGD nanospacing on differentiation of stem cells. *Biomaterials* **2013,** *34* (12), 2865-2874.
188. Chen, C. S.; Mrksich, M.; Huang, S.; Whitesides, G. M.; Ingber, D. E., Micropatterned Surfaces for Control of Cell Shape, Position, and Function. *Biotechnology Progress* **1998,** *14* (3), 356-363.
189. McMurray, R. J.; Gadegaard, N.; Tsimbouri, P. M.; Burgess, K. V.; McNamara, L. E.; Tare, R.; Murawski, K.; Kingham, E.; Oreffo, R. O. C.; Dalby, M. J., Nanoscale surfaces for the long-term maintenance of mesenchymal stem cell phenotype and multipotency. *Nat Mater* **2011,** *10* (8), 637-644.
190. Dalby, M. J.; McCloy, D.; Robertson, M.; Wilkinson, C. D. W.; Oreffo, R. O. C., Osteoprogenitor response to defined topographies with nanoscale depths. *Biomaterials* **2006,** *27* (8), 1306-1315.
191. Davison, M. J.; McMurray, R. J.; Smith, C.-A.; Dalby, M. J.; Meek, R. M. D., Nanopit-induced osteoprogenitor cell differentiation: The effect of nanopit depth. *Journal of Tissue Engineering* **2016,** *7*, 2041731416652778.
192. Abagnale, G.; Steger, M.; Nguyen, V. H.; Hersch, N.; Sechi, A.; Joussen, S.; Denecke, B.; Merkel, R.; Hoffmann, B.; Dreser, A.; Schnakenberg, U.; Gillner, A.; Wagner, W., Surface topography enhances differentiation of mesenchymal stem cells towards osteogenic and adipogenic lineages. *Biomaterials* **2015,** *61*, 316-326.
193. Engler, A. J.; Sen, S.; Sweeney, H. L.; Discher, D. E., Matrix Elasticity Directs Stem Cell Lineage Specification. *Cell* **2006,** *126* (4), 677-689.
194. Olivares-Navarrete, R.; Lee, E. M.; Smith, K.; Hyzy, S. L.; Doroudi, M.; Williams, J. K.; Gall, K.; Boyan, B. D.; Schwartz, Z., Substrate Stiffness Controls Osteoblastic and Chondrocytic Differentiation of Mesenchymal Stem Cells without Exogenous Stimuli. *PLoS ONE* **2017,** *12* (1), e0170312.
195. Huebsch, N.; Arany, P. R.; Mao, A. S.; Shvartsman, D.; Ali, O. A.; Bencherif, S. A.; Rivera-Feliciano, J.; Mooney, D. J., Harnessing traction-mediated manipulation of the cell/matrix interface to control stem-cell fate. *Nat Mater* **2010,** *9* (6), 518-526.
196. Keselowsky, B. G.; Collard, D. M.; García, A. J., Surface chemistry modulates fibronectin conformation and directs integrin binding and specificity to control cell adhesion. *Journal of Biomedical Materials Research Part A* **2003,** *66A* (2), 247-259.
197. Keselowsky, B. G.; Collard, D. M.; García, A. J., Integrin binding specificity regulates biomaterial surface chemistry effects on cell differentiation. *Proceedings of the National Academy of Sciences* **2005,** *102* (17), 5953-5957.

198. Benoit, D. S. W.; Schwartz, M. P.; Durney, A. R.; Anseth, K. S., Small functional groups for controlled differentiation of hydrogel-encapsulated human mesenchymal stem cells. *Nat Mater* **2008,** *7* (10), 816-823.
199. Horbett, T. A.; Schway, M. B., Correlations between mouse 3T3 cell spreading and serum fibronectin adsorption on glass and hydroxyethylmethacrylate–ethylmethacrylate copolymers. *Journal of Biomedical Materials Research* **1988,** *22* (9), 763-793.
200. Benavidez, T. E.; Garcia, C. D., Potential-Assisted Adsorption of Bovine Serum Albumin onto Optically-Transparent Carbon Electrodes. *Langmuir : the ACS journal of surfaces and colloids* **2013,** *29* (46), 10.1021/la4029657.
201. Vroman, L.; Adams, A. L., Identification of rapid changes at plasma–solid interfaces. *Journal of Biomedical Materials Research* **1969,** *3* (1), 43-67.
202. Ruoslahti, E.; Reed, J. C., Anchorage dependence, integrins, and apoptosis. *Cell* **1994,** *77* (4), 477-478.
203. McBeath, R.; Pirone, D. M.; Nelson, C. M.; Bhadriraju, K.; Chen, C. S., Cell Shape, Cytoskeletal Tension, and RhoA Regulate Stem Cell Lineage Commitment. *Developmental Cell* **2004,** *6* (4), 483-495.
204. Takebe, J.; Champagne, C. M.; Offenbacher, S.; Ishibashi, K.; Cooper, L. F., Titanium surface topography alters cell shape and modulates bone morphogenetic protein 2 expression in the J774A.1 macrophage cell line. *Journal of Biomedical Materials Research Part A* **2003,** *64A* (2), 207-216.
205. Schneider, G.; Burridge, K., Formation of Focal Adhesions by Osteoblasts Adhering to Different Substrata. *Experimental Cell Research* **1994,** *214* (1), 264-269.
206. Steele, J. G.; McFarland, C.; Dalton, B. A.; Johnson, G.; Evans, M. D. M.; Rolfe Howlett, C.; Underwood, P. A., Attachment of human bone cells to tissue culture polystyrene and to unmodified polystyrene: the effect of surface chemistry upon initial cell attachment. *Journal of Biomaterials Science, Polymer Edition* **1994,** *5* (3), 245-257.
207. Rabe, M.; Verdes, D.; Seeger, S., Understanding protein adsorption phenomena at solid surfaces. *Advances in Colloid and Interface Science* **2011,** *162* (1–2), 87-106.
208. Rezania, A.; Healy, K. E., Biomimetic Peptide Surfaces That Regulate Adhesion, Spreading, Cytoskeletal Organization, and Mineralization of the Matrix Deposited by Osteoblast-like Cells. *Biotechnology Progress* **1999,** *15* (1), 19-32.
209. Llopis-Hernández, V.; Rico, P.; Ballester-Beltrán, J.; Moratal, D.; Salmerón-Sánchez, M., Role of Surface Chemistry in Protein Remodeling at the Cell-Material Interface. *PLoS ONE* **2011,** *6* (5), e19610.
210. Bacakova, L.; Filova, E.; Parizek, M.; Ruml, T.; Svorcik, V., Modulation of cell adhesion, proliferation and differentiation on materials designed for body implants. *Biotechnology Advances* **2011,** *29* (6), 739-767.
211. Faia-Torres, A. B.; Goren, T.; Ihalainen, T. O.; Guimond-Lischer, S.; Charnley, M.; Rottmar, M.; Maniura-Weber, K.; Spencer, N. D.; Reis, R. L.; Textor, M.; Neves, N. M., Regulation of Human Mesenchymal Stem Cell Osteogenesis by Specific Surface Density of Fibronectin: a Gradient Study. *ACS Applied Materials & Interfaces* **2015,** *7* (4), 2367-2375.
212. Altankov, G.; Groth, T., Reorganization of substratum-bound fibronectin on hydrophilic and hydrophobic materials is related to biocompatibility. *Journal of Materials Science: Materials in Medicine* **1994,** *5* (9), 732-737.
213. Arima, Y.; Iwata, H., Effect of wettability and surface functional groups on protein adsorption and cell adhesion using well-defined mixed self-assembled monolayers. *Biomaterials* **2007,** *28* (20), 3074-3082.
214. Gessner, A.; Lieske, A.; Paulke, B. R.; Müller, R. H., Influence of surface charge density on protein adsorption on polymeric nanoparticles: analysis by two-dimensional electrophoresis. *European Journal of Pharmaceutics and Biopharmaceutics* **2002,** *54* (2), 165-170.

215. Hartvig, R. A.; van de Weert, M.; Østergaard, J.; Jorgensen, L.; Jensen, H., Protein Adsorption at Charged Surfaces: The Role of Electrostatic Interactions and Interfacial Charge Regulation. *Langmuir* **2011,** *27* (6), 2634-2643.
216. Fabrizius-Homan, D. J.; Cooper, S. L., Competitive adsorption of vitronection with albumin, fibrinogen, and fibronectin on polymeric biomaterials. *Journal of Biomedical Materials Research* **1991,** *25* (8), 953-971.
217. Slack, S. M.; Horbett, T. A., Physicochemical and biochemical aspects of fibrinogen adsorption from plasma and binary protein solutions onto polyethylene and glass. *Journal of Colloid and Interface Science* **1988,** *124* (2), 535-551.
218. Kilpadi, K. L.; Chang, P.-L.; Bellis, S. L., Hydroxylapatite binds more serum proteins, purified integrins, and osteoblast precursor cells than titanium or steel. *Journal of Biomedical Materials Research* **2001,** *57* (2), 258-267.
219. Ostuni, E.; Grzybowski, B. A.; Mrksich, M.; Roberts, C. S.; Whitesides, G. M., Adsorption of Proteins to Hydrophobic Sites on Mixed Self-Assembled Monolayers. *Langmuir* **2003,** *19* (5), 1861-1872.
220. Wei, Q.; Pohl, T. L. M.; Seckinger, A.; Spatz, J. P.; Cavalcanti-Adam, E. A., Regulation of integrin and growth factor signaling in biomaterials for osteodifferentiation. *Beilstein Journal of Organic Chemistry* **2015,** *11*, 773-783.
221. Ramirez, F.; Rifkin, D. B., Cell signaling events: a view from the matrix. *Matrix Biology* **2003,** *22* (2), 101-107.
222. Keshaw, H.; Forbes, A.; Day, R. M., Release of angiogenic growth factors from cells encapsulated in alginate beads with bioactive glass. *Biomaterials* **2005,** *26* (19), 4171-4179.
223. Schwab, E. H.; Pohl, T. L. M.; Haraszti, T.; Schwaerzer, G. K.; Hiepen, C.; Spatz, J. P.; Knaus, P.; Cavalcanti-Adam, E. A., Nanoscale Control of Surface Immobilized BMP-2: Toward a Quantitative Assessment of BMP-Mediated Signaling Events. *Nano Letters* **2015,** *15* (3), 1526-1534.
224. Hudalla, G. A.; Murphy, W. L., Biomaterials that regulate growth factor activity via bioinspired interactions. *Advanced functional materials* **2011,** *21* (10), 1754-1768.
225. Zara, J. N.; Siu, R. K.; Zhang, X.; Shen, J.; Ngo, R.; Lee, M.; Li, W.; Chiang, M.; Chung, J.; Kwak, J.; Wu, B. M.; Ting, K.; Soo, C., High Doses of Bone Morphogenetic Protein 2 Induce Structurally Abnormal Bone and Inflammation In Vivo. *Tissue Engineering. Part A* **2011,** *17* (9-10), 1389-1399.
226. Babitt, J. L.; Huang, F. W.; Xia, Y.; Sidis, Y.; Andrews, N. C.; Lin, H. Y., Modulation of bone morphogenetic protein signaling in vivo regulates systemic iron balance. *Journal of Clinical Investigation* **2007,** *117* (7), 1933-1939.
227. Pohl, T. L. M.; Schwab, E. H.; Cavalcanti-Adam, E. A., Covalent Binding of BMP-2 on Surfaces Using a Self-assembled Monolayer Approach. *Journal of Visualized Experiments : JoVE* **2013,** (78), 50842.
228. Luginbuehl, V.; Meinel, L.; Merkle, H. P.; Gander, B., Localized delivery of growth factors for bone repair. *European Journal of Pharmaceutics and Biopharmaceutics* **2004,** *58* (2), 197-208.
229. Migliorini, E.; Valat, A.; Picart, C.; Cavalcanti-Adam, E. A., Tuning cellular responses to BMP-2 with material surfaces. *Cytokine & Growth Factor Reviews*.
230. Farokhi, M.; Mottaghitalab, F.; Shokrgozar, M. A.; Ou, K.-L.; Mao, C.; Hosseinkhani, H., Importance of dual delivery systems for bone tissue engineering. *Journal of Controlled Release* **2016,** *225*, 152-169.
231. Cao, X.; Yu, W.-q.; Qiu, J.; Zhao, Y.-f.; Zhang, Y.-l.; Zhang, F.-q., RGD peptide immobilized on TiO2 nanotubes for increased bone marrow stromal cells adhesion and osteogenic gene expression. *Journal of Materials Science: Materials in Medicine* **2012,** *23* (2), 527-536.
232. Nakaoka, R.; Hirano, Y.; Mooney, D. J.; Tsuchiya, T.; Matsuoka, A., Study on the potential of RGD- and PHSRN-modified alginates as artificial extracellular matrices for engineering bone. *Journal of Artificial Organs* **2013,** *16* (3), 284-293.
233. Jones, E. A.; Kinsey, S. E.; English, A.; Jones, R. A.; Straszynski, L.; Meredith, D. M.; Markham, A. F.; Jack, A.; Emery, P.; McGonagle, D., Isolation and

characterization of bone marrow multipotential mesenchymal progenitor cells. *Arthritis & Rheumatism* **2002,** *46* (12), 3349-3360.
234. Bellis, S. L., Advantages of RGD peptides for directing cell association with biomaterials. *Biomaterials* **2011,** *32* (18), 4205-4210.
235. Zhong, C.; Chrzanowska-Wodnicka, M.; Brown, J.; Shaub, A.; Belkin, A. M.; Burridge, K., Rho-mediated Contractility Exposes a Cryptic Site in Fibronectin and Induces Fibronectin Matrix Assembly. *The Journal of Cell Biology* **1998,** *141* (2), 539-551.
236. Klotzsch, E.; Smith, M. L.; Kubow, K. E.; Muntwyler, S.; Little, W. C.; Beyeler, F.; Gourdon, D.; Nelson, B. J.; Vogel, V., Fibronectin forms the most extensible biological fibers displaying switchable force-exposed cryptic binding sites. *Proceedings of the National Academy of Sciences* **2009,** *106* (43), 18267-18272.
237. Vadillo-Rodríguez, V.; Pacha-Olivenza, M. A.; Gónzalez-Martín, M. L.; Bruque, J. M.; Gallardo-Moreno, A. M., Adsorption behavior of human plasma fibronectin on hydrophobic and hydrophilic Ti6Al4V substrata and its influence on bacterial adhesion and detachment. *Journal of Biomedical Materials Research Part A* **2013,** *101A* (5), 1397-1404.
238. Meadows, P. Y.; Walker, G. C., Force Microscopy Studies of Fibronectin Adsorption and Subsequent Cellular Adhesion to Substrates with Well-Defined Surface Chemistries. *Langmuir* **2005,** *21* (9), 4096-4107.
239. Bergkvist, M.; Carlsson, J.; Oscarsson, S., Surface-dependent conformations of human plasma fibronectin adsorbed to silica, mica, and hydrophobic surfaces, studied with use of Atomic Force Microscopy. *Journal of Biomedical Materials Research Part A* **2003,** *64A* (2), 349-356.
240. Hovgaard, M. B.; Rechendorff, K.; Chevallier, J.; Foss, M.; Besenbacher, F., Fibronectin Adsorption on Tantalum: The Influence of Nanoroughness. *The Journal of Physical Chemistry B* **2008,** *112* (28), 8241-8249.
241. González-García, C.; Sousa, S. R.; Moratal, D.; Rico, P.; Salmerón-Sánchez, M., Effect of nanoscale topography on fibronectin adsorption, focal adhesion size and matrix organisation. *Colloids and Surfaces B: Biointerfaces* **2010,** *77* (2), 181-190.
242. Llopis-Hernández, V.; Rico, P.; Moratal, D.; Altankov, G.; Salmerón-Sánchez, M., Role of Material-Driven Fibronectin Fibrillogenesis in Protein Remodeling. *BioResearch Open Access* **2013,** *2* (5), 364-373.
243. Vanterpool, F. A.; Cantini, M.; Seib, F. P.; Salmerón-Sánchez, M., A Material-Based Platform to Modulate Fibronectin Activity and Focal Adhesion Assembly. *BioResearch Open Access* **2014,** *3* (6), 286-296.
244. Llopis-Hernández, V.; Cantini, M.; González-García, C.; Cheng, Z. A.; Yang, J.; Tsimbouri, P. M.; García, A. J.; Dalby, M. J.; Salmerón-Sánchez, M., Material-driven fibronectin assembly for high-efficiency presentation of growth factors. *Science Advances* **2016,** *2* (8).
245. Baneyx, G.; Baugh, L.; Vogel, V., Coexisting conformations of fibronectin in cell culture imaged using fluorescence resonance energy transfer. *Proceedings of the National Academy of Sciences of the United States of America* **2001,** *98* (25), 14464-14468.
246. Gudzenko, T.; Franz, C. M., Studying early stages of fibronectin fibrillogenesis in living cells by atomic force microscopy. *Molecular Biology of the Cell* **2015,** *26* (18), 3190-3204.
247. Sethuraman, A.; Han, M.; Kane, R. S.; Belfort, G., Effect of Surface Wettability on the Adhesion of Proteins. *Langmuir* **2004,** *20* (18), 7779-7788.
248. Hao, L.; Fu, X.; Li, T.; Zhao, N.; Shi, X.; Cui, F.; Du, C.; Wang, Y., Surface chemistry from wettability and charge for the control of mesenchymal stem cell fate through self-assembled monolayers. *Colloids and Surfaces B: Biointerfaces* **2016,** *148*, 549-556.
249. Lam, C. N. C.; Wu, R.; Li, D.; Hair, M. L.; Neumann, A. W., Study of the advancing and receding contact angles: liquid sorption as a cause of contact angle hysteresis. *Advances in Colloid and Interface Science* **2002,** *96* (1–3), 169-191.

250. Smith, M. L.; Gourdon, D.; Little, W. C.; Kubow, K. E.; Eguiluz, R. A.; Luna-Morris, S.; Vogel, V., Force-Induced Unfolding of Fibronectin in the Extracellular Matrix of Living Cells. *PLoS Biology* **2007,** *5* (10), e268.
251. Stephansson, S. N.; Byers, B. A.; García, A. J., Enhanced expression of the osteoblastic phenotype on substrates that modulate fibronectin conformation and integrin receptor binding. *Biomaterials* **2002,** *23* (12), 2527-2534.
252. Vogel, S.; Arnoldini, S.; Möller, S.; Schnabelrauch, M.; Hempel, U., Sulfated hyaluronan alters fibronectin matrix assembly and promotes osteogenic differentiation of human bone marrow stromal cells. *Scientific Reports* **2016,** *6*, 36418.
253. Humphries, M. J., Cell Adhesion Assays. In *Extracellular Matrix Protocols: Second Edition*, Even-Ram, S.; Artym, V., Eds. Humana Press: Totowa, NJ, 2009; pp 203-210.
254. Berginski, M. E.; Gomez, S. M., The Focal Adhesion Analysis Server: a web tool for analyzing focal adhesion dynamics. *F1000Research* **2013,** *2*, 68.
255. Geiger, B.; Bershadsky, A.; Pankov, R.; Yamada, K. M., Transmembrane crosstalk between the extracellular matrix and the cytoskeleton. *Nat Rev Mol Cell Biol* **2001,** *2* (11), 793-805.
256. Biggs, M. J. P.; Dalby, M. J., Focal adhesions in osteoneogenesis. *Proceedings of the Institution of Mechanical Engineers. Part H, Journal of engineering in medicine* **2010,** *224* (12), 1441-1453.
257. Ahmad Khalili, A.; Ahmad, M. R., A Review of Cell Adhesion Studies for Biomedical and Biological Applications. *International Journal of Molecular Sciences* **2015,** *16* (8), 18149-18184.
258. Hersel, U.; Dahmen, C.; Kessler, H., RGD modified polymers: biomaterials for stimulated cell adhesion and beyond. *Biomaterials* **2003,** *24* (24), 4385-4415.
259. Grant, R. P.; Spitzfaden, C.; Altroff, H.; Campbell, I. D.; Mardon, H. J., Structural Requirements for Biological Activity of the Ninth and Tenth FIII Domains of Human Fibronectin. *The Journal of biological chemistry* **1997,** *272* (10), 6159-6166.
260. Martino, M. M.; Briquez, P. S.; Güç, E.; Tortelli, F.; Kilarski, W. W.; Metzger, S.; Rice, J. J.; Kuhn, G. A.; Müller, R.; Swartz, M. A.; Hubbell, J. A., Growth Factors Engineered for Super-Affinity to the Extracellular Matrix Enhance Tissue Healing. *Science* **2014,** *343* (6173), 885.
261. Fitzpatrick, V.; Fourel, L.; Destaing, O.; Gilde, F.; Albigès-Rizo, C.; Picart, C.; Boudou, T., Signal mingle: Micropatterns of BMP-2 and fibronectin on soft biopolymeric films regulate myoblast shape and SMAD signaling. *Scientific Reports* **2017,** *7*, 41479.
262. Lin, F.; Ren, X.-D.; Pan, Z.; Macri, L.; Zong, W.-X.; Tonnesen, M. G.; Rafailovich, M.; Bar-Sagi, D.; Clark, R. A. F., Fibronectin Growth Factor-Binding Domains Are Required for Fibroblast Survival. *J Invest Dermatol* **2011,** *131* (1), 84-98.
263. Fraioli, R.; Dashnyam, K.; Kim, J.-H.; Perez, R. A.; Kim, H.-W.; Gil, J.; Ginebra, M.-P.; Manero, J. M.; Mas-Moruno, C., Surface guidance of stem cell behavior: Chemically tailored co-presentation of integrin-binding peptides stimulates osteogenic differentiation in vitro and bone formation in vivo. *Acta Biomaterialia* **2016,** *43*, 269-281.
264. Bilem, I.; Chevallier, P.; Plawinski, L.; Sone, E. D.; Durrieu, M. C.; Laroche, G., RGD and BMP-2 mimetic peptide crosstalk enhances osteogenic commitment of human bone marrow stem cells. *Acta Biomaterialia* **2016,** *36*, 132-142.
265. Takahashi, K.; Tanabe, K.; Ohnuki, M.; Narita, M.; Ichisaka, T.; Tomoda, K.; Yamanaka, S., Induction of Pluripotent Stem Cells from Adult Human Fibroblasts by Defined Factors. *Cell* **2007,** *131* (5), 861-872.
266. Yu, Z.; Gauthier, P.; Tran, Q. T.; El-Ayachi, I.; Bhatti, F.-U.-R.; Bahabri, R.; Al-Habib, M.; Huang, G. T. J., Differential Properties of Human ALP(+) Periodontal Ligament Stem Cells vs Their ALP(-) Counterparts. *Journal of stem cell research & therapy* **2015,** *5* (7), 292.
267. Sobiesiak, M.; Sivasubramaniyan, K.; Hermann, C.; Tan, C.; Örgel, M.; Treml, S.; Cerabona, F.; de Zwart, P.; Ochs, U.; Müller, C. A.; Gargett, C. E.; Kalbacher, H.; Bühring, H.-J., The Mesenchymal Stem Cell Antigen MSCA-1 is Identical to Tissue

Non-specific Alkaline Phosphatase. *Stem Cells and Development* **2009,** *19* (5), 669-677.
268. Lee, K.-S.; Kim, H.-J.; Li, Q.-L.; Chi, X.-Z.; Ueta, C.; Komori, T.; Wozney, J. M.; Kim, E.-G.; Choi, J.-Y.; Ryoo, H.-M.; Bae, S.-C., Runx2 Is a Common Target of Transforming Growth Factor β1 and Bone Morphogenetic Protein 2, and Cooperation between Runx2 and Smad5 Induces Osteoblast-Specific Gene Expression in the Pluripotent Mesenchymal Precursor Cell Line C2C12. *Molecular and Cellular Biology* **2000,** *20* (23), 8783-8792.
269. Martino, M. M.; Tortelli, F.; Mochizuki, M.; Traub, S.; Ben-David, D.; Kuhn, G. A.; Müller, R.; Livne, E.; Eming, S. A.; Hubbell, J. A., Engineering the Growth Factor Microenvironment with Fibronectin Domains to Promote Wound and Bone Tissue Healing. *Science Translational Medicine* **2011,** *3* (100), 100ra89.
270. Lauffenburger, D. A.; Horwitz, A. F., Cell Migration: A Physically Integrated Molecular Process. *Cell* **1996,** *84* (3), 359-369.
271. Ehrlicher, A. J.; Nakamura, F.; Hartwig, J. H.; Weitz, D. A.; Stossel, T. P., Mechanical strain in actin networks regulates FilGAP and integrin binding to filamin A. *Nature* **2011,** *478* (7368), 260-263.
272. del Rio, A.; Perez-Jimenez, R.; Liu, R.; Roca-Cusachs, P.; Fernandez, J. M.; Sheetz, M. P., Stretching Single Talin Rod Molecules Activates Vinculin Binding. *Science* **2009,** *323* (5914), 638.
273. Mallick, P.; Kuster, B., Proteomics: a pragmatic perspective. *Nat Biotech* **2010,** *28* (7), 695-709.
274. Wasinger, V. C.; Cordwell, S. J.; Cerpa-Poljak, A.; Yan, J. X.; Gooley, A. A.; Wilkins, M. R.; Duncan, M. W.; Harris, R.; Williams, K. L.; Humphery-Smith, I., Progress with gene-product mapping of the Mollicutes: Mycoplasma genitalium. *ELECTROPHORESIS* **1995,** *16* (1), 1090-1094.
275. Zaidel-Bar, R.; Geiger, B., The switchable integrin adhesome. *Journal of Cell Science* **2010,** *123* (9), 1385.
276. Winograd-Katz, S. E.; Fässler, R.; Geiger, B.; Legate, K. R., The integrin adhesome: from genes and proteins to human disease. *Nat Rev Mol Cell Biol* **2014,** *15* (4), 273-288.
277. Zamir, E.; Geiger, B.; Kam, Z., Quantitative Multicolor Compositional Imaging Resolves Molecular Domains in Cell-Matrix Adhesions. *PLOS ONE* **2008,** *3* (4), e1901.
278. Schiller, H. B.; Friedel, C. C.; Boulegue, C.; Fässler, R., Quantitative proteomics of the integrin adhesome show a myosin II-dependent recruitment of LIM domain proteins. *EMBO Reports* **2011,** *12* (3), 259-266.
279. Zaidel-Bar, R.; Itzkovitz, S.; Ma'ayan, A.; Iyengar, R.; Geiger, B., Functional atlas of the integrin adhesome. *Nat Cell Biol* **2007,** *9* (8), 858-867.
280. Beaumont, Kristin G.; Mrksich, M., The Mechanostability of Isolated Focal Adhesions Is Strongly Dependent on pH. *Chemistry & Biology* **2012,** *19* (6), 711-720.
281. Kuo, J.-C.; Han, X.; Hsiao, C.-T.; Yates Iii, J. R.; Waterman, C. M., Analysis of the myosin-II-responsive focal adhesion proteome reveals a role for [beta]-Pix in negative regulation of focal adhesion maturation. *Nat Cell Biol* **2011,** *13* (4), 383-393.
282. Ajeian, J. N.; Horton, E. R.; Astudillo, P.; Byron, A.; Askari, J. A.; Millon‐Frémillon, A.; Knight, D.; Kimber, S. J.; Humphries, M. J.; Humphries, J. D., Proteomic analysis of integrin‐associated complexes from mesenchymal stem cells. *Proteomics. Clinical Applications* **2016,** *10* (1), 51-57.
283. Allet, N.; Barrillat, N.; Baussant, T.; Boiteau, C.; Botti, P.; Bougueleret, L.; Budin, N.; Canet, D.; Carraud, S.; Chiappe, D.; Christmann, N.; Colinge, J.; Cusin, I.; Dafflon, N.; Depresle, B.; Fasso, I.; Frauchiger, P.; Gaertner, H.; Gleizes, A.; Gonzalez-Couto, E.; Jeandenans, C.; Karmime, A.; Kowall, T.; Lagache, S.; Mahé, E.; Masselot, A.; Mattou, H.; Moniatte, M.; Niknejad, A.; Paolini, M.; Perret, F.; Pinaud, N.; Ranno, F.; Raimondi, S.; Reffas, S.; Regamey, P.-O.; Rey, P.-A.; Rodriguez-Tomé, P.; Rose, K.; Rossellat, G.; Saudrais, C.; Schmidt, C.; Villain, M.; Zwahlen, C., In vitro and in silico processes to identify differentially expressed proteins. *PROTEOMICS* **2004,** *4* (8), 2333-2351.

284. Ong, S.-E.; Mann, M., Mass spectrometry-based proteomics turns quantitative. *Nat Chem Biol* **2005,** *1* (5), 252-262.
285. Rappsilber, J.; Ryder, U.; Lamond, A. I.; Mann, M., Large-Scale Proteomic Analysis of the Human Spliceosome. *Genome Research* **2002,** *12* (8), 1231-1245.
286. Ishihama, Y.; Oda, Y.; Tabata, T.; Sato, T.; Nagasu, T.; Rappsilber, J.; Mann, M., Exponentially Modified Protein Abundance Index (emPAI) for Estimation of Absolute Protein Amount in Proteomics by the Number of Sequenced Peptides per Protein. *Molecular & Cellular Proteomics* **2005,** *4* (9), 1265-1272.
287. Mi, H.; Muruganujan, A.; Casagrande, J. T.; Thomas, P. D., Large-scale gene function analysis with the PANTHER classification system. *Nat. Protocols* **2013,** *8* (8), 1551-1566.
288. Huang, D. W.; Sherman, B. T.; Lempicki, R. A., Systematic and integrative analysis of large gene lists using DAVID bioinformatics resources. *Nat. Protocols* **2008,** *4* (1), 44-57.
289. Kanehisa, M.; Furumichi, M.; Tanabe, M.; Sato, Y.; Morishima, K., KEGG: new perspectives on genomes, pathways, diseases and drugs. *Nucleic Acids Research* **2017,** *45* (D1), D353-D361.
290. Humphries, J. D.; Byron, A.; Bass, M. D.; Craig, S. E.; Pinney, J. W.; Knight, D.; Humphries, M. J., Proteomic Analysis of Integrin-Associated Complexes Identifies RCC2 as a Dual Regulator of Rac1 and Arf6. *Science signaling* **2009,** *2* (87), ra51-ra51.
291. Horton, E. R.; Byron, A.; Askari, J. A.; Ng, D. H. J.; Millon-Frémillon, A.; Robertson, J.; Koper, E. J.; Paul, N. R.; Warwood, S.; Knight, D.; Humphries, J. D.; Humphries, M. J., Definition of a consensus integrin adhesome and its dynamics during adhesion complex assembly and disassembly. *Nature cell biology* **2015,** *17* (12), 1577-1587.
292. Chew, C. S.; Parente, J. A.; Zhou, C. J.; Baranco, E.; Chen, X., Lasp-1 is a regulated phosphoprotein within the cAMP signaling pathway in the gastric parietal cell. *American Journal of Physiology - Cell Physiology* **1998,** *275* (1), C56.
293. Chew, C. S.; Chen, X.; Parente, J. A.; Tarrer, S.; Okamoto, C.; Qin, H.-Y., Lasp-1 binds to non-muscle F-actin in vitro and is localized within multiple sites of dynamic actin assembly in vivo. *Journal of Cell Science* **2002,** *115* (24), 4787.
294. Li, B.; Zhuang, L.; Trueb, B., Zyxin Interacts with the SH3 Domains of the Cytoskeletal Proteins LIM-nebulette and Lasp-1. *Journal of Biological Chemistry* **2004,** *279* (19), 20401-20410.
295. Lin, Y. H.; Park, Z.-Y.; Lin, D.; Brahmbhatt, A. A.; Rio, M.-C.; Yates, J. R.; Klemke, R. L., Regulation of cell migration and survival by focal adhesion targeting of Lasp-1. *The Journal of Cell Biology* **2004,** *165* (3), 421-432.
296. Grunewald, T. G. P.; Kammerer, U.; Schulze, E.; Schindler, D.; Honig, A.; Zimmer, M.; Butt, E., Silencing of LASP-1 influences zyxin localization, inhibits proliferation and reduces migration in breast cancer cells. *Experimental Cell Research* **2006,** *312* (7), 974-982.
297. Hamada, K.; Shimizu, T.; Matsui, T.; Tsukita, S.; Tsukita, S.; Hakoshima, T., Structural basis of the membrane-targeting and unmasking mechanisms of the radixin FERM domain. *The EMBO Journal* **2000,** *19* (17), 4449-4462.
298. Tang, P.; Cao, C.; Xu, M.; Zhang, L., Cytoskeletal protein radixin activates integrin αMβ2 by binding to its cytoplasmic tail. *FEBS Letters* **2007,** *581* (6), 1103-1108.
299. Rintoul, R. C.; Buttery, R. C.; Mackinnon, A. C.; Wong, W. S.; Mosher, D.; Haslett, C.; Sethi, T., Cross-Linking CD98 Promotes Integrin-like Signaling and Anchorage-independent Growth. *Molecular Biology of the Cell* **2002,** *13* (8), 2841-2852.
300. Zent, R.; Fenczik, C. A.; Calderwood, D. A.; Liu, S.; Dellos, M.; Ginsberg, M. H., Class- and Splice Variant-specific Association of CD98 with Integrin β Cytoplasmic Domains. *Journal of Biological Chemistry* **2000,** *275* (7), 5059-5064.
301. Dang, H.; Lin, A. L.; Zhang, B.; Zhang, H.-M.; Katz, M. S.; Yeh, C.-K., A Role for Notch Signaling in Salivary Acinar Cell Growth and Differentiation. *Developmental*

dynamics : an official publication of the American Association of Anatomists **2009,** *238* (3), 724-731.
302. Broers, J. L. V.; Rot, M. K.; Vooijs, G. P.; Ramaekers, F. C. S.; de Leij, L.; ter Haar, A.; Lane, E. B.; Leigh, I. M.; Wagenaar, S. S., Expression of intermediate filament proteins in fetal and adult human lung tissues. *Differentiation* **1989,** *40* (2), 119-128.
303. Kreis, S.; Schönfeld, H.-J.; Melchior, C.; Steiner, B.; Kieffer, N., The intermediate filament protein vimentin binds specifically to a recombinant integrin α2/β1 cytoplasmic tail complex and co-localizes with native α2/β1 in endothelial cell focal adhesions. *Experimental Cell Research* **2005,** *305* (1), 110-121.
304. Homan, S. M.; Martinez, R.; Benware, A.; LaFlamme, S. E., Regulation of the Association of α6β4 with Vimentin Intermediate Filaments in Endothelial Cells. *Experimental Cell Research* **2002,** *281* (1), 107-114.
305. Kim, J.; Jang, J.; Yang, C.; Kim, E. J.; Jung, H.; Kim, C., Vimentin filament controls integrin α5β1-mediated cell adhesion by binding to integrin through its Ser38 residue. *FEBS Letters* **2016,** *590* (20), 3517-3525.
306. Calderwood, D. A.; Ginsberg, M. H., Talin forges the links between integrins and actin. *Nat Cell Biol* **2003,** *5* (8), 694-697.
307. Vadlamudi, R. K.; Li, F.; Adam, L.; Nguyen, D.; Ohta, Y.; Stossel, T. P.; Kumar, R., Filamin is essential in actin cytoskeletal assembly mediated by p21-activated kinase 1. *Nat Cell Biol* **2002,** *4* (9), 681-690.
308. Hampton, C. M.; Taylor, D. W.; Taylor, K. A., Novel Structures for α-Actinin:F-Actin Interactions and their Implications for Actin–Membrane Attachment and Tension Sensing in the Cytoskeleton. *Journal of Molecular Biology* **2007,** *368* (1), 92-104.
309. Wiche, G.; Winter, L., Plectin isoforms as organizers of intermediate filament cytoarchitecture. *Bioarchitecture* **2011,** *1* (1), 14-20.
310. Favre, B.; Schneider, Y.; Lingasamy, P.; Bouameur, J.-E.; Begré, N.; Gontier, Y.; Steiner-Champliaud, M.-F.; Frias, M. A.; Borradori, L.; Fontao, L., Plectin interacts with the rod domain of type III intermediate filament proteins desmin and vimentin. *European Journal of Cell Biology* **2011,** *90* (5), 390-400.
311. Kuo, J.-C.; Han, X.; Yates, J. R.; Waterman, C. M., Isolation of Focal Adhesion Proteins for Biochemical and Proteomic Analysis. *Methods in molecular biology (Clifton, N.J.)* **2012,** *757*, 297-323.
312. Sahai, E., Mechanisms of cancer cell invasion. *Current Opinion in Genetics & Development* **2005,** *15* (1), 87-96.
313. Vicente-Manzanares, M.; Webb, D. J.; Horwitz, A. R., Cell migration at a glance. *Journal of Cell Science* **2005,** *118* (21).
314. Theveneau, E.; Mayor, R., Collective cell migration of epithelial and mesenchymal cells. *Cellular and Molecular Life Sciences* **2013,** *70* (19), 3481-3492.
315. Nourshargh, S.; Alon, R., Leukocyte Migration into Inflamed Tissues. *Immunity 41* (5), 694-707.
316. Friedl, P.; Wolf, K., Plasticity of cell migration: a multiscale tuning model. *The Journal of Cell Biology* **2010,** *188* (1), 11-19.
317. Mayor, R.; Etienne-Manneville, S., The front and rear of collective cell migration. *Nat Rev Mol Cell Biol* **2016,** *17* (2), 97-109.
318. Campanale, J. P.; Sun, T. Y.; Montell, D. J., Development and dynamics of cell polarity at a glance. *Journal of Cell Science* **2017,** *130* (7), 1201.
319. Huttenlocher, A.; Horwitz, A. R., Integrins in Cell Migration. *Cold Spring Harbor Perspectives in Biology* **2011,** *3* (9).
320. Lo, C. M.; Wang, H. B.; Dembo, M.; Wang, Y. L., Cell movement is guided by the rigidity of the substrate. *Biophysical Journal* **2000,** *79* (1), 144-152.
321. Raab, M.; Swift, J.; P. Dingal, P. C. D.; Shah, P.; Shin, J.-W.; Discher, D. E., Crawling from soft to stiff matrix polarizes the cytoskeleton and phosphoregulates myosin-II heavy chain. *The Journal of Cell Biology* **2012,** *199* (4), 669-683.
322. Pelham, R. J.; Wang, Y.-l., Cell locomotion and focal adhesions are regulated by substrate flexibility. *Proceedings of the National Academy of Sciences* **1997,** *94* (25), 13661-13665.

323. Isenberg, B. C.; DiMilla, P. A.; Walker, M.; Kim, S.; Wong, J. Y., Vascular Smooth Muscle Cell Durotaxis Depends on Substrate Stiffness Gradient Strength. *Biophysical Journal* **2009,** *97* (5), 1313-1322.
324. Schlaepfer, D. D.; Mitra, S. K., Multiple connections link FAK to cell motility and invasion. *Current Opinion in Genetics & Development* **2004,** *14* (1), 92-101.
325. Hu, Y.-L.; Lu, S.; Szeto, K. W.; Sun, J.; Wang, Y.; Lasheras, J. C.; Chien, S., FAK and paxillin dynamics at focal adhesions in the protrusions of migrating cells. *Scientific Reports* **2014,** *4*, 6024.
326. Schiller, H. B.; Hermann, M.-R.; Polleux, J.; Vignaud, T.; Zanivan, S.; Friedel, C. C.; Sun, Z.; Raducanu, A.; Gottschalk, K.-E.; Théry, M.; Mann, M.; Fässler, R., β1- and αv-class integrins cooperate to regulate myosin II during rigidity sensing of fibronectin-based microenvironments. *Nat Cell Biol* **2013,** *15* (6), 625-636.
327. Danen, E. H. J.; van Rheenen, J.; Franken, W.; Huveneers, S.; Sonneveld, P.; Jalink, K.; Sonnenberg, A., Integrins control motile strategy through a Rho–cofilin pathway. *The Journal of Cell Biology* **2005,** *169* (3), 515-526.
328. Wozniak, M. A.; Modzelewska, K.; Kwong, L.; Keely, P. J., Focal adhesion regulation of cell behavior. *Biochimica et Biophysica Acta (BBA) - Molecular Cell Research* **2004,** *1692* (2–3), 103-119.
329. Beningo, K. A.; Dembo, M.; Kaverina, I.; Small, J. V.; Wang, Y.-l., Nascent Focal Adhesions Are Responsible for the Generation of Strong Propulsive Forces in Migrating Fibroblasts. *The Journal of Cell Biology* **2001,** *153* (4), 881-888.
330. Slater, J. H.; Boyce, P. J.; Jancaitis, M. P.; Gaubert, H. E.; Chang, A. L.; Markey, M. K.; Frey, W., Modulation of Endothelial Cell Migration via Manipulation of Adhesion Site Growth Using Nanopatterned Surfaces. *ACS Applied Materials & Interfaces* **2015,** *7* (7), 4390-4400.
331. Palecek, S. P.; Loftus, J. C.; Ginsberg, M. H.; Lauffenburger, D. A.; Horwitz, A. F., Integrin-ligand binding properties govern cell migration speed through cell-substratum adhesiveness. *Nature* **1997,** *385* (6616), 537-540.
332. Bergman, A. J.; Zygourakis, K., Migration of lymphocytes on fibronectin-coated surfaces: temporal evolution of migratory parameters. *Biomaterials* **1999,** *20* (23–24), 2235-2244.
333. Maximal migration of human smooth muscle cells on fibronectin and type IV collagen occurs at an intermediate attachment strength. *The Journal of Cell Biology* **1993,** *122* (3), 729-737.
334. DiMilla, P. A.; Stone, J. A.; Quinn, J. A.; Albelda, S. M.; Lauffenburger, D. A., Maximal migration of human smooth muscle cells on fibronectin and type IV collagen occurs at an intermediate attachment strength. *The Journal of Cell Biology* **1993,** *122* (3), 729.
335. Liu, D.; Che Abdullah, C. A.; Sear, R. P.; Keddie, J. L., Cell adhesion on nanopatterned fibronectin substrates. *Soft Matter* **2010,** *6* (21), 5408-5416.
336. Lee, M. H.; Ducheyne, P.; Lynch, L.; Boettiger, D.; Composto, R. J., Effect of biomaterial surface properties on fibronectin–α5β1 integrin interaction and cellular attachment. *Biomaterials* **2006,** *27* (9), 1907-1916.
337. Kim, M.-C.; Neal, D. M.; Kamm, R. D.; Asada, H. H., Dynamic Modeling of Cell Migration and Spreading Behaviors on Fibronectin Coated Planar Substrates and Micropatterned Geometries. *PLoS Comput Biol* **2013,** *9* (2), e1002926.
338. Rajagopalan, P.; Marganski, W. A.; Brown, X. Q.; Wong, J. Y., Direct Comparison of the Spread Area, Contractility, and Migration of balb/c 3T3 Fibroblasts Adhered to Fibronectin- and RGD-Modified Substrata. *Biophysical Journal* **2004,** *87* (4), 2818-2827.
339. Clark, R. A. F.; An, J.-Q.; Greiling, D.; Khan, A.; Schwarzbauer, J. E., Fibroblast Migration on Fibronectin Requires Three Distinct Functional Domains. **2003,** *121* (4), 695-705.
340. Mooradian, D. L.; McCarthy, J. B.; Skubitz, A. P.; Cameron, J. D.; Furcht, L. T., Characterization of FN-C/H-V, a novel synthetic peptide from fibronectin that promotes rabbit corneal epithelial cell adhesion, spreading, and motility. *Investigative Ophthalmology & Visual Science* **1993,** *34* (1), 153-164.

341. Huebsch, J. C.; McCarthy, J. B.; Diglio, C. A.; Mooradian, D. L., Endothelial Cell Interactions With Synthetic Peptides From the Carboxyl-Terminal Heparin-Binding Domains of Fibronectin. *Circulation Research* **1995,** *77* (1), 43-53.
342. Kimura, K.; Hattori, A.; Usui, Y.; Kitazawa, K.; Naganuma, M.; Kawamoto, K.; Teranishi, S.; Nomizu, M.; Nishida, T., Stimulation of Corneal Epithelial Migration by a Synthetic Peptide (PHSRN) Corresponding to the Second Cell-Binding Site of Fibronectin. *Investigative Ophthalmology & Visual Science* **2007,** *48* (3), 1110-1118.
343. Livant, D. L.; Brabec, R. K.; Kurachi, K.; Allen, D. L.; Wu, Y.; Haaseth, R.; Andrews, P.; Ethier, S. P.; Markwart, S., The PHSRN sequence induces extracellular matrix invasion and accelerates wound healing in obese diabetic mice. *Journal of Clinical Investigation* **2000,** *105* (11), 1537-1545.
344. Kim, D.-H.; Wirtz, D., Focal adhesion size uniquely predicts cell migration. *The FASEB Journal* **2013,** *27* (4), 1351-1361.
345. Halfter, W.; Liverani, D.; Vigny, M.; Monard, D., Deposition of extracellular matrix along the pathways of migrating fibroblasts. *Cell and Tissue Research* **1990,** *262* (3), 467-481.
346. Sun, W.; Kurniawan, N. A.; Kumar, A. P.; Rajagopalan, R.; Lim, C. T., Effects of Migrating Cell-Induced Matrix Reorganization on 3D Cancer Cell Migration. *Cellular and Molecular Bioengineering* **2014,** *7* (2), 205-217.
347. Provenzano, P. P.; Inman, D. R.; Eliceiri, K. W.; Trier, S. M.; Keely, P. J., Contact Guidance Mediated Three-Dimensional Cell Migration is Regulated by Rho/ROCK-Dependent Matrix Reorganization. *Biophysical Journal* **2008,** *95* (11), 5374-5384.
348. Altankov, G.; Groth, T., Fibronectin matrix formation and the biocompatibility of materials. *Journal of Materials Science: Materials in Medicine* **1996,** *7* (7), 425-429.
349. Li, L.; Clevers, H., Coexistence of Quiescent and Active Adult Stem Cells in Mammals. *Science* **2010,** *327* (5965), 542.
350. Horwitz, E. M.; Prockop, D. J.; Fitzpatrick, L. A.; Koo, W. W. K.; Gordon, P. L.; Neel, M.; Sussman, M.; Orchard, P.; Marx, J. C.; Pyeritz, R. E.; Brenner, M. K., Transplantability and therapeutic effects of bone marrow-derived mesenchymal cells in children with osteogenesis imperfecta. *Nat Med* **1999,** *5* (3), 309-313.
351. Sacco, A.; Doyonnas, R.; Kraft, P.; Vitorovic, S.; Blau, H. M., Self-renewal and expansion of single transplanted muscle stem cells. *Nature* **2008,** *456* (7221), 502-506.
352. Dalby, M. J.; Gadegaard, N.; Tare, R.; Andar, A.; Riehle, M. O.; Herzyk, P.; Wilkinson, C. D. W.; Oreffo, R. O. C., The control of human mesenchymal cell differentiation using nanoscale symmetry and disorder. *Nat Mater* **2007,** *6* (12), 997-1003.
353. Salmerón-Sánchez , M.; Ricoa, P.; Moratal, D.; Lee, T. T.; Schwarzbauer, E. J.; Garcia, J. A., Role of material-driven fibronectin fibrillogenesis in cell differentiation. Biomaterials: 2011; Vol. 32.
354. Stratton, S.; Shelke, N. B.; Hoshino, K.; Rudraiah, S.; Kumbar, S. G., Bioactive polymeric scaffolds for tissue engineering. *Bioactive Materials* **2016,** *1* (2), 93-108.
355. Lo, K. W. H.; Ulery, B. D.; Ashe, K. M.; Laurencin, C. T., Studies of Bone Morphogenetic Protein based Surgical Repair. *Advanced drug delivery reviews* **2012,** *64* (12), 1277-1291.
356. James, A. W.; LaChaud, G.; Shen, J.; Asatrian, G.; Nguyen, V.; Zhang, X.; Ting, K.; Soo, C., A Review of the Clinical Side Effects of Bone Morphogenetic Protein-2. *Tissue Engineering Part B: Reviews* **2016,** *22* (4), 284-297.
357. Vuento, M.; Vartio, T.; Saraste, M.; Von Bonsdorff, C.-H.; Vaheri, A., Spontaneous and Polyamine-Induced Formation of Filamentous Polymers from Soluble Fibronectin. *European Journal of Biochemistry* **1980,** *105* (1), 33-42.
358. Moulisová, V.; Gonzalez-García, C.; Cantini, M.; Rodrigo-Navarro, A.; Weaver, J.; Costell, M.; Sabater i Serra, R.; Dalby, M. J.; García, A. J.; Salmerón-Sánchez, M., Engineered microenvironments for synergistic VEGF – Integrin signalling during vascularization. *Biomaterials* **2017,** *126*, 61-74.

359. Mnatsakanyan, H.; Rico, P.; Grigoriou, E.; Candelas, A. M.; Rodrigo-Navarro, A.; Salmeron-Sanchez, M.; Sabater i Serra, R., Controlled Assembly of Fibronectin Nanofibrils Triggered by Random Copolymer Chemistry. *ACS Applied Materials & Interfaces* **2015,** *7* (32), 18125-18135.